THE UNIVERSITY OF HULL

Physical, Chemical, Biological and Management Aspects of Coastal Ecosystems Facing Eutrophication: The Guaymas Bay, Sonora, México.

being a Thesis submitted for the Degree of
Doctor of Philosophy
in the University of Hull

by

MARTIN A. BOTELLO-RUVALCABA, BSc., MSc.
(Universidad Autonoma de Baja California;
The University of Hull)

June 1999

Contents

Acknowledgements

I would like to thanks Dr. Michelle Elliott, my supervisor, for his advice and valuable help in editing this manuscript.

I would to acknowledge the Universidad de Sonora, STAUS, CONACyT-Mexico and The British Council, for the financial support.

I am grateful to DICTUS for their support, especially to those involved in the present work.

I am grateful to Dr. Roger Uglow of the University of Hull, and the Dr. Wim van Raaphorts of NIOZ in The Netherlands for their important critiques and contributions to the present work. Also thanks to Dr. Victor de Jonge of RICZ in The Netherlands for their encouragement.

A special thanks goes for "The Guaymas Team Task Force" (Isidro Vasquez, Fernando Enriquez, Grethel Ramirez, Lourdez Tejeda, and Francisco Muñoz) for their valuable help during the fieldwork. Especially to my friends Fernando Enriquez and the "*Doctore*" Fco. Muñoz for their help and encourage through the whole work.

I wish to thanks the valuable helps provided by CIBNOR-Guyamas, an especially thanks goes for M.C. Alfredo Arreola and Ing. Sara Burrola.

Tanks to ITMAR (M.C. Antonio Gonzales and M.C. Pedro Grano).

A very special thanks goes for my family (Andreas, Karla and Silvia) source of inspiration of this enterprise. Thanks Silvia, for sheering this project.

To Amalia for their support and encourage through this project.

To my parents for their encourage and support.

Finally, To my friends thanks for being there

To Trinidad Botello, Don Trini.

Abstract

The present study has encompassed a series of field observations and theoretical considerations related to physical, chemical, and biological factors defining the process of eutrophication in the Guaymas system. Additionally, the work has produced the basic ecosystem model of the system through the modelling of the hydrodynamics, sediment dynamics, budget dynamics, net ecosystem metabolism and the potential for eutrophication. These findings produce an overall assessment of the system, which together with the environmental legislation and socio-economic concerns, allows those factors influencing decision making to be highlighted. In general, the knowledge of the hydrodynamic features indicates that the flushing capacity of the system may be insufficient to remove pollution discharged into the Guaymas sub-system and Estero el Rancho. There is a residual mass of water that exchanges from the Empalme sub-system to the Guaymas sub-system. Simulation of the trends for potential net transport of sediment indicates that bedload transport is likely to occur toward the head of the Guaymas sub-system. For the Empalme sub-system, there was a net bedload displacement toward the mouth. Mathematical interrelationships between measured phytoplankton biomass and environmental parameters shows through a MRA model that nearly 100% of its variance is influenced by nutrients, pH, temperature and salinity. The stoichiometric Redfield approach indicates that nitrogen is a limiting factor of the phytoplankton biomass growth in the Guaymas system, when other factors such as light, sinking, grazing, temperature and salinity gradients are not. However, an analysis of the two major sub-systems shows that nutrients limiting in the Guaymas sub-system are closely related to phosphorus loads from wastewater sources, whereas for the Empalme sub-system, nutrient limitation was alternately by nitrogen and phosphorus. A primary quantitative outcome of the eutrophic status is given, using a simple biochemical budgetary approach, indicating that the Guaymas system is a net heterotrophic system, with a value of -4811.72 $mmol.C.m^{-2}.y^{-1}$. Using a simple box model to characterise the potential hyper-trophic conditions suggests that phosphorus reduction in the system is accompanied by an improvement in water quality, hence management strategies must encourage P control from wastewater discharges into the sub-system. An analysis of the particular case of the Guaymas system in the context of the Mexican Environmental Legislation indicates that the quality standards set for the system will depend very much upon the designation ultimately used for the system. For instance, if some areas of the Guaymas sub-basin are designated for industrial use, a polluted influence is likely to occur in an area near the development. However, the areas influenced by this development must not pose a threat for the people living the Guaymas basin as stated in the Mexican Environmental Legislation.

CHAPTER 1

General Introduction

1.1 Introduction.

The coastal zone is of considerable socio-economic importance world-wide, it can be defined as the space in which terrestrial and marine environments influence each other (Carter 1988). In Mexico the coastal zone extends for more than 11122 km, including both Atlantic and Pacific Mexican coasts, with nearly 14 million people settled permanently in this zone (INEGI, 1998; SEMARNAP, 1998). This area of transition between land and ocean supports important industries such as fishing, aquaculture, shipping, oil extraction, mining and tourism, which represents important sources of food (protein) supply and economic incomes. Moreover, it is a strategic area for national security reasons.

Considering the multi-user availability of the Mexican coastal zone, an Integrated Coastal Zone Management programme is required in order to minimise pressure in the use of the ecosystem, conflicts between users, and to optimise resources through the integration of national and regional management programme, which allows reduction of costs and minimisation of losses from uncoordinated duplicative management (Kildow, 1997). An Integral Coastal Zone Management (ICZM) programme is *a dynamic process where a co-ordinated strategy is implemented for the conservation and sustainable use of environmental, sociocultural and institutional resources in the coastal zone* (Carter, 1988; French, 1997; Sorensen, 1997). In this context, coastal management strategies must include a combination of economics, social and environmental options, regarding the coastal zone response to this options.

ICZM includes those programmes that provide the required policy and legislation at national and state level, allowing the generation of ICZM plans and strategies, as well as; those issues dealing with a single case basis or local level, where a strategy is generated and implemented.

Disregard for the importance of coastal management strategies very often leads to negative processes and affects against coastal developments. Thus, eutrophication processes and heavy metal pollution from waste disposal, the need for coastal protection against flooding from hurricanes and sea level rise, drought and species succession from oceanographic events such as El Niño, uncontrolled sediment erosion and accretion from either natural or man-induced coastal destabilisation, and saline intrusion are some of the well-documented processes and events that require an ICZM approach in order to be prevented, controlled or solved (Altamirano-Cortez, 1987; Makrama, 1994; Rainbow, 1995; Wu, 1995; French, 1997).

For example, the need for an adequate coastal strategy can be seen in several coastal systems where the actual and potential eutrophic condition represents a risk to human and ecosystem health (Carter, 1988; Cederwall and Elmgren, 1990; Nixon, 1995;). The increase in documented cases of red tides, water de-oxygenation and fish kills are associated with the growing imbalance between the very large increase in tourism, industry or urban population against the improvement of wastewater disposal (Altamirano-Cortez, 1987; Carter 1988; Nixon, 1995).

Thus, coastal management can only be achieved through an understanding of coastal systems. Research is particularly important to produce information for the management of coastal ecosystems, this will allow the optimal use of resources to benefit society and the ecosystem as a whole.

Considering the wide scope and complexity of the ICZM issues, the present study focuses at the local basis, taking as study case the Guaymas system in Guaymas, Sonora, North

West of Mexico. In addition, the final chapters aim to provide a critical analysis of the coastal management status at national level in Mexico.

1.2 Case of study and management tools.

The present work centres on the Guaymas System in the Mexican Pacific coast as a characteristic coastal system representative of the coastal zone problems in Mexico (Figure 1.1).

The Guaymas system is located at 110° 54' West and 28° 40' North in the central-oriental coast of the Gulf of California and it is the most important port in the State of Sonora, Mexico (Figure 1.1). The system itself is a semi-enclosed coastal system with a restricted exchange with the open sea and low fresh water inputs (Rosales-Grano, *et al.* 1995). The system can be generally sub-divided into two sub-systems, the Guaymas bay in the West with the Guaymas city as main watershed, and; the Laguna and Estero El Rancho at Northeast, which include the Empalme city in their watershed (Figure 1.2).

The Guaymas sub-system. The Guaymas watershed is restricted by topographic features of the Guaymas basin and comprises the major percentage of the Guaymas City (Figure 2). Population in Guaymas city is around 91,500 (INEGI 1998), and freshwater requirements for domestic and industrial uses are satisfied with 0.6 m^3s^{-1} (COAPAES, 1996). A poorly-efficient oxidation lagoon represents municipal wastewater treatment facilities, the capacity of which is 0.16 m^3s^{-1} (Figure 1.2). Thus, wastewaters into the Guaymas Bay are estimated to be around 0.1 m^3s^{-1}, which represents the 16.6% or the total fresh water requirements of the city (Figure 1.3; COAPAES, 1996). Industrial activities within this basin include, seafood product industrialisation including cannery and packing, shipping, shipyard, reception and storage facilities for oil and other chemicals, tourism, and commerce (Figure 1.3).

Figure 1.1. The Guaymas System.

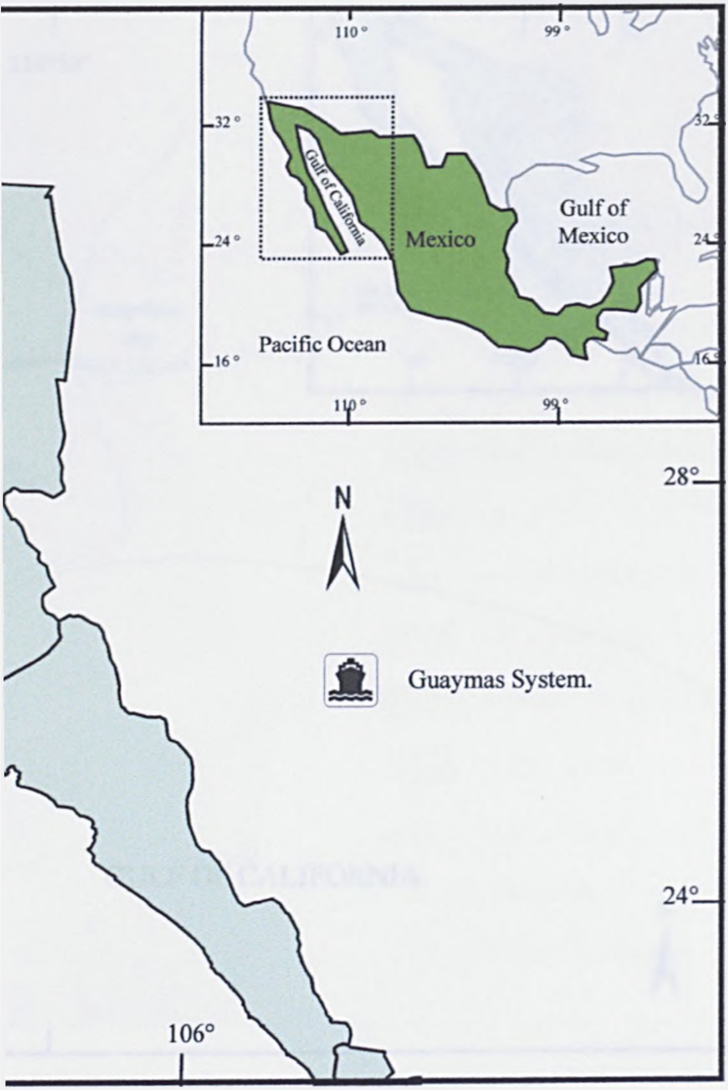
110°
99°
32°
24°
16°
Gulf of California
Mexico
Gulf of Mexico
Pacific Ocean
28°
24°
N
Guaymas System.
106°

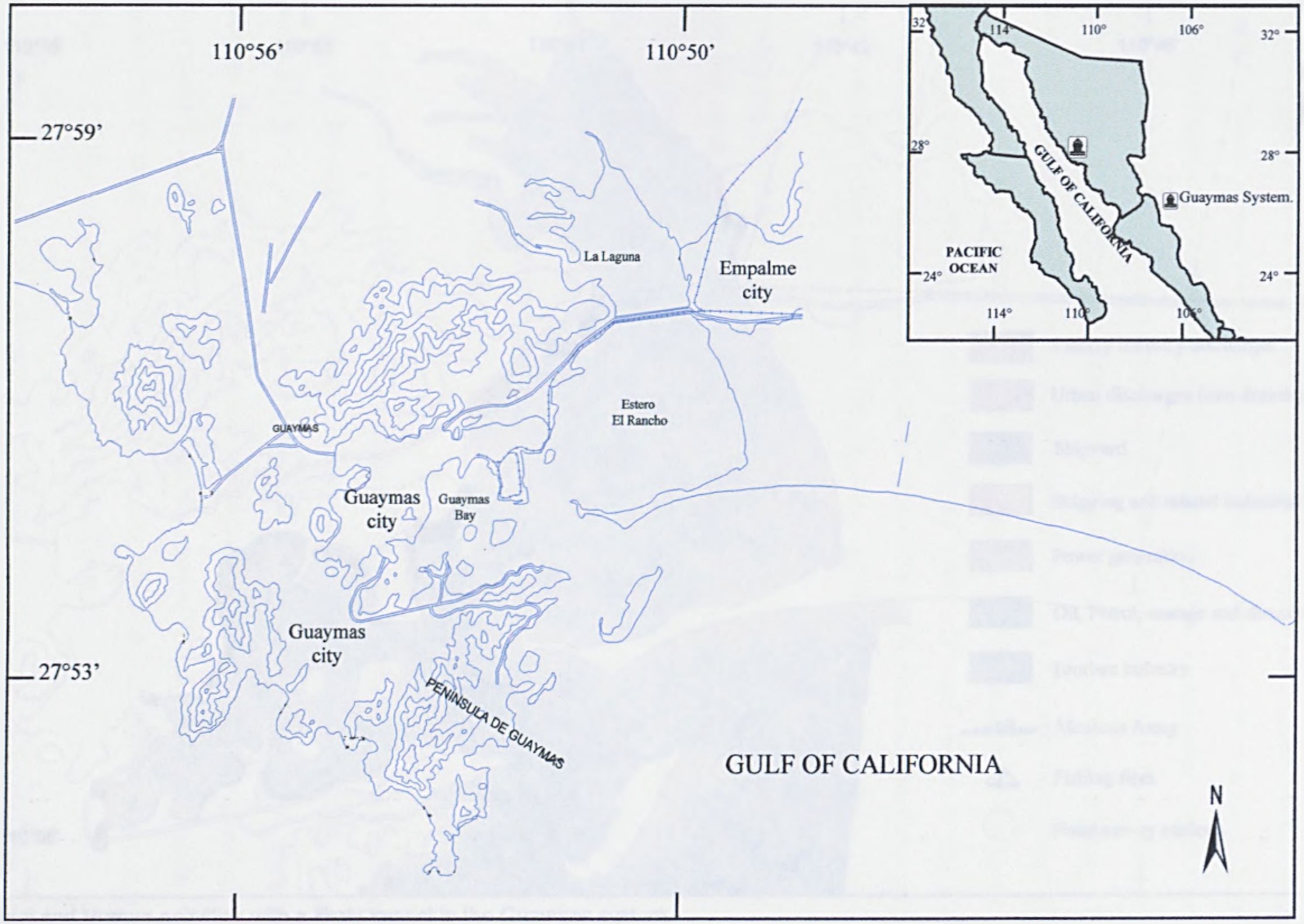

Figure 1.2. Location of the Guaymas System in the State of Sonora, United State of Mexico.

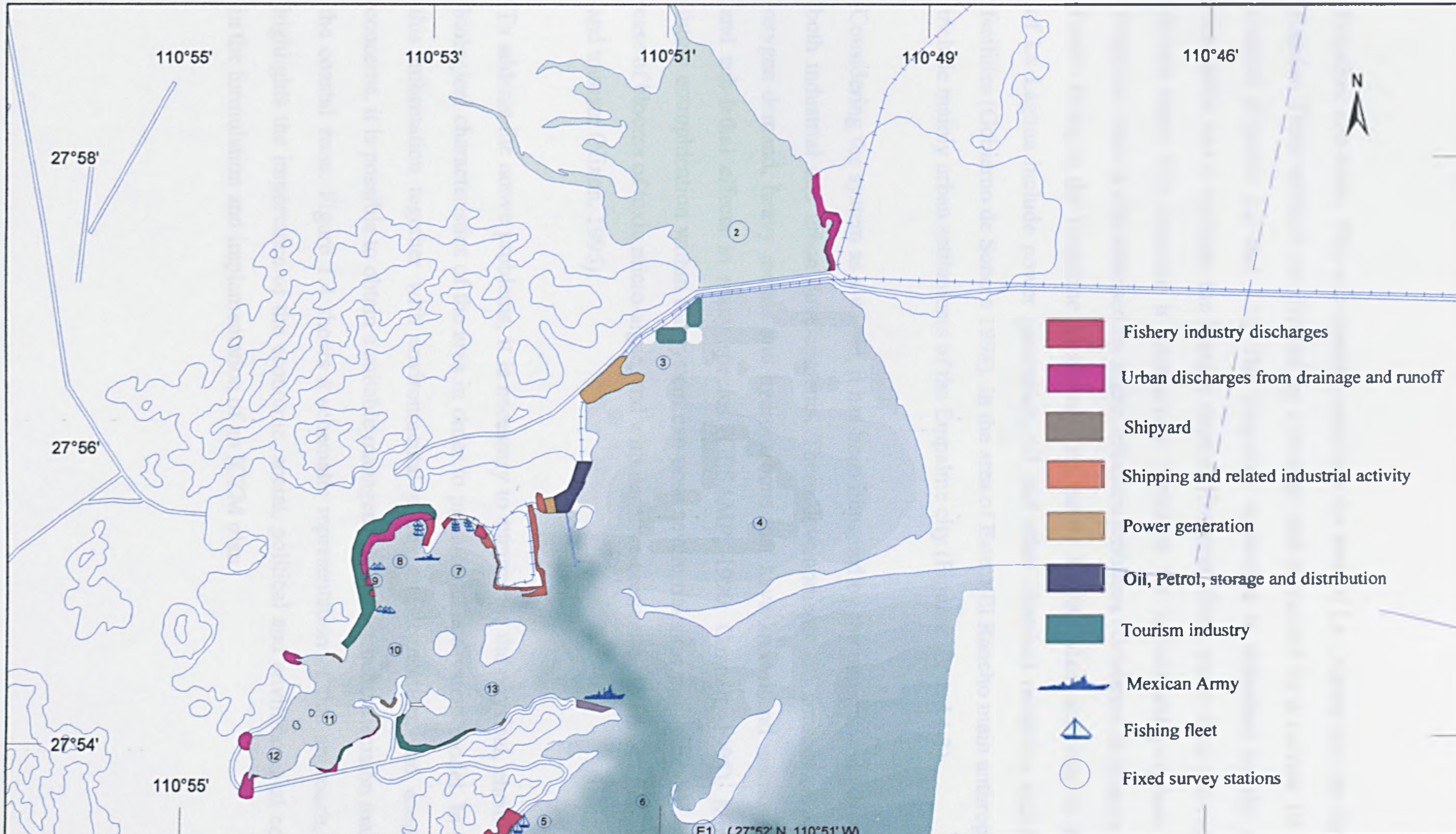

Figure 1.3. Industrial and Human activities with a likely impact in the Guaymas system.

Empalme sub-basis. This sub-system comprises the area of La Laguna and the Estero El Rancho. These systems are divided by a barrage and connected by a narrow 10 metres channel (Figures 1.2 and 1.3). The Empalme watershed is delimited by the nearest mountains and it includes the Matape stream. However, fresh water does not reach the system since this resource is extensively exploited for agricultural purposes. Thus, Empalme basis is characterised by saline intrusion problems (Gobierno de Sonora 1998). People living in the Empalme urban area total nearly 38,000. Main activities in the area of La Laguna include power generation, oil and other chemical reception and storage facilities (Gobierno de Sonora 1998). In the area of Estero El Rancho main anthropogenic include mainly urban settlements of the Empalme city (Figures 1.2 and 1.3).

Considering the system as a whole, it has been impacted by the unregulated growth from both industrial and urban developments. These developments are sources of nutrients, oxygen demand, heavy metals and hydrocarbons that have known and unknown lethal and sub-lethal effects in many species (GESAMP, 1990; Connell, 1995). Moreover, future eutrophication within the system can pose severe risks for public health as in the case of blooms of toxic micro-algae, and with negative economic effects in local fisheries and tourism (Nixon, 1995).

To address the above problems, it is necessary to summarise the physical, chemical and biological characteristics of the area in order to produce an ecosystem model. In linking this information together with environmental policy and legislation, and economical concerns, it is possible to obtain a suitable management tool for better decision making in the coastal zone. Figure 1.4 shows a schematic representation of this approach, which highlights the importance of the economic, social, political and environmental concerns in the formulation and implementation of an ICZM plan.

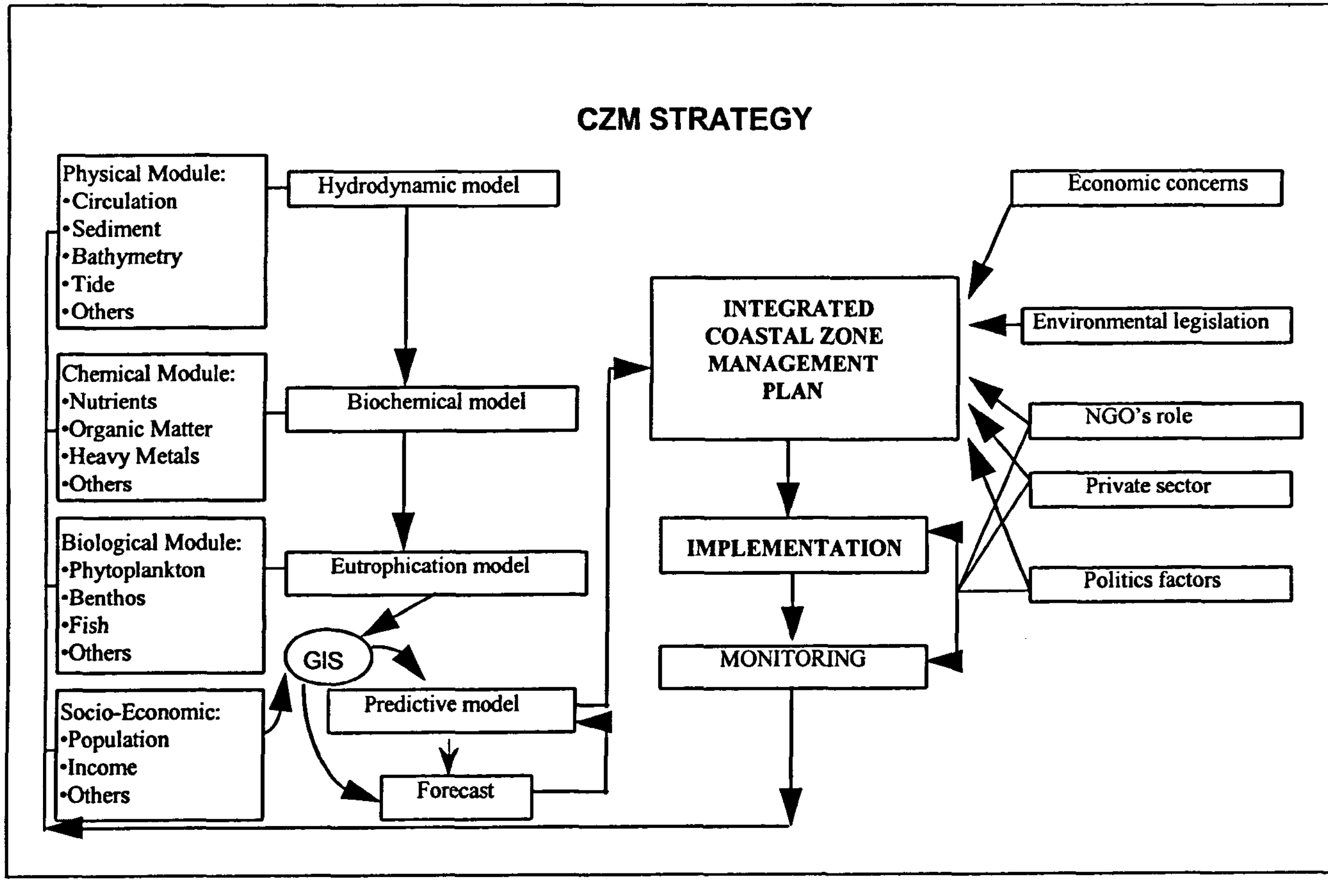

Figure 1.4. Schematic representation of a coastal zone strategy.

1.3. Aims

This work aims to create the basic ecosystem modelling that allows a better management of the Guaymas coastal zone, especially for future development projects. Additionally, based on the information generated by the present case study, to evaluate the trophic status of the system against the background of the repercussions of the Mexican environmental policy and legislation and their likely implications at international level.

In order to perform the above objectives, the initial chapters here characterise the main physical and environmental conditions of this particular ecosystem. This information is summarised in later chapters which aim to produce an overall assessment of the system in the ICZM context.

Chapter 3 characterises the hydrophysical regime, including tidal components, and current velocity field within the Guaymas system. This information is then used in Chapter 4 to characterise the sediment dynamics within the system.

Chapter 5 produces a physical-chemical and biological budgetary approach to give a first approximation for the trophic status of the system, highlighting areas that represent a net source or sink for nutrients and identifying those compartments which are net producers or consumers of organic matter.

Chapter 6 characterises the variation of biotic and abiotic parameters, with the aims to produce empirical models based on statistical analysis of observed trends. Also, using information derived from previous chapters, Chapter 6 evaluates the potential for eutrophication within the Guaymas system.

Chapter 7 presents the general conclusion, producing an overall assessment of the system and, together with environmental legislation and socio-economic concerns, it allows those factors influencing decision making to be highlighted. Finally, the Chapter presents future work.

CHAPTER 2.

General Materials and Methods

2.1 Survey Strategy.

In order to ensure the accuracy and validity of the information used for the assessment, it was necessary to develop a spatial and temporal field survey within the Guaymas System. The survey especially included those physical, chemical and biological factors that provide an overview of how the ecosystem operates, providing the basic knowledge to assess the likely impact of human activities within the system. In order to ensure the above, the following criteria were considered (Elliott, *et al.* 1994):

1. An estimation of the degree of freshwater (if any) and tidal flushing leading to a calculation of exchange rate. This information to provides the capacity of the system to retain or to flush-out materials such as pollutants and phytoplankton.

2. The characterisation of the physical conditions under which potential primary producers can grow, such as turbidity regime, light penetration/light availability, type of bed substratum, degree of wind, tidal, and density gradients (from temperature and salinity). This information indicates the way in which physical environmental variables limit primary production, and it establishes basic relationships suited for ecosystem models.

3. The estimation of nutrient inputs (N & P species) to the area from main sources, regarding the system watershed. When other physical variables are not limiting for phytoplankton growth the N and P species concentration may be regarded as the limiting factors. The study aimed to consider the repercussions of increased N and P concentration

up to several orders of magnitude, and hence the increase of potential harmful phytoplankton blooms within the system.

4. The calculation of the residence time for nutrients, together with the levels of nutrients in the area and in the open coast. As in the case of other materials, nutrient residence times determine their availability to be assimilated by phytoplankton. In addition, nutrient budget dynamics allow a first approximation for the trophic status of the system, highlighting areas that represent a net source or sink for nutrients and identifying which are net producers or consumers of organic matter.

5. Nitrification/denitrification characteristics of the system. These include the nutrient dynamics within the area, i.e. their conservative or otherwise behaviour, their uptake or release by biotic and non-biotic components, and the estimation of molar N:P values to determine primary production mechanisms (and the need for nitrification/denitrification levels). Nitrogen and Phosphorus relationships give an insight into whether nutrients are limiting for primary producers. In addition, stoichiometric N:P linkages may suggest the N fixation or denitrification within the system, and their likely relationship with anthropogenic activities.

6. An assessment of the trophic status of the area includes adverse symptoms of hypernutrification or eutrophication including any oxygen deficiency.

A summary of the above information including physical, chemical and biological aspects of the system will allow establishing an overall assessment of the system. In turn, this assessment, together with environmental legislation and economic concern, will allow management strategies to be established.

2.2 Temporal characteristics.

A total of 10 sampling surveys were performed within a one year period. Situations beyond the control of the present study, such as unwanted equipment failure, were responsible for slips on time for June and August, reducing the survey time series from 12 to 10 surveys. In order to characterise the best retention conditions within the system, the surveys were done preferentially during neap tide. Sampling collection started from open sea to the head of the system keeping this pattern during all surveys.

2.3 Spatial characteristics.

After an extensive baseline survey which analysed 25 sampling stations, a total of 13 stations were considered as the most representative of the system. The main criteria utilised to discriminate the number a location of the survey stations were: the non-significant differences between immediate survey stations, the number of stations in one hydrographic unit, and the logistical problems to survey a representative number of stations with the available resources. Thus, from the above cost-effective considerations and for the purpose of this thesis, samples were taken at 13 fixed stations located within the system and adjacent sea (Figure 1.3). Sampling depths were surface (0.5 m) and bottom, depending upon the bathymetry of the area (10 m; stations E1, 5 and 6).

Water samples were obtained using Niskin hydrographic sampler bottles. Sub-samples for Chlorophyll-*a*, nutrients, phytoplankton, zooplankton, salinity, and seston were collected in acid washed polyethylene bottles. Oxygen samples were obtained using acid-washed biochemical oxygen demand bottles (BOD) following the technique of Strickland and Parsons (1972).

In the case of benthos and sediment analysis, sampling was carried-out from at least 3 sub-samples in each sampling station using a 5 kg capacity Van-Veen drag. Samples were transferred to acid washed plastic bags.

2.4 Samples storage.

On board. Samples for chlorophyll-*a*, benthos, seston, sediment analysis, and nutrients were kept in the dark and cooled-down immediately to nearly 0 °C using salt-saturated ice. Samples for phytoplankton taxonomy were fixed using a Lugol's iodine solution, zooplankton samples were preserved using 10% formol solution, sediments for benthos identification were preserved with 10 % formol solution before being cooled. Oxygen samples were fixed accord to Strickland and Parsons (1972). All fixed and preserved samples, except the benthos, were kept at room temperature.

Laboratory. Samples for chlorophyll-*a* were filtered using with 0.45 μ Watman filters and frozen to -20°C; samples for nutrients were frozen to –40°C until further analysis (Grasshoff, *et al.* 1983). Analyses and determinations were made within a month period. Benthos sediment was washed and sorted using a 0.5 sieve, subsequent samples were fixed using the vital stain Rose Bengal solution and keep in plastic containers for future identification. Samples for oxygen, seston, organic and inorganic matter and carbonates in sediment, were analysed within the following two days. Samples for phytoplankton, benthos, and sediment granulometry were kept at room temperature until further analysis.

2.5 Measured and Collected Sample Parameters

Measurements for temperature, pH, light irradiation, Sechi disc, and geographical position were done on board the vessel during each survey. In addition, data for tide, current velocity, precipitation and evaporation were collected for each survey (when it was possible) from research institutions within the Guaymas System (Rosales-Grano, *et al.* 1995; Comision Nacional del Agua, 1998).

2.6 Methods

2.6.1 Temperature.

Water temperature was measured using a bucket thermometer with a 0 to 50°C range. The samples were read immediately within the Niskin bottles with a precision ± 0.1°C.

2.6.2. Salinity.

An induction technique was used to measure salinity. Seawater samples were analysed with a Beckman Induction Salinometer (Model SR10). The analyses were performed at the University of Baja California, Ensenada Unit. Calibration was carried out using Copenhagen seawater standards. The accuracy was ± 0.003 practical salinity units (psu), including unavoidable errors encountered with good technique (Beckman-Industrial, 1986).

2.6.3 pH.

The pH determinations were performed from sub-samples at the shore-base laboratory using a Cole Palmer 5983 potentiometer. The electrode was calibrated using buffer solutions (Merck) at 4, 7 and 10 pH units.

2.6.4 Oxygen

Samples were taken from the Niskin bottles to BOD bottles avoiding bubble formation. The samples were fixed on board (1 ml of Manganous sulphate reagent + and 1 ml of alkaline Iodine solution). Determinations were performed at the laboratory within the next two days. In the laboratory, the samples were acidified with 1.0 ml of concentrated (sp gr 1.84) sulphuric acid, shaken until the precipitate was dissolved. Finally, three 50 ml samples of solution were titrated with standard 0.01 N thiosulphate, using starch as indicator. Further calculation and considerations were done according to the methodology described by Strickand and Parsons (1972).

2.6.5 Light

Light penetration in the water column was estimated using a secchi disk and an LI-192SA Underwater Quantum Sensor.

Secchi disk depth. A 30 centimetres diameter secchi disk was used to measure secchi depths (Sd), lectures were registered in meters.

Atmospheric and underwater, photosynthetically-active radiation (PAR) readings were performed using a LI-192SA Underwater Quantum Sensor and a LI 1000 data logger. The sensor measure the 400-700 nm quantum response. Sensitivity: Typically 3 µA per 1000 ±mol s^{-1} m^{-2}.

2.6.6 Chlorophyll-*a*

One litre of seawater was filtered using Watman filters with 2.5 cm diameter and 0.45 micron pore size. During filtration, two drops of MgCO3 were added as preservative. Filters were frozen and kept at –25°C until further analysis. Determinations of Chlorophyll-*a* were performed by the spectrophotometric methods described by Parsons, *et al.* (1984). Pigment extraction was done with 15 ml of spectrophotometric grade acetone (90% v/v) during 24 hours at 3°C. After centrifugation, the supernatant liquid was measured at 480, 510, 630, 647, 664, and 750 nm in a Perkin-Elmer Lambda 2 UV/VIS spectrometer. The concentration of chlorophyll-*a* was computed as stated by

Parsons *et al.* (1984). The precision of the method at 5 μg level was $\pm 0.21/n^2$ chlorophyll-*a*

2.6.7 Nutrients.

In the present study, total nitrogen compounds were characterised as nitrate, nitrite and ammonia, and total phosphorus as inorganic phosphate. Nutrient analyses were performed for nitrate and nitrite through the spectrophotometric techniques described by Parsons, *et al.* (1984). For the case of phosphate and ammonia the analyses were performed through clean flow injection techniques set-up in the present work. As a general condition, water grade HPLC and analytic grade chemicals (SIGMA, MERCK and SPECTRUM) were used. All glassware and plastic material were rinsed with phosphate-free Dextran and/or HCl solution (10% v/v).

Nitrate and Nitrite. Nitrite in seawater samples was determined by diazotizing with sulphanilamide and N-1 napthyl-elthylendiamide (Parsons, *et al.* 1984). Measurements were done with a spectrophotometer Perkin-Elmer Lamda 2 UV/VIS. Nitrate in seawater samples were reduced to nitrite through a cadmium-copper reduction column. The concentrations of nitrate were obtained by subtracting the nitrite concentration from the original sample (Parsons, *et al.* 1984). For nitrite precision at 1.0 μM level was $\pm 0.03/n^2$ μM, and for nitrate precision at 20 μM level was $\pm 0.5/n^2$ μM.

Ammonia. The technique involves the use of a flow injection, gas diffusion technique adapted by Clinch *et al.* (1988), and cited by Hunter and Uglow (1993) and Gomez-Jimenez (1998; Figure 2.1).

As a general consideration, and in order to avoid the formation of any salt precipitate that may interfere with the technique, the flow-injection system was periodically washed/flushed with 10% HCl followed by HPLC water, and the membrane replaced.

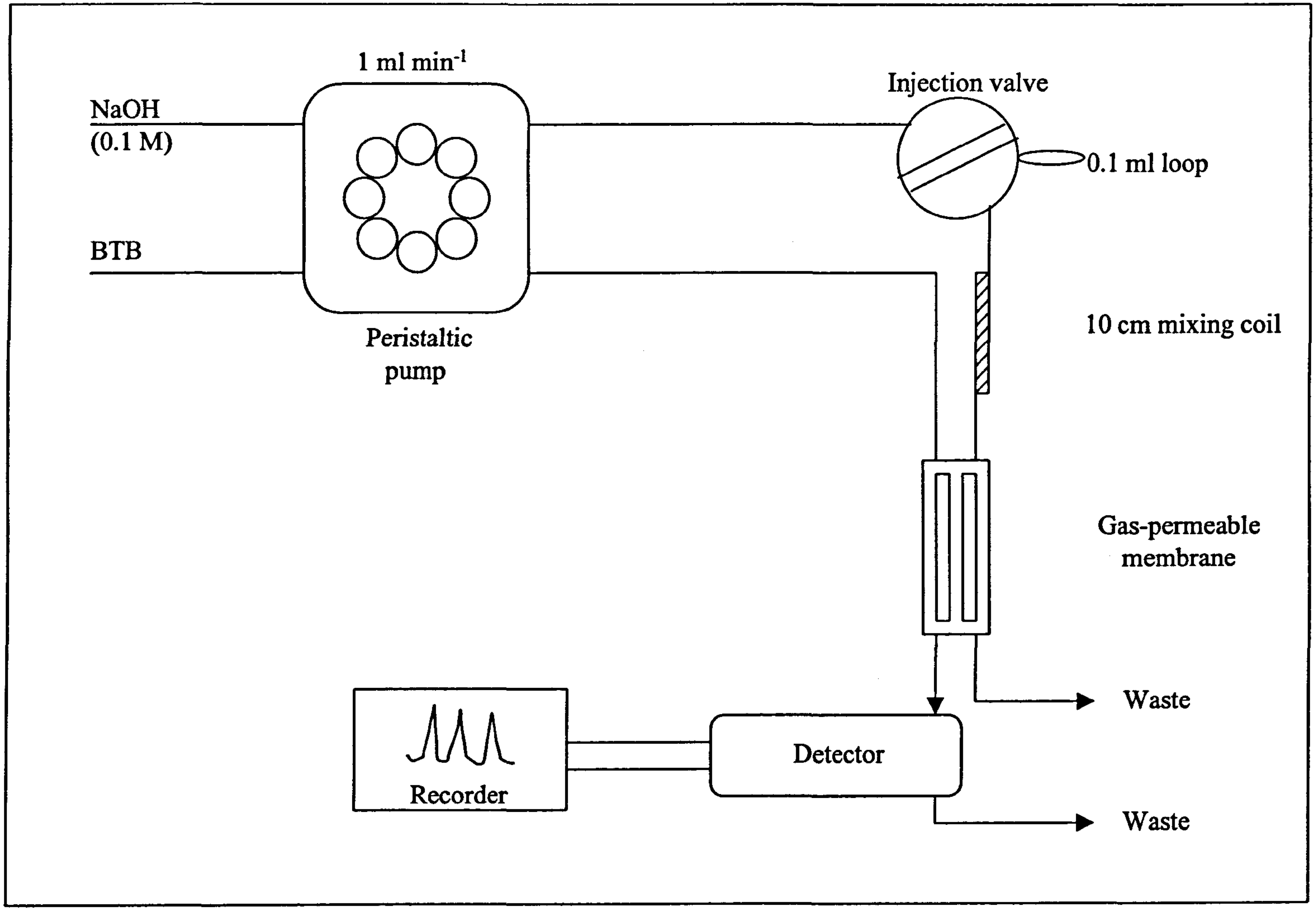

Figure 2.1. Flow Injection Analysis manifold used for the determination of ammonia in seawater samples.

The sample is injected into an alkaline carrier stream of 0.1 M NaOH, which transforms all the ammonium ions (NH_4^+) in to free gaseous ammonia (NH_3). This carrier stream is passed on one side of a gas permeable membrane (PTFE), on the other side of which flows a pH sensitive indicator Bromothymol Blue (BTB: 0.4 g L^{-1} ultrapure water). There is a NH_3 diffusion across the permeable membrane that reacts with BTB in the alkaline form. The BTB reaction produces a change in colour that was measured spectrophotometrically (635 nm) and the potential difference produced was recorded graphically through a computer, using software package (PICOLOG®).

Ammonia concentrations within the sample produce a proportional relationship with the magnitude of the colour change. Standard solutions of $(NH_4)SO_4$ with known concentrations within the expected range for ammonium in seawater were used to produce a linear regression, from which ammonium concentrations in samples were calculated.

Phosphate. Phosphate was analysed in the present work using a reversed flow injection technique. A flow injection system was set-up following the indications suggested by Kenneth and Petty (1982) and the modifications done in this work. Modifications to the primary system were done mainly in relation to flow velocity, length and internal diameter of the tubing, wave length and chemical concentrations (Figure 2.2).

A mixed reactive (H_2SO_4 125/500 ml v/v; (NH4)6Mo7O24.4H2O 47.5 gr/500 ml; K(SbO)C6H4O6 16.25/500 ml) and Ascorbic Acid (35 gr/500ml) were combined in a 1 metre mixing coil, and injected into the sample that works as a carrier. The carrier stream is passed through a 1.5 metres reaction coil (50°C) and the reactions produces a change in colour that was measured spectrophotometrically (733 nm). The potential difference produced was recorded graphically through a computer, using a software package (PICOLOG®).

PAGE(S) MISSING IN ORIGINAL

Phosphate concentrations within the sample produce a proportional relationship with the magnitude of the colour change. Known KH_2PO_4 standard solutions within the expected range for phosphate in seawater were used to produce a linear regression, from which phosphate concentrations were calculated.

2.6.8 Seston Analysis.

Samples were analysed through the ignition and gravimetric method cited by Strickland and Parsons (1972).

One litre of seawater was filtered using Watman GF/C filters with 2.5 cm diameter and 0.45 μ pore size. Filters were placed into an oven at 100°C during 1 hour. Dry weight was registered through a gravimetric scale (Mettler-100). Further, filters were put into the oven at 450°C during 4 hours. The percentage of organic and inorganic matter was obtained by difference with respect to the dry weight.

2.6.9 Sediment analysis.

Organic and inorganic matter, and carbonates were analysed in sediments. The technique involves the use of the thermal differential analysis cited by Walter (1974). Sediment samples (≅ 10 grams) were placed into an oven at 100°C for 1 hour for dry weight, at 550°C for 1 hour for organic carbon elimination, and at 1000°C for 1 hour for carbonate elimination. Weight difference from the fractions were used to obtain the percentages of dry weight, organic matter, and carbonate.

CHAPTER 3.

Hydrodynamics of the System

3.1 Introduction.

The Guaymas system is a shallow, coastal lagoon with moderated tidal forcing, a mixed diurnal/semidiurnal tide type with a predominate diurnal tide, narrow tidal flats, variable channel cross-sections, and null riverflow (Rosales-Grano, *et al.* 1996). In this kind of system, hydrodynamic characteristics such as current velocity, tide and sediment transport strongly influence the coastal lagoon's stability (Dyer, 1986). Modification of these characteristics may largely influence their geological evolution, navigability, as well as the chemical and biological health of the system (Pethick, 1984; Carter, 1988). Therefore, knowledge of the hydrodynamic conditions represents the first step towards the understanding of many environmental processes, and provides the basic framework for coastal zone management.

In this context, the present chapter aims to provide a better understanding of the hydrodynamics of the Guaymas system. The first section of the present chapter describes as information background the basic elements influencing circulation patterns, highlighting those characteristics for which knowledge is needed in order to produce hydrodynamics. Finally, hydrodynamics of the Guaymas system, is modellated through a the numerical model (HydroTrack©.)

3.1.1 Tide in shallow systems.

Tide forcing is a major process controlling circulation in small and shallow coastal lagoons. Knowledge of tidal characteristics is important, since these processes influence other physical, chemical and biological features.

In semi-enclosed coastal systems, the tidal process is mainly influenced by relative positions of the moon and earth; the solar influence during the day, and the effects on tide wave due to sheer stress, land obstruction with geographic wells, and seabed. All these influences are reflected in a series of regular sinusoidal variations with a characteristic amplitude and phase known as tidal constituents or components (Dyer, 1986). Furthermore, non-linear advection and other bathymetric and geometric effects very often present in these systems are described as additional higher harmonic components (e.g. M4, M6 and M8), which are fractions of the astronomic diurnal and semi-diurnal constituents (Howarth and Pugh, 1983; Aubrey and Speer, 1985). Table 3.1 describes the main tidal constituents for shallow waters.

Tidal constituents can be derived from sea surface elevation time-series, the most used methods are the harmonic or response analysis (Howarth and Pugh, 1983), the response and admittance method (Aubrey and Speer, 1985; and authors therein), and the least squares harmonic analysis (Aubrey and Speer, 1985). The least squares harmonic method for a limited data time-series can achieve better resolution compared with the traditional Fourier harmonic analysis. However, this high resolution is likely to be affected by noise of other tide signals such as storms and surges, thus limiting accuracy and requiring a noise filter or longer time series to overcome these effects (Howarth and Pugh, 1983).

Although tides can be measured and modelled mathematically, the development of a mathematical model for tide predictions are beyond the present work. Thus, this section specifically aims to characterise the main tide species and constituents within the system using a standard Fourier harmonic analysis. Tidal height elevations at the mouth of the system are obtained using both time-series data from field time series recorded data and predicted elevations from the programme PREDOB©. For tidal height elevation within the system, heights are approximated through the tide prediction programme HydroTrack©.

Table 3.1. Principal tidal constituents in shallow waters (Dyer, 1986).

Name	Constituent	Period (h)	Relative size (%)
Lunar semidiurnal	M2*	12.4	100
Solar semidiurnal	S2*	12.0	47
Lunar elliptic	N2*	12.7	19
Luni-Solar-semidiurnal	K2	11.97	13
Luni-Solar-diurnal	K1*	23.9	58
Lunar diurnal	O1*	25.8	42
Solar diurnal	P1	24.1	19
Lunar fortnightly	Mf*	328	17
Lunar monthly	Mn*	661.3	

* components identified in the present work.

3.1.2 Circulation

Circulation patterns are important to understand both physical dynamics and water quality processes in coastal environments. The importance of these processes has encouraged steady progress in the development of sophisticated numerical models for water circulation in coastal systems. Thus, current modelling represents a valuable management tool, which allows the study and control of the effects associated with anthropogenic and natural perturbations such as sediment transport, pollution and eutrophication for coastal environments (Aubrey, 1986; van de Kreeke, 1986; Aksnes *et al.* 1995; Kuusisto *et al.* 1998).

Circulation in coastal systems is mainly driven by tide, wind, fresh water flows, density gradient and earth rotational forces such as Coriolis forces. However, the balance of forces defining circulation depends very much upon the characteristics of the particular coastal system and the interaction of circulation patterns with the topography.

For well-mixed and shallow coastal lagoons, tidal and wind-induced currents represent the major components inducing circulation (Dyer, 1986; Huang *et al.*, 1986; Prandle, 1986). In these environments, circulation is also highly influenced by seabed friction and morphology of the system (Aubrey and Speer, 1985). Energy can be increased or dissipated depending on the irregular bathymetry of the area, and strong currents can be produced by hydraulic pressure gradients in local straits. These currents strain are associated with processes such as stratification, turbulence and waterfronts.

Circulation structure and their characteristics in coastal lagoons are determined by:

Tidal currents. Tidal currents are defined as the horizontal water displacements associated with the vertical tide oscillation (Bearman *et al.* 1993). For small shallow water systems, where tidal range volume constitutes a significant fraction of the total water volume, tidal currents mainly determine the dynamics of the system (Dyer, 1986; Huang *et al.* 1986).

There is a strong correlation between those factors determining tidal constituents and tidal currents. Thus, tidal constituents contain a dominant proportion of the total energy in relation to currents (Cheng and Gartner, 1985).

Wind-induced currents. Local wind force and direction can play a major role in shallow waters, and may explain a large proportion of the total transport within coastal lagoons (Cheng and Gartner, 1985; Smith, 1990). Wind forces often overcame Coriolis and other frictional forces in shallow waters, influencing the magnitude and direction of the resultant circulation currents. Also, waves, produced locally by wind, can increase or decrease the surface water motion, inducing turbulent processes. Re-suspension of small sediment particles or turbidity affects directly other physical, chemical and biological properties of the system (Pethick 1984; Bearman *et al.* 1993).

Geostrophic currents. The driven current resultant from a horizontal density gradient and earth rotation is known as geostrophic current. Although the general Coriolis effect for the northern hemisphere shows a right-hand lateral deflection of water currents, it can be neglected for small shallow systems where bottom friction, system geometry and sustained wind blowing balance or overcome these earth rotation forces (Aubrey, 1986; Kjerfve, 1986; Bearman *et al.* 1993).

Density-driven currents. Density gradients during slack periods can drive horizontal and vertical water currents. Horizontal, density-induced currents different from geostrophic currents, are not significantly driven by Coriolis forces, instead local topography highly determines their direction. For coastal lagoon systems where fresh water inputs are limited and highly seasonal, salinity increases toward the head. This highly saline water tends to sink and flow seaward near the seabed, representing a negative circulation (Bearman *et al.* 1993). Further, this circulation can be disrupted by mixing processes induced by tide and wind (de Silva, 1989), and seasonal fresh water inputs, where water runoff from the watershed may invert circulation patterns.

3.1.2.1 Residual currents.

Residual currents are important in the net transport of dissolved and suspended materials in shallow systems. They can provide help to explain the amount of substance retained by the system after a tidal cycle, i.e. the rate of displacement of substance over tide (Huang *et al.* 1986; Cheng *et al.* 1986; Uncles *et al.* 1986; Dyer 1997).

For the transport of substances (e.g. pollutants, phytoplankton), it is important to distinguish the difference between Eulerian and Lagrangian residual currents. Eulerian residual currents represent the time period averaged currents for a fixed location. Thus, Eulerian residual currents are the mean current velocities in a fixed location averaged over the tide period (Dyer, 1986). An approximation can be obtained by averaging data from currents registered at regular intervals through a period of 24 hours 50 minutes (Lunar day).

A Lagrangian residual current is the Lagrangian displacement of a labelled water parcel per tidal period. An approximation to the main Lagrangian residual is given by the expression:

Lagrangian residual current = Eulerian residual current + Stokes drift current (3.1)

This residual is defined as the mass transport velocity or first order Lagrangian residual current and is accurate and valid for weakly, non-linear systems (Cheng *et al.* 1986; Huang *et al.* 1986). Where Stokes drift current is defined as:

a)

$$Us = \int_{\theta_0}^{\theta_0+\theta}\left[\int_{\theta_0}^{\theta}(\hat{u}dt'.\ \nabla\hat{u})\right] dt \qquad (3.2)$$

Where θ_0 is the initial time, θ represents tide period, $\hat{u}$ is the depth mean horizontal velocity vector and ∇ is the horizontal operator $\partial/\partial x$, $\partial/\partial y$.

b) A solution for the Stokes drift was expressed by Cheng *et al.*, (1986) as:

$$Us(u,v) = <(\partial u_0/\partial x_0)_0\xi> + <(\partial u_0/\partial y_0)_0\eta>, <(\partial v_0/\partial x_0)_0\xi> + <(\partial v_0/\partial y_0)_0\eta> \qquad (3.3)$$

Where the terms < > represents notation for the time averaging operator, tide period; $(\ )_0$, are arguments evaluated at x_0 and y_0, finally (ξ,η) is the Lagrangian water parcel displacement denoted by:

$$(\xi,\eta) = \int_{\theta_0}^{\theta}\left[u_l(x_0,y_0,\theta),v_l(x_0,y_0,\theta)\right] d\theta \qquad (3.4)$$

Here, (u_l,v_l) are Lagrangian tidal velocities and θ is the time or tide period.

However, non-uniform velocity field is often the case in coastal systems. For dynamic coastal lagoons, where topographic characteristics influence circulation, the difference between Lagrangian velocity and the residual transport velocity has been indicated to be very important (Pingree and Maddock, 1977; Cheng *et al.*, 1986). A second order correction, Lagrangian drift velocity, was introduced by Cheng *et al.* (1986) to improve accuracy between predicted and observed Lagrangian residual currents, concluding that high order corrections improve substantially the representation of residual transport. Cheng *et al.*, (1986) define Lagrangian residual velocity as:

Lagrangian		Eulerian		Stokes'		Lagrangian	(3.5)
Residual	=	Residual	+	Drift	+	k Drift	
Current		Current		Velocity		Velocity	

Where Lagrangian drift velocity is given by:

$$1/[2\{u'^{2}_{ld} + u''^{2}_{ld} + v'^{2}_{ld} + v''^{2}_{ld} \pm [(u'^{2}_{ld} + u''^{2}_{ld} + v'^{2}_{ld} + v''^{2}_{ld})^{2} - 4(u'^{2}_{ld}\, v'^{2}_{ld} - u''^{2}_{ld}\, v''^{2}_{ld})^{2}]^{½}\}^{½}]^{½} \quad (3.6)$$

Details for $(u,v)_{ld}'$ and $(u,v)_{ld}''$ Lagrangian velocities are given by Cheng *et al.*, (1986).

Figure 3.1 shows a schematic representation between the three residuals for a depth-averaged modelled system.

Further evolution of mass transport equations is given by Garcia-Martinez and Flores-Tovar (1998) introducing a fourth-order velocity interpolation, minimising the difference between predicted and observed Lagrangian residual current.

3.1.3 Modelling Tide and Currents.

The state-of-the-art models allow an approximation for the circulation processes description in coastal environments. The present section provides those basic elements used for modelling as used in this work. There is a set of governing partial differential equations from which the description of the basic hydrodynamic process in coastal lagoons can be provided. For a co-ordinate system (x,y,z) the basic governing equations are represented by:

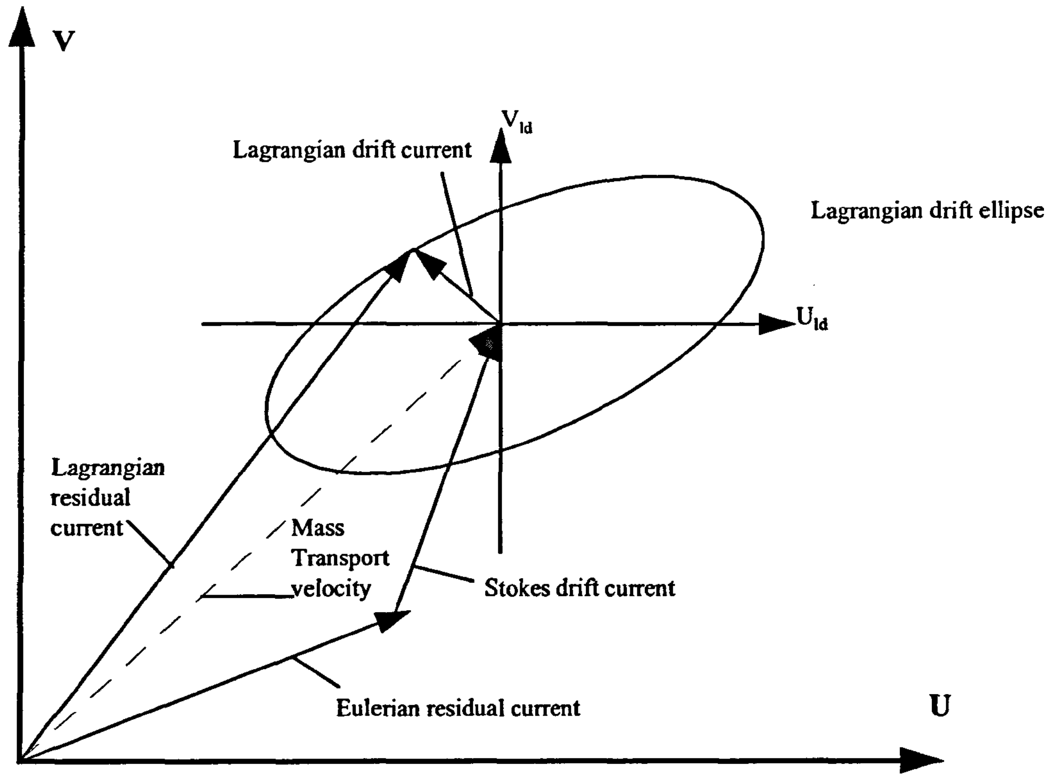

Figure 3.1. Schematic representation of the relationship among Eulerian residual current, Stokes drift current, Mass transport velocity and Lagrangian residual currents. Figure taken from Cheng (1986).

Conservation of mass equation.

$$\partial U/\partial x + \partial V/\partial y + \partial W/\partial z = 0 \tag{3.7}$$

Conservation of momentum equation in (x,y,z) direction

$$\begin{aligned} \partial U/\partial t + \partial U^2/\partial x + \partial VU/\partial y + \partial WU/\partial z &= Ex \\ \partial V/\partial t + \partial V^2/\partial y + \partial UV/\partial x + \partial WV/\partial z &= Ey \\ \partial W/\partial t + \partial W^2/\partial z + \partial UW/\partial x + \partial VW/\partial y &= Ez \end{aligned} \tag{3.8}$$

Further complicated considerations in terms of boundary conditions and the forces acting on a fluid particle in well-mixed shallow coastal lagoons, such as gravity, friction, pressure gradients and Coriolis force must also be represented.

Boundary Conditions. The formulation of the limits in time and space for the computational domain are essential for the finite difference equation solution. Close boundaries represent the time and computation region limits. This close boundary region must be regarded as impermeable, hence it does not allow flow-through. Open boundaries are those regions with a free exchange of properties between in and outside the computational domain. Further boundaries conditions are given in terms of coefficients such as bed friction, wind shear stress, etc. (Knauss, 1978).

Turbulent or eddy viscosity coefficients. The coefficient of eddy viscosity depends of the degree of turbulence. This coefficient is not conservative in relation to the fluid properties and varies with time and space, depending mainly on boundary roughness and distance of the boundary layer. Common values range from 10^{-2}-10^{2} kg(m.s)$^{-1}$ for vertical eddy viscosity coefficients, and 10^4 to 10^8 kg(m.s)$^{-1}$ for horizontal eddy viscosity coefficient (Bearman *et al.*, 1993).

In homogenous waters or well-mixed systems, the eddy diffusion (K_2) and eddy viscosity (N_2) can be regards as equal with a dimension of m^2s^{-1}, N_2 is given by:

$$N_2 = N_0(1 + 10\,Ri)^{-1/4} \qquad (3.9)$$

Here, N_0 is the eddy coefficient at zero stratification is defined as 4.1 x 10^{-5} W^2 at the surface and 2.4 x 10^{-3} U_0h at the sea bed; W, is wind velocity at 10 meters height; $U_{0,}$ is equal to the tidal current amplitude; h, is the water depth, and; Ri, the Richarson number, which is defined as the relative magnitude of the stabilising density forces and the destabilising forces of the shear induced turbulence, and can be approximated to 0.25 (Dyer, 1997). Alternatively, Ri can be obtained from the expression:

$$Ri = [(\Delta\rho/\rho)gh_u].(u^2)^{-1} \qquad (3.10)$$

Where h_u is the depth of the upper layer, for an unstratified system h_u represents the total depth, ρ is the density (Knauss, 1978; Dyer, 1997).

Lin and Falconer (1995) have used a useful expression for depth mean horizontal eddy viscosity, it has the form:

$$N_{hD} = 0.15U_{*}h \qquad (3.11)$$

Where U_* is defined as friction velocity at the water depth h. Friction velocity can be approximated using the expression (Bearman *et al.*, 1993):

$$U_* = \Delta\hat{U}(5.75\ \Delta\ln z)^{-1} \qquad (3.12)$$

From this formula, z is the height above seabed and $\hat{U}$ represents mean current velocity in ($m.s^{-1}$). Alternatively, friction velocity can be expressed as (Mushenheim *et al.* 1986):

$$U_* = 0.4\ \hat{U}[(\ln(z/z_0)] \quad (3.13)$$

Where z_0 is the bed roughness length, usually a few centimetres (Officer, 1976). Table 3.2 shows values of z_0 and C_D for different seabed types.

Bottom friction. There is a reduction in flow velocity due to friction with the solid boundary, walls and seabed. This boundary shear stress is defined as the product between the square of friction velocity and the density, ρ.

$$\tau_0 = \rho\ U_*^2 \quad (3.14)$$

For well-mixed, shallow waters, this reduction in flow velocity may roughly decrease logarithmic up to the surface (Dyer, 1986). An experimental approximation to bed shear stress or bottom friction stress (τ_0) is stated by the quadratic friction law as:

$$\tau_0 = \rho\ C_D U^2 \quad (3.15)$$

here U is flow velocity and C_D represents the drag coefficient, which can be approximated using the relation:

$$C_D = (\ k\ )/\ (\ln 100/z_0) \quad (3.16)$$

Were k is the von Korman's constant approximated to 0.4 (Officer, 1976; Dyer 1986). Alternatively, the bed drag coefficient can be obtained regarding the specific vertical distance from seabed (z) (Dyer, 1997).

$$C_D = 0.16\ (\ln z/z_0)^2 \quad (3.17)$$

Table 3.2. Bed roughness length and drag coefficient sea bed. Table taken from Dyer (1986).

Bottom type	z_0 (cm)	Drag Coefficient (C_{100})
Mud	0.020	0.0022
Mud/sand	0.070	0.0030
Silt/sand	0.002	0.0014
Sand (unrippled)	0.040	0.0026
Sand (rippled)	0.600	0.0061
Sand/shell	0.030	0.0024
Sand/gravel	0.030	0.0024
Mud/sand/gravel	0.030	0.0024
Gravel	0.300	0.0047

Experimental values of C_D for small vertical averaged systems can be setup from 0.005-0.025 (Knauss, 1978; Ip *et al.*, 1998). Although these values are an order of magnitude higher than those presented by Dyer (1986) shown in table 3.2.

A theoretical expression of bottom friction in terms of conservation variables for vertical averaged systems is showed by Garcia and Kahawita (1986) using a Manning approximation, where $S_{f(x,y)}$ represents bottom friction slope:

$$S_{f(x,y)} = \frac{n^2 U (U^2 + V^2)^{1/2}}{H^{10\,3}} \tag{3.18}$$

Here H = h(x,y,t), U = u(x,y,t,)h(x,y,t), V = v(x,y,t)h(x,y,t) and *n* is the Manning coefficient which either can be chosen from 0.01 to 0.05 or alternatively computed using the expression:

$$\boldsymbol{n} = 1.49\,(0.5\,h)^{1/6}.(8/C_D)^{-1/2} \tag{3.19}$$

Where h is water depth (Officer, 1976; Dyer, 1986).

Wind-induced surface stress. There is an analogue representation of the quadratic friction law for wind stress (τ_s) where:

$$\tau_s = -C_d \rho_a W^2 \tag{3.20}$$

Here, wind stress is proportional to the product of the square wind velocity (W, 10 m height), density of the air (ρ_a), and the empirical dimensionless wind drag coefficient (C_d). Values of C_d increase with wind speed and sea surface roughness, an approximation to these values can be obtained through the relation $C_d \approx 3\%$ of W. For coastal systems C_d usually range between 1.3 x10^{-3} and 0.02 (Officer, 1976; Knauss, 1978; Alvarez *et al.*, 1989; Bearman *et al.* 1993).

Coriolis Effect. Some authors consider that this has a small contribution in shallow and well mixed coastal lagoons (de Silva, 1989; Bearman *et al.*, 1993), but the effect is present in all coastal environments and potentially may affect those coastal lagoons characterised by slack periods, considerable depth basin and geographic smooth properties. Coriolis effect is proportional to the sine of the latitude and is given by:

$$\text{Coriolis “force”} \;\; C_f = m\, f\, u \tag{3.21}$$

Where m is a mass moving at speed u, f is the Coriolis parameter given by the expression

$$f = 2\,\Omega\,\sin\phi \tag{3.22}$$

Here Ω represents the angular velocity of the earth and ϕ is the latitude (Bearman *et al.*, 1993).

3.1.3.1 Finite difference methods.

In order to select a set of partial differential equations and the finite difference methods to solve them, it is important to consider the answer that the model aims to provide, the physical characteristics of the system, the degree of accuracy required, and the computational efficiency (Garcia and Kahawita, 1986; Owens, 1986). There are, in the literature, many explicit finite difference methodologies that have been developed to provide specific hydrodynamic solutions and representation applied to two and three dimensions. The difference between schemes such as MacCORMACK time-splitting scheme, Galarkin method, QUICKEST, and ULTIMATE QUICKEST is mostly related with grid representation and the characteristics derived of this representation, which gives their degree of accuracy and computational efficiency (Garcia and Kahawita, 1986; Owens, 1986; Lin and Falconer, 1995; Ip *et al.*, 1998).

The hydrodynamics outcome of the present work is based in the HydroTrack® model, which uses the MacCORMACK time-splitting finite-difference scheme to provide a numerical solution to the set of resultant equations. The scheme divides the complicated finite-difference operator into a sequence of simpler ones. The model uses a fully dense grid where all dependent variables are defined at the cell center, thus the values represent the average cell properties (Garcia and Kahawita, 1986).

3.1.4 HydroTrack Model.

The program aims to simulate coastal sea level, Eulerian circulation and pollutant Lagrangian transport. The software is coded in FORTRAN 77, run in MS-Windows using Windows environment (Rodriguez-Molina and Garcia-Martinez, 1998). The graphical user interface, which communicates with the user, is composed of six subsystems, as shown in figure 3.2.

The Model's subsystem comprises the current and the pollutant transport modes. Within the current model, the program simulates wind and tidal-induced currents for shallow waters, using a two-dimensional, vertically averaged equation to calculate water level and the unsteady velocity field. The depth-averaged equation for water motion with a free surface is obtained by integration of the three-dimensional Navier-Stokes equation over depth (Garcia and Kahawita, 1986; Lin and Falconer 1995). The resultant governing equations are equation 3.7 and 3.8:

Conservation of mass equation

$$\partial U/\partial x + \partial V/\partial y + \partial W/\partial z = 0 \qquad (3.7)$$

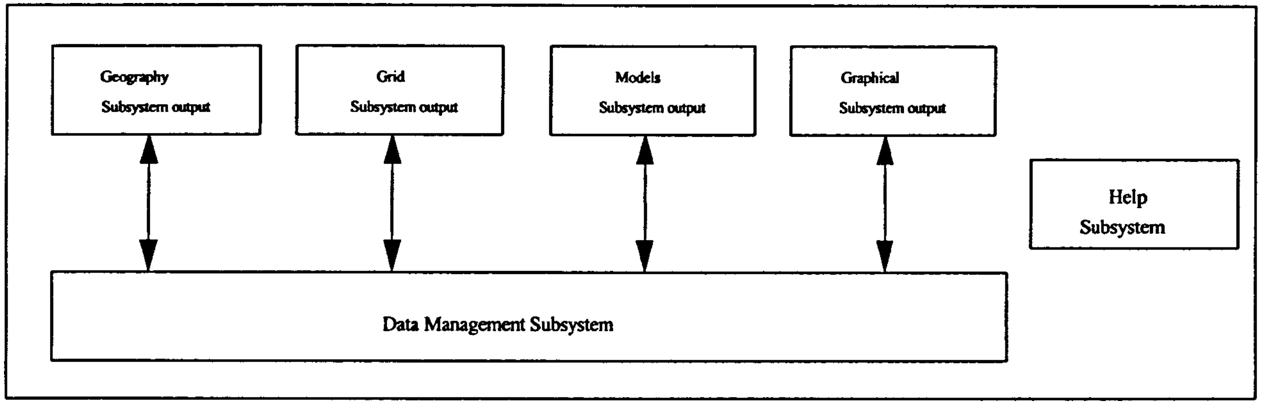

Figure 3.2. HydroTrack structure. Diagram representation taken from Rodriguez-Molina and Garcia Martinez (1998).

Conservation of momentum equation (3.8) is written in (x,y) direction as:

$$\partial U/\partial t + \partial F/\partial x + \partial G/\partial y = Ex$$
$$\partial V/\partial t + \partial G/\partial x + \partial S/\partial y = Ey \qquad (3.23)$$

Where E(x,y) is given in terms of water depth, depth averaged velocities (x,y), Coriolis parameter, gravitational acceleration, bed elevation, bottom bed slopes, bottom friction slopes, wind induced surface stresses, eddy coefficient and water density. Further explanation for the F, G, and S terms is given by Garcia and Kahawita (1986).

3.2 Aims.

This chapter aims to characterise the main hydrographic features, tide and currents, within the Guaymas system. In order to achieve the above objective, the work describes: The tidal constituents for the system; the tide height within the coastal lagoon, and a non-stationary current field, including a Lagrangian transport for the system.

3.3 Materials and Methods

3.3.1 Tide and currents data.

Tide data were obtained from direct measurements made near the mouth of the system (Figure 1.3). Also, data were taken from tide measurements made by Rosales-Grano *et al.* (1996) and estimations using the software-packet PREDOB developed by the Centro de Investigaci6n Científica y Eseñansa Superior de Ensenada (CICESE, 1995).

Tidal data from the PREDOB programme are provided for a specific station (27° 56' N and 110° 54' W) within the Guaymas system (Figure 1.3). Tide height calculations are based on continous measurements registered for the Universidad Autonóma de México (UNAM). Details and methodology for the tide and currents measurements produced by Rosales-Grano *et al.* (1996), and used in the present work are described further in this section.

3.3.2 Tide and Currents measurements.

Data for tide and currents were obtained from tide prediction tables produced by the PREDOB programme and currents and tide data produced by the ITMAR (Rosales-Grano, *et al.* 1996) those date were generated through oceanographic sensors, Inter Ocean Model S4DW. Tides were recorded using a high-resolution (4 mm) pressure-sensor and water motion was measured through an electromagnetic current-meter (±1 $cm.s^{-1}$ and 2°). The signals were stored in a solid state memory as hydrostatic pressure p, and vector of magnitude u, v.

3.4 Data analysis and Modelling.

Tide constituents were characterised through a spectral analysis using both predicted and field measured data. A non-stationary current field was constructed in order to characterise water circulation within the system during a typical ebb and neap periods. Lagrangian transport representation was obtained in order to provide a transport insight in the system.

3.4.1 Tide.

A spectral density analysis of tide was performed, using the time series obtained from the data measurements and those predicted by the PREDOB model. Mathematically, the spectral density analysis expresses the variation of a time series as the sum of a series of sinusoidal components, it uses a standard Fourier transformation. The programme used to obtain the variance decomposition into main constituents was SPSS for Windows version 7.5.1.

Tide height elevations within the system were computed from tide elevation at the open boundary (mouth of the system) through the HydroTrack programme.

3.4.2 Circulation.

Data input. The programme require the arrangement of the following data:

i. Tide and currents. Water elevation and velocity at the open boundaries were fed using the American Standard Code for Information Interchange, ASCII code. Time in hours and water height as tide range in metres were ordered in two columns. For water current, three columns were required in order to include time in hours, and water velocity ($m.s^{-1}$) for x and y directions. Enclosed data files for tide and currents were labelled with extension HVT and UVT respectively.

ii. Water depth. Bathymetry of the system was set-up for the computational in a cell by cell basis, allowing the program to interpolate for those cells without values.

iii. Wind velocity. An average wind velocity value at 10 m is required to compute the wind induced current component. This value is given in a straight form in a dialogue box.

iv. Wind dragging coefficient. A value of 0.02 was chosen, which produces an accuracy within a factor of two or better (Bearman et.al. 1993).

v. Eddy viscosity coefficient. A explain value of 0.01 was chosen.

vi. Bottom roughness (Manning) coefficients. A mean value of 0.2 was chosen.

vii. Latitude of the simulation site. This value was computed as 27° 55' Latitude North.

3.5. Results and Discussion

For the purpose of this work, it is assumed that mathematical considerations of the model are strongly supported by the background literature. Thus, the present section describes firstly the tide, circulation and transport features, and secondly considers the management significance of these hydrographic features.

3.5.1 Tide

The Guaymas system presented a mixed, diurnal and semi-diurnal tide, with a predominantly diurnal form. Figure 3.3, shows an example of the tide curves representative of spring and neap tide periods.

Principal tidal constituents identified for the Guaymas system were: M_2, N_2, K_1, O_1, M_f, and M_n (Table 3.1 and Figure 3.4). The major contribution to the variance was produced by the Luni-Solar-diurnal component (K_1), and Lunar diurnal (O_1), followed by the semi-diurnal components Lunar semidiurnal (M_2) and solar semi-diurnal, S_2 (Figure 3.4; Table 3.1). The diurnal semidiurnal ratio can be used to characterise the diurnal semidiurnal form (F) for tide in coastal systems (Aubrey and Speer, 1985). Thus, a form number can be defined to characterise tide types where $F = (O_1 + K_1)/(M_2 + S_2)$, the values of F for semidiurnal dominant types is $F<0.25$, for diurnal dominant $F>3.0$ and for mixed tide F range between 0.25 to 3. The computed value for this system was 2, which indicates a mixed diurnal and semidiurnal with a slight diurnal dominant.

As is discussed further in this section, tide constituents are distorted toward the interior of the system, with a likely effect on diurnal and semidiurnal characteristics of tide.

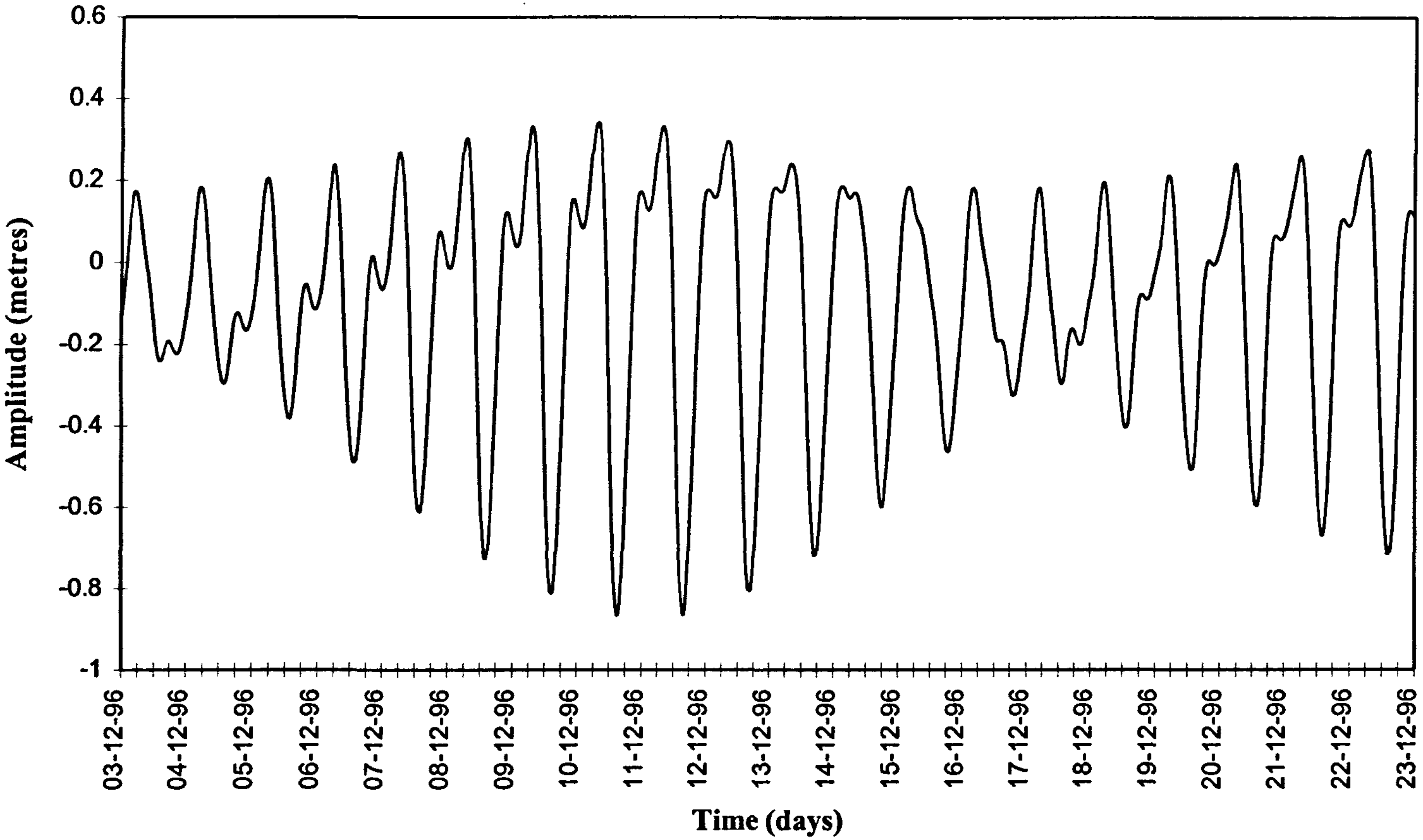

Figure 3.3. Example of tide curve representative of a spring and neap tide periods for the Guaymas system. The graph shows the predicted tide range for the period between the 3 of December to 23 December 1996 near the mouth of the system. The 0 in the Y axes represents the mean sea level .

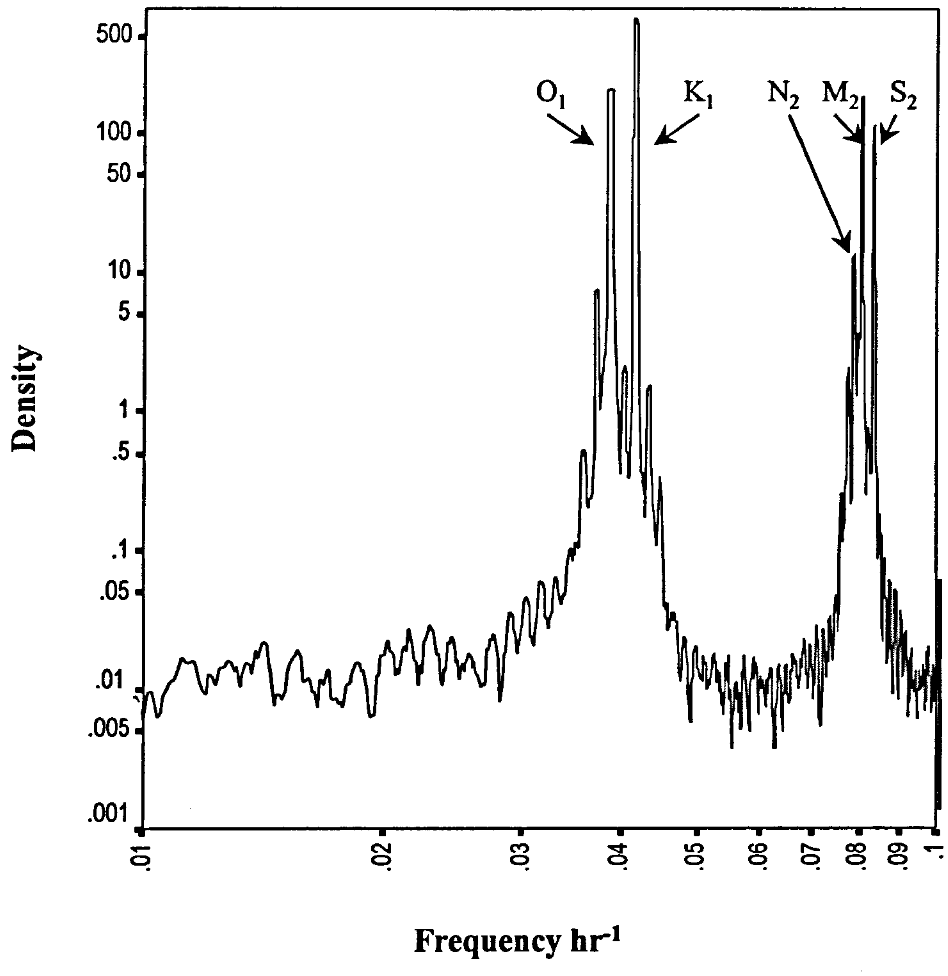

Figure 3.4. Density spectrum of tide height (amplitude in metres) for the Guaymas System. The arrows show the identified tidal components.

Considering this, further work must be developed to produce reliable estimates of tide amplitude and velocity time series measurements, in order to identify F for each sub-system.

Tide amplitude for the period is presented in Figure 3.3 is 0.38 m, however the maximum annual amplitude for the whole year was 0.65 m, other estimations for the system have approached 0.46 m (UNAM, 1987).

Tide constituents are affected as the tide propagates toward the head of the system by topographic and bathymetric conditions. Thus, this asymmetric effect is probably enhanced by resonance at the mouth of the system and Guaymas sub-basins, and shallowness at the interior of both the Empalme and Guaymas sub-basins (Figures 3.5 and 3.6).

In general, tide amplitude slightly increases from the mouth of the system to the head (Figures 3.5 and 3.6). For the Estero El Rancho, tide influences are disrupted by an artificial barrage and the narrow communication with the Laguna area. Thus, tide amplitude induced by spring and neap tides is substantially reduced for this confined system (Figure 3.5).

These results provide an insight that the tide cycle influences longitudinal transport by forcing general flooding and draining on the lagoon, and by affecting the variation of pressure over the horizontal surface or barotropic pressure gradient of this well-mixed system. Flooding and drainage characteristics may be differentiated for both systems where flooding and drainage seems to be more efficient at the Guaymas sub-system, regarding the topographic and man-induced circulation restrictions in the Empalme sub-system.

For management considerations, those tide features described above provide the way for further and more specific studies related with tide and tide-induced mixing. This includes,

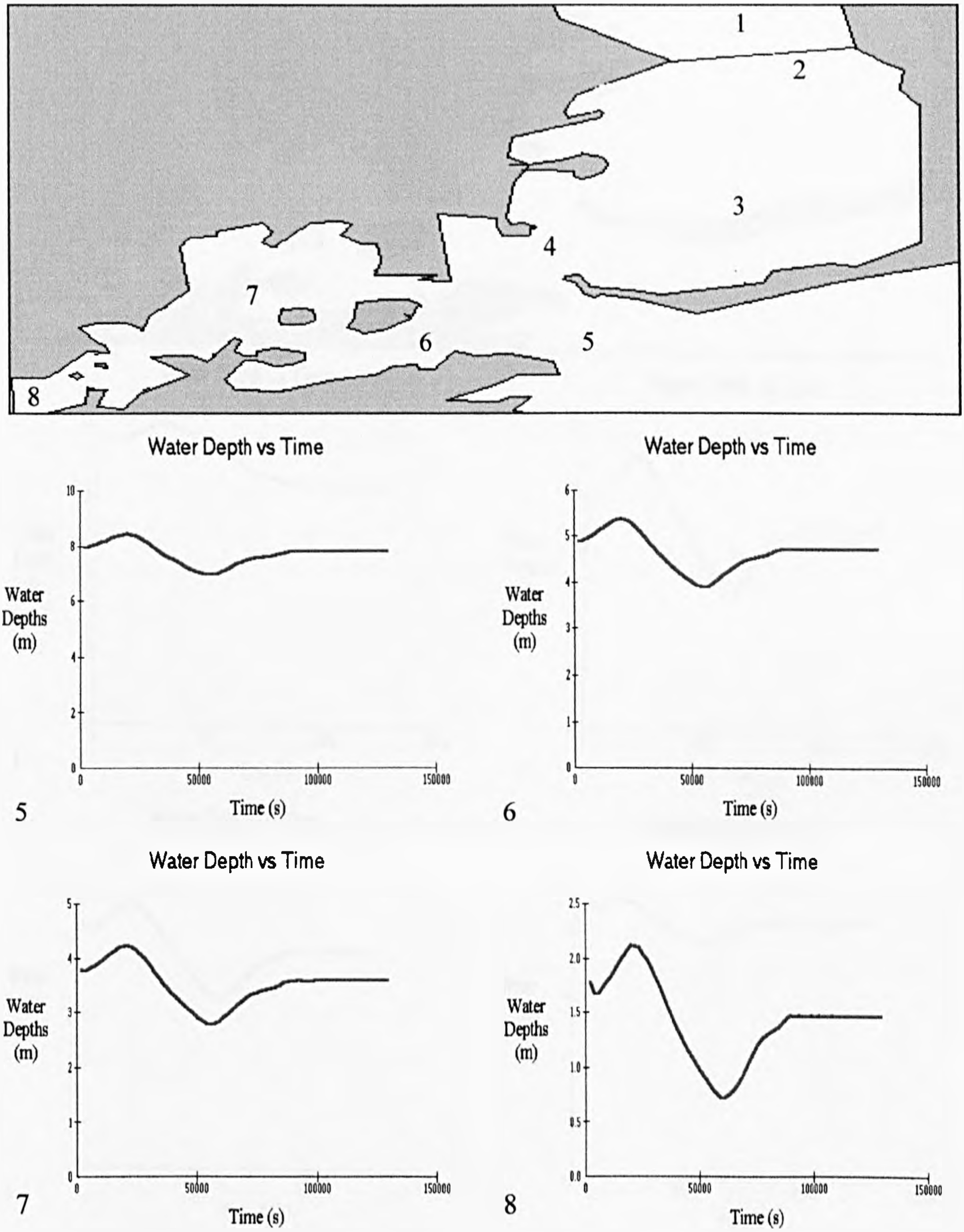

Figure 3.5. Tide elevation within the Empalme sub-system. The figure numbers represent the location in the system.

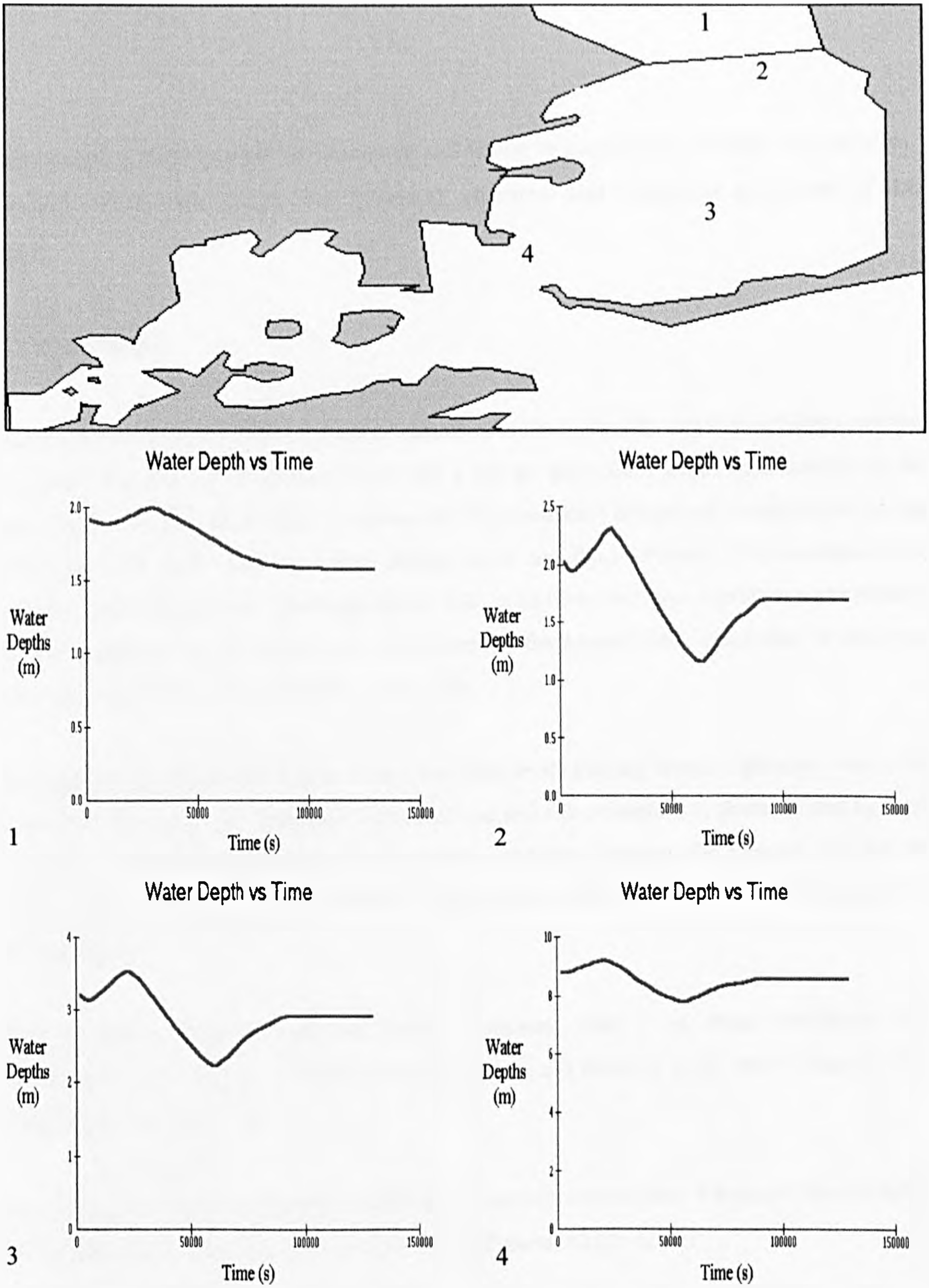

Figure 3.6. Tide elevation within the Empalme sub-system. The figure numbers represent the location in the system.

water mixing induced turbulent processes and hence re-suspension of sediment particles. Turbidity effects also affect other physical, chemical and biological properties of the system.

3.5.2 Circulation.

A current velocity field simulation was produced in order to identify circulation features within the system. The finite grid square cells of 250 x 250 m, provided a good representation of the current field when the whole field is represented. The simulation comprised a complete lunar day period (24 hours 50.47 minutes), which include flood and ebb conditions. It is considered that given the small difference in tide range among tides, a 25 hours scenario provide a representative circulation patterns for the system. For the purpose of the present work, simulation is presented with 1 hr synoptic frequency (Figures 3.7 to 3.19).

Slack conditions. Simulation begins from a zero tide level, moving toward light neap tide in the next 0.5 hrs (Figure 3.7a). Transition between flood and ebb conditions is characterised by slack conditions (Figure 3.10a). There is a slip in tide conditions between the Laguna area and the Estero El Rancho because the barrage effect in the system, this effect is reflected in Figure 3.10a and thereafter.

Flood conditions. Flood conditions became dominant after 1 hr, these conditions were maintained during the next 5 hours of the simulation, and from 18 to 25 hours (Figure 3.7a to 3.9b; Figure 3.15b to 3.19b).

Ebb conditions. Flushing conditions of the system are represented after 7 hours of the simulation, this pattern is held them for a period of 10 hours (Figures 3.11 to 3.15a)

In general, circulation follows topographic and bathymetric features. Thus, strong currents were associated to channel depths and hydraulic pressure gradients produced by local strains, especially those associated with the island narrows passages at the mouth of

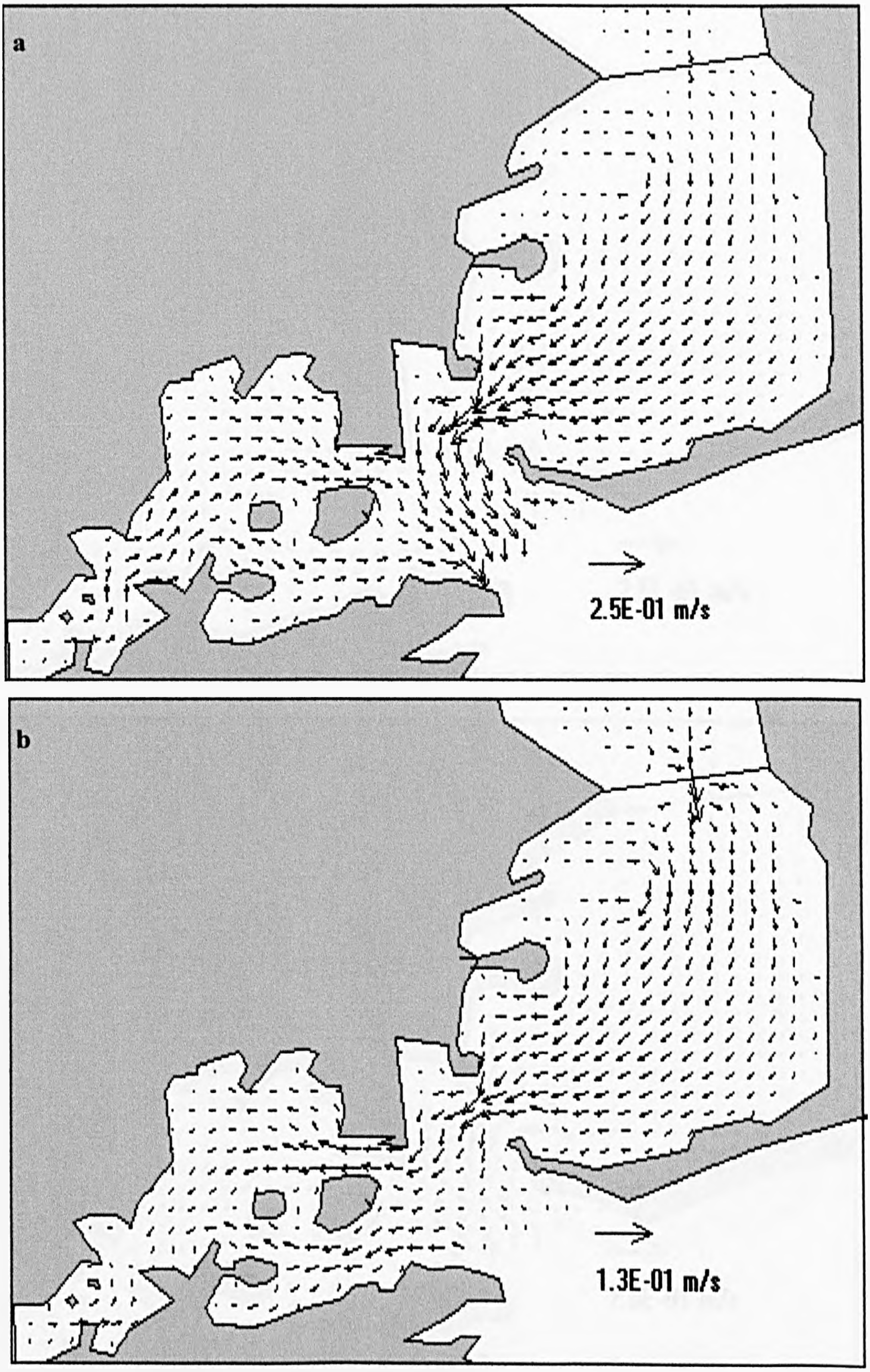

Figure 3.7. Simulated Velocity field for the Guaymas system. Figures a and b represent the velocity field after 0.5 and 1 hour respectively. The grid mesh is 250 meters.

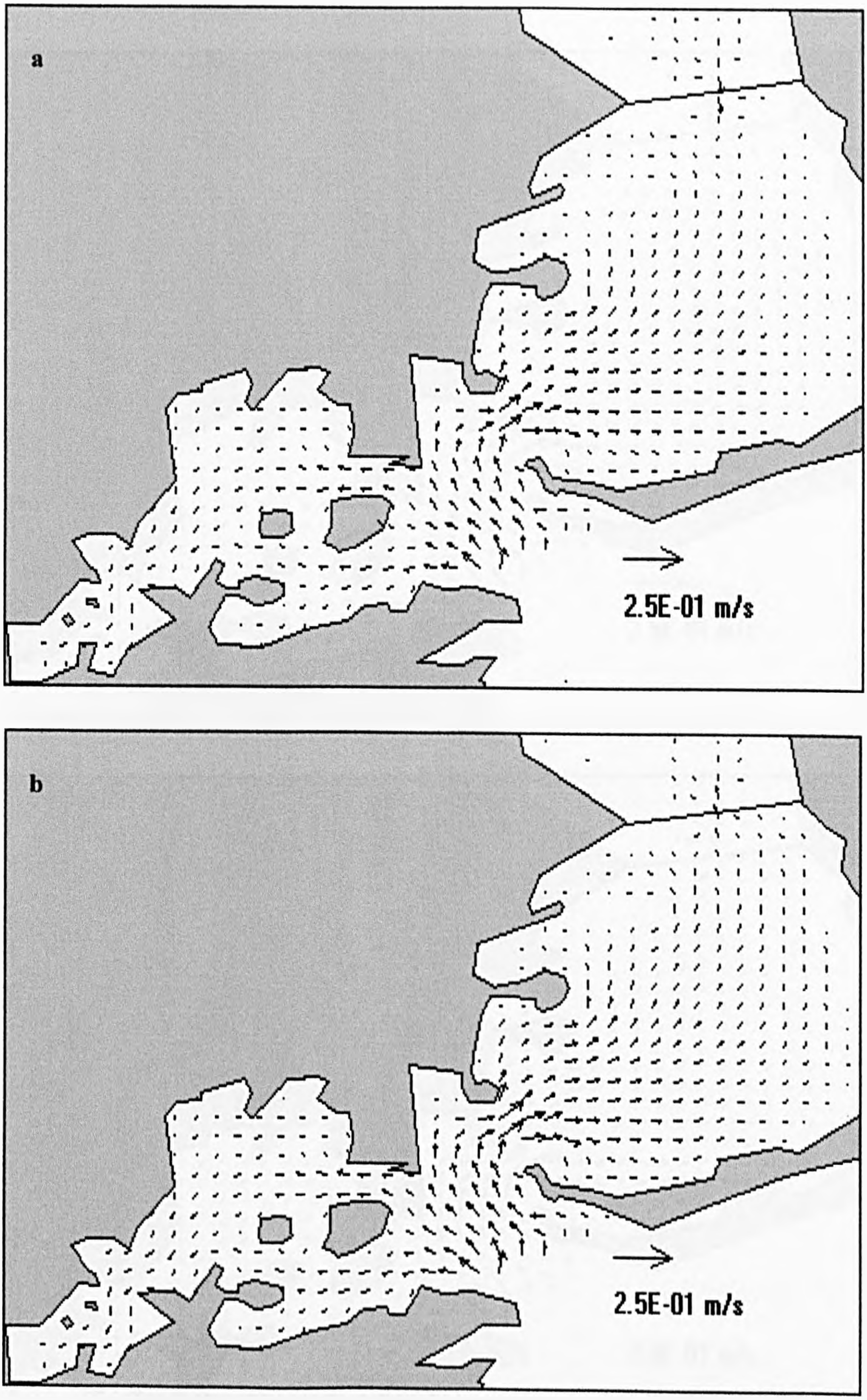

Figure 3.8. Simulated Velocity field for the Guaymas system. Figures a and b represent the velocity field after 2 and 3 hours respectively. The grid mesh is 250 metres.

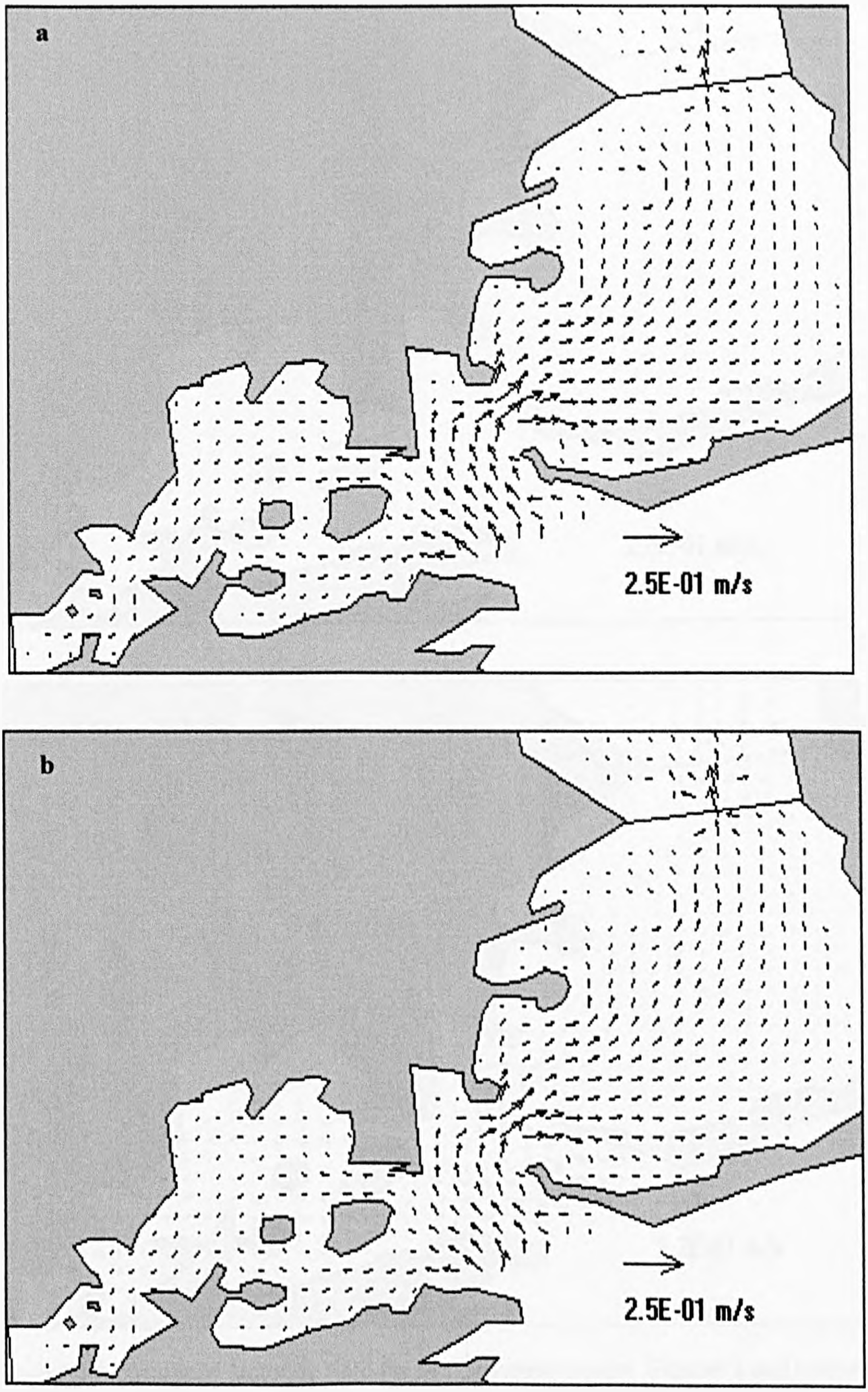

Figure 3.9. Simulated Velocity field for the Guaymas system. Figures a and b represent the velocity field after 4 and 5 hours respectively. The grid mesh is 250 metres.

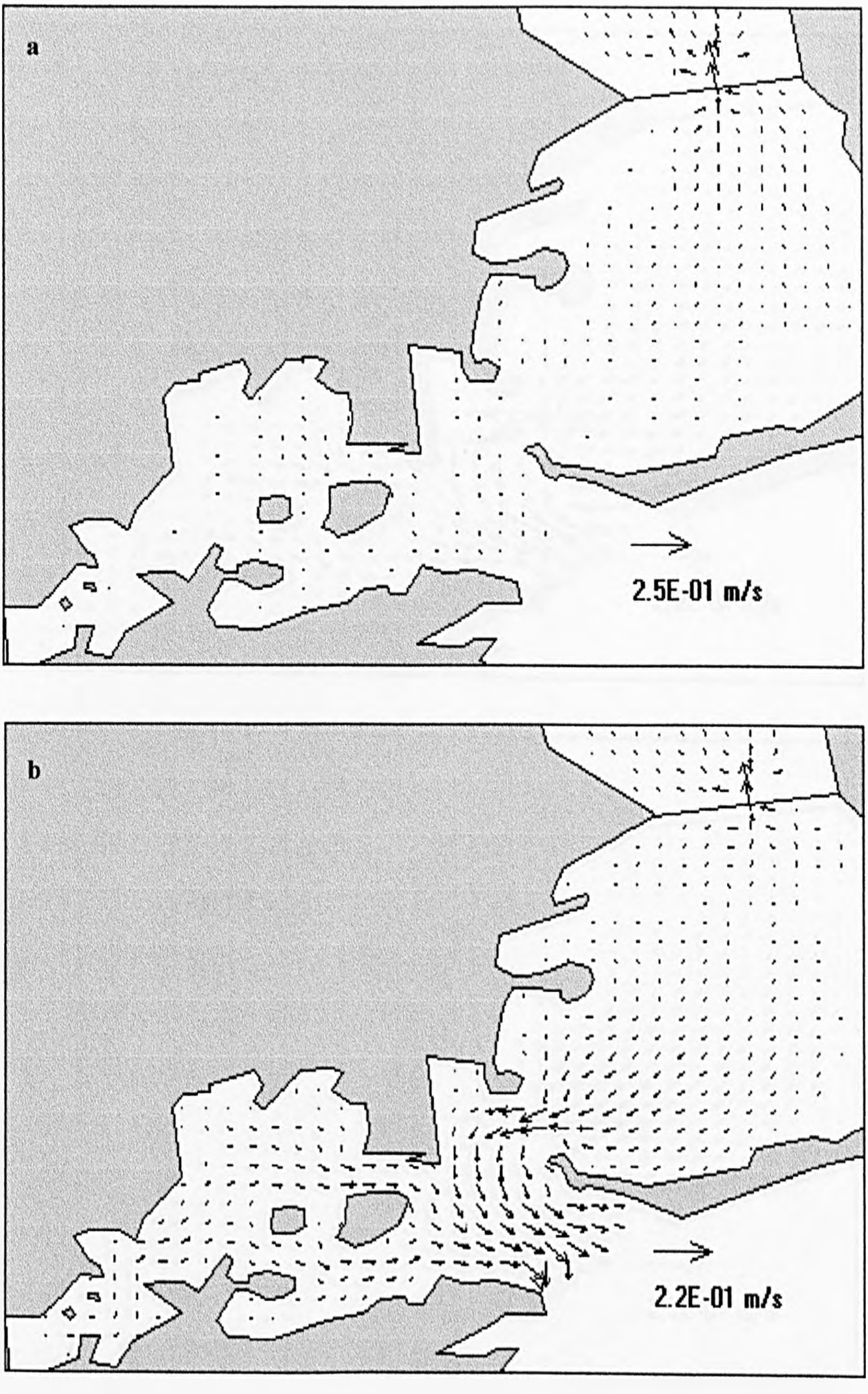

Figure 3.10. Simulated Velocity field for the Guaymas system. Figures a and b represent the velocity field after 6 and 7 hours respectively. The grid mesh is 250 metres.

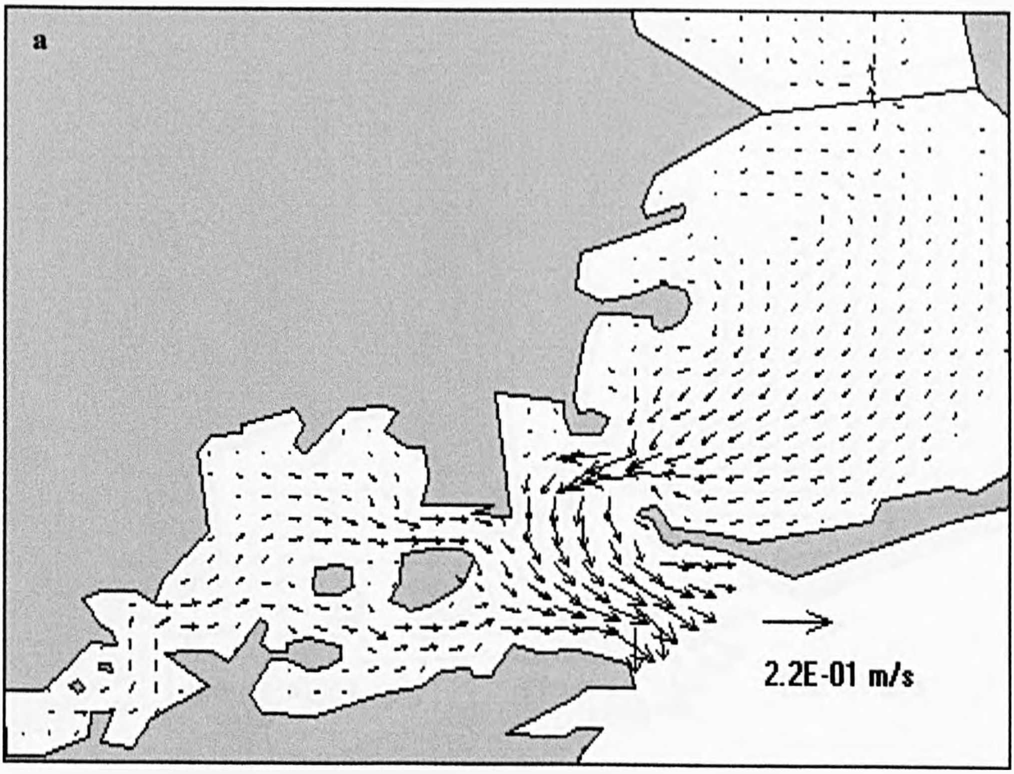

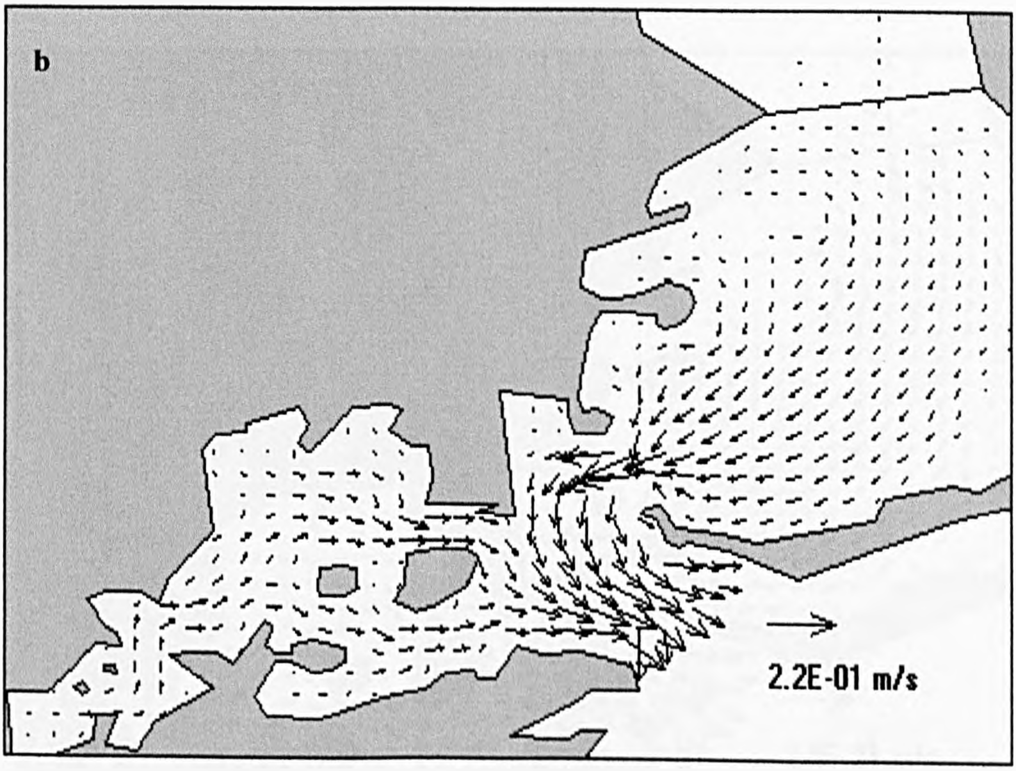

Figure 3.11. Simulated Velocity field for the Guaymas system. Figures a and b represent the velocity field after 8 and 9 hours respectively. The grid mesh is 250 metres.

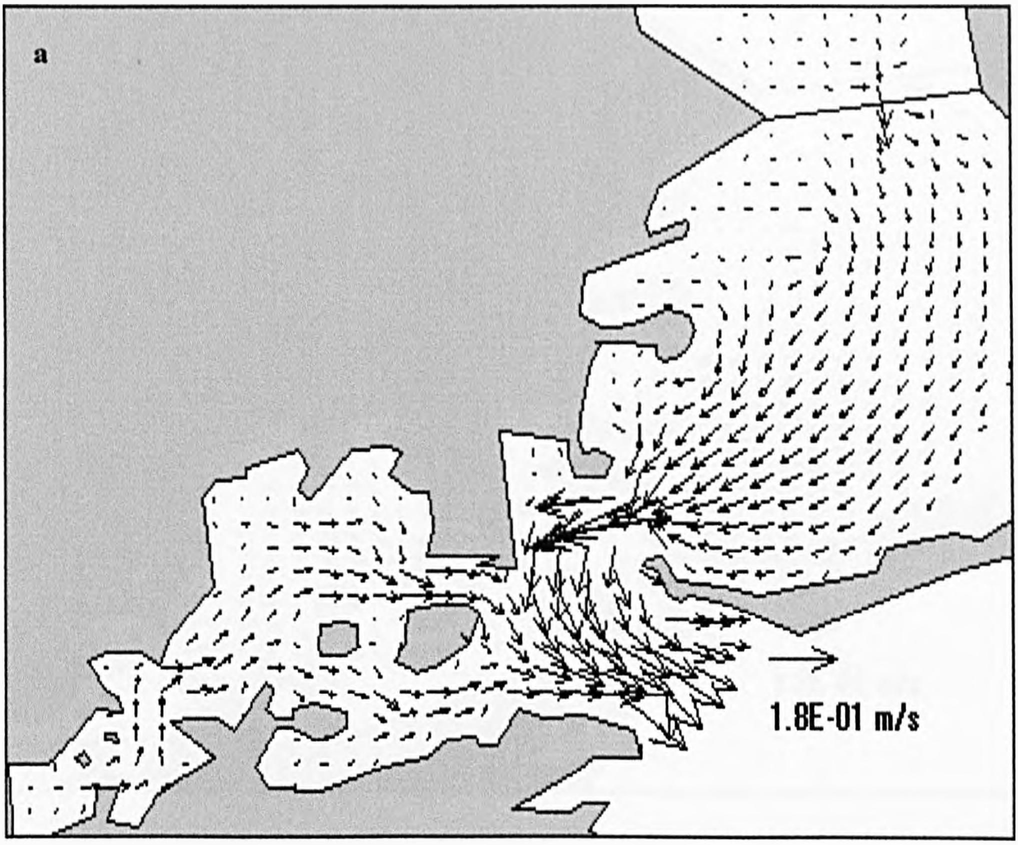

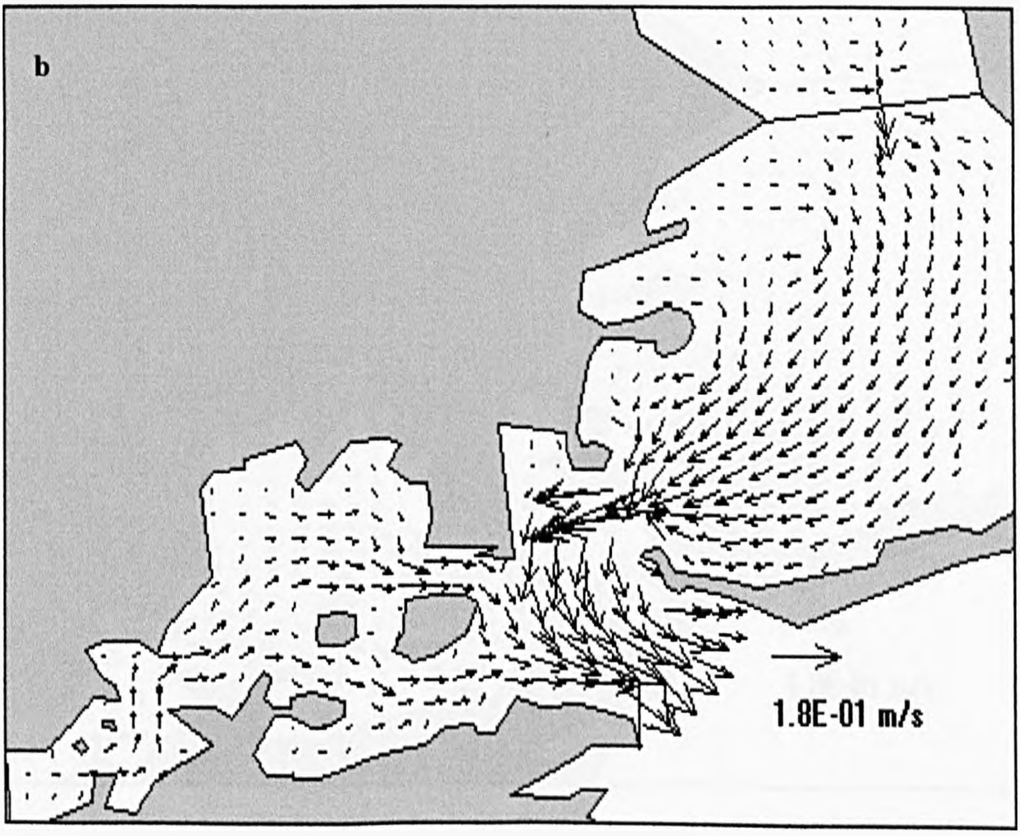

Figure 3.12. Simulated Velocity field for the Guaymas system. Figures a and b represent the velocity field after 10 and 11 hours respectively. The grid mesh is 250 metres.

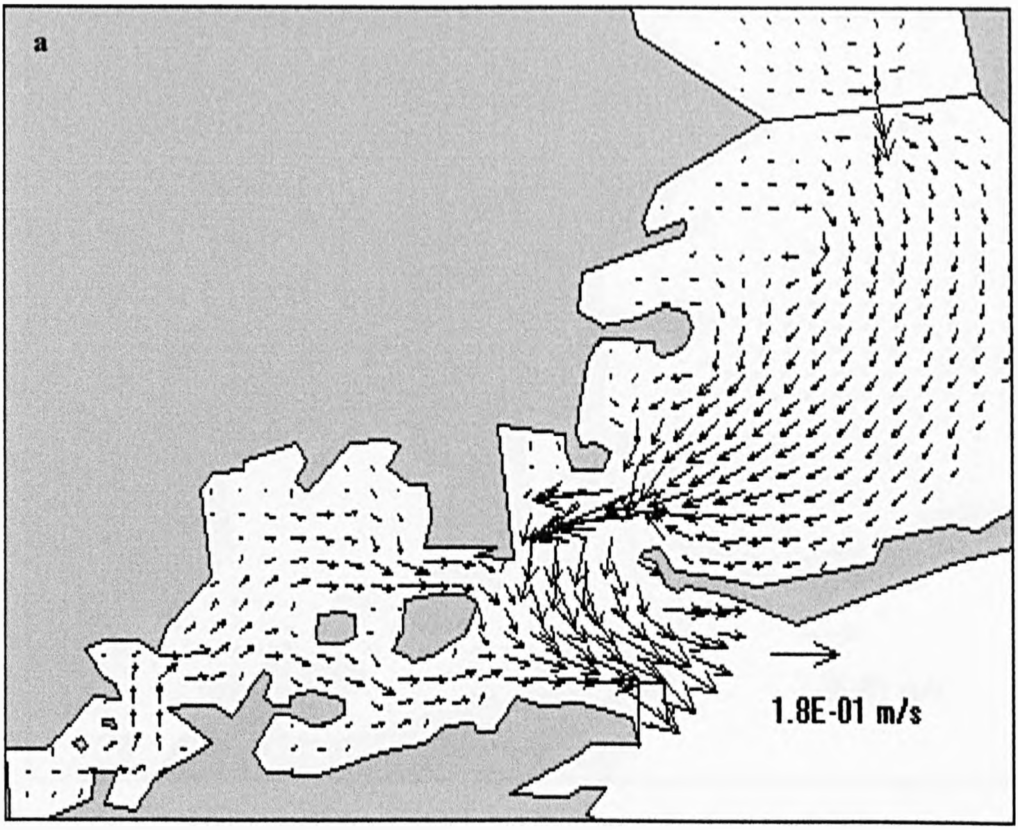

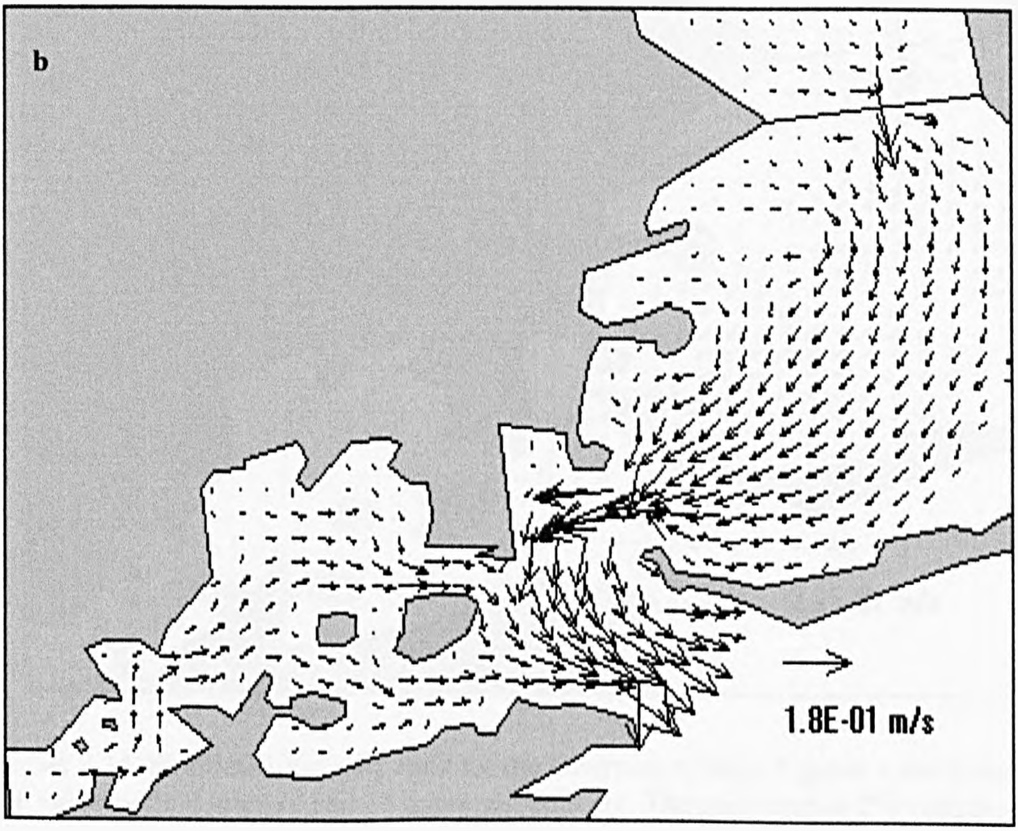

Figure 3.13. Simulated Velocity field for the Guaymas system. Figures a and b represent the velocity field after 12 and 13 hours respectively. The grid mesh is 250 metres.

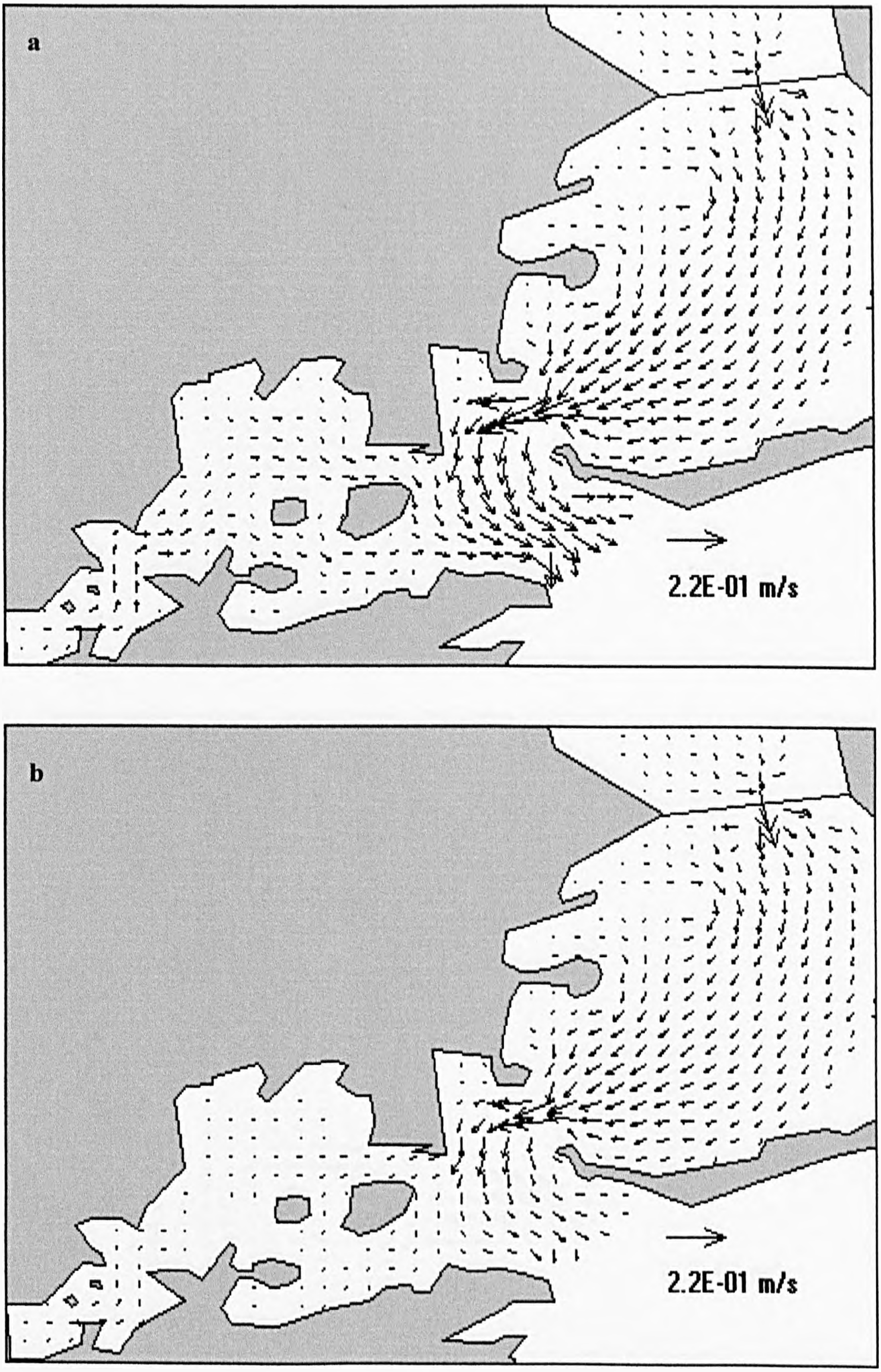

Figure 3.14. Simulated Velocity field for the Guaymas system. Figures a and b represent the velocity field after 15 and 16 hours respectively. The grid mesh is 250 metres.

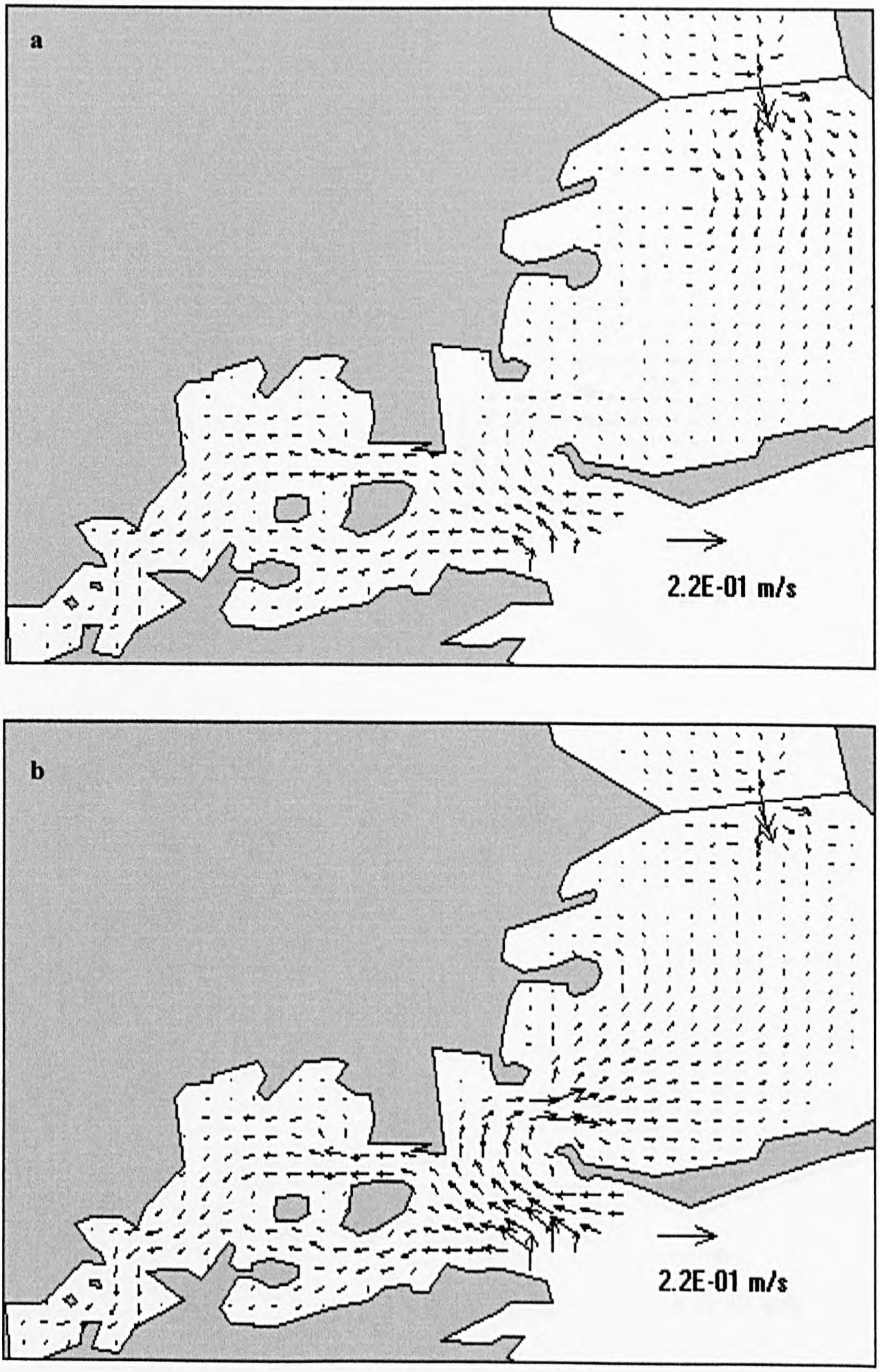

Figure 3.15. Simulated Velocity field for the Guaymas system. Figures a and b represent the velocity field after 17 and 18 hours respectively. The grid mesh is 250 metres.

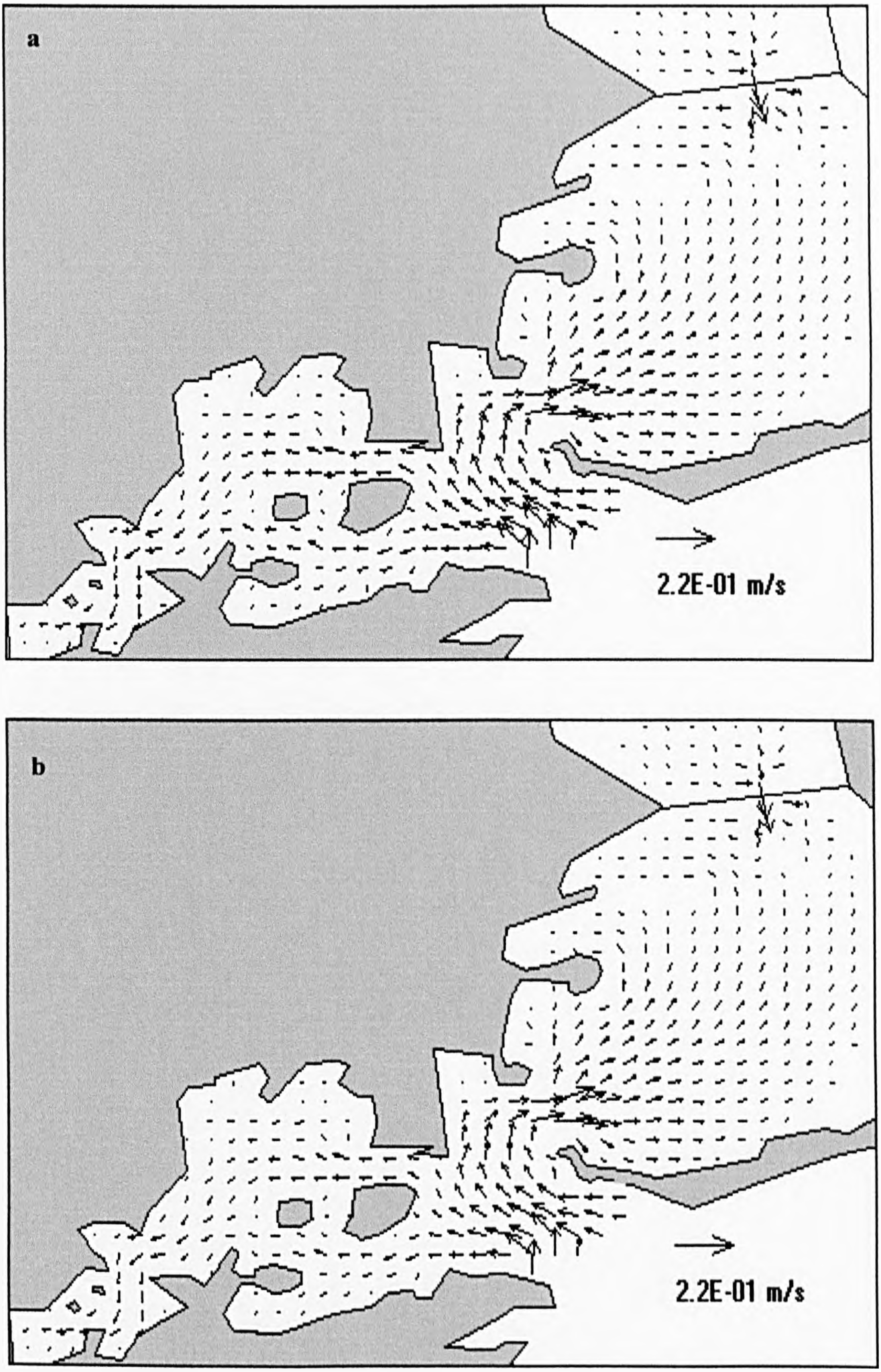

Figure 3.16. Simulated Velocity field for the Guaymas system. Figures a and b represent the velocity field after 19 and 20 hours respectively. The grid mesh is 250 metres.

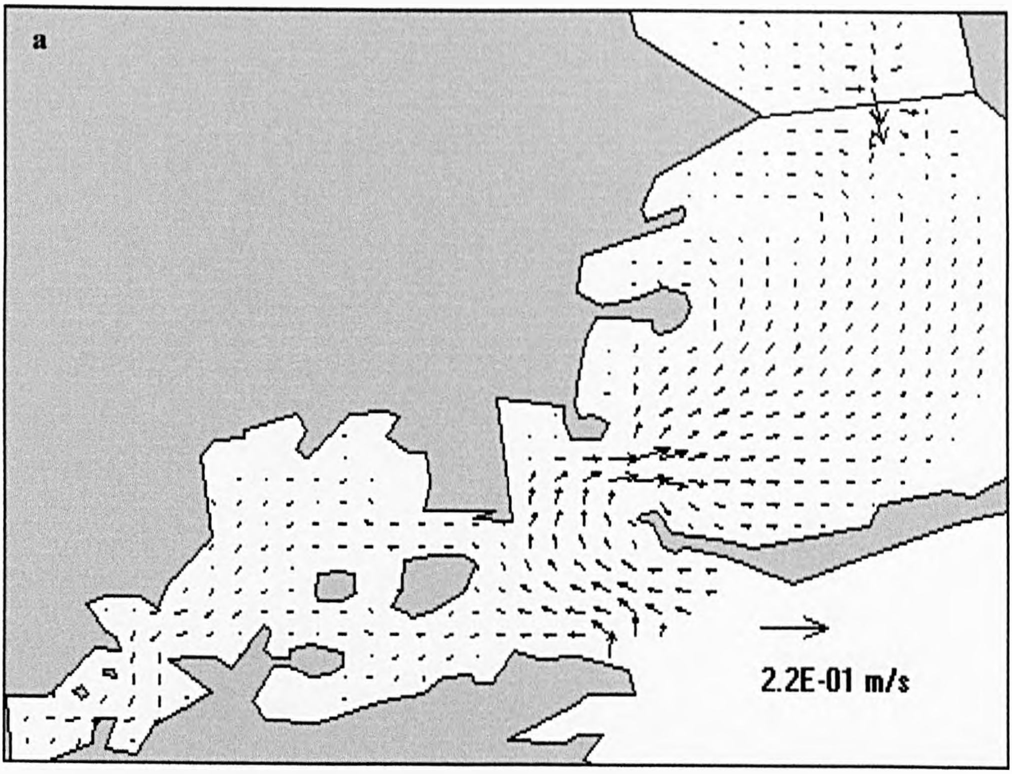

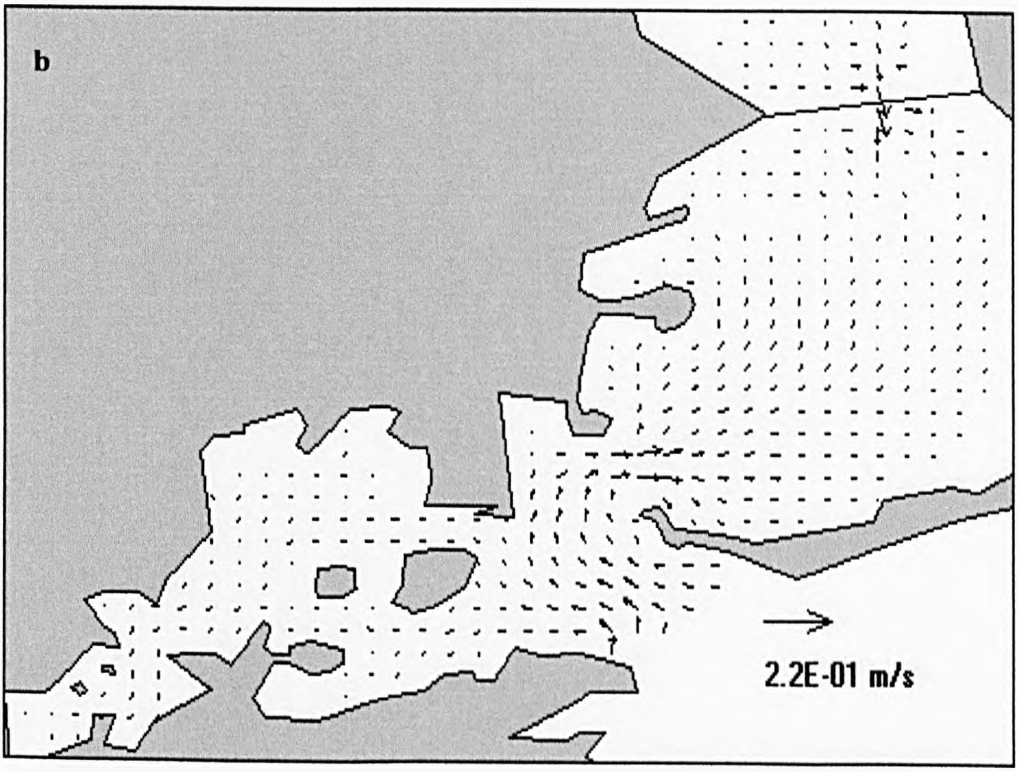

Figure 3.17. Simulated Velocity field for the Guaymas system. Figures a and b represent the velocity field after 21 and 22 hours respectively. The grid mesh is 250 metres.

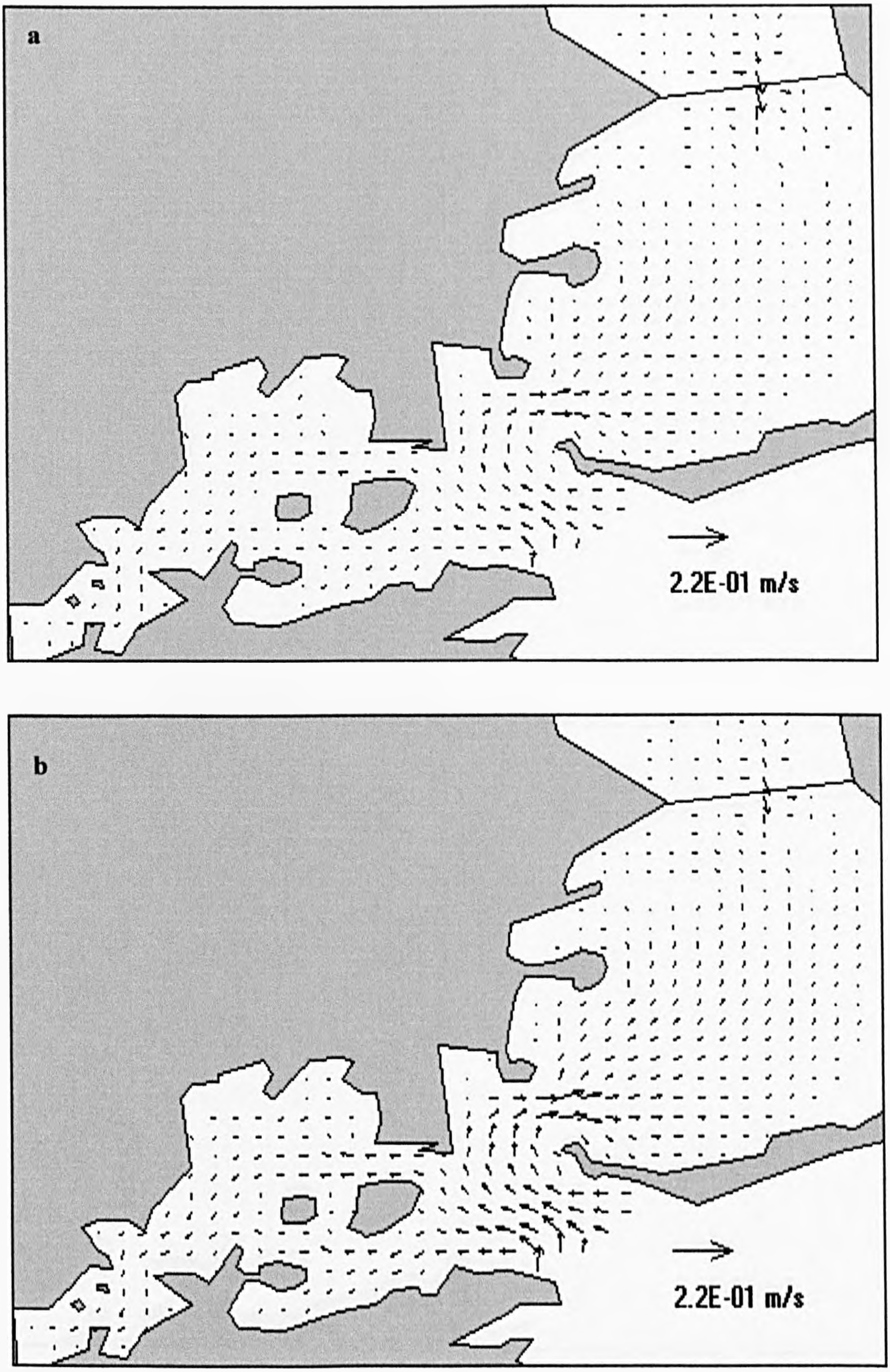

Figure 3.18. Simulated Velocity field for the Guaymas system. Figures a and b represent the velocity field after 23 and 24 hours respectively. The grid mesh is 250 metres.

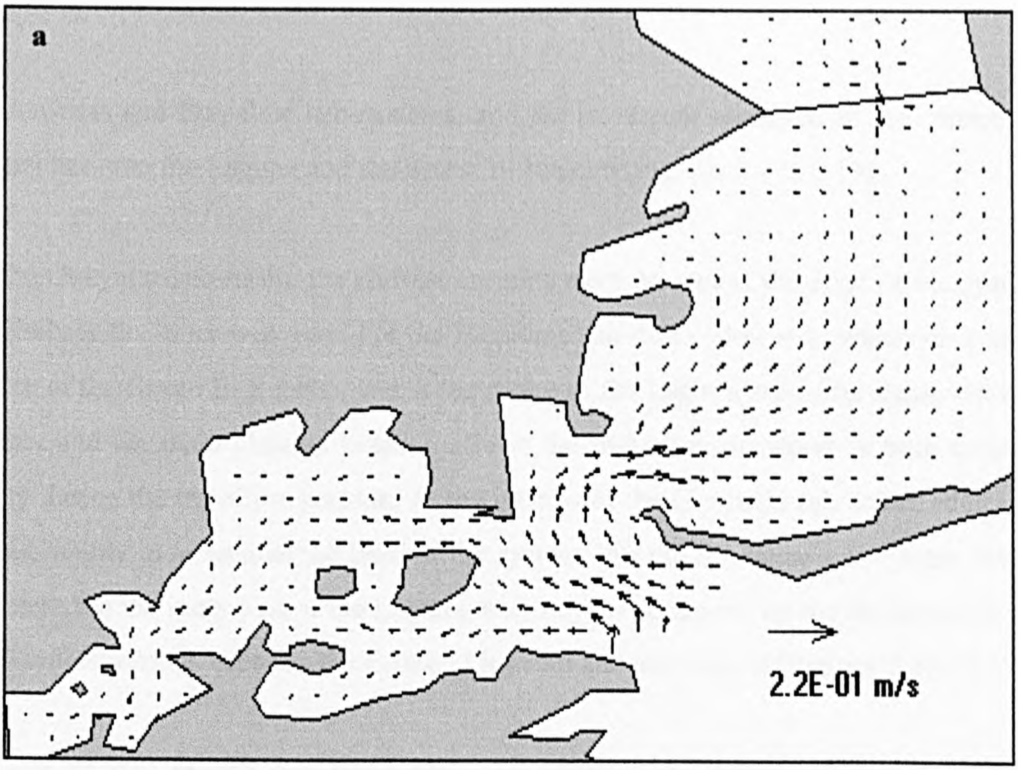

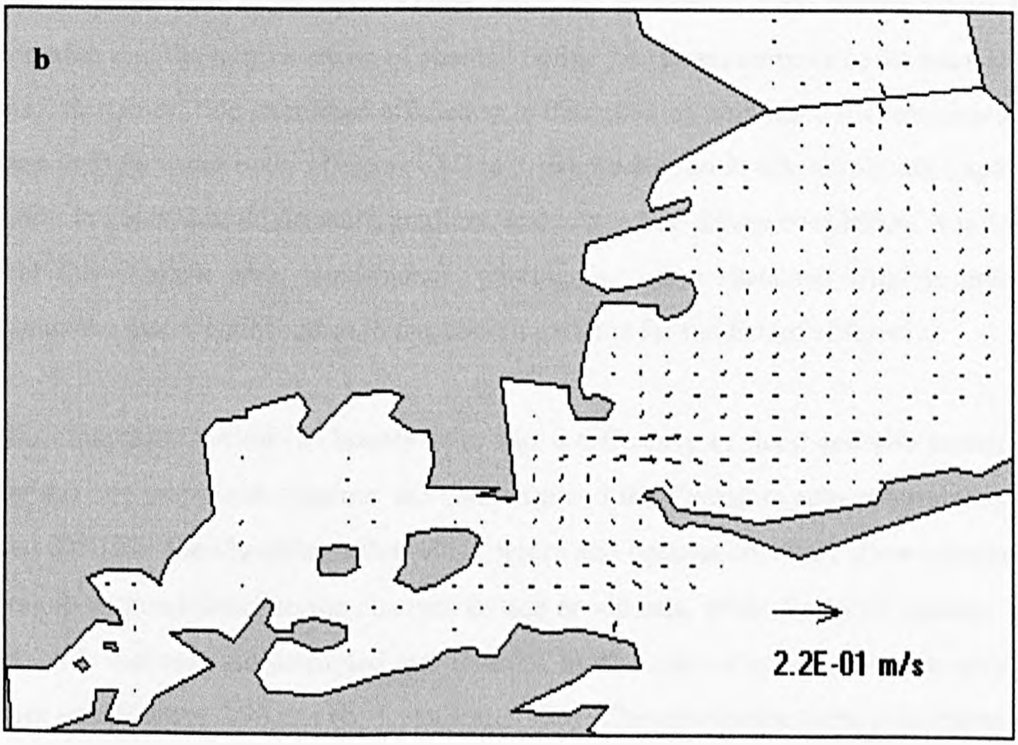

Figure 3.19. Simulated Velocity field for the Guaymas system. Figures a and b represent the velocity field after 24 and 25 hours respectively. The grid mesh is 250 metres.

the Guaymas and Empalme sub-systems, and the jet stream produced in the connection channel between the Laguna and the Estero El Rancho (Figures 3.7 to 3.19).

For the Guaymas sub-basin, the slowest currents were present at the head of the system, especially in the inner-west part. For the Empalme sub-basin, slower currents occur at the interior of the Estero El Rancho, and at the centre of the Lagoon area. The shallowness of the area and the main channel position allows the formation of eddies in both systems, mainly during the transition periods. At the interior of the Guaymas sub-basin, eddies are formed mainly in areas near the head of the system. For the Empalme sub-system, eddies are formed in the inner part of the Laguna, and they are enhanced by the difference in ebb and flood conditions between the Estero el Rancho and the Laguna (Figures 3.7 to 3.19).

The discrepancy in ebb and flood condition between the Estero El Rancho and the Laguna are determined firstly by tide level. Thus, the differential slope between these two water bodies and the narrow shape of channel define jet-stream currents at the connection channel. Certainly, tide exchange efficiency is disrupted by this narrow communication between the two water bodies (Figures 3.7 to 3.19). Reduction in tide amplitude implies a reduction in the hydraulic pressure gradient, and hence tide driven circulation. It is likely that for this shallow area, wind-induced circulation, when sustained wind is present, represents the major contribution to circulation patterns for the Estero el Rancho.

For this simulation period (24 hours) there was a difference in flood and ebb conditions among the two major sub-systems, the Guaymas and the Empalme sub-systems (Figures 3.5 and 3.6). For the Guaymas sub-system, wider and deepest channels allow circulation patterns to respond faster to the changes in tide conditions, while for the Empalme sub-system, tide currents are disrupted and delayed by the narrow communication with the adjacent sea (Figures 3.7b, 3.14b, 3.15a and 3.19b). This circulation feature indicates that the Empalme system is an ebb-dominant system, during the simulated period. Thus, the Empalme sub-system is characterised by a stronger ebb current. Ebb-dominant systems are often characterised by extensive wetlands with a long tidal excursion and strong ebb currents that guarantee its stability from sediment accretion problems (Aubrey and Speer, 1985). This is important in terms of management, since tide asymmetry and currents favour ebb transport, minimising sediment deposition or accretion within this sub-system (Aubrey and Speer, 1985). However, it is important to highlight that, in the present simulation, ebb-dominance can be enhanced by neap tide conditions. Therefore further work is required to analyse a longer time series that includes complete spring and neap tide cycles.

The above characteristic from the Empalme sub-system does not extend to the Estero el Rancho in which water exchange is restricted and hence the system works as a sediment trap. This system is likely to be have large accretion problems, with the subsequent effect on ecosystem and navigability.

For the Guaymas sub-system, the ebb-dominance is not as clear as in the Empalme sub-system. However the system has a large exchange with the adjacent sea (Figures 3.7 to 3.19).

The difference between the ebb and flood characteristics of both systems produces a residual water movement towards the Guaymas system, as is indicated in figures 3.7b, 3.14b and 3.15b. This may be significant in terms of management since the mouth of the Empalme system has oil and other chemical facilities, and hence contingency plans take note of these considerations.

3.5.3 Lagrangian residual transport.

The present work assessed the Lagrangian residual current using a Lagrangian particle-tracking dispersion model. This was represented by a tracking a parcel of water labelled with non-reactive and neutral buoyancy particles through the tide cycle (24 hours 50.47 minutes). Particles were released during flood-tide in order to represent the most likely worse conditions during the modelled time period.

Two scenarios were created to simulate the Lagrangian residual, the first in an area known to be affected by sewage discharges, and the second in an area used as an oil terminal, which might be potentially affected by oil spills. Time conditions were set-up to 24 hours considering phytoplankton response to induces and natural changes in the diurnal scale, and time of response from cleanup-teams in the case of an oil spill accident.

Scenario 1. A 24 hours Lagrangian particles-tracking model simulated the likely displacement of labelled particles within the sub-system of Guaymas. Table 3.3 shows the initial conditions for the modelling. The particles created in the model were intentionally set-up near a major wastewater discharge area (Figures 1.3, 3.20 and 3.21). The simulation is presented in a 4 hours frequency snap-shots time series (Figures 3.20 and 3.21). During the first 6 hours, there is a net displacement toward the inner part of the system. After 8 hours the plume changed direction toward the centre of the system, this pattern was kept until 16 hours when a change in tide currents produced a retreat or inwards movement of particles. During the next 8 hours (20 and 24 hours) particles spread over the two internal bays within the sub-Guaymas system (Figures 1.3, 3.20 and 3.21).

In general, the Lagrangian displacement of the particles over a diurnal period (24 hours) indicates that only a small proportion of the labelled water parcel was flushed out under the conditions set-up in this modelling. Moreover, the simulation produces an insight which indicates that particles will be spread in a limited area near the point of release (Figure 3.21). In terms of management, long residence times of reactive particles may intensify the effect of acute materials, as in the case of nutrients and heavy metals, potentially affecting human health (Rosenberg, *et al.* 1990).

Scenario 2. A 24 hours Lagrangian particle-tracking release was set-up in the oil-receiving facilities area, at the mouth of the Empalme sub-system (Figures 1.3, 3.22 and 3.23). Certainly, the Lagrangian displacement aims to provide an insight of a hypothetical

Table 3.3. Initial condition for particles transport model.

Conditions	Scenario 1	Scenario 2
Discharge position (Figure 1.3)	Major wastewater discharge within the Guaymas sub-system.	PEMEX, oil reception terminal. Yeti area.
Discharge volume (m^3)	1000	1000
Number of particles	1000	10000
Discharge duration (hours)	1	1
Total simulation time (hours)	25	25

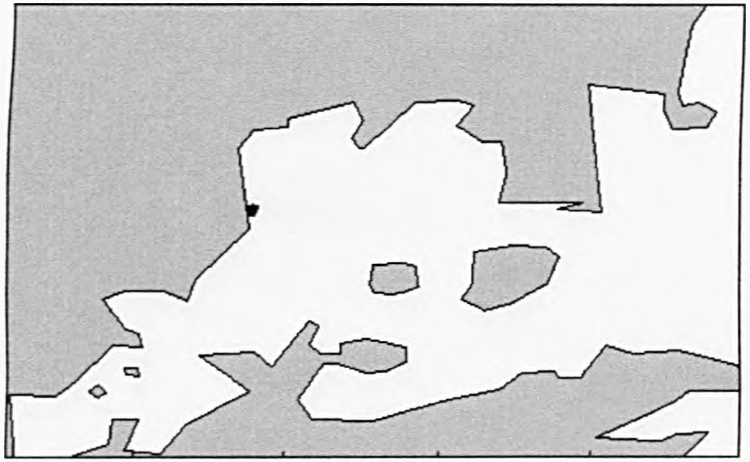

Particles trajectory 1 hours

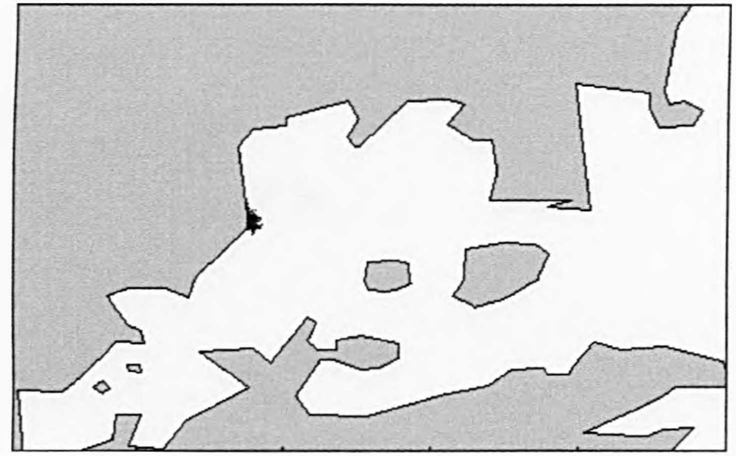

Particles trajectory 4 hours

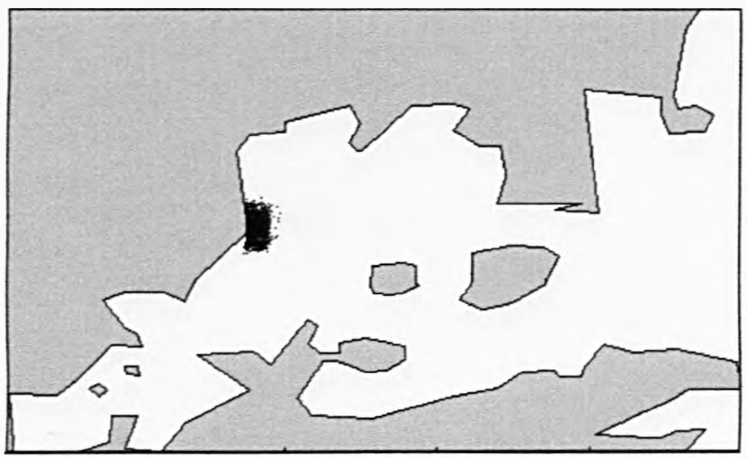

Particles trajectory 6 hours

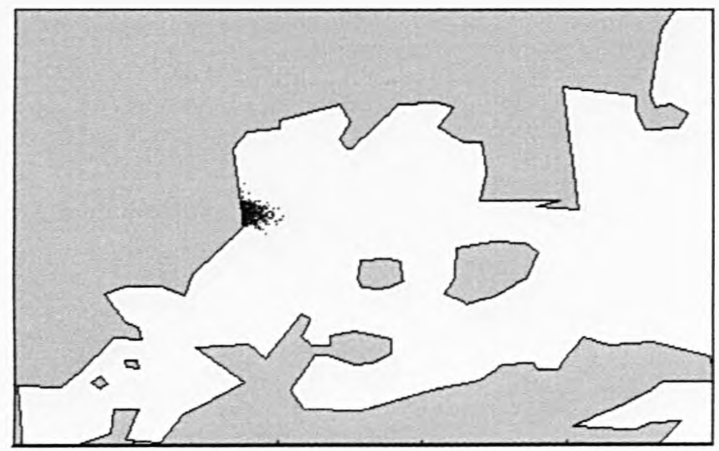

Particles trajectory 8 hours

Figure 3.20. Lagrangian particles' trajectory for a simulation pollutant discharge at Guaymas sub-system.

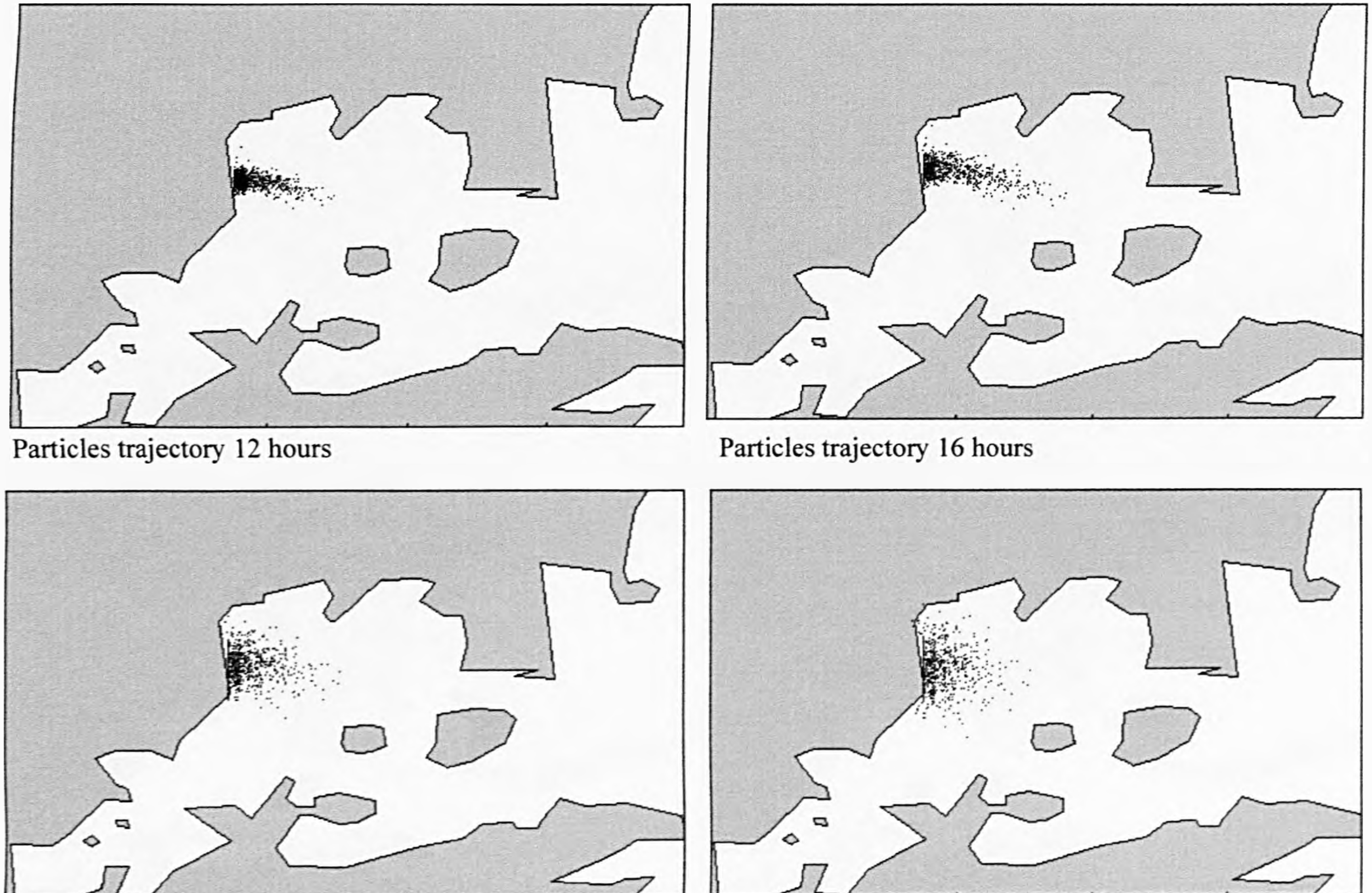

Particles trajectory 12 hours

Particles trajectory 16 hours

Particles trajectory 20 hours

Particles trajectory 24 hours

Figure 3.21. Lagrangian particles' trajectory for a simulation pollutant discharge at Guaymas sub-system.

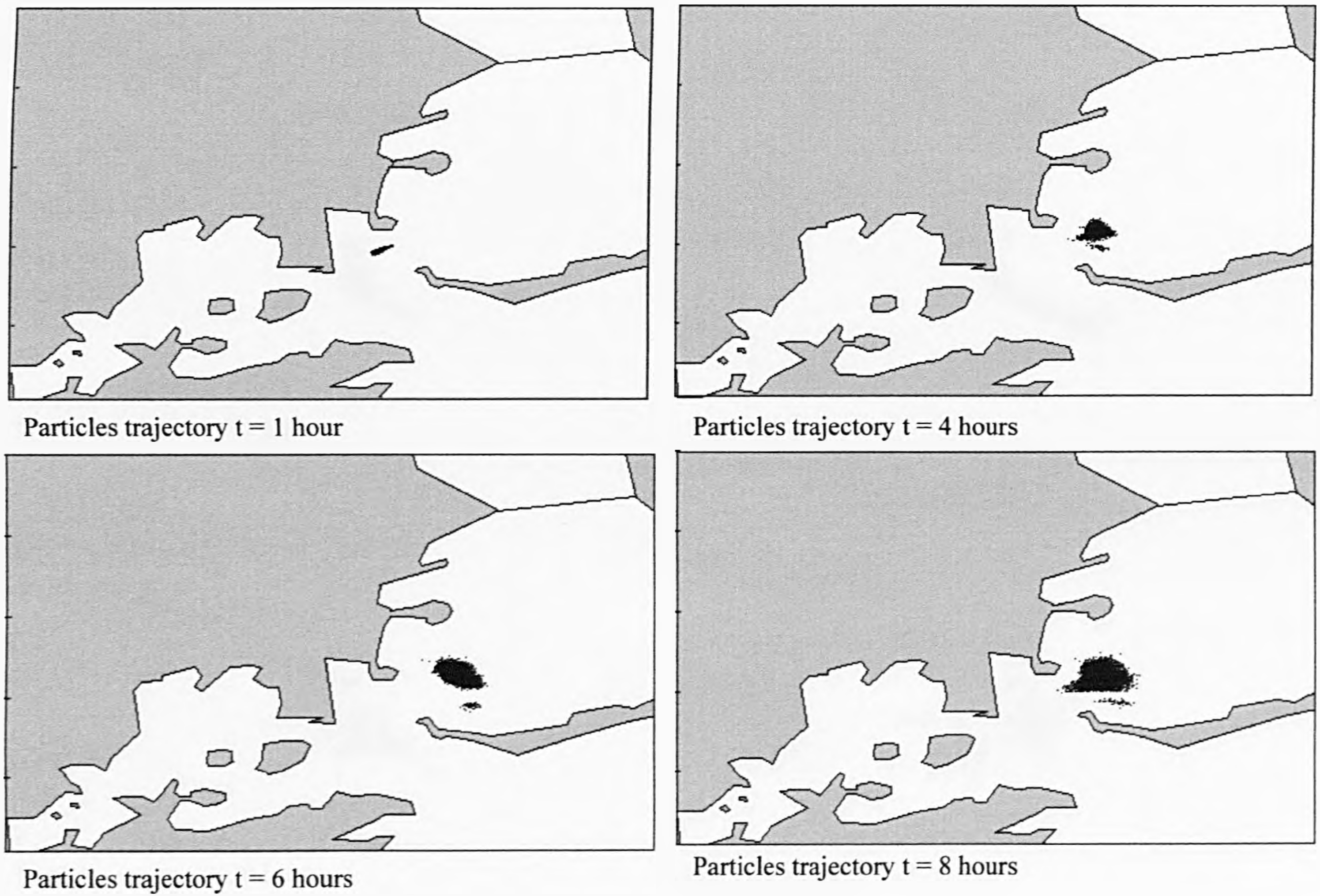

Particles trajectory t = 1 hour

Particles trajectory t = 4 hours

Particles trajectory t = 6 hours

Particles trajectory t = 8 hours

Figure 3.22. Lagrangian particles' trajectory for a simulation pollutant discharge at the mouth of the Empalme sub-system.

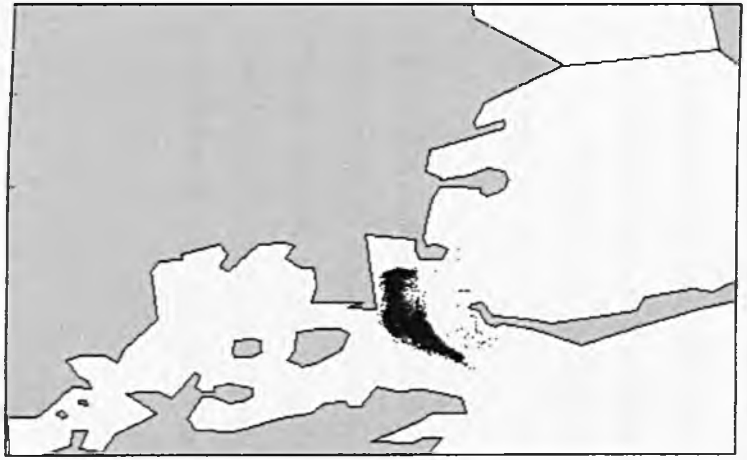

Particles trajectory 12 hours

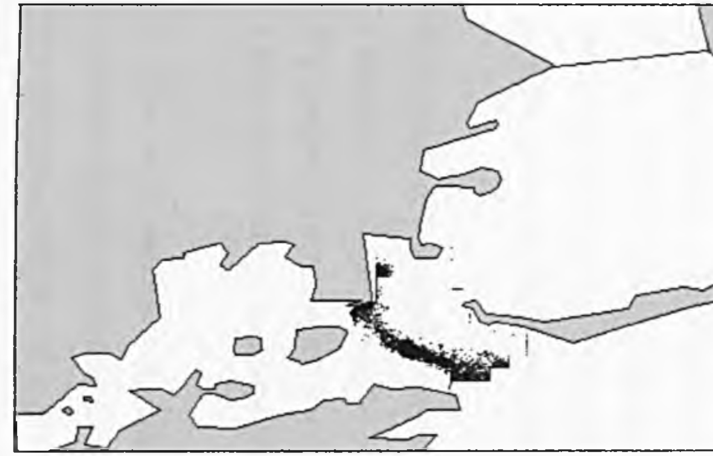

Particles trajectory 16 hours

Particles trajectory 20 hours

Particles trajectory 24 hours

Figure 3.23. Lagrangian particles' trajectory for a simulation pollutant discharge at the mouth of the Empalme sub-system.

but potential oil spill on this area. The model set-up conditions are described in Table 3.3. The Lagrangian displacement of particles at the mouth of the Empalme system shows net flushing conditions during the first hour. However, since currents are heavily influenced by tides, current direction changes with position in the tide cycle and hence the particle's trajectory. Thus, after 6 hours the labelled particles move to the centre of the Laguna (Figure 3.22). After 8 hours, particles are strongly flushed-out by tide currents. This pattern is kept until 16 hours where a spring tide drives flood conditions into both sub-systems, and hence distributes particles through both sub-systems (Figure 3.23).

For scenario 2, Lagrangian displacement shows that large proportions of the particles are washed out of the sub-system by tide currents. It also provides an insight into the residual displacement of the labelled water parcel from the Empalme sub-system to the Guaymas sub-system during the modelled period.

In terms of management, dispersion of particles for some materials is often associated with dilution. However, in small semi-enclosed and shallows systems such as Guaymas, some materials, such as oil, may produce a more severe impact if they are spread through the system. Although this Lagrangian representation aims to provide water displacement, it indicates the time in which tracked materials reach the Guaymas sub-system. For this short period of time, it is unlikely that materials such as oil can be diluted, degraded by bacteria, evaporated or sunk (Daling and Strom, 1998; Fingas, 1998; Shin-ichi-Sugioka, *et al.* 1998).

In general, Lagrangian residual currents provide an approximation of the likely residual excursion of the mass of water, and hence the transport of dissolved and suspended materials in this shallow system. This allows comparison between predicting and observed water mass displacement. However, it is important to perform future validation experiments such as dye release particles in order to corroborate the above arguments.

3.6. Concluding Remarks and Future Work.

The findings obtained in the present work provide the basic foundation for characterising the hydrodynamics of the Guaymas system. It also provides the primary framework for the development of sediment transport, water quality, geochemical and ecosystem models. The study has identified the following:

- for the system, circulation follows topographic and bathymetric features, where strong currents were associated to channel depths and local hydraulic pressure gradients;
- this circulation feature indicates that the Empalme system is an ebb-dominant system, during the simulated period;
- the difference between the ebb and flood characteristics of both systems produces a residual water movement towards the Guaymas system.

Further work

Although this work produces an insight of the hydrodynamics of the system, it is important to highlight that this is a large research area in which further investigation must be conducted. This would also prove and to validate the hypotheses and modelling produced in the present work. Thus, the present work has identified the following research necessities:

Modelling validation and calibration. Although, modelling is run with real data measured within the system, it is necessary to develop a specific survey campaign that allows the validation and further calibration of the produced model. This must include: Simultaneous tide amplitude and current velocity measurements along the two main sub-systems, in order to identify tide constituents, the ratio of semidiurnal to diurnal constituents (F), and current velocities. These measurements must be done for at least two spring and neap tide periods, and if possible, to indicate of how these vary seasonally within the Guaymas System.

Finally, Lagrangian transport velocity provides an approximation of water transport, although, validation must be carried out. Dye releases and tracking particles through fluorescence techniques, provide a good feedback to the model, allowing validation for the field current model and further calibration in the Lagrangian transport model.

CHAPTER 4

Sediment Dynamics

4.1 Introduction.

Studies of the sediment dynamics aim to provide a greater understanding on which to base coastal zone management decisions. In coastal systems, physical changes are either the product of natural processes and events, or the result of anthropogenic activities. Most of these physical coastal changes are related to sediment dynamics, where the deposition and erosion processes may directly impact upon both human activities (e.g. navigation) and environment (e.g. geological stability, chemical and biological conditions).

Environmental changes or episodic events such as surges, storms, drought and flooding can significantly alter sediment patterns, affecting the geological evolution of the system (Carter, 1988). Anthropogenic activities represented by engineering works such as tide barrages, dragging, pipe-line installation, land reclamation among others, may affect directly the whole hydrology of the system including sediment transport (Hooke, *et al.* 1996; Lin and Falconer, 1997). In addition, indirect effects caused by pollution can alter sediment transport, since water quality conditions greatly determine biological community structure and chemical speciation for the water column and seabed (Thomann, 1983; Harris, *et al.* 1984).

Biological communities significantly contribute to keep a balance in sediment processes, either through sediment retention such in the case of polycheate tubes, seagrass, and mucus coating produced by some diatoms; or by enhancing sediment transport through bioturbation in the case of sediment borrowers (Heip, 1995). Geochemical conditions also are involved in sediment dynamics, and processes such as speciation, chelation, dissociation, and mineralisation may by important defining sediment stability. For instance, cohesive sediment characteristics influence the erosion and accretion balance, and sediment settling velocity (Pethick,1984).

In shallow coastal lagoons, bed sediment transport mainly occurs through tide and wind-induced currents, when the velocity of the current is sufficiently strong to lift or move sediment grains (Dyer, 1986). For these shallow systems, transport is often enhanced by wave motion, which works as a stirring mechanism decreasing current energy requirements to move sediment. In addition, sediment gradation responds differently to current stress. Finer sediment fractions are likely to move in suspension and to travel longest distances whereas the largest grains will move through saltation (hopping), and/or rolling over the seabed with a relative short displacement (Pethick, 1984; Dyer, 1986).

The above complex interactions, together with the difficulties to obtain reliable measurements near seabed, have compromised steady-progress for sediment transport understanding (Owen, 1986; Dyer, 1997). However, a fair sediment transport approximation for shallow systems can be obtained determining the interactions between sediment size, tidal asymmetry, field currents, ebb/flood characteristics, and local waves induced by sustained wind blowing (Dyer, 1997). In addition, chemical speciation and biological processes must be considered. In this context, the present chapter aims to provide an insight of the sediment transport within the Guaymas system.

4.1.1 Sediment Classification.

Sediment classification relies on two grain properties, shape and size. Because of the wide variety in sediment shapes, it is generally assumed that grains are roughly spheroid in shape, this assumption allows the simplification of sediment measurements and theory (Dyer, 1986). Thus, the range of sediment sizes contained in a sample is analysed using the diameter of the normalised sphere shape for the grain. The most widely accepted grade scale for grain size is the Wentworth scale (Table 4.1; Pethick, 1984; Dyer, 1986).

Table 4.1 Sediments grain size classification, Wentworth size classes and ϕ relation.

Classification	Phi ϕ	Millimetres mm
Gravel:	-6 to -1	60 to 2
Sand:		
very coarse	0	1.00000
coarse	+1	0.50000
medium	+2	0.25000
fine	+3	0.12500
very fine	+4	0.06250
Silt:		
coarse	+5	0.03125
medium	+6	0.01562
fine	+7	0.00781
very fine	+8	0.00391
Clay:		
coarse	+9	0.00195
medium	+10	0.00098
fine	+11	0.00049
very fine	+12	0.00024

$\phi = -\log_2 (mm)$

The most used methods to measure sediment particle size include sieving (wet and dry), pipette analysis, the use of Coulter Counter, and Laser diameter measurement techniques (Dyer, 1979; Pethick, 1984).

4.1.2. Sediment transport.

For sediment transport modelling, the representative diameter chosen for the sample is a particular important parameter. Experimental work and literature reviews made by Ackers and White (1973) and Owen (1986) respectively, show that a simple mean diameter can be recommended as representative of sediment diameters. The diameter, D_{35} instead of the expected median diameter, D_{50}, is recommended for graded sediments, the subscript is the percentage by weight of sediment finer than that diameter, this number came from multiple laboratory simulations and field validation works (Ackers and White 1973; Owen, 1986; Jing-Wen, *et al.* 1997). Different size fractions can be very complex to model and highly computational time-consuming (Owen, 1986). However, size fraction data may be required, depending upon the phenomena to be studied, e.g. sediment load transport, suspended sediment transport, or deposition and erosion processes (Jing-Wen, *et al.* 1997).

Sediment displacement within coastal lagoons can be presented as bedload, suspended load and wash load (Pethick, 1984). Bedload represents those particles that move close to the seabed through rolling, sliding and saltation. The sediment load, movement depends very much on the maximum current velocity, and their net transport is most related to the system flood/ebb characteristic (Pethick, 1984; Dyer, 1997). Suspended load comprises more fine grains, which can be lifted and transported by currents (Dyer, 1997). The distance of their movement depends on the time prior to settlement and the sustained tidal current characteristics. Finally, wash loads are those finest grains with a positive or neutral buoyancy, these sediments are always are in suspension (Pethick, 1984).

In order to determine the relative amounts by which suspended sediment load or bedload are important for the system, it is possible to consider the ratio of settling velocity (w_s) and shear velocity (U_*). This relation is known as Entrainment velocity, P_s.

$$P_s = w_s / k\,U_* \tag{4.1}$$

Where k is the von Karman's constant = 0.4, U_* is given by the expression 3.13, w_s is further described in section 4.1.2.2. Suspended load transport occur when $P_s < 2$, shear velocity overcoming settling velocity, while negligible suspended sediment will occur when $P_s > 2$, this means that settling velocity is larger than shear velocity (Dyer, 1997).

4.1.2.1 Threshold of sediment movement. The critical shear stress, τ_c, is the flow force for the initial motion of sediment or threshold velocity, V_{*c}, and the relation is:

$$V_{*c} = (\tau_c/\rho)^{1/2} \tag{4.2}$$

Values of τ_c can be obtained from Chepil (1958) cited in Dyer (1986) as:

$$\tau_c = \frac{0.66Dg(\rho_s - \rho)N\tan\alpha}{(1 + 0.85\tan\alpha)T} \tag{4.3}$$

N represents the ratio of mean drag and lift forces over the bed in relation to the drag and lift of the protruding grains, N ranges between 0.2 and 0.3. The parameter α represents the dynamic friction angle approximated to $\approx 24°$, and T is the turbulence factor defining instantaneous shear stress $\approx$ 2.2 to 2.5.

A widely-used sediment threshold formula is given by Shields (1939) and cited by Pethick (1984), Dyer, (1986), and Owen (1986). This combines the threshold shear stress and the gravitational grain force to produce the dimensionless Shields' threshold coefficient, θ_c.

$$\theta_c = \frac{\tau_c}{Dg(\rho_s - \rho)} \tag{4.4}$$

Combining equation 4.3 and 4.4:

$$\frac{\tau_c}{Dg(\rho_s - \rho)} = \frac{0.66N\tan\alpha}{(1 + 0.85\tan\alpha)T} = \theta_c \tag{4.5}$$

then, substituting the constant values for N, α and T

$$\frac{\tau_c}{Dg(\rho_s - \rho)} = \theta_c = 0.425 \tag{4.6}$$

and from equation 4.2

$$V_{*c} = (\tau_c/\rho)^{½} = [\{0.425\ Dg(\rho_s - \rho)\}/\rho]^{½} \tag{4.7}$$

Alternatively, values for threshold sediment movement can be obtained from the figure 4.1. The theory may not always hold due to natural processes such as non-uniform sediments, armouring, changes in bed roughness by benthic flora and fauna, and chemical effects in sediment very often occur, altering terminal shear stress and velocities (Dyer, 1986; Owen, 1986).

Threshold of sediment movement enhanced by wave oscillation. In shallow systems where tidal amplitude is moderate to small, local meteorological conditions such as wind can play a major role in defining the vertical structure of the water column. Wind may have a sustained speed and sufficient duration and direction to produce a fully-developed sea, where the energy transmitted by wind is proportional to the wave energy dissipation,

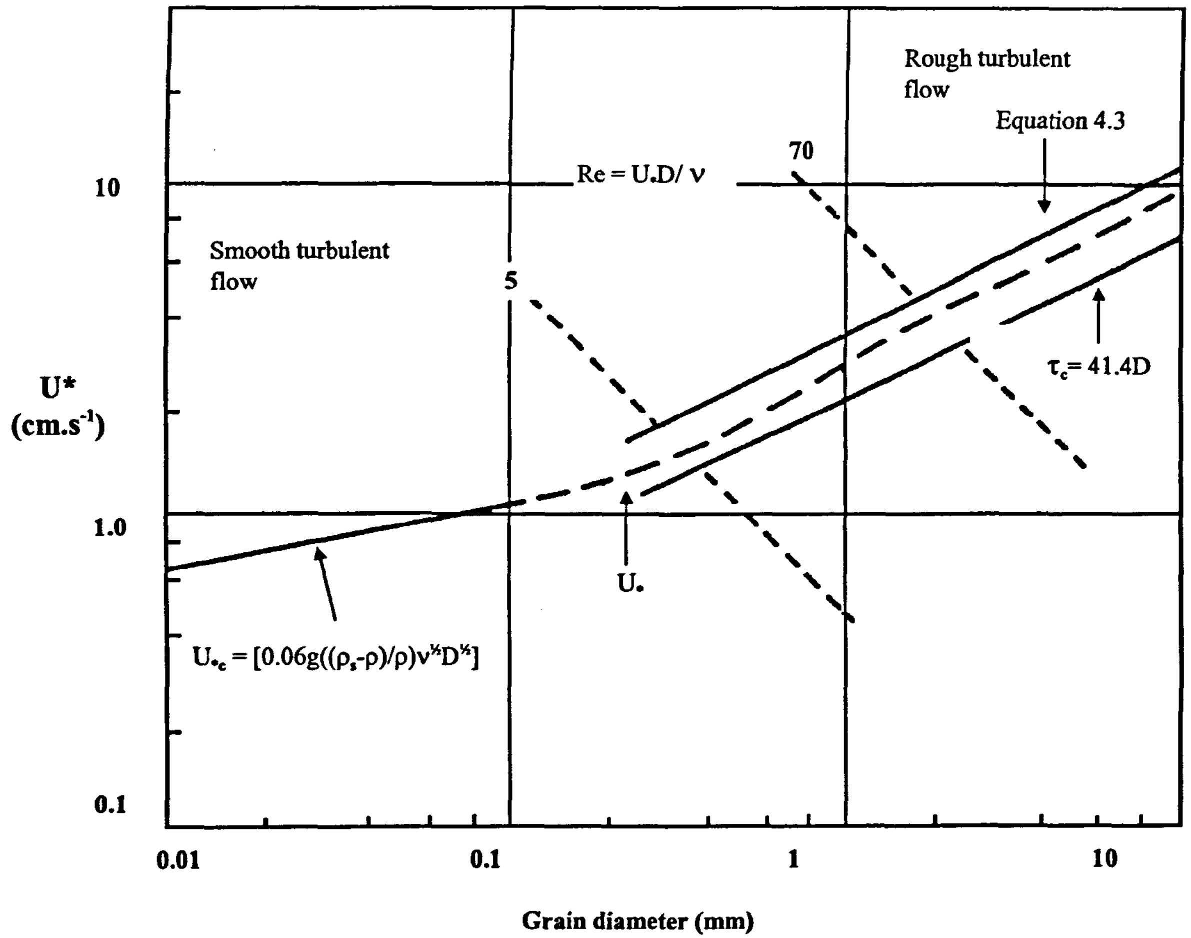

Figure 4.1. Threshold friction velocity for sediment movement. The figure shows different relations of U_* and τ_c for sediment size. Semi-dashed lines indicate the Reynolds number limits for smooth turbulent flow (5) and rough turbulent flow (70). The diagram is taken from Dyer (1986).

and in which wave characteristics became constant (Bearman *et al.*, 1993). Although a fully-developed sea is unlikely to occur in natural systems, the concept gives a relatively good indication of the relationship between wind speed and wave height for coastal lagoons. Table 4.2 shows the wind speed and waves height relationship for a fully developed sea. An alternative relationship between wind and seawater surface is given in chapter 3, sections 3.1.2 and 3.1.3.

The threshold of sediment movement is enhanced under wave oscillation, the effective depth limit for wave influence in shallow waters is $h < \lambda/20$, where λ is the wave length, with a horizontal water motion amplitude, A_b, and maximum wave orbital velocity, U_m. A_b is obtained as:

$$A_b = [a/(\sin h\ (2\pi h/\lambda))] \tag{4.8}$$

whereas U_m is expressed as:

$$U_m = H/2\ (g/h)^{1/2} \tag{4.9}$$

a represents wave amplitude, H is wave height and h is water depth. The magnitude of wave orbital velocity highly influences threshold sediment, since it increases turbulence.

4.1.2.2 Settling velocity. Once the sediment has been put in movement, the finest fractions are likely to be suspended by turbulent processes, the velocity in which these fine grains settle is an important characteristic of sediments. In theory, setting velocity (w_s) is the fall velocity of a particle though a motionless fluid (Pethick, 1984). This velocity is achieved by a particle when the friction forces balance the weight-immersed forces. There are several formulae considering theoretical and experimental observations for w_s. For particles finer than 0.1 mm, Stokes Law states that:

$$w_s = \frac{(s-1)gD^2}{18\nu} \quad \text{or} \quad w_s = \frac{D^2(\rho_s - \rho)g}{18\mu} \tag{4.10}$$

Owen (1986) shows for particles from 0.1 mm to 1.0 mm the relationship:

Table 4.2 Relation between wind speed and wave height for a fully developed sea from Beaufort Wind Scale (Bearman 1989).

Beaufort No.	Name	Wind Speed (ms^{-1})	Wave Height (m)
0	Calm	0.0 - 0.2	0
1	Light air	0.3-1.5	0.1-0.2
2	Light breeze	1.6-3.3	0.3-0.5
3	Gentle breeze	3.4-5.4	0.6-1
4	Moderate breeze	5.5-7.9	1.5
5	Fresh breeze	8.0-10.7	2
6	Strong breeze	10.8-13.8	3.5

Wave height as averaged one-third highest waves over a time period.

$$w_s = \frac{(10\,\nu)}{D}\left[(1 + 0.01(s-1)gD^3/\nu)^{½}\right] - 1 \tag{4.11}$$

And for larger grains, settling velocity is proportional to the square root of the grain diameter (Pethick, 1984; Owen, 1986).

$$w_s = 1.1((s-1)gD)^{½} \tag{4.12}$$

Where s represents the relative sediment density $((\rho_s - \rho)/\rho)$, ν is the kinematics viscosity (μ/ρ), and μ the coefficient of molecular viscosity.

Although these good approximations aim to consider hydraulic, size, shape, density and chemical properties of the analysed particles, a limitation is that the leading theory still came from the study of sphere particles in still fluid, hence there is a disagreement between theoretical and field settle velocity observations. Certainly, in coastal systems other complex and partially understood processes such as flocculation in clays and silts increase settle velocity (Pethick, 1984). Also, elicoidal or spin fall developed from determined particle shape and oscillatory flows negatively affect w_s, and the turbulence present in the fluid increases friction and therefore decreases settle velocities (Dyer, 1997). There are many studies regarding each one of the above processes, however, a few of them have general practical applicability with a significant increase in accuracy (Ackers and White, 1974; Pethick, 1984; Owen, 1986 and Dyer, 1997).

4.1.2.3 Tide influence. In coastal lagoons, a large proportion of the sediment transport is likely occur with tide currents. In combination with waves and wind, tide currents define the inward or outward sediment transport for a system. A detailed explanation of tide and current velocity relationship was given in Chapter 3.

Tidal asymmetry. The hydraulic geometry, i.e. the morphology and volume of the tidal prism of a lagoon, highly determines the residual current direction, hence the ebb or flood dominance of a system (Chapter 3). For coastal lagoons with complex hydraulic geometry or/and large tidal flat areas, tides are asymmetric in retarding the flood processes and increasing flushing during the ebb period (Aubrey and Speer, 1985). These environments are known as ebb-dominant systems as reflected by flushing capacity, they are often characterised by a net oceanward sediment transport. A flood-dominant system is characterised by an intense flood and weak longer ebb, those systems are often represented by smooth channels with narrow or absent tidal flats, and often reflect a net landward sediment transport (Aubrey, 1986). Frequently, coastal lagoons tend to reach an apparent balance between the sedimentary infilling and sediment flushing, preventing further long-term accretion or erosion. This balance reflects a self-adjusting control between tide, hydraulic geometry and sediment; Dyer (1997) defined those systems as Equilibrium Estuaries and this concept can be applied to coastal lagoons.

An useful indicator of the flood or ebb dominance in coastal system is given by the ratio of tidal range to water depth (a/h), in which values > 0.3 represents flood-dominant, whereas systems with values <0.3 are ebb-dominants. Figure 4.2 shows the relationship used by Friedrichs and Aubrey (1988), and modified by Dyer (1997).

Alternatively, ebb or flood dominance may be obtained by the M_4/M_2 ratio. For an elevation phase ($2M_4/M_2$) between 0 and 180° flood will be dominant, while for phases of 180-360° ebb will dominate. The ebb- or flood- magnitude is obtained by the M_4/M_2 ratio, i.e. whichever the dominance in the ratio represents largest ebb or flood (Aubrey, 1986; Friedrichs and Aubrey, 1988; Dyer, 1997).

4.1.3 Modelling sediment transport rate for well mixed coastal lagoons.

Modelling the transport of noncohesive sediment is a complex process. Many of the theories and approaches aiming to predict sediment transport rely very much on different

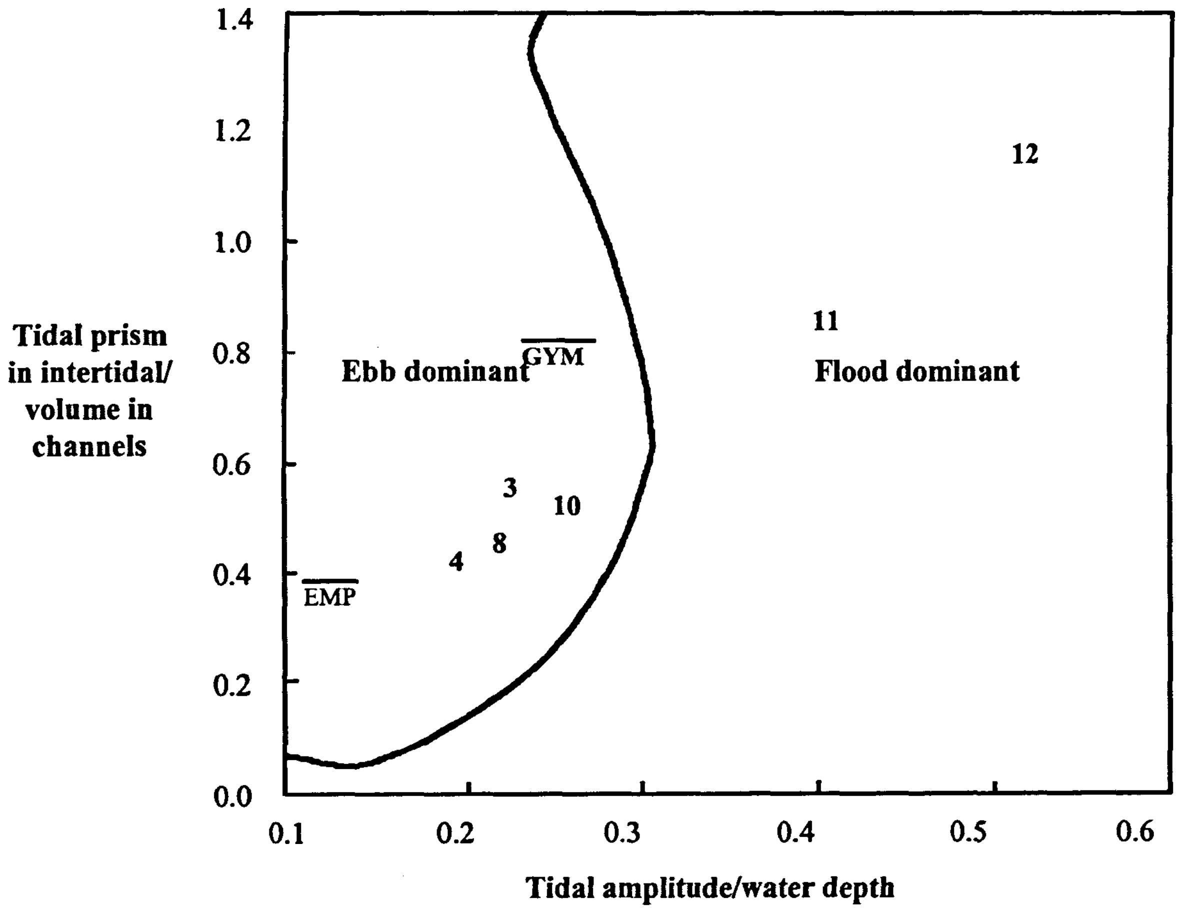

Figure 4.2. Flood or Ebb dominance in coastal systems in relation to their hydraulic geometry. Diagram taken from Dyer (1997). The numbers represent the survey stations and the labels GYM and EMP represents the average values for the Guaymas and Empalme sub-systems respectively.

empirical approximations and, therefore, often there is a discrepancy between them (Einstein,1950; Ackers and White,1973; Bagnold, 1966). In addition, some of these formulations are difficult to apply given the data required. Bearing this in mind, the present work adopts the Bagnold (1966) and Ackers and White (1973) approaches for sediment flux. These approaches provide an approximation for sediment flux from easy-to-measure parameters, without compromising accuracy.

4.1.3.1. Bedload transport. A commonly-accepted approach to represent sediment bedload transport is that given by Bagnold (1966). This concept considers the work efficiency required by the fluid in order to move sediment, this is expressed as:

$$q = K\,W = K\,\tau_o \hat{U} \tag{4.13}$$

where K is the efficiency proportional constant and W represents work. This equation was expressed by Kachel and Sterber in Dyer (1986) as:

$$q_b = K\,U_*^3 \tag{4.14}$$

here U_* represents shear or friction velocity. For coastal environments, it is required to normalise the variables U_* and K under wave and currents. Friction velocity is approximated as $U_* \approx U_{*s}$ where U_{*s} represents the bed friction velocity influenced by waves and currents. U_{*s} can be expressed as:

$$U_{*s} = \left(\frac{\eta V^2}{7.5 U_*^2} + 1 \right)^{1/2} U_* \tag{4.15}$$

η is a proportionality factor ≈ 0.6, h is depth and V is the root mean square of wave velocity (C), C for inter-medium waters is given by:

$$C = [\,(g\lambda/2\pi) \tan h\,(2\pi h/\lambda)]^{1/2} \tag{4.16}$$

for shallow waters

$$C = (gh)^{½} \tag{4.17}$$

where λ is the wave longitude and h is water depth.

The efficiency-proportional constant, K, is given in terms of sediment diameter, D, bed shear stress, τ_o, and threshold shear stress, τ_c. K can be approximated as Sternberg (Dyer, 1986). For grains size less than 0.25 mm:

$$K = 0.005 \exp 0.7 [(\tau_o - \tau_c)/\tau_c] \tag{4.18}$$

and for grains >0.25mm and <0.30 mm, K is equal to:

$$K = 0.005 \exp[((D/140) - 1.5) ((\tau_o - \tau_c)/\tau_c] \tag{4.19}$$

In order to normalise K under waves and currents, the Bijker approach is used where $\tau_o \approx \tau_{wc}$, and τ_{wc} represents the bed shear stress under waves and currents (Dyer, 1986).

$$\tau_{wc} = 1 + ½ [\xi(U_m/ \hat{U})]^2 . \tau_0 \tag{4.20}$$

Here, U_m and $\hat{U}$ are orbital velocity and mean velocity respectively, ξ is a factor computed as $\xi = p \ln [(h/z_0)-1]$ where z_0 is the sediment roughness can be chosen from Chapter 3 in Table 3.2. As the bed load sediment direction is not necessarily the same as the average current direction, the sediment transport vector direction can be obtained as $\tan^{-1} \tau_2/\tau_1$ where τ_1 and τ_2 are given by:

$$\tau_1 = 1 - N [\xi (U_m/ \hat{U})]^{1.5} . \tau_0 \tag{4.21}$$

And

$$\tau_2 = 1 - M [\xi (U_m/ \hat{U})]^{1.25} . \tau_0 \tag{4.22}$$

M is the mobility number equal to 0.36 - 0.14 cos 2φ, and N is the number of grains moving and can be set as 0.205 sin 2φ, where φ is the angle between waves and current direction. Alternatively, M can be set as M_c, the critical mobility number. For grains < 0.5 mm $M_c = 0.30\ (A_b/D)^{1/4}$, and for grains > 0.5 mm $M_c = 0.55(A_b/D)^{1/4}$, A_b represents amplitude of the near-bed oscillatory water motion. A_b, is given by equation 4.8.

Table 4.3 summarizes the properties of the system that must be known in order to compute the transport of bedload sediment, and Figure 4.3 shows the calculation procedure for bedload sediment transport.

4.1.3.2 Combined suspended and bedload transport. A practical approach developed by Ackers and White (1973) considers sediment transport as a function of three dimensionless groups: D_{gr} (sediment grain diameter), F_{gr} (sediment mobility) and G_{gr} (sediment transport). This empirical approach aims to integrate the effects of the bed forms such as ripple and dune configurations.

Sediment transport is based on the waters stream power, fine sediments are moved by the total stream power, whereas large sediments use the product of net grain shear and the stream velocity as the power per unit area of bed. The transport rate of sediment, q, takes the form:

$$q = [(G_{gr}\rho_s D/g\rho h)/(U_*/\hat{U})^n \qquad (4.23)$$

where G_g is the dimensionless sediment transport, which was set as a function of sediment mobility from which the efficiency is dependent, and the dimensionless grain diameter:

$$G_{gr} = C(F_{gr}/A - 1)^m \qquad (4.24)$$

Table 4.3 Properties of the system required to compute the transport of bedload sediment (q_b).

Symbol	Value/unit	Explanation
λ	meters	Field observation
h	meters	Field observation
H	meters	Field observation
φ	Value in °	Field observation
$\hat{U}$	$m.s^{-1}$	Field observation/ Modelation
D	mm	Field observ/ Laboratory analysis
ρ	$Kg.L^{-1}$	Field observ/Temp. & Salin. dep.
ρ_s	$Kg.L^{-1}$	Field observ/Sediment concent.
N	0.2-0.3	Assumed constant
α	24°	Assumed constant
T	2.2-2.5	Assumed constant
z_0	Table 3.4	Assumed constant
η	0.6	Constant
g	$9.8\ m.s^2$	Constant
π	3.1416	Constant

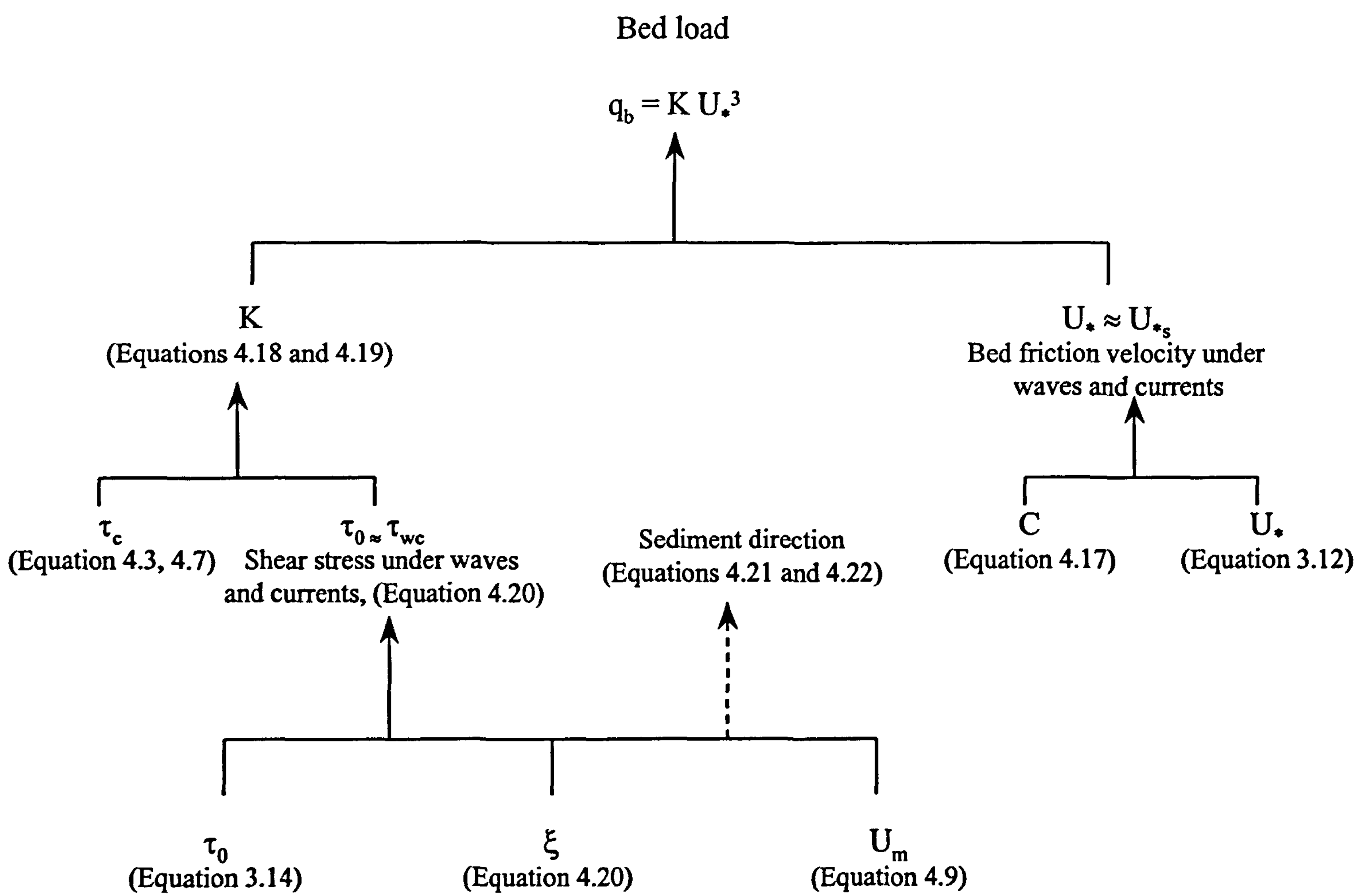

Figure 4.3. Calculation procedure for sediment bed load.

In order to integrate the wave and current effects, $U_* \approx U_{*s}$ where U_{*s} is taken from equation 4.15. It is assumed that *C*, *A*, m and n will all vary with sediment size. For sediments > 2.5 mm $A = 0.17$, $C = 0.025$, m = 1.5 and n = 0; for sediments between 0.04 and 2.5 mm. The coefficient, *C*, in the sediment transport function is:

$$\log C = 2.86 \log D_{gr} - (\log D_{gr})^2 - 3.53 \tag{4.25}$$

A represents the value of F_{gr} at nominal initial motion, and is given by:

$$A = 0.23(D_{gr})^{-½} + 0.14 \tag{4.26}$$

The exponent "m" in the sediment function (Equation 4.24) and the transition exponent "n" (Equation 4.23) are given by:

$$m = 9.66D_{gr}\text{-}1 + 1.34 \tag{4.27}$$

$$n = 1.00 - 0.56D_{gr} \tag{4.28}$$

The dimensionless expression for grain diameter, D_{gr}, is derived by eliminating shear stress from two Shields parameters of equation 4.21; or, from the drag coefficient and Reynolds Number of a settling particle, by eliminating the settling velocity. Using the latter, D_{gr} is:

$$D_{gr} = D\,[\,g((\rho_s - \rho)/\rho)\,v^{-2}]^{⅓} \tag{4.29}$$

Sediment Mobility, F_{gr}, is described as the ratio of the shear force on unit area of the seabed to the immerse weight of a layer of grains. The mobility number F_{gr} is denoted by:

$$F_{gr} = \frac{U_*^{\,n}}{(gD(\rho_s - \rho)/\rho)}\left[\frac{\hat{U}}{(32)^{½}\log(10hD)}\right]^{1-n} \tag{4.30}$$

For coarse sediment n = 0, and for fine n = 1. Thus, n range from 1 to 0 and the value depend primarily on D_{gr}.

Table 4.4 summarizes the properties of the system that must be known to compute sediment transport using Ackers and White formulation, and Figure 4.4 shows the calculation procedure for total sediment flux.

4.2 Aims.

The present chapter aims to provide a better understanding of the sediment dynamics within the Guaymas system through the characterization of the following parameters:

- ebb- or-flood dominance of the system;
- the rate in which suspended sediment load or bedload are important, and;
- the likely sediment load movement within the system.

4.3. Methods.

Sampling procedure is described in the methods section, Chapter 2.

4.3.1 Sediment Analysis.

Sieve fraction. For the sieve fraction, 60 gr dry weight sediment sample were hydrated and sieved wet using 0 (1 mm) and 1 ϕ (0.5 mm) mesh size sieves. Each fraction was dried and weighed, the fines fraction, size < 0 ϕ, was analysed through an instrumental technique (Dyer, 1997). Organic matter was not removed, as this fraction is regarded as representing, for some stations, an important part of the whole sample.

Table 4.4 Properties of the system required to compute combined sediment transport.

Symbol	Value/unit	Explanation
λ	meters	Field observation
h	meters	Field observation
$\hat{U}$	$m.s^{-1}$	Field observation/ Modelation
z	meters	Field observation
D	mm	Field observ/ Laboratory analysis
ρ	$Kg.L^{-1}$	Field observ/Temp. & Salin. dep.
ρ s	$Kg.L^{-1}$	Field observ/Sediment concent.
ν	L^2T^{-1}	Assumed constant
μ	$10.9\text{-}8.5 \times 10^{-3}\ ML^{-1}.T^{-1}$	Assumed constant
z_0	Table 4.3	Assumed constant
η	0.6	Constant
g	$9.8\ m.s^2$	Constant
π	3.1416	Constant

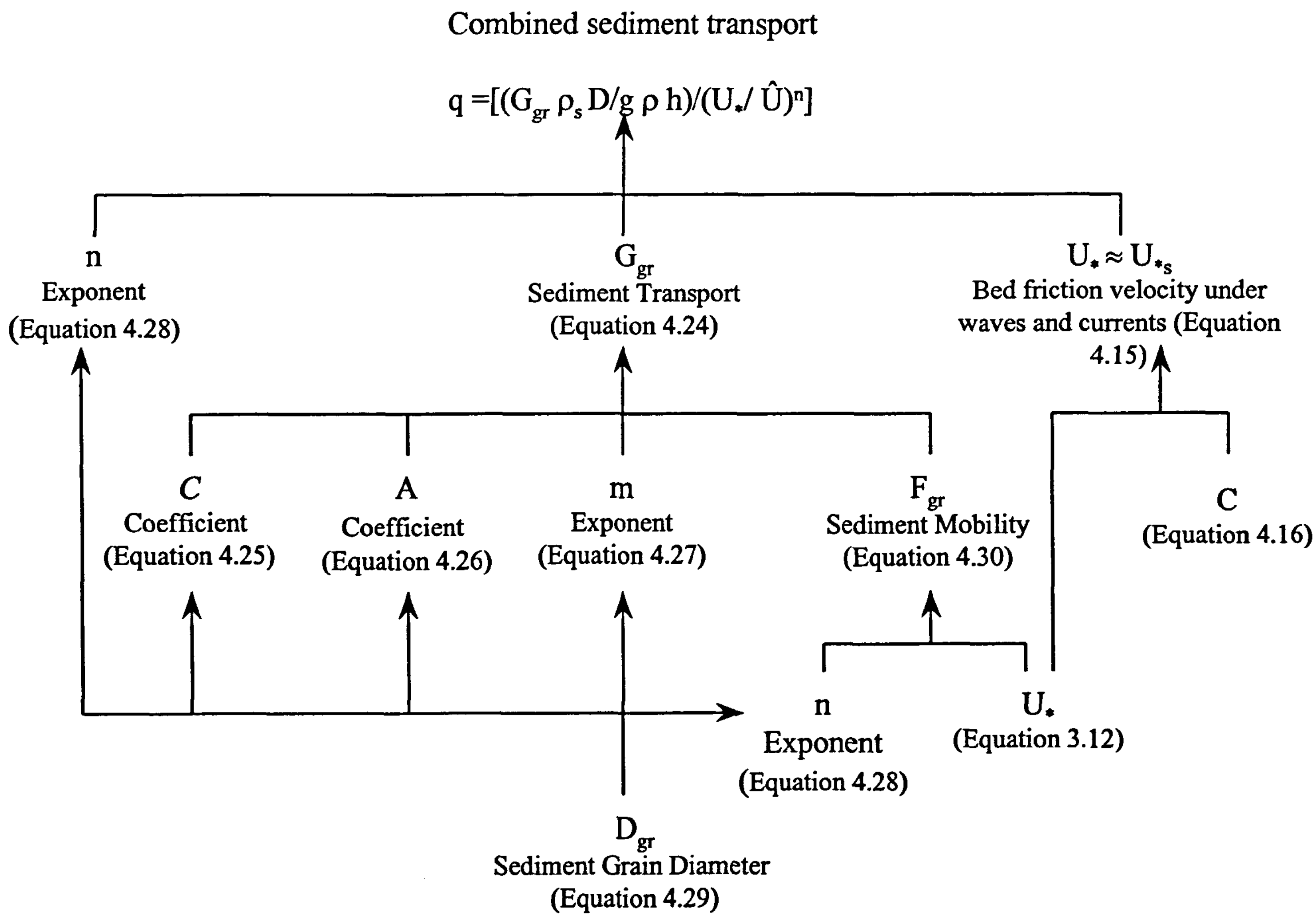

Figure 4.4. Calculation procedure for combined sediment transport.

4.3.2. Ebb or flood dominance of the system.

As an indicator of the flood- or ebb-dominance of the system, the ratio of tidal range to water depth (a/h) was used. The results were compared with the Friedrichs and Aubrey (1988) relationship shown in Figure 4.2.

4.3.3. Modelling .

Sediment bedload was modelled following the procedure shown in Figure 4.3. Mean current velocities were obtained from water field prediction (see Chapter 2).

4.4. Results and Discussion.

Entrainment velocity values (*P*s) indicated for most of the modelled periods are above 2 units, indicating that sediment bedload represents an important part of sediment transport within the system (Table 4.5). Although washed load sediments must not be discounted, bedload is considered of practical significance in most situations considering sediment transport (Sleath, 1995). Accordingly, the present section aims to provide an insight of the likely bedload pattern during a tide cycle. Bedload transport considers those sediments with a size > 0.01 mm, and particles < 0.01 mm were considered as sediment washed load (Sleath, 1995).

Sediment net flux from tide asymmetry. For the system, the transport of sediment load depends very much of the maximum current velocity, consequently its transport may be determined by flood/ebb-dominance. The Guaymas system showed a differentiation between the two major subsystems, Guaymas and the Empalme. For the Guaymas sub-system stations 12 and 11 presented a/h values of 0.54 and 0.4 respectively, indicating flood-dominance, whereas there is a progressive ebb dominance towards the mouth of the system with values for stations 10 and 8 of approximately 0.24 and 0.22 respectively. The

Table 4.5. Entrainment velocity. $P_s = W_s / kU_*$

Time	station 12	station 11	station 10	station 8	station 4	station 3	station 2
0	0.424866	0.349822	0.908089	0.807245	0.807245	2.152653	2.494618
1	0.672704	0.874555	48.43143	2.391837	1.291592	4.612828	1.164155
2	0.896939	0.816251	2.421572	1.793878	1.345408	5.381633	1.179887
3	0.849732	0.765236	2.201429	1.61449	0.9497	4.036225	2.494618
4	1.009056	0.890456	2.201429	1.61449	0.807245	3.587755	1.164155
5	2.018112	2.448754	3.302143	2.583184	0.807245	3.587755	0.727597
6	8.07245	4.897508	24.21572	6.45796	0.645796	5.381633	0.545698
7	0.896939	0.765236	2.136681	1.076327	1.291592	5.381633	0.545698
8	0.576604	0.544168	1.513482	0.922566	0.717551	3.398926	0.739929
9	0.461283	0.445228	1.210786	0.807245	0.587087	2.690817	2.910387
10	0.424866	0.422199	1.153129	0.849732	0.529341	2.391837	1.091395
11	0.436349	0.445228	1.231308	1.009056	0.504528	2.323007	0.698493
12	0.448469	0.470914	1.320857	1.076327	0.496766	2.306414	0.582077
13	0.448469	0.470914	1.345318	1.041606	0.496766	2.226883	0.529161
14	0.436349	0.462029	1.345318	1.113441	0.496766	2.21923	0.513598
15	0.107633	0.544168	1.816179	2.583184	0.538163	2.33984	0.498924
16	0.849732	4.081256	4.540447	2.152653	0.645796	2.935436	0.485065
17	0.47485	0.544168	1.816179	1.041606	0.645796	4.967661	0.471955
18	0.358776	0.437277	1.39706	0.978479	1.291592	4.612828	0.485065
19	0.336352	0.422199	1.274511	1.153207	0.872697	3.22898	0.498924
20	0.448469	0.544168	1.729694	1.537609	0.849732	3.22898	0.513598
21	2.018112	1.224377	3.632357	4.612828	1.076327	3.7988	0.529161
22	2.018112	2.040628	6.604286	4.967661	1.291592	4.967661	0.545698
23	1.345408	1.440443	4.540447	3.22898	1.467718	5.381633	0.623654
24	0.896939	0.979502	2.594541	1.8994	1.153207	4.967661	0.671628
average	1.077103	1.093067	4.995375	1.9726	0.86429	3.684348	0.908205

average value for the sub-system was > 0.3 (0.22), indicating the ebb-dominance. The flood, dominance at stations 12 and 11 suggests that the tide asymmetry produced at the head of the sub-system may be responsible for flood dominance in that area.

The Empalme sub-system is shown to have an ebb-dominance for the three stations, the minimum value was computed for station 2 with 0.036, while stations 4 and 3 presented values of 0.19 and 0.22 respectively. The average value for the sub-system indicates ebb dominance. The whole hydraulic geometry of the sub-system is likely to determine ebb dominance and hence flushing condition dominates. Residual bedload transport must also follow these patterns. The ebb dominance for the inner part of the Empalme sub-system, the Estero El Rancho, was defined by the hydraulic gradient against the Laguna.

Figure 4.2 shows the flood- and ebb-dominance for the system with respect to their hydraulic geometry, which re-produces the patterns described below.

Sediment modelling: Bangor's formula under wave and tide oscillation. It is considered for the purpose of the present work that the combined effect of waves and currents exceed bed shear stress, and hence induce bedload sediments fluxes through the system. The above assumption is likely to occur in very shallow systems such as the Guaymas system. Thus, as an illustration, it is considered the particular case of bedload transport under waves and currents in the Guaymas system. Assumptions for some parameters such as local wave characteristics were made in relation to:

<u>Wave length (λ).</u> Assumed values of 0.5 m for station 2, 1m for stations 12, 11, and 3, and 2 m for stations 10, 8 and 4 were chosen. These values are similar to other semi-enclosed shallow systems, where waves are induced preferentially by local wind.

<u>Wave height (H).</u> A standard value of 0.3 m was used. In assuming that sustained wind blowing is responsible for H, 0.3 m corresponds to an induced wind speed of 1.6 $m.^{-1}$ when the Beaufort wind scale is applied (Table 4.2). This wind velocity is an averaged

value resulting from wind measurements reported within the Guaymas system (Rosales-Grano, *et al.* 1996).

Angle between currents and waves (φ). Bedload transport (q_s) is greatest when φ is very small or collinear (same direction that) to currents, which is the likely case for the system of Guaymas. In general, if assuming that waves are induced by sustained wind blowing, wind direction during winter is dominantly from Northwest to Southeast, inverting the pattern during summer (Rosales-Grano, *et al.* 1996). Moreover, the topographic conditions of the system likely to maintain this pattern (Figure 1.2).

Sediment density was assumed constant to 2650 kg/m^3 (Owen, 1986; Sleath, 1995).

Sediment diameter was incorporated following sediment analysis practised within this work. These data are stations 12 and 2, D_{35} = 0.0625 mm, for stations 11, 4 and 3, D_{35} = 0.12 mm and station 10 D_{35} = 0.25 mm. Finally, mean currents at each site were obtained using the hydrodynamic model outcomes (Chapter 3). The model shows that flood conditions in the Guaymas sub-system are associated with strongest inward currents and hence major inward sediment transport (Figure 4.5). During ebb conditions, there is also a displacement toward the mouth of the system. However, although ebbs are dominant and present during a consistently long period, the induced tide currents are slightly weaker than those induced by flood conditions, resulting in less bedload transport. The above highlight that the model is particular sensitive to U_*. Thus, coarse sediment displacement is strongly related to current strength and wave effects on the seabed. For this particular, simulation q_s is determined mainly by tide currents, since the wave effect for demonstration has been set-up constant. There are spatial differences in q_s within the sub-system, also as the result of tide asymmetry, and hence in tide currents (Figure 4.5).

For the Empalme sub-system, station 2 (Estero El Rancho) presents a very low tide range and tide currents (Figure 4.6). Low current velocity alone seems to be unable to re-suspend coarse sediments. The projected bedload transport is likely to be the result of

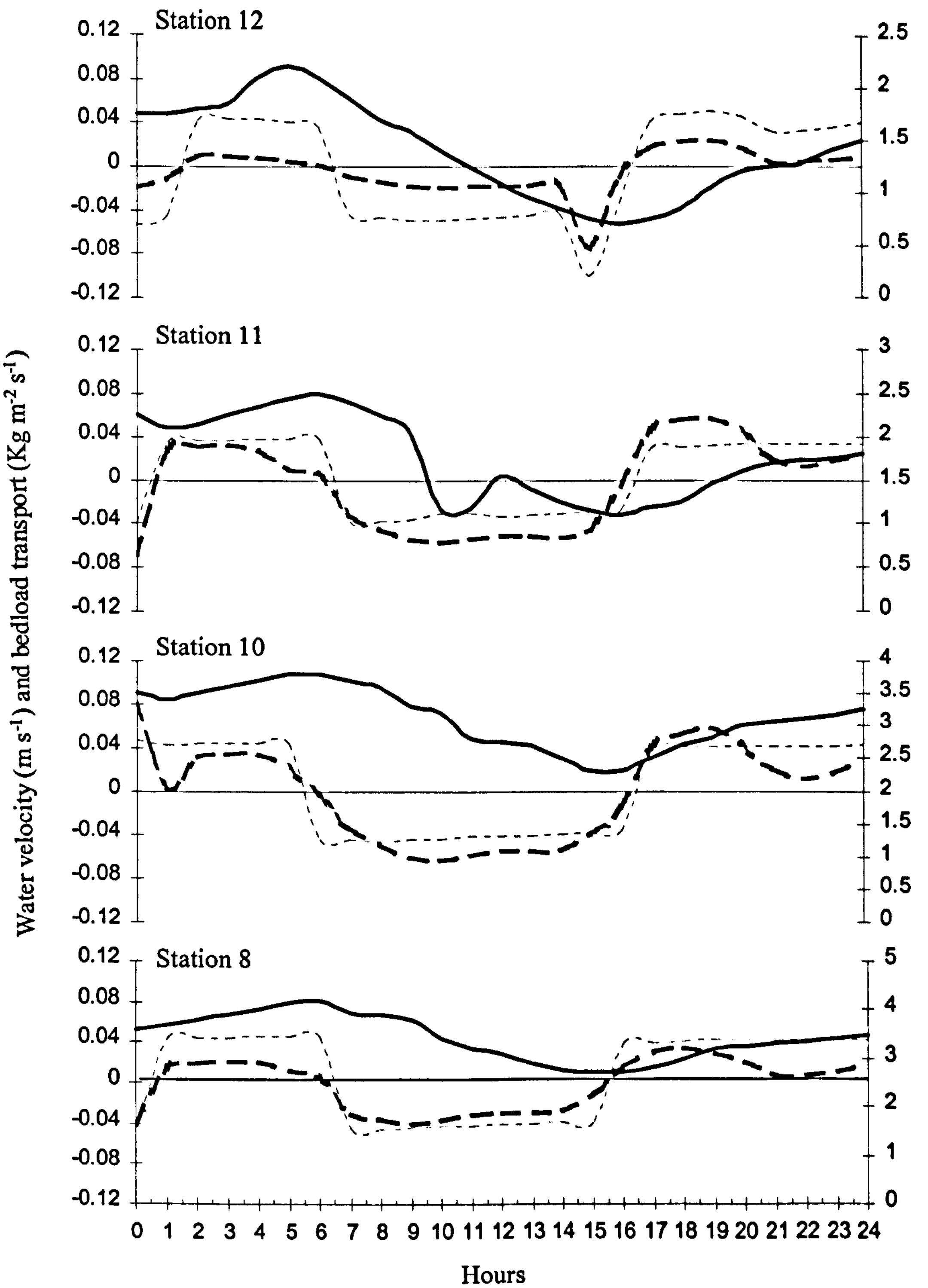

Figure 4.5 . Water velocity and bedload transport at four stations, across the Guaymas sub-system for a neap tide period. The ____ represents water depth, the _ _ _ represents water velocity and .... represents sediment load transport. The sings represent ebb (-) and flood (+) conditions.

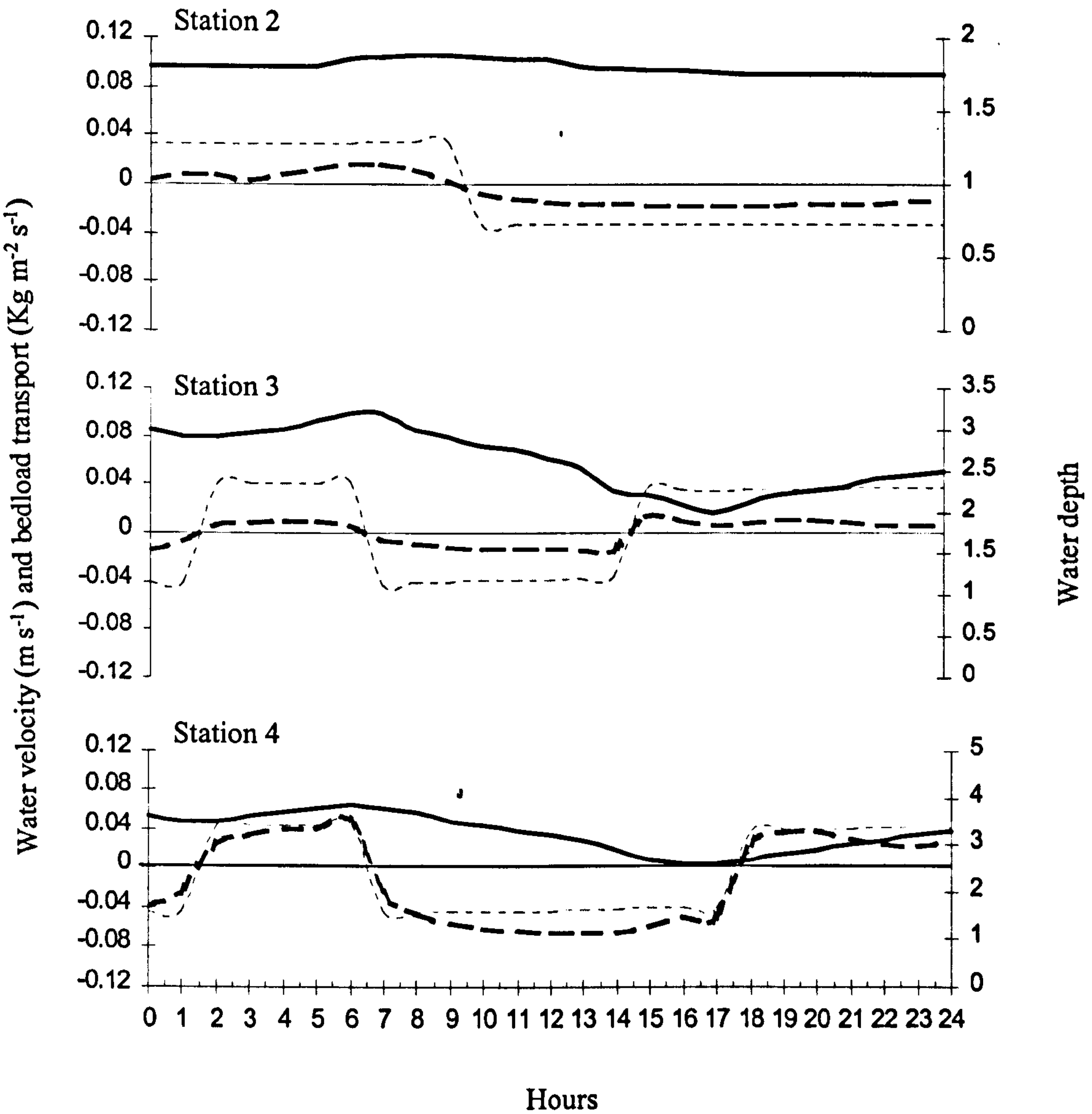

Figure 4.6. Water velocity and bedload transport at three stations, across the Empalme sub-system for a neap tide period. The ____ represents water depth, the _ _ _ represents water velocity and .... represents sediment load transport. The sings represent ebb (-) and flood (+) conditions.

wave effects over sediment, whereas transport direction was determined by the collinear resultant between waves and currents. Therefore, it was mainly determined by the tide currents. Also, this station presents longer outward movement than inward, which can be expected, considering that the modelled period is more representatives of neap tides.

For the rest of the sub-system, station 3 presents very low currents and consequently, q_s is more associated with the wave effect (Figure 4.6). For this particular station, inward currents are dominant, and likely to be associated with the formation of a dominant clockwise eddy, enhanced by the barrage effect (Estero El Rancho), the shallowness of the area and tide asymmetry (Figures 3.7 to 3.19). Station 4 was located in the main channel of the Laguna, where currents seems to be strongly associated with q_s, as can be seen in Figure 3.6.

Residual values: The residual bedload transport, defined for the purpose of this work as the average load sediment transported over a complete tide cycle, produces a net displacement towards the head of the Guaymas sub-system (Figure 4.7). The highest residual values were predicted for the sites 8 (0.008718 $kg.m^{-1}.s^{-1}$) and 10 (0.005367 $kg.m^{-1}.s^{-1}$), and lowest values for the sites 11 (0.00462 $kg.m^{-1}.s^{-1}$) and 12 (0.004271 $kg.m^{-1}.s^{-1}$; Table 4.6; Figure 4.7).

For the Empalme sub-system, there is a net bedload residual transport toward the mouth of the system, with the exception of station 3 that presents a net landward flux (Table 4.6; Figure 4.7). Station 3 patterns might be strongly influenced by local circulation which, in turn, is defined by tidal currents and the shallowness of the area (Figures 3.7 to 3.10). Stations 2 and 3 produced the higher bedload residual values of -0.00654 $kgm^{-1}s^{-1}$ and 0.00686 $kgm^{-1}s^{-1}$, and the same residual value was found for station 4, with -0.00686 $kgm^{-1}s^{-1}$, where the sing represents flood (+) and flushing (-) conditions.

For the whole Guaymas system, modelling of bedload transport under currents and waves, using the output of a depth averaged circulation model shows that the bedload

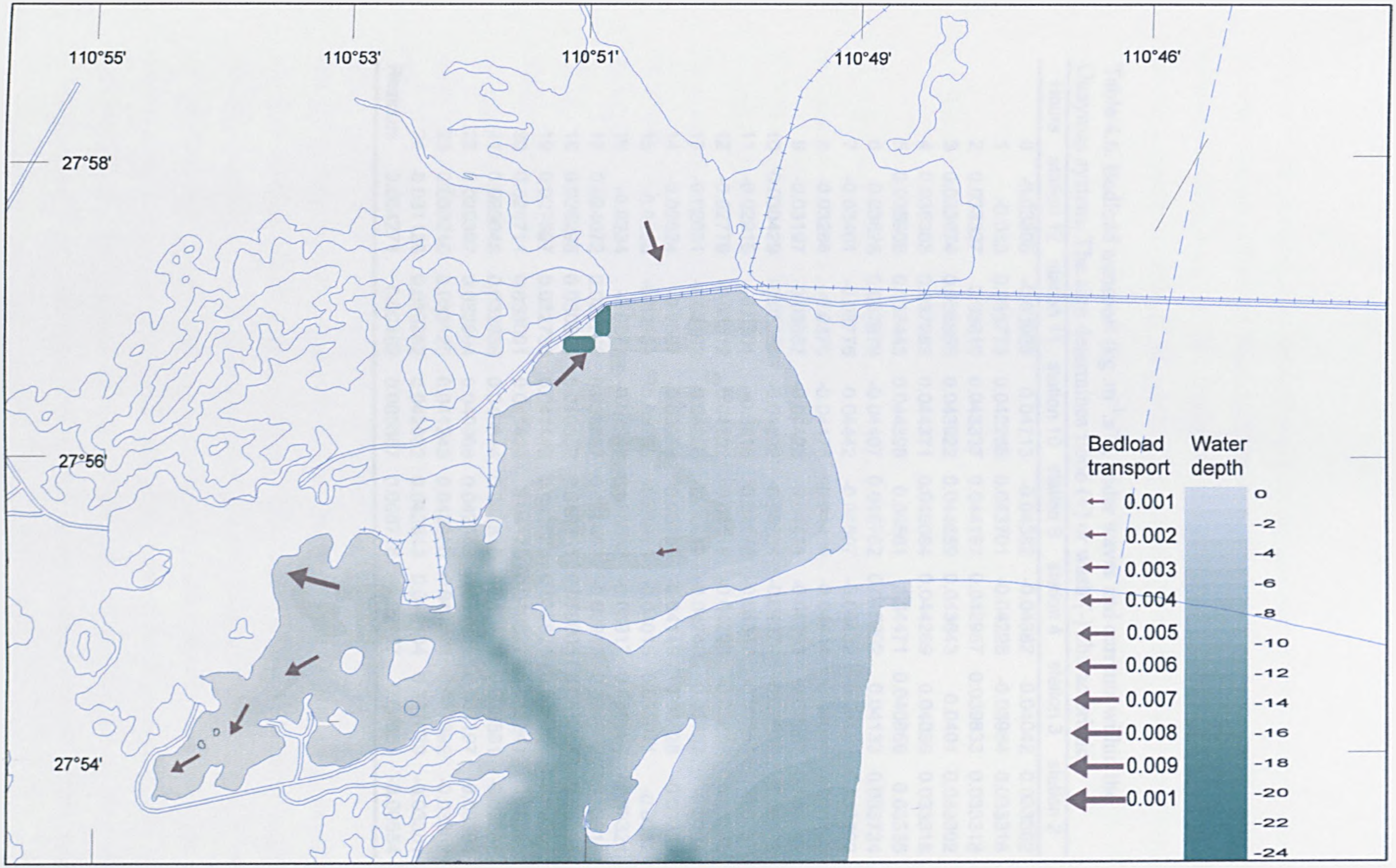

Figure 4.7. Residual bedload transport within the Guaymas system. The arrows represents the magnitude and direction of the transport.

Table 4.6. Bedload transport (kg .m^{-1}.s^{-1}), under waves and currents within the Guaymas system. The sign determines flood (+) or wash (-) characteristics.

Hours	station 12	station 11	station 10	station 8	station 4	station 3	station 2
0	-0.03308	-0.03936	0.04713	-0.04382	-0.04382	-0.04042	0.033302
1	-0.033	0.035773	0.042268	0.043701	-0.04298	-0.03984	0.033318
2	0.033327	0.03616	0.043337	0.044197	0.042957	0.039833	0.033318
3	0.033674	0.036855	0.043922	0.044659	0.043643	0.0401	0.033302
4	0.035303	0.037283	0.044371	0.045084	0.044269	0.04036	0.033318
5	0.035906	0.037443	0.044398	0.04561	0.04471	0.040859	0.03335
6	0.03528	0.037679	-0.04407	0.045762	0.045292	0.04133	0.033734
7	-0.03401	-0.03775	-0.04442	-0.04507	-0.04432	-0.04133	0.033802
8	-0.03266	-0.0375	-0.04475	-0.04499	-0.04444	-0.04036	0.033896
9	-0.03197	-0.03687	-0.04423	-0.04471	-0.04393	-0.03987	0.033849
10	0.030429	-0.03039	-0.04399	-0.04284	-0.04374	-0.03937	-0.03373
11	-0.02916	-0.0301	-0.0416	-0.04172	-0.04342	-0.03911	-0.0337
12	-0.02779	-0.03312	-0.04102	-0.04118	-0.04298	-0.03857	-0.03372
13	-0.02631	-0.03192	-0.04068	-0.04019	-0.04248	-0.03797	-0.0334
14	-0.02524	-0.0307	-0.03956	-0.03936	-0.04146	-0.03628	-0.03333
15	-0.0258	-0.02933	-0.03753	-0.03883	-0.04015	0.035971	-0.0332
16	-0.0234	-0.0277	-0.03667	0.038852	-0.03917	0.035324	-0.03321
17	0.024072	0.029786	0.038697	0.039667	-0.03917	0.034655	-0.03314
18	0.025296	0.030894	0.040539	0.040751	0.039005	0.035297	-0.03306
19	0.027397	0.032733	0.041443	0.041623	0.039825	0.035937	-0.03306
20	0.028711	0.033091	0.041499	0.04173	0.040377	0.036241	-0.03305
21	0.029048	0.032836	0.040844	0.041815	0.040678	0.036531	-0.03305
22	0.029307	0.032894	0.040908	0.042049	0.041071	0.037107	-0.03304
23	0.030316	0.033125	0.041243	0.042306	0.041506	0.037392	-0.03302
24	0.031126	0.033682	0.042082	0.042843	0.042104	0.037679	-0.03301
Residual	0.004271	0.00462	0.005367	0.008718	-0.00187	0.00686	-0.00654

transport is in the direction to the net current circulation, when wave direction is collinear to currents. In spite of the ebb characteristics of the Guaymas sub-system, it presents a net landward bedload transport. The Empalme sub-system presents a slightly net outward bedload transport. Because of this, an area of sediment accumulation may be anticipated in the regions for which there is a net landward transport (Pethick, 1984; Owen, 1986; Carter, 1988; Dyer, 1997).

4.5. Remarks and further work.

The importance of the present work and modelling relies in its potential to be used as a management tool for assessing the effects associated with bedload movement. In this context, the model should be used as a predictive tool only when satisfactory agreement is obtained between the field measurements and the assumptions and theory contained in the model. Further field verifications are needed in order to ensure accuracy and trust in the model. Thus, since the model is largely empirical in nature, a number of laboratory and field tests are still needed to describe quantitatively the transport of bedload.

The present bedload predictions can only be used for comparative or qualitative studies, providing the path in which further research efforts must be addressed in order reduce uncertainties. The latter are particularly necessary because of the dependence of transport rate on grain size. In addition, further work is needed to test the model effectiveness. These efforts must include a comprehensive survey that overcomes the lack of information related with sediment dynamics within the system. This must comprise: a temporal variation including spring and neap tides, and a well-spread spatial variation, including channels and shallow waters, ensuring representative data for the system. Also, surveys must include simultaneous measurements of both bed sediments and suspended sediments, including a complete profile through the water column, particularly near to the bed. Wash load is an important fraction of total sediment displacement in some areas, mainly in those close to the head of the system, in which direct research efforts must be addressed. Since the model relies on predicted velocity vectors, any substantial improvement in such predictions will result in a proportional improvement in sediment dynamics understanding.

Finally, the identification and characterization of fine grid littoral cells for sediment circulation will allow a better framework for shoreline management to be suggested.

CHAPTER 5

NET AND GROSS METABOLISM AND NUTRIENT BUDGET DYNAMICS

5.1 Introduction.

The Guaymas system is a multi-user area in which may exist potential eutrophication problems due to untreated industrial and urban water discharges into the marine environment. High inputs of nutrients and organic matter in coastal environments with restricted water exchange, generally increase primary production by pelagic and benthic algae and produce changes in community structure, anoxic conditions, and blooms of opportunistic species, including toxic microalgae (Elliott, *et al.* 1994). In this context, biochemical modelling, defined in this chapter as the combination between the mass balance calculation of a specific variable and known stoichiometric relationships resulting from biological processes, can be applied to studies related with fate and effects of contaminants, and eutrophication (Wulff, *et al.* 1990; Johnson, *et al.* 1995; Gordon, *et al.* 1996). Biochemical budgets can be seen as a valuable management tool, which summarises the existing information in order to provide an insight of the trophic status of the ecosystem. These budget models may produce exploratory predictions of the consequences of environmental changes, which are valuable in the coastal zone decision-making process (Johnson, *et al.* 1995). Biochemical modelling also leads to the development of more specific numerical models, mainly those related to local and low-scale processes, for instance, identifying areas, net producers of organic matter in which the resolution of sophisticated numerical models may be successfully applied.

5.1.1 Biochemical budget.

A budget model can be defined as a mass balance calculation for specific areas and time periods. This approach provides an estimation of the integrated ecosystem performance.

Their scope ranges from the global to the local scale, and the approach is able to compare other similar areas through known stoichiometric relationships, such as Redfield ratios (Redfield, *et al.* 1963; Jacinto, *et al.* 1998). The basic principle of the budgetary approach is the conservation of mass (Officer, 1976; Dyer, 1997). It is assumed that either water volume remains constant or that changes of water volume through time are known. Essentially, this principle is kept for water, sediment, conservative and non-conservative solutes throughout the calculations (Wulff, *et al.* 1990; Gordon, *et al.* 1995).

Biochemical budgetary approaches provide the first predictive values for management strategies. This approach is generally well-suited for systems where there is a lack of information or data are ill defined or collected for different purposes, and for relatively homogeneous systems where exchange processes are simple. Also, this modelling can be applied to a wide range of dynamic processes in the coastal zone, for instance the description of Water Exchange (WE), Nutrient Fluxes (ΔN) and Net Ecosystem Metabolism (NEM) at the land sea interface of coastal systems (Smith, et al 1991, 1997). However, budget models are limited in their ability to describe in detail the processes occurring within the system, and to allow refined predictions of the system functioning under new conditions. Therefore, often the spatial and temporal scale of the study needs to be increased in order to overcome high-frequency events such as tide and irradiation cycles, and phytoplankton and nutrient concentration patchiness (Wulff, *et al.* 1990; Gordon, *et al.* 1996; Smith, et al 1997).

This chapter regards the limitations of this approach and hold that its resolution relies heavily on the information that the model is expected to provide. Thus, in this study, biochemical budgets are refered to as stoichiometrically linked water-salt-nutrient budgets, and the study aims to question whether a simple budgetary approach using salt, phosphorus and nitrogen fluxes in relatively small compartments can provide an overall assessment of the nitrified and eutrophic status for the Guaymas Coastal System.

5.2 Methods.

5.2.1. Physiography of the Guaymas system.

The characteristics of this semi-enclosed hypersaline coastal lagoon, which imply strong salinity gradients and particular topographic features such as sub-basins, islands, variable cross-section channels, and areas semi-isolated by artificial barrages, allow the definition of physiographic units. The system is divided in two sub-basins, the Guaymas bay with the Guaymas City as main watershed, and the Empalme basin, which includes the Guaymas valley and Empalme valley as its watershed (Chapter 2.2). These physiographic features allow the use of a simple water and salt budget for water mix, and nonconservative materials budgets for nutrient dynamics and net ecosystem metabolism. Nutrient dynamics within a system can largely define the eutrophic status, hence the net ecosystem metabolism.

5.2.2 Boundary Definition.

An essential part of any modelling is to clearly define the spatial domain to be modelled, as well as the temporal scale of the model. These spatial and time scales must be strictly connected to the objectives and the questions that the model is expected to provide. Despite this, boundary conditions still remain a major uncertainty for modelling. As an initial attempt to choose an appropriate scale in time and space, aspects such as topography, bathymetry, salt gradient, nutrient gradient and human activities were considered.

Evaluating different scenarios.

In order to determine the best spatial and temporal scale, in which budgetary calculations can offer the best representation of the NEM and nitrified status of the system, five different scenarios were considered. The evaluation considers scenarios from one compartment to those with multiple boxes. These spatial differences were represented by the number and size of the boxes into which the system was divided. Temporal distinctions among scenarios were established regarding two averaged seasons (winter and summer) and monthly.

Scenario I.

The system is considering a simple box that exchanges with the adjacent sea. Boundary conditions are set up at the mouth of the system as stated in Figure 5.1. Table 5.1 summarises the physical characteristics for the compartment.

Scenario II.

For this scenario the system was divided regarding the two major sub-basins. The eastern part of the system, the Empalme basin (box 1), and western part that comprises the Guaymas basin (box 2). Both boxes were connected to the adjacent sea through the box labelled as MS, which is considered here and in the remaining scenarios only as a transitional box (Figure 5.2). Finally, box MS is connected with the adjacent sea, OS. Tables 5.2 summarise the physical characteristics of each box.

Scenario III.

The system was divided in four big compartments dependent on the major topographic characteristics of the system (Figure 5.3). The Empalme basin was subdivided in two boxes, El Estero el Rancho as Box 1 and La Laguna as Box 2. These two systems are connected by narrow and complex 10-metres channel, and divided physically by a barrage built to connect the Guaymas and Empalme cities. The entire Guaymas basin was labelled as Box 3. Box 3 and Box 2 were connected into the open sea through Box MS, which represents the mouth of the system (Figure 5.3). Tables 5.3 summarise the physical characteristics of each box.

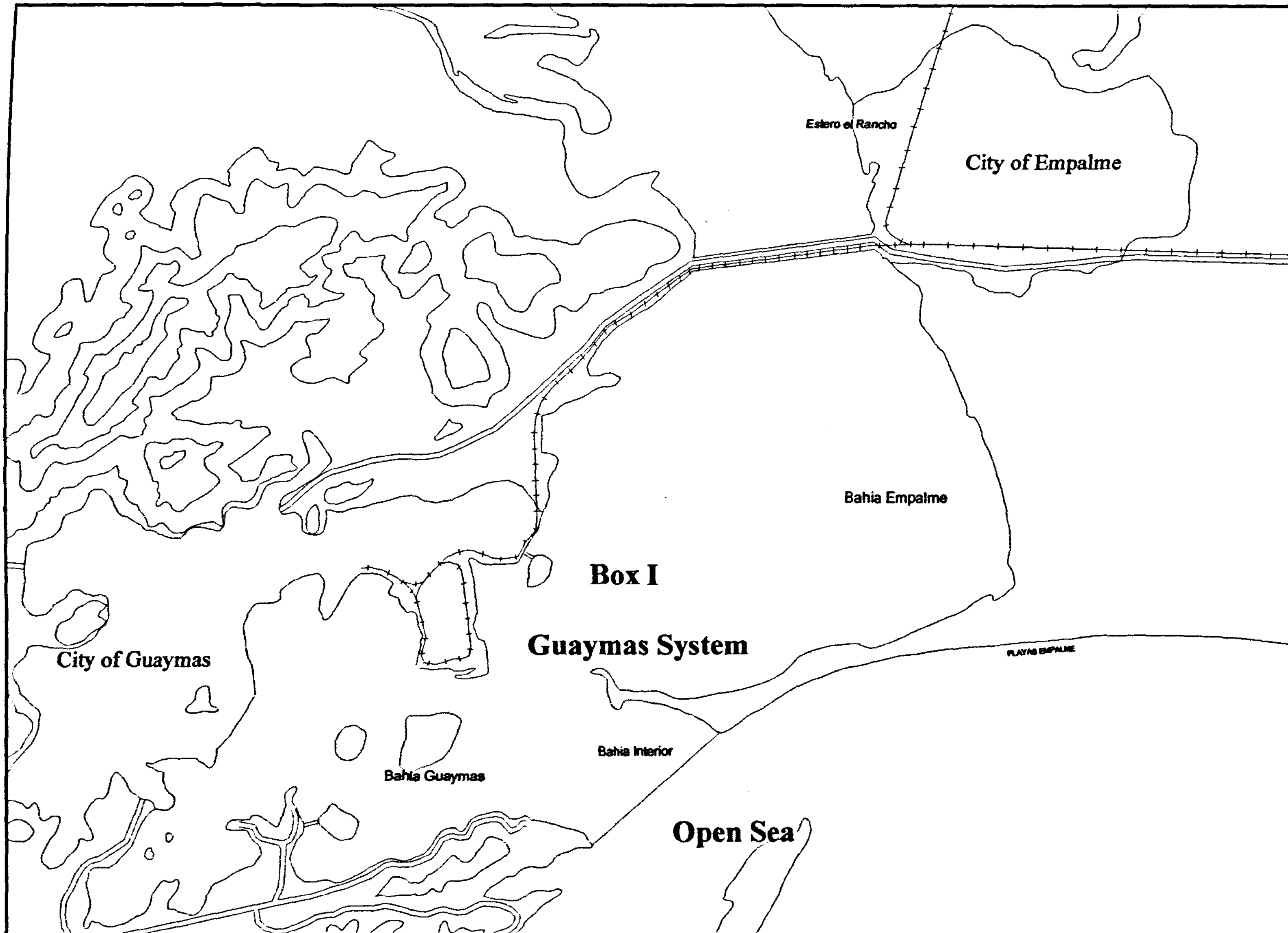

Figure 5.1. Map showing the compartment distribution for scenario 1.

Table 5.1. Input data used for scenario I. Topographic features of the Guaymas System.

	BOX 1
Box Area m^2	34367934
Box Depth m	3.468598
Box Volume m^3	119208560.7

Table 5.2. Input data used for scenario II. Topographic features of the Guaymas System.

	BOX 1	BOX 2	MS
Box Area m^2	23873590	7579939	2914405
Box Depth m	2.43	4.62	9
Box Volume m^3	57958653	35020263	26229645

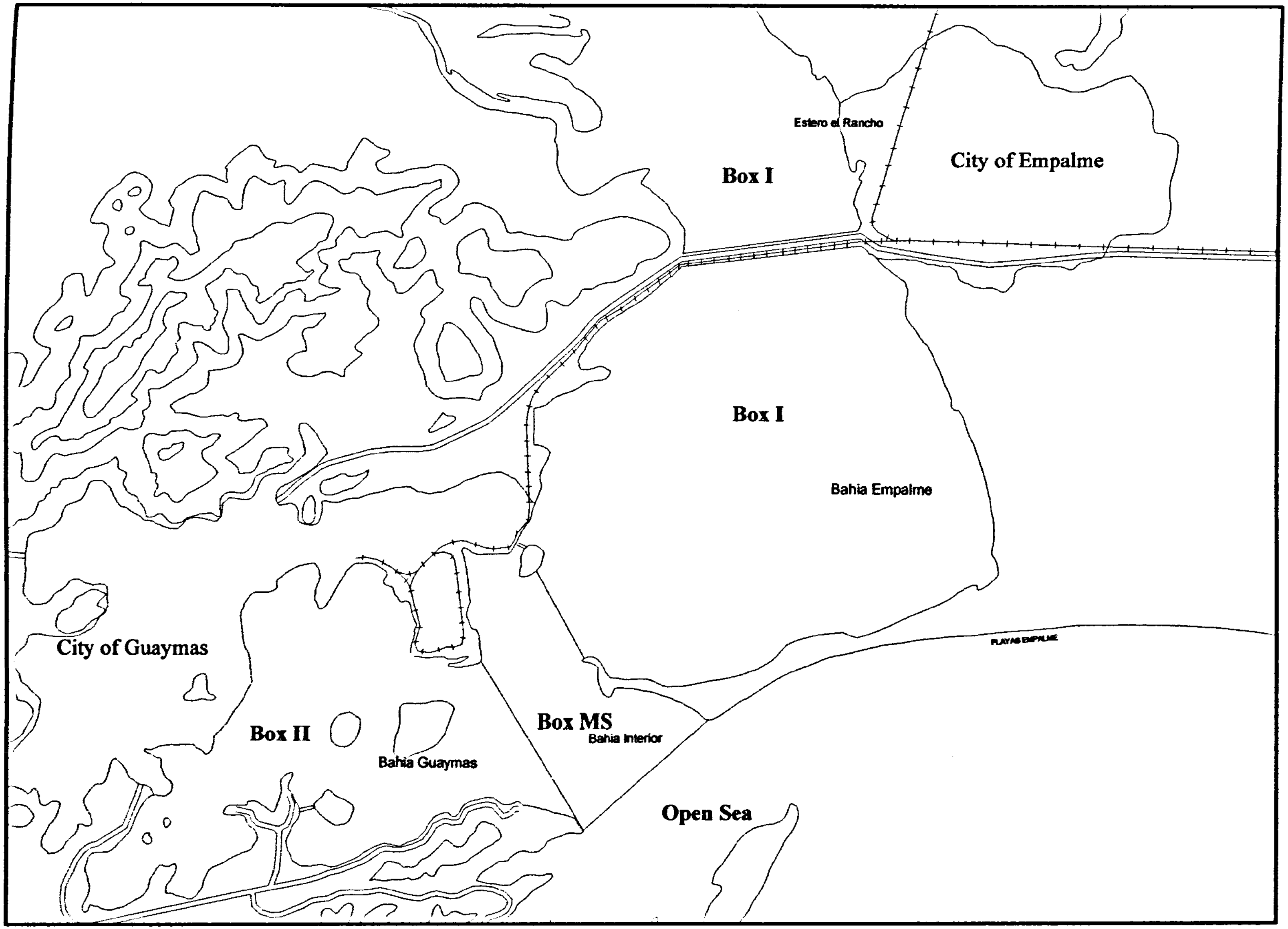

Figure 5.2. Map showing the compartment distribution for scenario 2.

Table 5.3. Input data used for scenario IV. Topographic features of the Guaymas System.

	BOX 1	BOX 2	BOX 3	MS
Box Area m^2	7590065	16283525	7579939	2914405
Box Depth m	1.2	3	4.620125	9
Box Volume m^3	9108078	48850575	35020263	26229645

Table 5.4. Input data used for scenario IV. Topographic features of the Guaymas System.

	BOX 1	BOX 2	BOX 3	BOX 4	MS
Box Area m^2	7590065	16283525	2099509	5480430	2914405
Box Depth m	1.2	3	2.5	5.4	9
Box Volume m^3	9108078	48850575	5253736	29766527	26229645

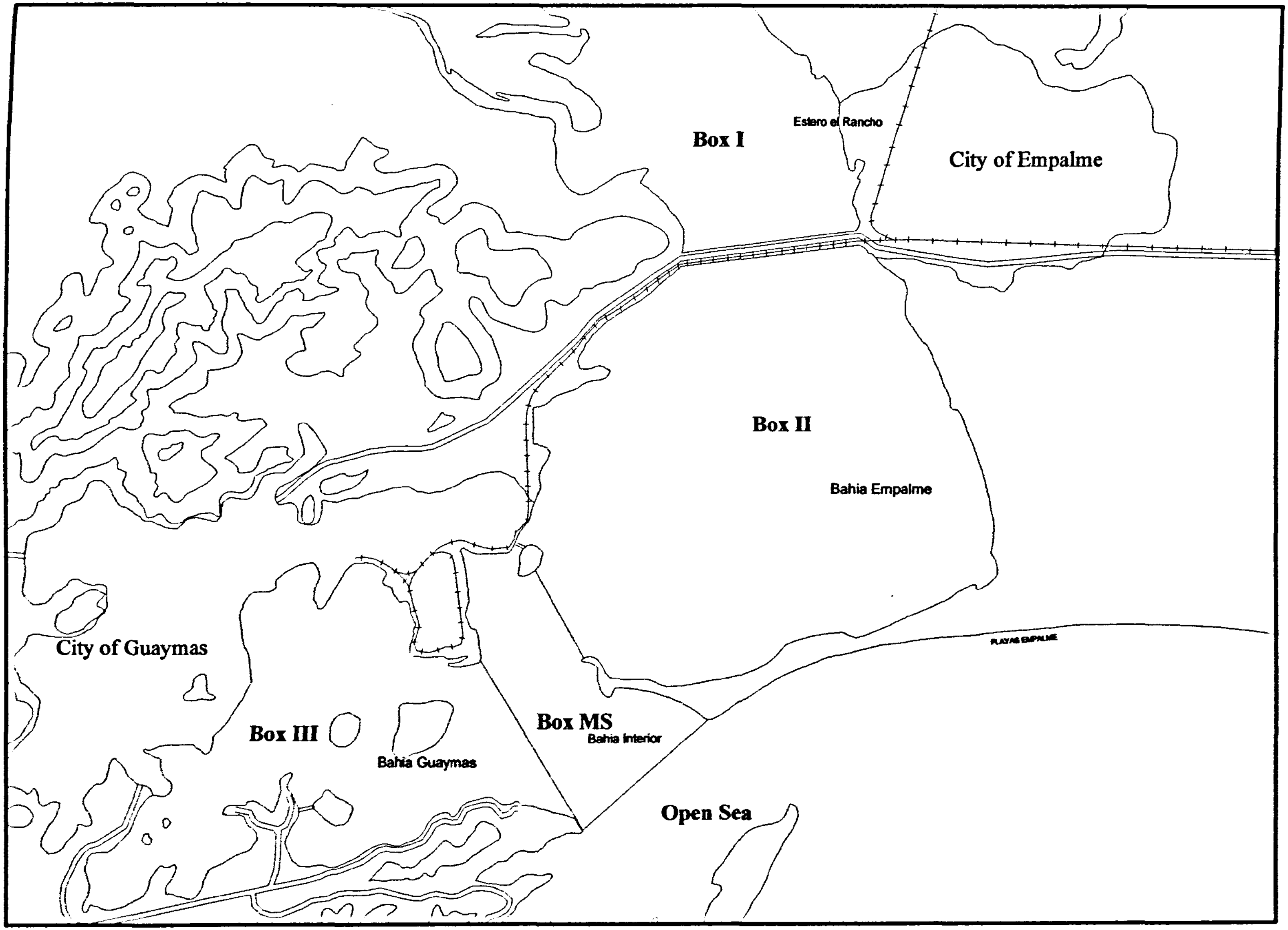

Figure 5.3. Map showing the compartment distribution for scenario 3.

PAGE(S) MISSING IN ORIGINAL

Scenario IV.

The system was subdivided into 5 boxes. From the previous scenario, Box 3 was divided into boxes 3 and 4. Box 3 represents the inner part of the Guaymas basin, whereas box 4 characterises urban and industrial activities. Box 4 was connected to the open sea through Box MS (Figure 5.4). Table 5.4 summarises the physical characteristics of each box.

Scenario V.

The system was subdivided into 7 boxes, again compartments within the Guaymas bay were subdivided according to activities in the area, highlighting those areas receiving majors inputs of organic matter. Box 3 represents the inner part of the Guaymas basin. Box 4 collects the drainage of two small bays within the system and thus is the basin receiving two minor seasonal streams. Box 5 characterises a heavily-polluted area from both industrial and urban discharges. Box 6 represents a transition zone that connect the box 4, 5 and MS (Figure 5.5). Tables 5.5 summarise the physical characteristics of each box.

5.2.3 Data.

Budget calculation data were taken from monthly surveys performed at 12 fixed stations from October 1996 to September 1997 (Chapter 2; Figure 1.3). For all the scenarios, station 5 was excluded, and considered as out-side of the present system.

Values for total Nitrogen (N) were computed as $NO_2 + NO_3 + NH_3$, and Phosphate (P) was computed as PO_4, nutrient analyses were performed through clean Flow Injection Techniques (Chapter 2). Phytoplankton biomass was obtains from Chlorophyll-*a* measurements (Parsons, *et al.* 1984). Salinity was calculated using an induction salinometer (Beckman RS10) and temperature using mercury thermometers. Monthly average precipitation and evaporation data were collected from the Comision Nacional

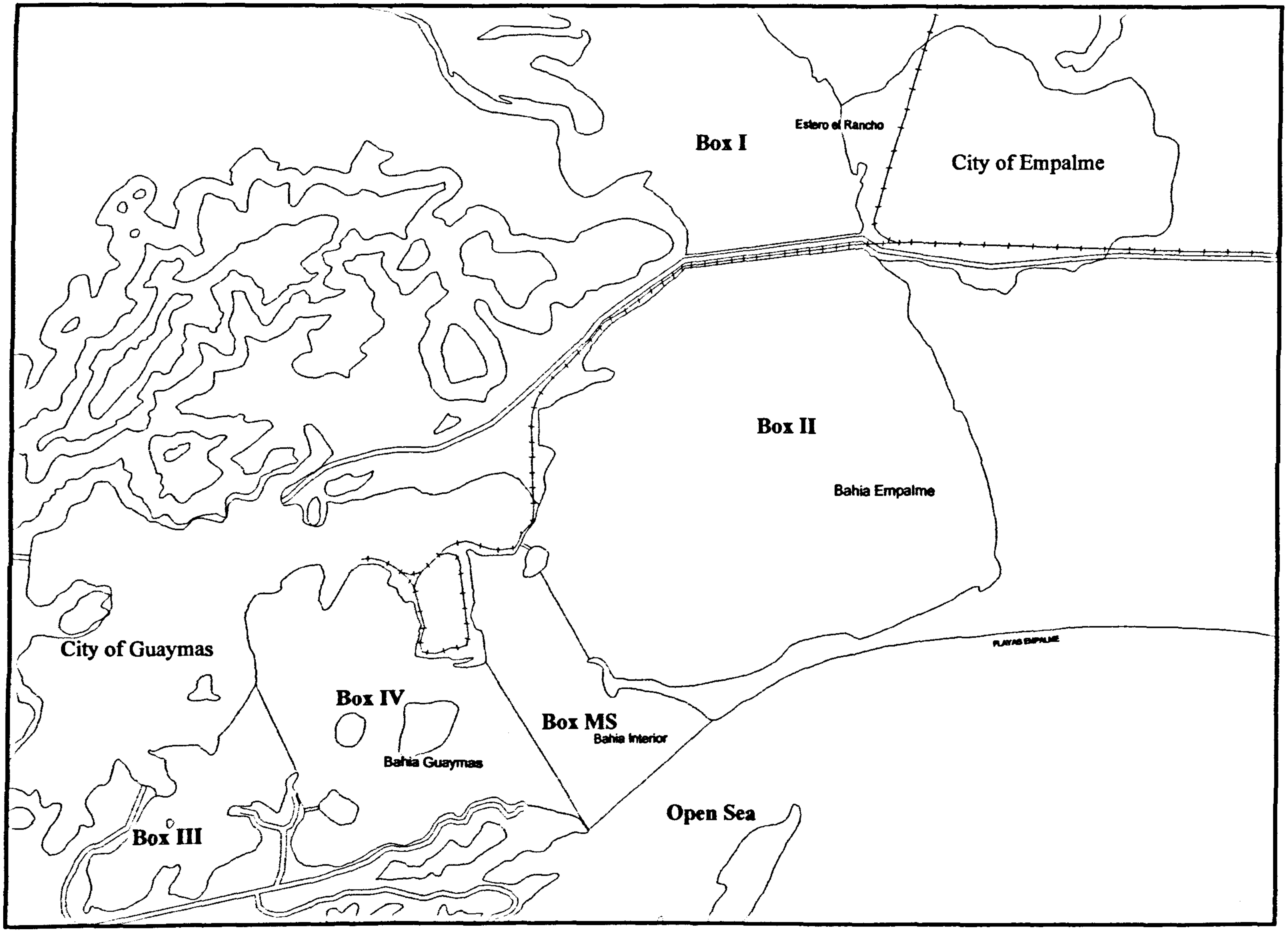

Figure 5.4. Map showing the compartment distribution for scenario 4.

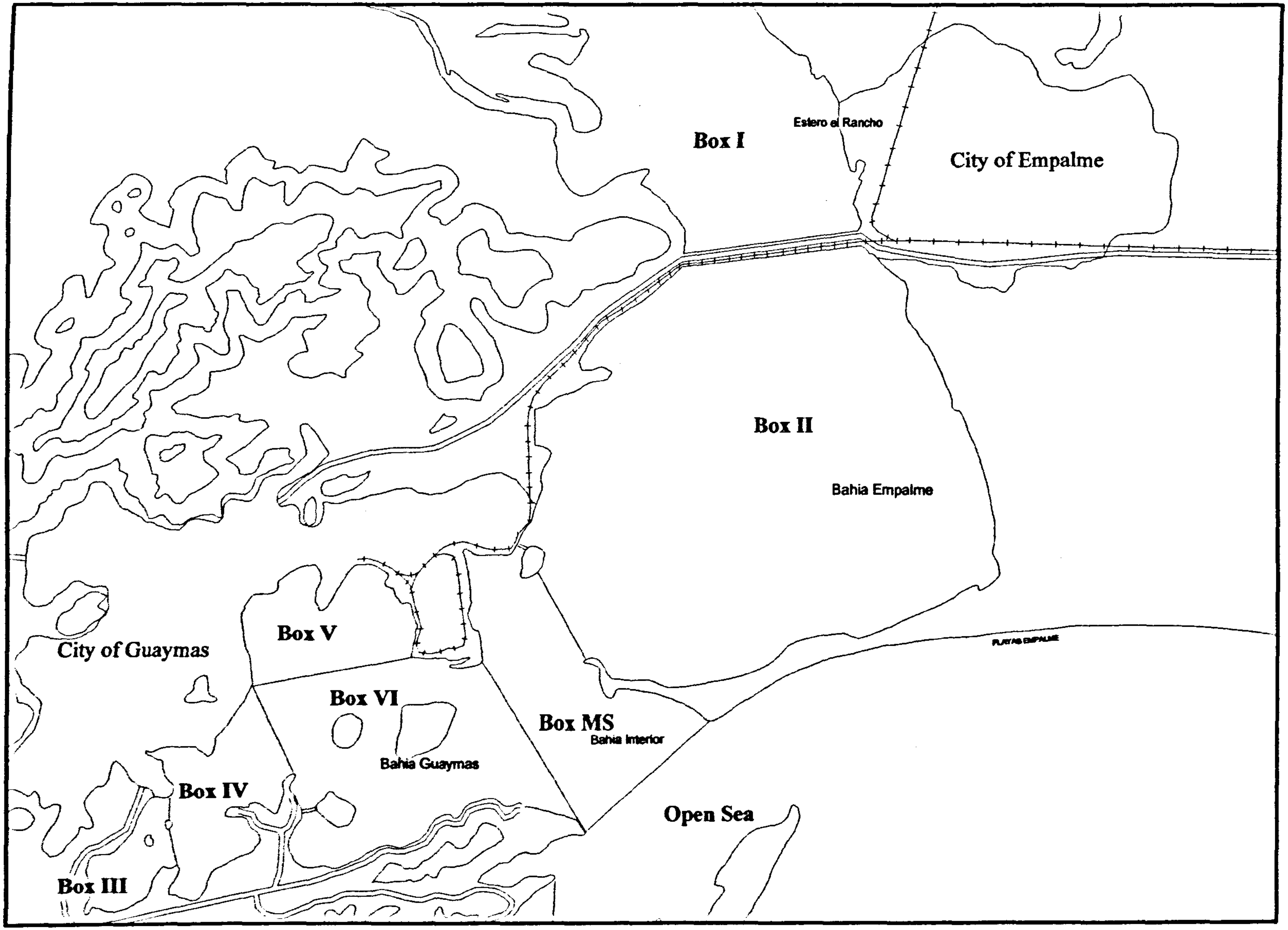

Figure 5.5. Map showing the compartment distribution for scenario 5.

Table 5.5. Input data used for scenario V. Topographic features of the Guaymas system.

	BOX 1	BOX 2	BOX 3	BOX 4	BOX 5	BOX 6	MS
Box Area m^2	7590065	16283525	592769	1506740	1553851	3926609	2914405
Box Depth m	1.2	3	2	2.7	4.5	5.8	9
Box Volume	9108078	48850575	1185538	4068198	6992195	22774332	26229645

del Agua (CNA), Empalme Station (Figure 1.2). Data for precipitation and evaporation during winter were not available for the 1996-1997 period, so, an historic 10 years average time series is assumed to be an approximation for that season.

5.2.4 Budgetary Approach.

The present work employs the stoichiometrically-linked water-salt-nutrient budgets (Wulff, *et al.* 1990; Smith, *et al.* 1991; Johnson, *et al.* 1996; Gordon, *et al.* 1996; Smith, *et al.* 1997), and incorporates the use of relatively small compartments. The model moves from a water mass balance, which considers the gain and loss of water across boundaries to a salt balance which, in turn, refines the water budget. The next step incorporates budgets for non-conservative materials e.g. P and N. Finally, the use of known stoichiometric relationships, such that stated by Redfield, *et al.* (1973) allows the calculation of N fixation/denitrification and net ecosystem metabolism.

5.2.4.1 Water Budgets:

The model is driven by the conservation of water mass, where water balance is represented by:

$$dV/dt = V_Q + V_P + V_G + V_O + V_{IN} - V_E - V_{OUT} \qquad (1)$$

here V_Q = rivers, streams and runoff, V_P = precipitation, V_G = groundwater, V_O = other sources, V_{IN} = advective inflow, V_E = evaporation, and V_{OUT} = advective output. For most coastal systems V_Q typically represents major freshwater contributor, however in desert coastal lagoons such as the Guaymas system V_Q can be considered as negligible (Chapter 2; Botello-Ruvalcaba and Valdez Holguin, 1997; Delgadillo-Hinojosa and Segobia-Zavala, 1997, Lechuga-Deveze, 1997). Thus, for this desert coastal lagoon the major freshwater source is V_P, which also is minimum throughout the whole year (annual average = 150 mm; CNA, 1998). Other sources, including V_G, are unlikely to represent a significant contribution. Hence the difference between V_{in} and V_{out} is likely to be the residual flow V_R driven by the water budget and to calculate V_R for each box:

$$V_R = V_{IN} - V_{OUT} = dV/dt - V_Q - V_P - V_G - V_O - (-V_E) \qquad (2)$$

In order to assume a steady state ($dV/dt = 0$) in equation 2, it is necessary to integrate those processes that drive water exchange. The major processes responsible for water exchange within the system can be assumed to be tide and wind-induced currents; density-driven currents, in spite of the strong salinity gradients, are unlikely to be a major contributor given the complex bathymetry of the system (Chapter 3). For this budget approach, it is assumed that for periods longer than a tide cycle the difference between the water inputs and outputs driven by currents will lead to 0, i.e., assuming steady state. In the present work, the highest survey frequency was monthly, which comprised a two spring-neap tide cycle modulation. Regarding the above, equation 2 can be rewritten as:

$$V_R = -V_P - (-V_E) \qquad (3)$$

5.2.4.2 Salt Balance and Mixing Volume.

Mixing is a major physical oceanography processes taking place through circulation, advection and diffusion processes (Officer, 1976). These fluxes carry water constituents into and out of the computational domain. Exchange fluxes budgets can be calculated through the addition of the volume fluxes multiplied by the salinity of each, as:

$$dV_1S_1/dt = V_QS_Q + V_PS_P + V_GS_G + V_OS_O + (-V_E S_E) + V_RS_R + V_XS_2 - V_XS_1 \quad (4)$$

Where S_1 and V_1 are the inside-box salinity and volume, S_2 represents the outside- box salinity (Figure 5.1). S_R is the salinity of the residual flow and represents the boundary between inside and outside the box, and is defined as the average between S_1 and S_2. Mixing volume, V_X, represents the exchange between compartments and is defined by the resultant ratio from the product of residual salinity and the residual volume divided by the difference in saline between inside and outside-box (Equation 6). Assuming steady state ($dV/dt = 0$) and considering that all freshwater sources are likely to have salinity near 0, equation 4 can be rewritten as:

$$0 = V_R S_R + V_X(S_2 - S_1) \qquad (5)$$

The mixing volume V_X is then:

$$V_X = -V_R S_R / (S_2 - S_1) \qquad (6)$$

Considering the Guaymas system as a well-mixed system (Chapter 2), an approximation to the residual time (τ) can be calculated as equation 7. In a coastal system, residual time results from complex interactions among the different transport fields, therefore τ is expected to be different from the observed residual time. Considering the above, the calculated τ may alternatively be held in terms of residual rate rather than strictly residual time. Then the residual rate can be computed as:

$$\tau = V_{SYS} / (V_X + V_R) \qquad (7)$$

here V_{SYS} is the total volume of the inside-box (Figures 5.6a and 5.6b).

5.2.4. Budgets of Nonconservative Materials.

Non-conservative materials are likely to be represented by sources similar to water and salt budgets, but, other sources including wastewater discharges in some systems are important (Forsberg, 1994; Jacinto, *et al.* 1998). Fluxes of non-conservative materials are calculated in a similar way to water and salinity fluxes:

$$dV_1Y_1/dt = V_QY_Q + V_PY_P + V_GY_G + V_OY_O + (-V_E\ Y_E) + V_RY_R + V_XY_2 - V_XY_1 + \Delta Y \qquad (8)$$

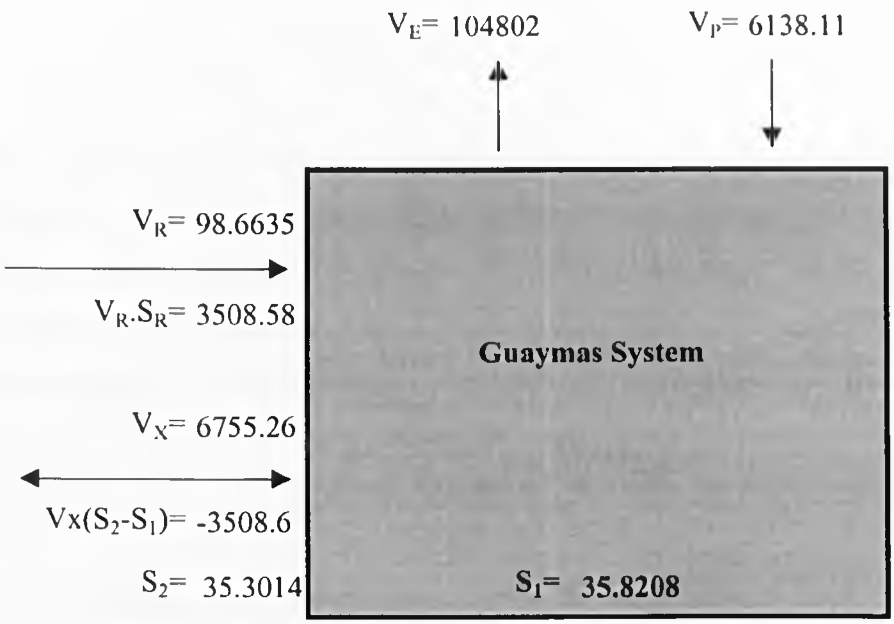

Figure 5.6a. Steady-state water and salt budgets for the Guaymas system. Water fluxes in 10^3 m^3 d^{-1}, Salt fluxes in 10^3 kg d^{-1}. The box represents the winter season.

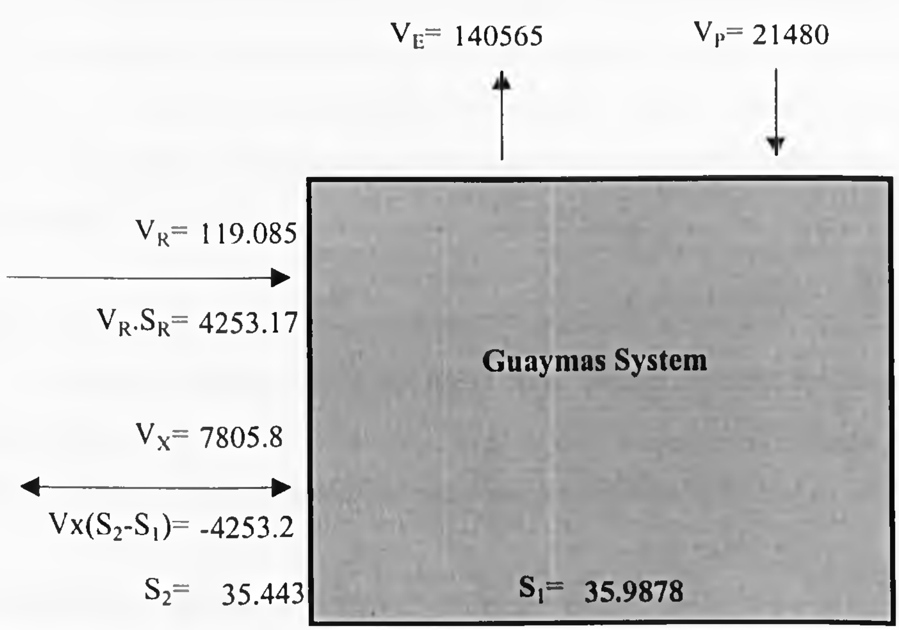

Figure 5.6b. Steady-state water and salt budgets for the Guaymas system. Water fluxes in 10^3 m^3 d^{-1}, Salt fluxes in 10^3 kg d^{-1}. The box represents the summer season.

Where Y_1 and Y_2 represents non-conservative material concentrations inside and outside the box, Y_R is the residual amount of the element Y and represents the concentration at the open boundary, this value is defined as the average between Y_1 and Y_2, and ΔY is the net internal source or sink (non-conservative material flux) of element Y. Assuming a steady state ($dV_1Y_1/dt = 0$) and that some sources are 0, ΔY is given as:

$$\Delta Y = -V_QY_Q - V_GY_G - V_OY_O - V_RY_R + V_X(Y_2 - Y_1) \quad (9)$$

5.2.4.4 Stoichiometric C:N:P linkages and Net System Metabolism.

The difference between production and oxidation of organic matter of a known relation C:N:P is supported by the primary reaction of dissolved inorganic P. It is, the C:P ratio of the organic particulate material is known (as stated by Redfield for instance) and the ΔDIP multiplied by this ratio, it represents a measure of the net ecosystem metabolism (Smith, *et al.* 1991). These arguments necessarily include a series of assumptions that must be considered carefully for each system. For the present system, these assumptions are described as follows:

Redox conditions. Redox condition highly determine adsorption and desorption of P from sediments, therefore this approach may be particularly sensible for systems characterised by eutrophic conditions. In eutrophic environments redox, conditions are likely to mediate phosphorus desorption from inorganic particles.

Phosphorus speciation. Although phosphorus can be present in the marine environment in a variety of dissolved and particulate forms, dissolved forms are more likely to be assimilated by primary producers. The major chemical speciation for dissolved phosphorus is orthophosphate ions, which comprise nearly 99 % of the total dissolved phosphorus (Reley and Chester, 1971). Dissolved Organic phosphorus (DOP) is related with decomposition, excretion products from marine organisms, and in coastal areas may be associated with organic pollution discharges. DOP may constitute a major proportion of the Total Dissolved Phosphorus (TDP), but this is limited to some particular areas mainly those related to pollution sources. Thus, very often, DOP is very small compared with DIP, as in the case of Tomales bay, a coastal ecosystem in the North American Pacific coast (Riley and Chester, 1971; Smith, *et al.* 1991; Gordon, *et al.* 1996). Particulate Phosphorus (PP) can be both organic and inorganic, and although this PP fraction must be considered, the total phosphorus in seawater may not be directly available for primary producers. Broadly, both TDP and PP can be more related with phosphorus regeneration or phosphorus turnover, which in turn will make available phosphorus for primary producers (de Jonge, 1990). Hence, it is valid to assume a small direct contribution of these fractions to primary producers.

Metabolic processes and stoichiometry. Organic carbon production in any ecosystem is the result of several metabolic processes. Primary producers in any system are characterised by phytoplankton and benthic macro and micro algae among others, which presents a variable/patchy distribution and variables C:P uptake ratios (Smith and M. Atkinson, 1980; Atkinson and Smith, 1983; de Jonge 1990; Johnson, *et al.* 1995; Jacinto, *et al.* 1998). The present work assumes that phytoplankton represents the major component responsible for the primary production of the system, hence the Redfield C:P ratio approach is utilised. This assumption has been recently successfully applied in budgets modelling for hypersaline coastal lagoons within the Gulf of California (Botello-Ruvalcaba and Valdez-Holguin, 1997; Delgadillo-Hinojosa and Segovia-Zavala, 1997; Lechuga-Deveze, 1997). Finally, as stated by Gordon *et al.* (1996), unidirectional stoichiometry of the reaction involving organic and inorganic carbon is has to be assumed for C:N:P linkages.

5.2.4.5 Nitrogen fixation-denitrification.

The flux of non-conservative materials ΔP and ΔN are used to estimate the apparent rate of nitrogen fixation minus denitrification (N_{fix}-N_{denit}) as the difference between observed and expected ΔN production (ΔN_{obs}-ΔN_{exp}), where ΔN_{exp} is the Redfield N:P molar ratio (16) of the reacting particulate organic matter.

$$(N_{fix}-N_{denit}) = \Delta N_{obs}-\Delta N_{exp} = \Delta N_{obs}- (N:P)_{part} \times \Delta P \qquad (10)$$

5.2.4.6. Net Ecosystem Metabolism.

The metabolism of the system is given by the integration of several processes and a measure of these integrated processes can be obtained through the use of Phosphorus fluxes (Gordon, *et al.* 1996). Certainly, assuming that most conversion between dissolved and particulate phosphorus involves organic material, the ΔP multiplied by the C:P ratio of the reacting organic matter is used to estimate Net Ecosystem Metabolism (NEM) or production - respiration (p -r) (Smith, *et al.* 1991; Gordon, *et al.* 1996) . This work assumes the Redfield C:P ratio approach (106:1) in order to obtain ΔDIC. However, this assumption must be carefully reconsidered, especially for those areas where processes other than those related with phytoplankton control phosphorus availability, absorption and disorption.

$$(p - r) = -(C:P)_{part} \times \Delta DIP \qquad (11)$$

It is likely that, in some areas of the Guaymas systems, especially those heavily-polluted, phosphorus availability is dominated by load discharge composition but wever whether or not the Redfield approach is a fair representation of NEM is matter of further discussion later in this chapter.

5.3 Results and Discussions.

For the purpose of the following description, the fluxes between individual compartments are shown in total mass units, while comparisons between compartments and other systems are scaled to rate per unit area. The discussion of scenario 1 is focused on the exchange between the system and adjacent sea. For the other scenarios, discussion is focused on the exchange between compartments.

5.3.1 Scenario 1.

Discussion is focused on the interaction between the system and the adjacent sea, and the NEM with other systems world-wide.

Water budget. In this system, evaporation processes exceed freshwater inputs, where precipitation represents the only source of fresh water. The residual volume, V_R, shows a net inward movement of water through the whole year (Table 5.6; Figures 5.6a and 5.6b). This inward water flux compensates the loss of water by evaporation, which increases during the summer months. The higher fluxes coincide with the period of higher evaporation rate, during the months of June-July (Table 5.6).

Salt budgets. There is a net salt delivery from the system to the adjacent sea during both seasons, winter and summer (Figures 5.6a and 5.6b). Thus, the system exports to the adjacent sea around 3508.6 $x10^3$ $kg.d^{-1}$ during winter and 4253.2 $x10^3$ $kg.d^{-1}$ during summer. This salt exchange is carried out through different mixing processes among the Guaymas system and the adjacent sea represented by the mixing volume, *Vx* (Figures 5.6a and 5.6b). This analysis highlights the hypersaline characteristics of the system, which operates as an evaporation basis, and therefore a source of salt.

Non-conservative budgets. Within this approach, *Vx* is considered to be the main pathway for non-conservative fluxes between the system and the adjacent sea. The

Table 5.6. Summary of budget properties for the Guaymas System.

	Oct-Nov	December	January	Februar	March	Winter	April	May	Jun-Jul	Aug-Sep	Summer
$V_R\,(10)^3 m^3 d^{-1}$	98.6634922	98.6634922	98.66349	98.663492	98.66349	98.66349	130.0483	130.162743	169.0765	119.0849	137.0931
$Vx\ (10)^3 m^3 d^{-1}$	4934.63854	5578.147575	8958.331	11261.152	6391.611	6755.257	5004.819	6871.15992	7944.6	7805.797	6729.357
τ days	23.6839673	20.99921229	13.16204	10.493882	18.36726	17.39276	23.21551	17.0265772	14.6923	15.04231	17.36102
ΔP mol.$m^2 d^{-1}$	0.19305892	0.004827669	0.632597	0.4317688	-0.272388	0.143037	0.126058	0.10107494	0.202143	-0.020121	0.105695
ΔN mol.$m^2 d^{-1}$	-0.0740274	0.229051556	-2.705069	-1.325203	-0.253255	-0.585944	0.837393	2.57314654	0.551714	2.373598	1.539375
N(*fix-denit*) mol.$m^2 d^{-1}$	-3.1629701	0.077242699	10.12156	-8.233504	4.104946	-2.874539	-1.179539	0.9559475	-2.68258	2.695542	-0.151748
NEM (p-r) mol.$m^2 d^{-1}$	-20.464245	-0.51173288	-67.05531	-45.76749	28.87308	-15.16194	-13.36217	-10.713944	-21.4272	2.695542	-11.20369

Vx = Mixing volume
t = Residential time
ΔP = Nonconservative flux of P
ΔN = Nonconservative flux of N
N(*fix-denit*) Difference between nitrogen fixation and denitrification
NEM (p-r) = Net Ecosystem Metabolism (production - respiration).

dissolved inorganic phosphorus fluxes within both seasons show a net P production, and therefore a net export of phosphorus from the system to the adjacent sea (Figures 5.7a and 5.7b). Phosphorus production within the system may be the result of the multiple industrial and urban effluents that discharge into the system. Nutrient load from industrial and urban discharges increase phosphorus concentrations within the system. However, other processes such as remineralization in the water column and sediment, must be considered; especially if the assumption of low phosphorous release from sediments may not hold for sediments associated with organic matter inputs from urban and industrial discharges.

In winter, the system delivers 49150 mol.d^{-1} of phosphorus, with a slightly smaller amount during summer, reaching 3632.5 mol.d^{-1}. At the monthly scale, March and August were the only months where the system operated as a net sink of phosphate. During these two months the average concentration of phosphate was slightly less than the concentration of the adjacent sea. Up-welling events may have affected E1 during winter (For March) and phosphate oxidation and fixation processes within the system during summer (August-September) may drive phosphate fluxes during these months. However, there are insufficient data to support the above arguments about the area outside the system. The generation of that information was beyond the scope of the present study.

Nitrogen fluxes show a different seasonal pattern as, during winter, the system appears to be a net sink of nitrogen, importing 20138 mol.d^{-1} (Figure 5.8a). For summer, this pattern is reversed, and the system is a net source of nitrogen, exporting 52905.2 mol.d^{-1} (Figure 5.8b). During winter the negative ΔDIN is driven by high DIN concentrations in the open sea. This differentiation in ΔDIN among seasons has been identified for other systems within the Gulf of California, and has been associated with the seasonal shift of the mass of water (Delgadillo-Hinojosa and Segovia-Zavala, 1997). Seasonal variation in the mass of water within the Gulf of California is characterised by cold water, rich in nutrients during cold months and warm oligotrophic water during summer (Badan-Dagon, *et al.*

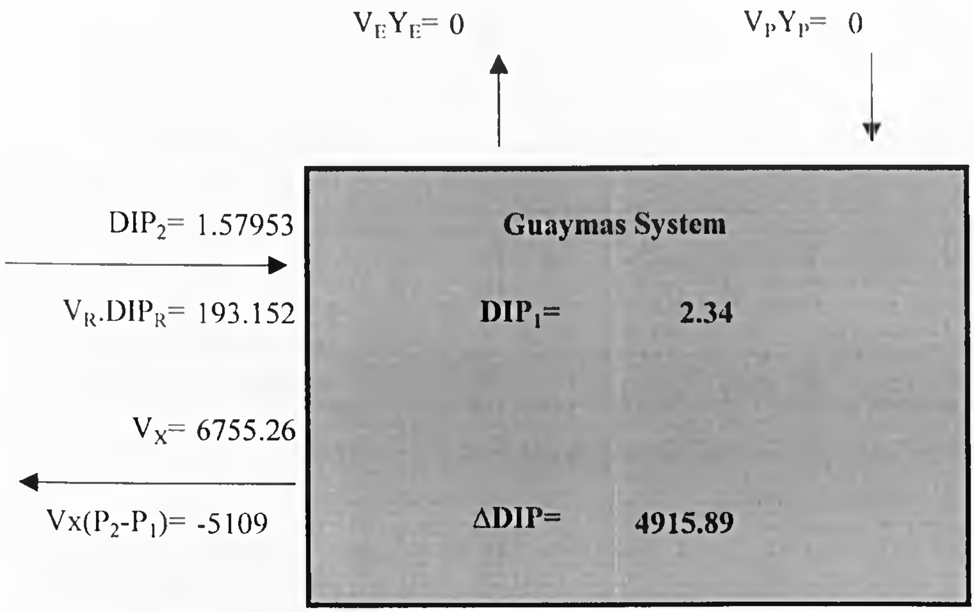

Figure 5.7a. Steady-state dissolved inorganic phophorus budget for the Guaymas system, during winter season. DIP concentrations are in $mmolm^{-3}$, Nutrient fluxes $mol.d^{-1}$.

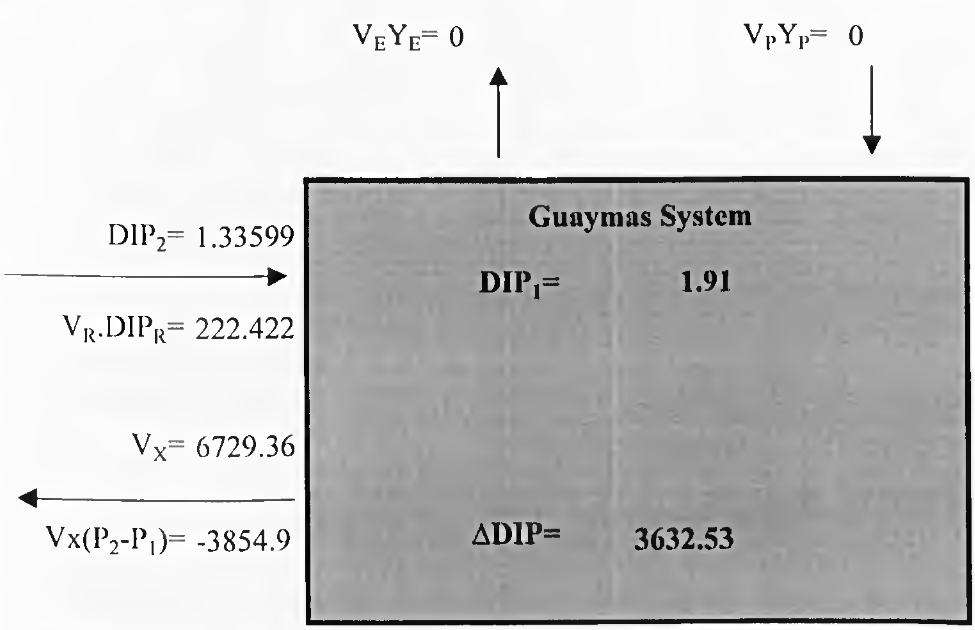

Figure 5.7b. Steady-state dissolved inorganic phophorus budget for the Guaymas system, during summer. DIP concentrations are in $mmolm^{-3}$, Nutrient fluxes $mol.d^{-1}$.

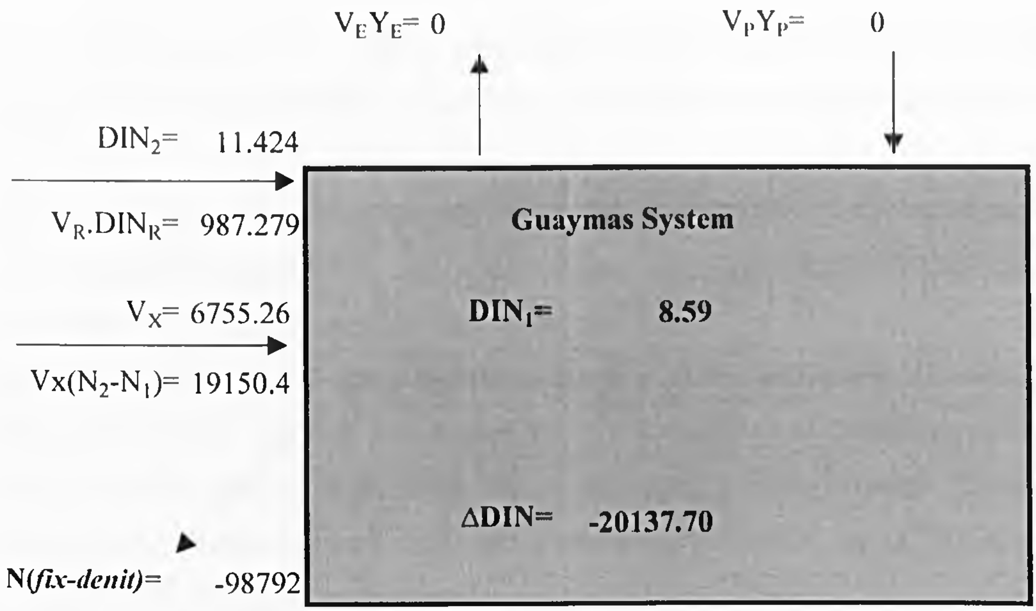

Figure 5.8.b. Steady-state dissolved inorganic Nitrogen budget for the Guaymas system, during winter season. DIN concentrations are in mmolm^{-3}, Nutrient fluxes mol.d^{-1}, and N(fix-dent) mol.d^{-1}.

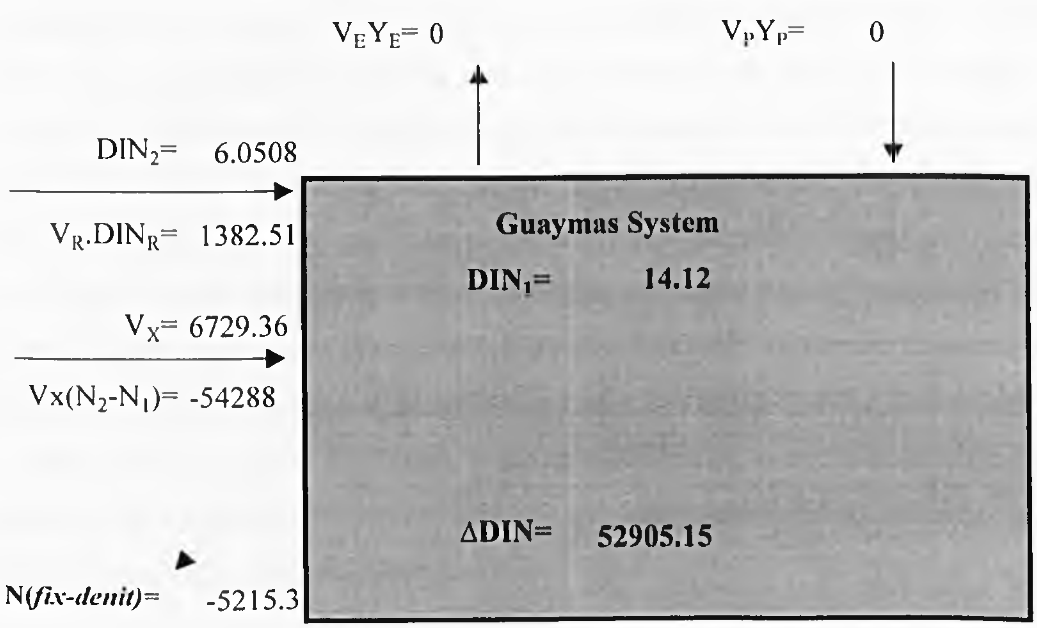

Figure 5.8.b. Steady-state dissolved inorganic phophorus budget for the Guaymas system during summer. DIN concentrations are in mmolm^{-3}, Nutrient fluxes mol.d-1, and N(fix-dent) mol.d^{-1}.

1985; Gaxiola-Castro, *et al.* 1995). Thus, during winter, nitrogen seems to be stored through burial processes or/and N uptake from production by benthic and pelagic algae.

Within seasons, December was the only month that did not follow the seasonal pattern, during this month appears to be a source of nitrogen rather than a sink, this may indicate that nitrogen is not production-limiting within the system for this month. A possible explanation for this pattern could be the composition of the load discharge within the system; December historically represents a peak in the activity of the fishing industry, which is a major contributor to the discharges within the system. However, it was not quantitatively possible to corroborate this correlation, given the lack of information coming from the fishing industry sector.

Nitrogen fixation-denitrification. The apparent rate of nitrogen fixation minus denitrification is assumed to be the difference between the observed and expected DIN production (ΔDIN_{obs} - ΔDIN_{exp}), where ΔDIN_{exp} is DIP multiplied by the N:P ratio of the reacting particulate organic matter, in this case the Redfield ratio (Section 5.2.4.5). The C:N:P ratio change depends upon the source of reacting particulate organic matter, for instance, areas dominated by animal wastes have a moderately low N:P ratio compared with the Redfield ratio (Flores-Verdugo and de la Lanza-Espino, 1997), whereas in systems dominated by organic discharges, the N:P is somewhat similar (eg. 15:1; Jacinto, *et al.* 1998;). In the Guaymas system, it is difficult to know the exact composition of the reacting organic matter given the diversity of it, therefore, it is assumed as appropriate that the N:P ratio of decomposition of organic matter is near the Redfield ratio (Smith, *et al.* 1991; Smith, *et al.* 1997; Jacinto, *et al.* 1998). Thus, a more valid result may be reached by characterising the C:N:P ratio for the different sources of reacting organic matter, although this requires further study.

Denitrification was a dominant process during winter and summer, representing the main loss of nitrogen in the Guaymas system (Figures 5.8a and 5.8b). Within seasons the N(fix-denit) alternates between the months when fixation was dominant and months characterised by the denitrification processes (Table 5.6). If a lower N:P ratio for the decomposition of organic matter is assumed, as suggested by Jacinto, *et al.* (1998), on a seasonal basis, only a small change in the magnitude of the denitrification processes will be observed, while on a monthly basis, changes from fixation to denitrification processes may be observed.

Net Ecosystem Metabolism (NEM). The Guaymas system can be regarded as a net heterotrophic system during both winter and summer (Table 5.6). The system maintains a positive ΔDIP through the year, hence also maintaining heterotrophic characteristics. Thus, the system seems to oxidise more organic matter that it produces. It is assumed that a large proportion of the reacting organic matter comes from industrial and urban discharges (Chapter 1; Figure 1.3), and therefore the system is strongly heterotrophic as should be expected for a system heavily-loaded with organic and inorganic matter from sewage discharges. Within seasons, the system became net autotrophic for March and slightly autotrophic during August-September (Table 5.6). As indicated for phosphates, upwelling events during winter and P-fixation during summer may be responsible for a important proportion for the NEM during these two months.

Table 5.7 shows a comparison between non-conservative materials fluxes, N(fix-denit) and NEM-scaled per unit of area for different systems world-wide. The NEM for the Guaymas system fits within the range of NEM computed for other systems world-wide, using the same budgetary approach. This gives support for the results computed in the present work. Thus, the system presents a NEM approximately –4811.27 $mmolm^{-2}d^{-1}$ above other values calculated for coastal ecosystem within the Gulf of California and Mexican Pacific coast, and below the 18000 $mmolm^{-2}d^{-1}$ calculated for the Manila Bay, an ecosystem somewhat similar to that analysed here.

Table 5.7. Nonconservative fluxes for P and N, and stoichiometric calculations for the Guaymas system other coastal systems. Stoichiometric linkages for C:N:P are obtained assuming the major proportion of production results from organic matter oxidation and using the Readfield ratio approach. The anterior assumption does not apply for Shark Bay where production is dominated by benthic algae and C:N:P ratio of 550:30:1 is applied.

System	Area ($10^6.m^2$)	Latitude	ΔDIP $mmolm^{-2}y^{-1}$	ΔDIN $mmolm^{-2}y^{-1}$	N(fix-denit) $mmolm^{-2}y^{-1}$	NEM (p-r) $mmolm^{-2}y^{-1}$	Authors
Tomales Bay, USA.	16	38 N, 123 W	34	237	960	-3604	Smith, *et al*. 1991.
Tokio, Japan.	1000	35.5 N, 139.9 E	-110	-2300	-540	11660	Smith and Yangi, 1996.
San Quintin, BC, Mexico	42	30,27N, 115,58W	-45	-80.3	-754.33	-3650	Camacho-Ibar, *et al*. 1997.
Guaymas, Sonora, Mexico	**34**	**27.9 N, 110.88 W**	**45.39**	**-134.63**	**-552.30**	**-4811.726603**	**The present study**
La Paz, BCS, Mexico.	45	24,08N, 110,22W	-16.42	21.9	273.75	1642.5	Lechuga-Deveze. 1997.
Manila Bay, Philippines	1700	15N, 121E	90	240	-1200	-18000	Jacinto, *et al*. 1996.
Shark Bay, Australia.	13119	26 S, 114 E	-1.46	-0.73	36.5	830	Smith and Atkinson. 1983.

5.3.2. Scenario 2.

The discussion here considers the exchange of properties between the two main sub-basins and their variability at seasonal and monthly level.

Salt and water budget. Since evaporation and precipitation drive water budgets in the whole system, the difference in V_R between compartments will be determined by their area. Certainly, Box 1 registered higher V_R than Box 2 through the whole year (Figures 5.9a and 5.9b). The evaporation process is dominant in the system, thus, there is a net flux of the mass of water into the two compartments that balance loss of water by the evaporation process. The above process is enhanced during summer, when high evaporation rates increases V_R values.

There is a net flux of salt toward the adjacent sea from both compartments, where compartment 1 contributes 75 % percent of the total (Figures 5.9a and 5.9b). The low proportion of salt exported from box 2 can be explained firstly by the small area of this box, but also through the fact that this box receives different inputs of water from different sources. Unfortunately, because of the large amount of small intermittent discharges, including industrial and domestic, it was not possible to determine their volume. The influence of these sources is more evident on a monthly basis when for March, May and June-July, compartment 2 presents an average salinity below compartment MS, against which it is balanced. This negative salinity gradient produces a negative Vx , which indicates that either salt is delivered into box 2 or it is diluted within the compartment. Another likely explanation may relate to the distribution of the survey stations within compartment 2, where some stations may not be the best representatives of the whole area in which these are located, but instead, they may be strongly-affected by small water source. This effect is magnified by the representation of the station within the system. It is important to highlight that either the lack of information about the volume of the load and water discharged and/or the representation of the station within the system may affect the interpretation of the water and salt budget for the

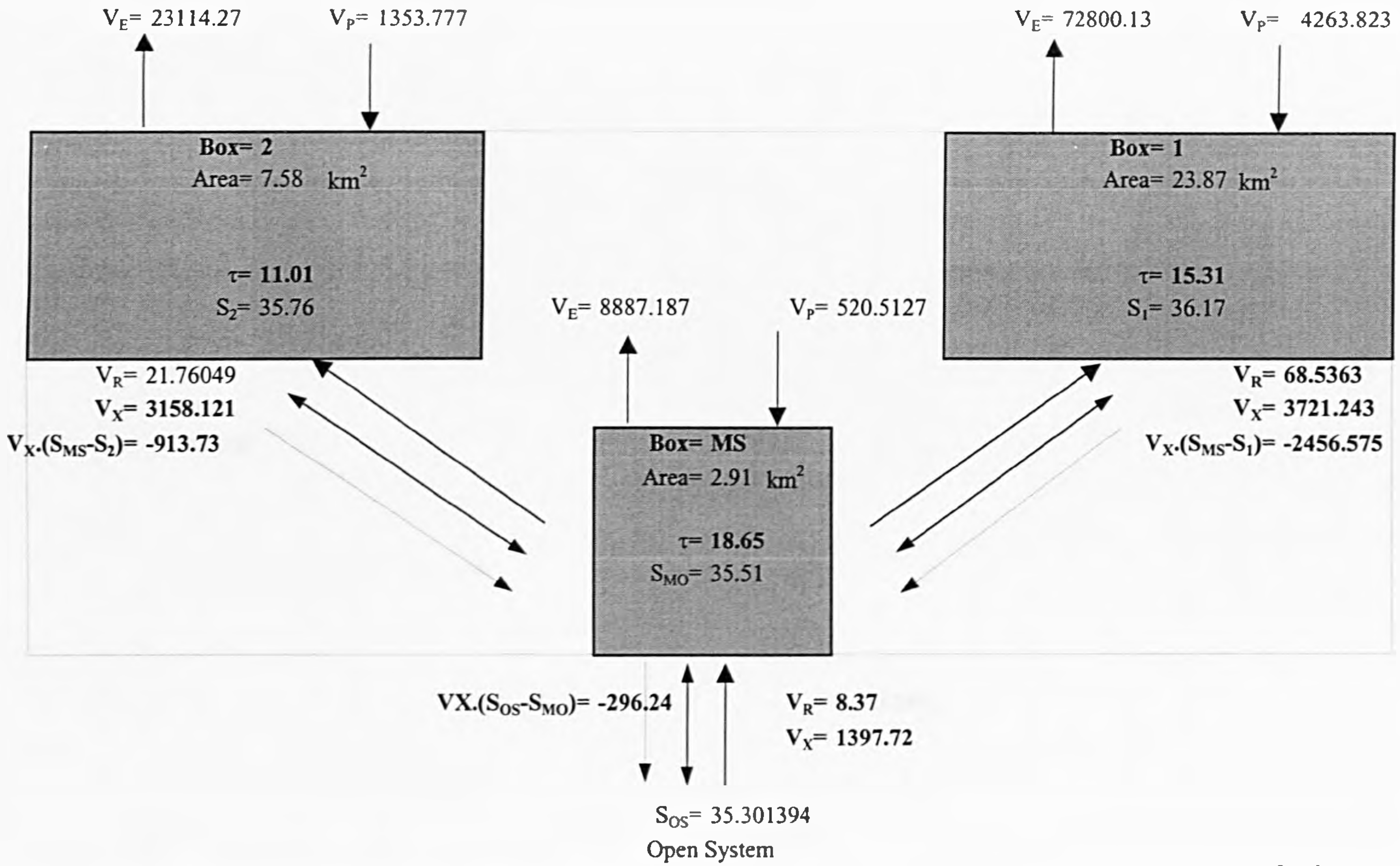

Figure 5.9a. Steady-state water and salt budgets for the Guaymas system, during winter season. Water fluxes in 103 m^3 d^{-1}, Salt fluxes in 10^3 kg d^{-1}. Arrows at the top of the boxes represent input and outputs from evaporation and precipitation processes; the wide head arrows represent the advective flows between compartments; the dashed arrows represent salt delivery; the double head arrows represent the mixing between compartments.

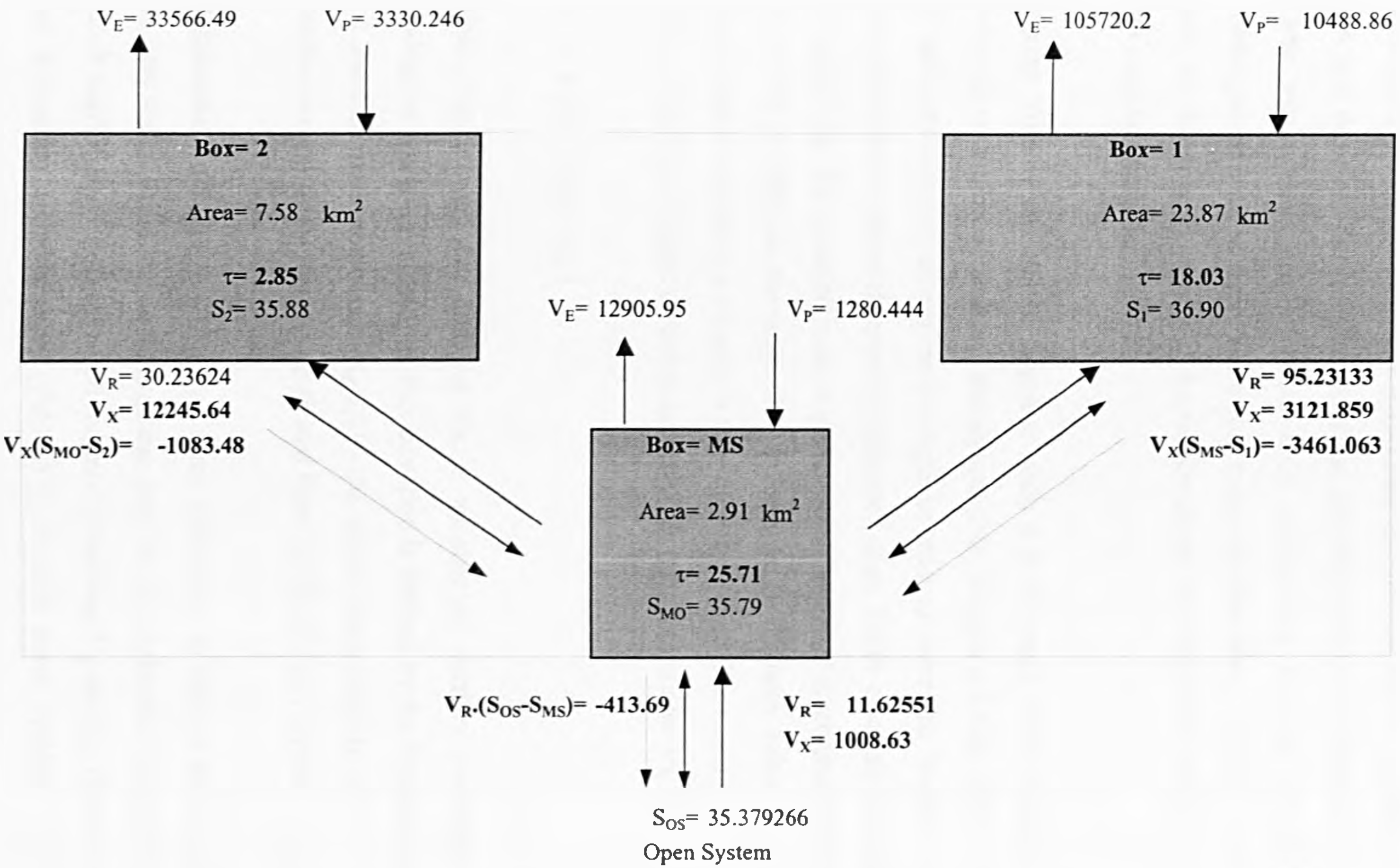

Figure 5.9b. Steady-state water and salt budgets for the Guaymas system, during summer season. Water fluxes in 10^3 m^3 d^{-1}, Salt fluxes in 10^3 kg d^{-1}. Arrows at the top of the boxes represent input and outputs from evaporation and precipitation processes; the wide head arrows represent the advective flows between compartments; the dashed arrows represent salt delivery; the double head arrows represent the mixing between compartments.

system, hence the modelling on this basis.

The present work assumes that the discharges are continuous in the short term (days to weeks) and the fresh water sources and their distribution are well-spread along the coastal line, and therefore the integration of the discharge volume is through the compartment. These assumptions are likely to hold, considering that the diurnal variations of discharges, as well as their dispersion, must stabilise after a complete tide cycle. In this case, the monthly frequency of the survey allows the integration of two completed spring and neap tide periods.

Mixing Volume can not be negative since it is the main mechanism for the fluxes of materials within the system and the adjacent sea (Section 5.2.4.2). So far, the definition of in- and out-boxe may determine this sign. In order to overcome the above problem either non-conservative materials may be estimated upon fluxes calculated through other kinds of modelling, for instance more sophisticated numerical mathematical models (Chapter 3), or it is possible to rearrange the Vx formula. In the latter option, those boxes where Vx is negative indicate a change in flux direction, such that a correction must be applied without the loss of water direction notion. This new formula for Vx must be written as:

$$V_X = -V_R S_R / - |(S_2 - S_1)| \qquad (12)$$

Where the denominator defining Vx, is an absolute number multiplied by -1, which produces a positive Vx, and the flux direction is defined by the number resultant between the absolute mark notation, $|(S_2 - S_1)|$. The above assumption is valid if it is considered that the sea is infinity large to be diluted from the fresh water inputs in the compartment.

Residential time. For this scenario, some differences in salinity between Box II and MS are very small. For instance during June-July, the ΔS difference between boxes was 0.02, which magnifies by a factor of 50 the product among V_R and S_R, therefore increasing Vx and decreasing τ considerably (Table 5.8). In such cases, residence times for the area must be considered though an alternative method. Thus, the result highlights that the sensibility of the estimations for τ can be more strongly associated to factors not related with the hydrodynamics of the system. Thus, τ depends directly from the salinity gradient between compartments, which in turn is affected for factors such as wastewater inputs, and high evaporation rates associated with the shallowness of the area.

Non-conservative budgets. There is a differentiation in the dissolved inorganic phosphorus fluxes for the two compartments, throughout the year (Figures 5.10a and 5.10b). Box 1 appears to be a net sink of phosphate, during both winter and summer, fixing nearly the double during summer. Box 2 is a net phosphate producer in both seasons. The major fluxes of ΔDIP from Box 2 are produced during summer with 9387.65 mold^{-1}, which represents a flux 6.5 greater than for winter. Thus, it seems that the net export of nitrogen from the whole system, as shown in scenario 1, is the result of the phosphorus production from the Guaymas basin. Moreover, Box 2 is likely to supply both the adjacent sea and the Empalme basin. These findings seems realistic considering that almost the total pollutant load from the discharges goes to the Guaymas basin, hence phosphate-loading from urban and industrial discharges. In this basin, high concentrations of phosphate are typically carried by sewage waters, and phosphate turnover within the system, indicates that organic matter decomposition may be the main factor controlling phosphate fluxes within the system. It is of note that, if the fluxes of the split boxes in scenario 2 are added, the resultant amount does not equal the total amount of P exported in scenario 1. As the budget procedure is based in the assumption that the averaged concentration of the non-conservative element is representative of the area in which it is averaged rather than integrated over it, some areas of the system are sub-estimated and other overestimated.

At monthly scale, Box 1 was characterised as a net DIP producer in February, May, June-July and August-September. For Box 2, January, February and August-September was a source of P. As in the case of the spatial variation, monthly frequencies show

Table 5.8. Summary of budget properties for the Guaymas System.

	Box-linka	Oct-Nov	December	January	February	March	Winter	April	May	Jun-Jul	Aug-Sep	Summer
V_R $(10)^3$ m^3 d^{-1}	I-MS	68.536302	68.5363022	68.5363	68.536302	68.5363	68.5363	90.33766	68.5363	68.5363	68.536302	95.23133
	II-MS	21.760489	21.7604889	21.76049	21.760489	21.76049	21.76049	28.68249	21.7605	21.76049	21.760489	30.23624
	MS-OS	8.3666739	8.36667387	8.366674	8.3666739	8.366674	8.366674	11.02811	8.36667	8.366674	8.3666739	11.62551
Vx $(10)^3m^3d^{-1}$	I-MS	3808.7742	3331.75565	4705.574	4246.8504	3011.38	3721.243	3120.461	2437.19	2210.448	2018.7827	3121.859
	II-MS	2726.5029	2032.85588	5031.776	1640.2233	11777.58	3158.121	1962.535	2716.47	48415.15	5981.7788	12245.64
	MS-OS	780.84078	1332.41331	1792.156	3180.8106	776.9198	1397.721	1083.358	538.996	610.7055	1249.7618	1008.626
τ days	I-MS	14.96213	17.0611302	12.15155	13.44325	18.83585	15.30771	18.06804	23.1521	25.45556	27.792984	18.0327
	II-MS	12.742344	17.0442126	6.929666	21.070795	2.967904	11.01278	17.58689	12.789	0.722988	5.8331122	2.852694
	MS-OS	33.235425	19.5629747	14.56779	8.2245805	33.40137	18.65434	23.96745	47.92	42.36928	20.848145	25.709
ΔP $mol.m^{-2}.d^{-1}$	I-MS	-0.207602	-0.03932895	-0.488878	0.0492392	-0.042275	-0.139874	-0.44169	0.07587	0.041086	0.044435	-0.054573
	II-MS	-0.516917	-0.1969486	1.146126	0.3359163	0.497384	0.177891	-0.18194	0.45032	14.04395	0.2102889	1.238491
	MS-OS	0.6612766	0.24011513	1.251303	-5.4873131	-0.417309	0.333336	0.780753	-0.07783	-0.106795	-0.161407	0.068428
ΔN $mol.m^{-2}.d^{-1}$	I-MS	1.3783304	-1.07089679	-0.14052	0.0492392	-0.179193	-0.029048	-0.73186	0.12948	0.088982	2.5374764	0.872453
	II-MS	3.3183854	-0.08642107	-1.600164	0.3359163	0.194241	0.682378	0.270685	6.74627	22.74532	-5.330606	6.828892
	MS-OS	-2.05311	1.59728062	-5.389747	-5.4873131	-0.289177	-1.825408	2.41084	0.28751	0.016108	4.614549	1.629997
N(*fix-denit*) $mol.m^{-2}.d^{-1}$	I-MS	4.6999592	-0.62926322	7.681535	0.2844854	0.4972	2.208941	6.335219	9.5E-27	-0.568395	1.8265158	1.745621
	II-MS	11.589057	-3.15117756	-19.93817	-7.3889908	-7.763911	-2.163885	3.181706	1.5E-23	-201.9578	-8.695228	-12.98696
	MS-OS	-12.63354	3.84184215	-25.41059	-5.6205225	6.387764	-7.158791	-10.0812	1.2E-23	1.724826	7.1970543	0.535157
NEM (p-r) $mol.m^{-2}.d^{-1}$	I-MS	22.005791	4.16886884	51.82111	1.558506	4.4811	14.82668	46.81942	-8.0422	-4.355127	-4.710114	5.78474
	II-MS	54.7932	20.8765514	-121.4893	-51.17751	-52.72276	-18.85649	19.28551	-47.734	-1488.658	-22.29062	-131.28
	MS-OS	-70.09532	-25.4522042	-132.6381	-0.882512	44.23473	-35.33366	-82.7598	8.24947	11.32026	17.109098	-7.25332

Vx = Mixing volume

t = Residential time

ΔP = Nonconservative flux of P

ΔN = Nonconservative flux of N

N(*fix-denit*)= Difference between nitrogen fixation and denitrification.

NEM (p-r) = Net Ecosystem Metabolism (production - respiration).

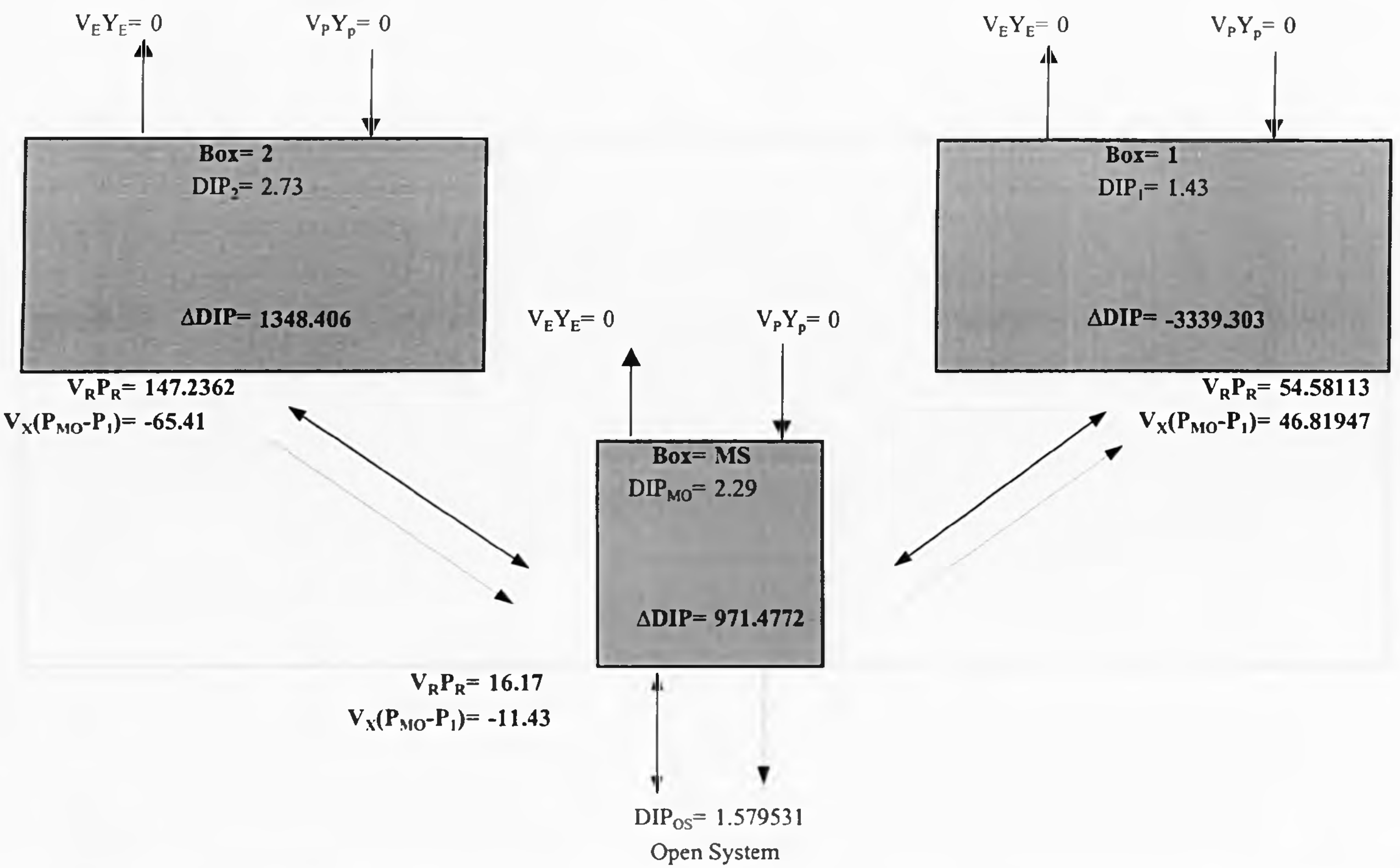

Figure 5.10a. Steady-state dissolved inorganic P budget for the Guaymas system, winter season. Phosphorus fluxes (ΔDIP) in $mold^{-1}$; $Vx.(S_{out}-S_{in})$ is given in $(10)^3 mmold^{-1}$. Arrows at the top of the boxes represent input and outputs from atmospheric processes; the double head arrows represent the mixing between compartments; and, the dashed arrows indicate the combined entrainment ($V_R Y_R$) and mixing ($V_X(Y_2-Y_1)$) fluxes.

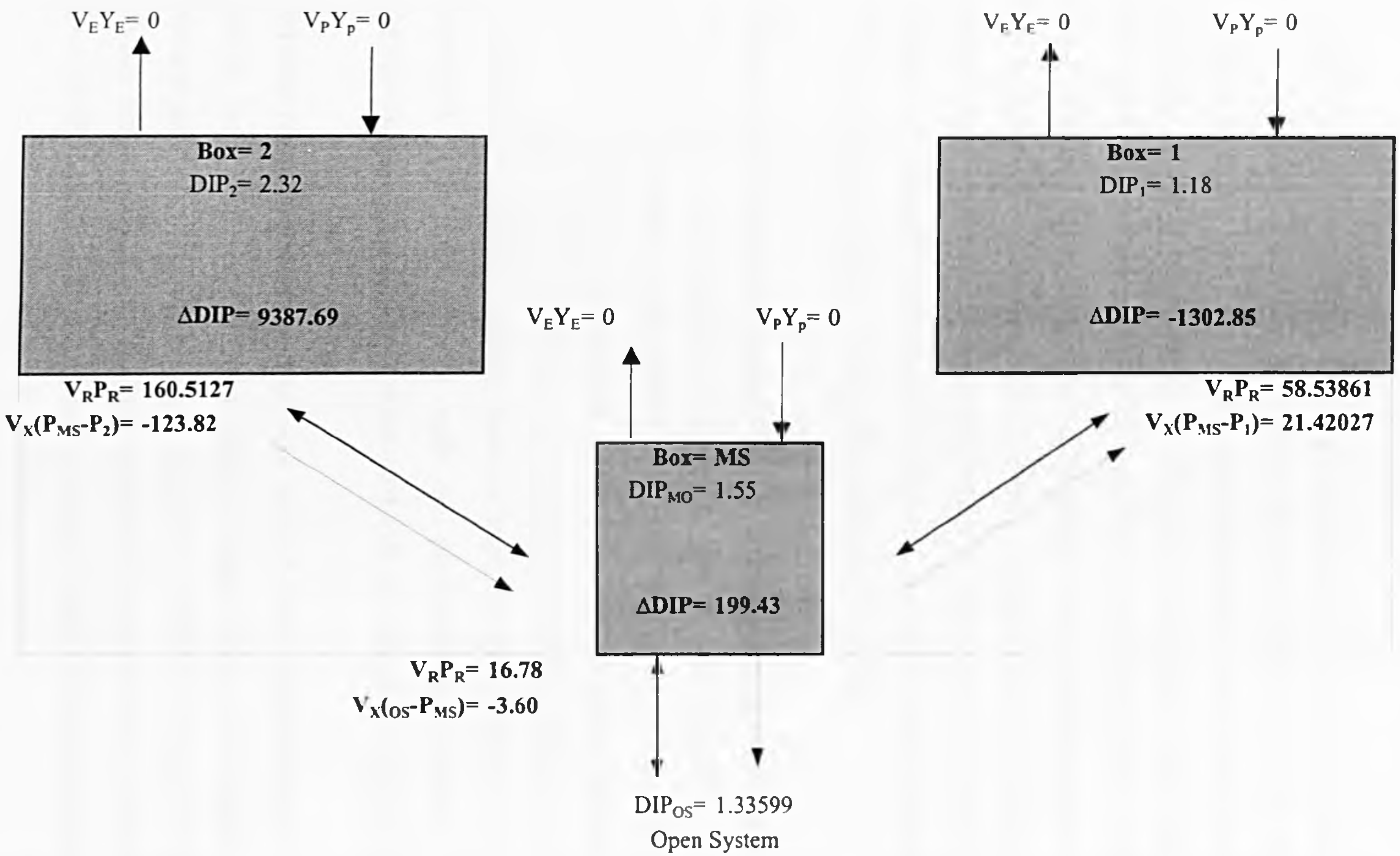

Figure 5.10b. Steady-state dissolved inorganic P budget for the Guaymas system, summer season. Phosphorus fluxes (ΔDIP) in mold^{-1}; $Vx.(S_{out}-S_{in})$ is given in $(10)^3$mmold^{-1}. Arrows at the top of the boxes represent input and outputs from atmospheric processes; the double head arrows represent the mixing between compartments; and, the dashed arrows indicate the combined entrainment (V_RYR) and mixing ($V_X(Y_2-Y_1)$) fluxes.

differences in phosphate fluxes, which are not indicated on a seasonal basis. Considering the above, increment in box segmentation and temporal survey frequency (from seasons to months) may increment resolution of the model in the case of the scenario II.

The non-conservative fluxes of nitrogen during winter show that the system is a sink for nitrogen, as indicated by the high DIN in the open sea (Figure 5.11a). In winter, Box 1 is a net sink of N and Box 2 works as a source of nitrogen. This scheme indicates that a high proportion of the N imported by the system during winter sinks in Box 1. In summer, both boxes work as net source of N, with Box 2 producing almost double the amount of Box 1 (Figure 5.11b). Within Box 2, as stated above, nitrogen production is associated with anthropogenic activities, while in Box 1, nitrogen production during summer may be associated with nitrification processes related to oxidation of organic matter within this system. On a monthly basis, as in the case of phosphate, both compartments display a marked variation, alternates from source to sink (Table 5.8).

Nitrogen fixation-denitrification. Box 1 is fixing nitrogen during the two-averaged seasons, winter and summer, whereas in Box 2, the denitrification processes is a dominant one through both seasons. The ratio of organic matter, oxidation provides an insight about the nitrogen production from Box 2, which may pump nitrogen to Box 1. On a monthly basis, both Boxes had a strong variation, which may indicate that the assumption reached for seasons does not apply at this frequency, but instead may be associated with local events such as phytoplankton blooms. Thus, persistent phytoplankton blooms had been associated with compartment 2 (chapter 6).

Net Ecosystem Metabolism. There is a marked spatial differentiation in the NEM of the system. Box 1 shows a positive NEM through winter and summer, indicating that primary production dominates over respiration. Production processes performed during the day are associated with the phytoplankton located in this compartment. For Box 2, since ΔDIP is positive in winter and summer, budget calculations indicate that the sub-

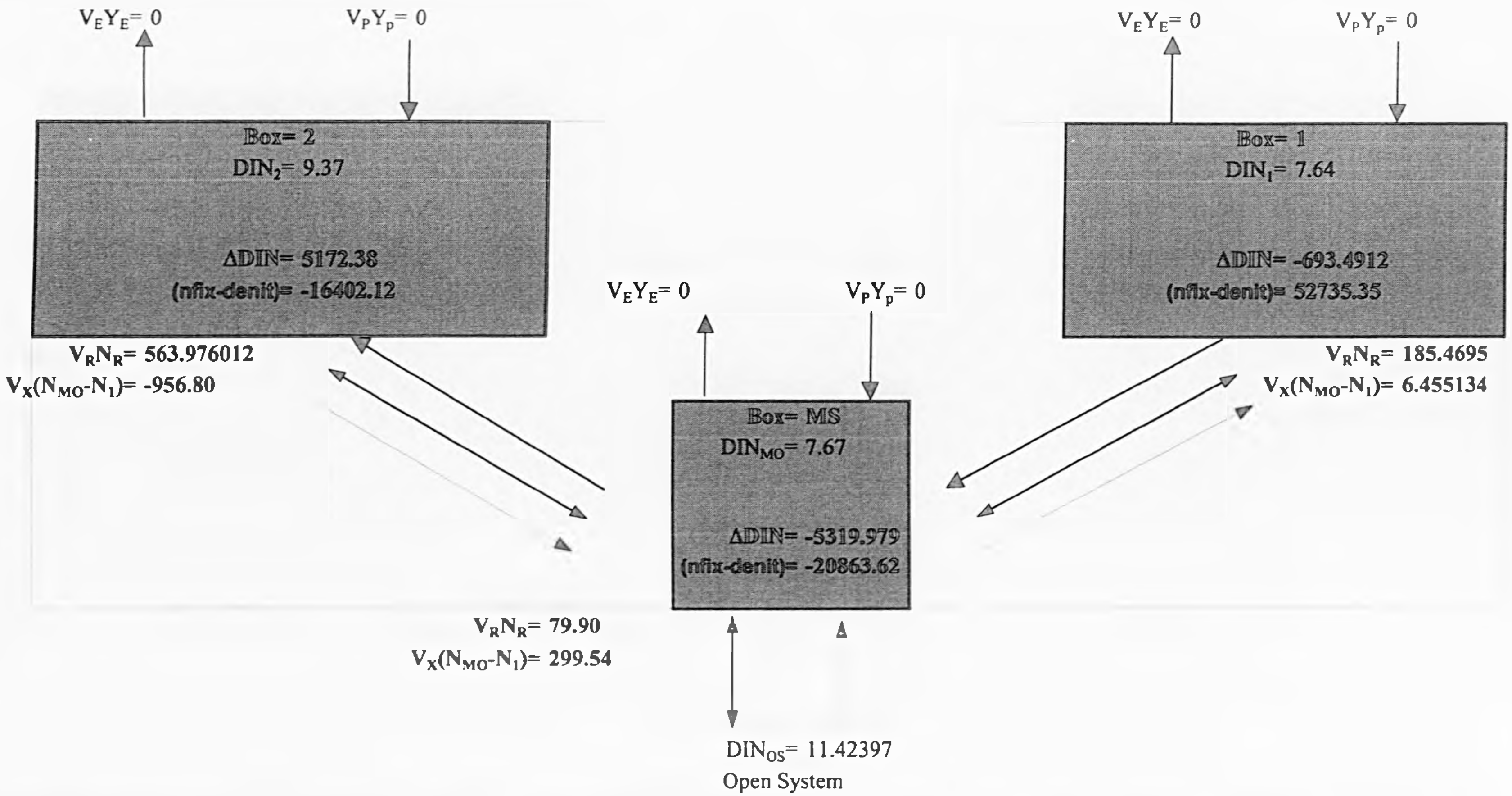

Figure 5.11a. Steady-state dissolved inorganic N budget for the Guaymas system, winter season. Nitrogen fluxes (ΔDIN) in mold^{-1}; $Vx.(S_{out}-S_{in})$ is given in $(10)^3$mmold^{-1}. Arrows at the top of the boxes represent input and outputs from atmospheric processes; the double head arrows represent the mixing between compartments; and, the dashed arrows indicate the combined entrainment (V_RY_R) and mixing ($V_X(Y_2-Y_1)$) fluxes.

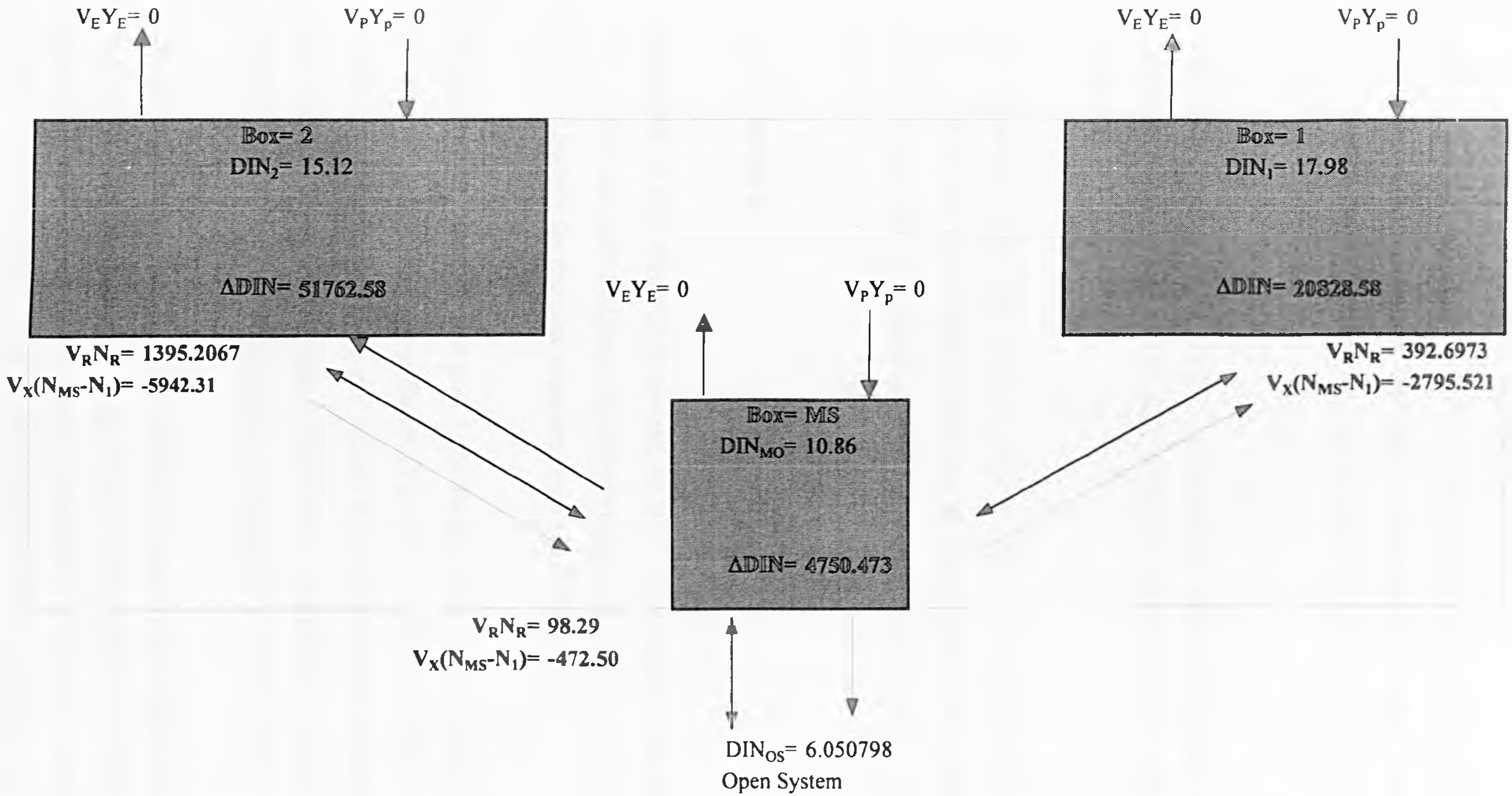

Figure 5.11b. Steady-state dissolved inorganic N budget for the Guaymas system, summer season. Nitrogen fluxes (ΔDIN) in mold^{-1}; $Vx.(S_{out}-S_{in})$ is given in $(10)^3$mmold^{-1}. Arrows at the top of the boxes represent input and outputs from atmospheric processes; the double head arrows represent the mixing between compartments; and, the dashed arrows indicate the combined entrainment (V_RY_R) and mixing ($V_X(Y_2-Y_1)$) fluxes.

system is net heterotrophic for both seasons. In winter the system consumes about 18.85 $molm^2d^{-1}$, and during summer this value is increased 7.3 times (Table 5.8). The increase in temperature during summer and the constant organic matter load increase respiration and oxidation processes.

Autotrophic conditions in Box 2 are associated with the coldest months (October to December), whereas box 1 only became slightly heterotrophic during the warmer months (Table 5.8).

The Guaymas sub-system is responsible for the heterotrophic behaviour of the system. The NEM of this sub-basin is consuming 6 times more organic matter from scenario 1, and, compared with other systems world-wide, the NEM is 50 % higher than Manila Bay (Table 5.7).

5.3.3 Scenario 3.

Discussion of this scenario is centred on the new division of the former box 1 (Figure 5.3). Water and salt budgets, nonconservative fluxes and stoichiometric linkages are discussed mainly for the new compartments box 1 and box 2.

Salt and water budget. The area from the new box 2 (16.28 km^2) represents the double the new box 1, therefore water fluxes (V_R) are near double in box 2 than in box 1. As in the former scenario, there is a net inward flux of seawater, which compensates for water lost by evaporation. During summer, there is an increment in V_R flux, mainly because of the high evaporation rate during summer (Figures 5.12a and 5.12b).

Salt was transferred from Box 1 to Box 2 and then to the adjacent sea. During summer, the system increases its capacity to export salt, mainly because the high evaporation rate and nearly null rainfall. Box 1 exports an average 957 x 10^3 kg d^{-1} to Box 2 and this system exports as much as 2009 x 10^3 kg d^{-1} to the Box MS. Residence time, τ, for Box 2 during

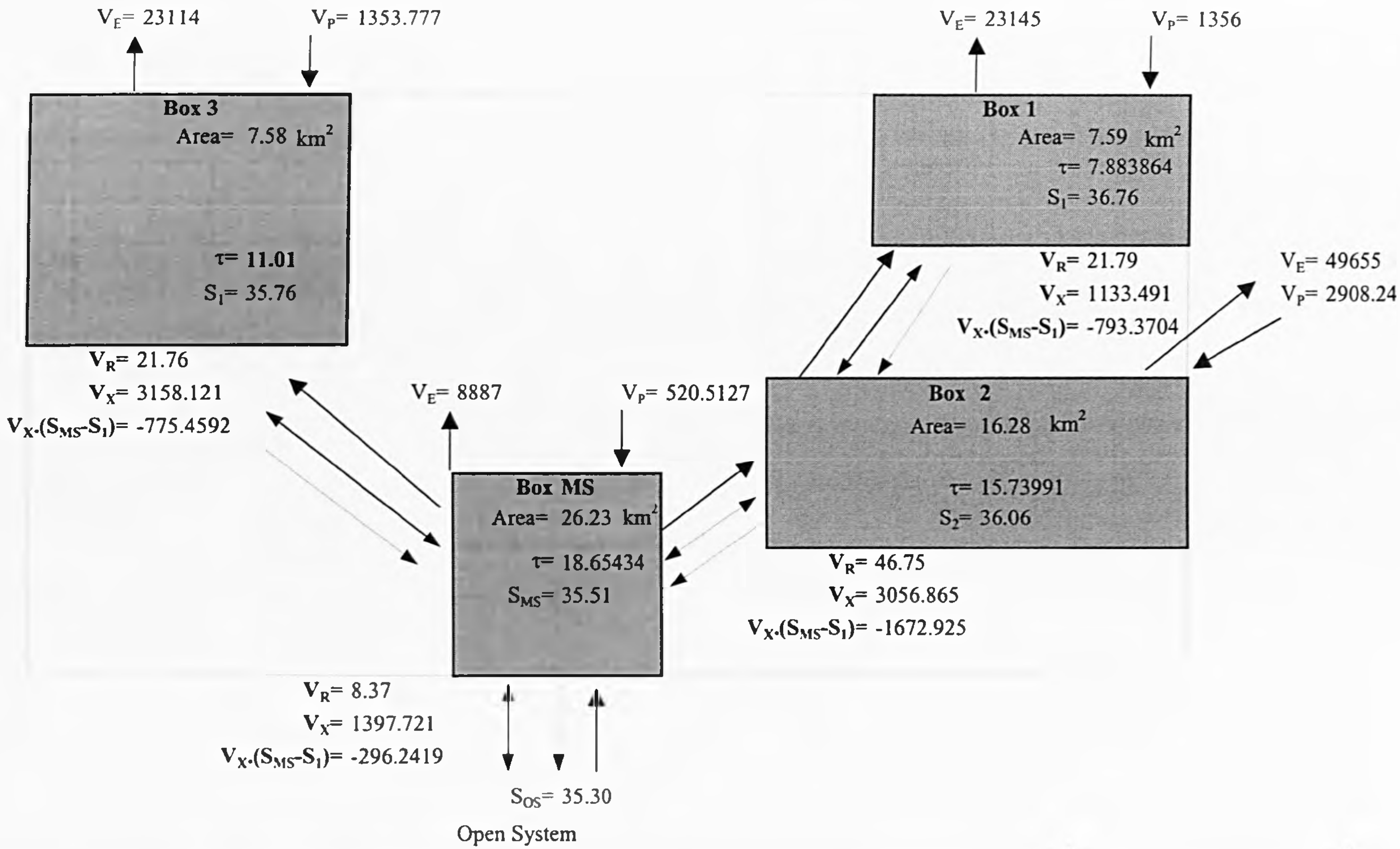

Figure 5.12a. Steady-state water and salt budgets for the Guaymas system, during winter season. Water fluxes in 10^3 m^3 d^{-1}, Salt fluxes in 10^3 kg d^{-1}. Arrows at the top of the boxes represent input and outputs by evaporation and precipitation processes; the wide head arrows represent the advective flows between compartments; the dashed arrows represent salt delivery; the double head arrows represent the mixing between compartments.

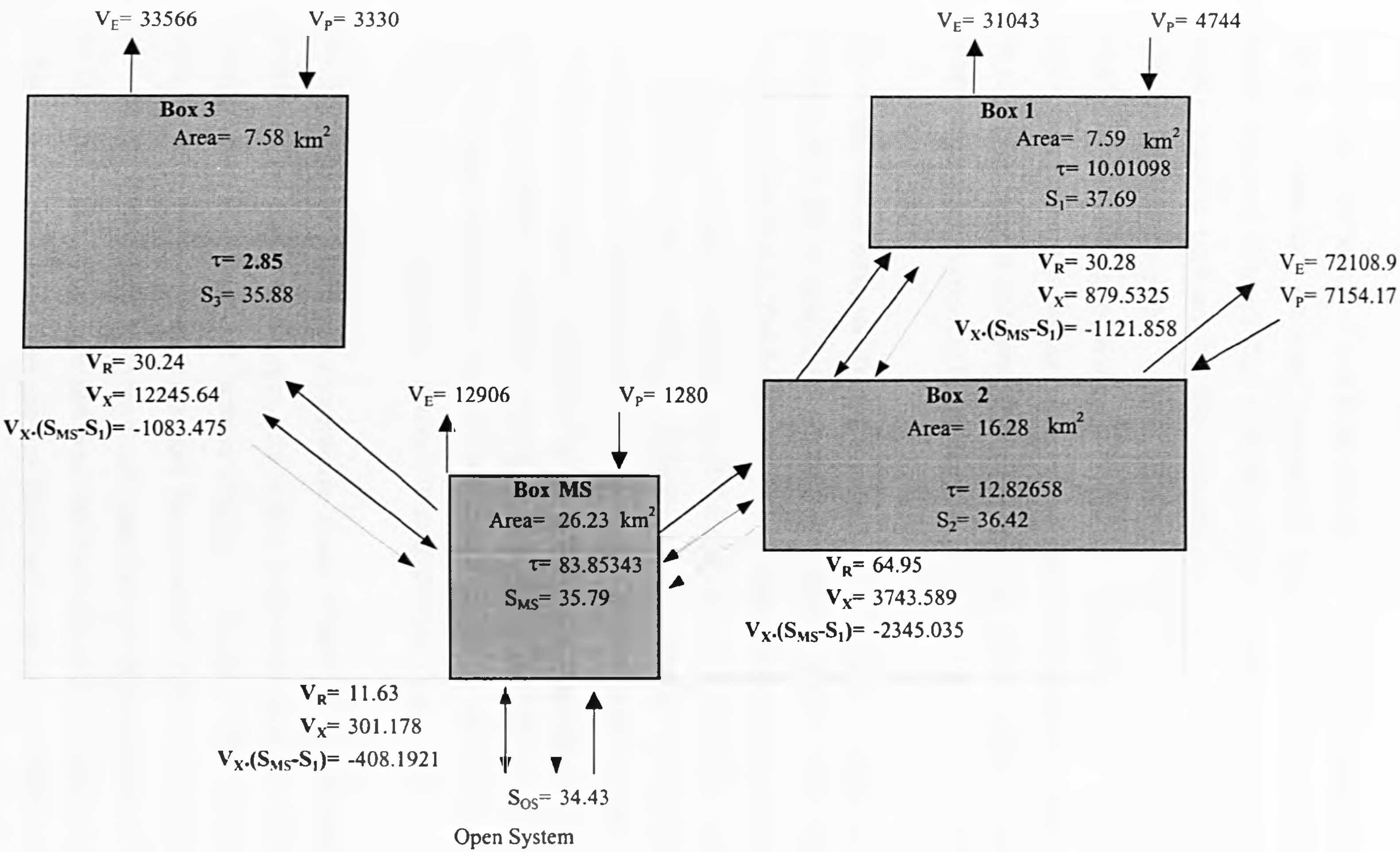

Figure 5.12b. Steady-state water and salt budgets for the Guaymas system, during winter summer. Water fluxes in 10^3 m^3 d^{-1}, Salt fluxes in 10^3 kg d^{-1}. Arrows at the top of the boxes represent input and outputs by evaporation and precipitation processes; the wide head arrows represent the advective flows between compartments; the dashed arrows represent salt delivery; the double head arrows represent the mixing between compartments.

winter is the double that of Box 1. In summer the residual exchange of Box 2 increased and the residual time for Box 1 became the longest (Figures 5.12a and 5.12b). This longest residence time for Box 1 during summer is associated to the increase in the salinity gradient between the two compartments. At a monthly level, January and February showed a very low τ, these values are associated with a very small gradient of salinity sampled during those months (Table 5.9). The above may be partly explained, as during the cold months such as January and February, the exchange of heat goes from the sea to the atmosphere, and hence in shallow areas the water tended to be more influenced by air temperature, decreasing the evaporation difference between the two boxes.

Non-conservative budgets. During winter there is a net flux of phosphorus from the transition Box MS to Box 2 and finally Box 1, (Figure 5.13a). ΔDIP in Box 1 is three times lower than Box 2. This highlights the importance of the source, Box MS, for Box 1, which is likely to be fed through Box 2. During summer there was a change in pattern, Box 1 became a slight source of P, while Box 2 is a net sink of ΔDIP receiving phosphate from both Box 1 and Box MS (Figure 5.13b). In particular, the Box 1 area is not characterised by intensive urban discharges and mud flat areas are limited. Therefore it is likely that the slight ΔDIP production is associated with phosphorus regeneration, organic matter decomposition and P released from sediments. On the monthly scale, both systems alternate sinks and source characteristics through the year (Table 5.9).

For the Empalme basin, non-conservative fluxes of nitrogen indicates that Box 1 was working as net source of nitrogen, whiles Box 2 was working as a net sink for the two averaged seasons, winter and summer (Figures 5.14a and 5.14b). Summer Box 1 was exporting in an order of magnitude more than in winter, whereas Box MS was producing more during winter. Box MS was closely associated with the seasonal activities within the Guaymas basin, which in winter were characterised by a high fishing season. For Box 1, high concentrations of nitrogen are likely to be associated with an increase in the reduction processes.

Table 5.9. Summary of budget properties for the Guaymas System.

	Box	Oct-Nov	December	January	February	March	Winter	April	May	Jun-Jul	Aug-Sep	Summer
Vx $(10)^3 m^3 d^{-1}$	I-II	851.4766428	851.4766428	2072.63659	52746.38795	654.951844	1133.49139	615.79081	1075.9515	1370.52433	708.795348	879.5324757
	II-MS	4977.723737	1638.379517	4231.08194	2934.217055	4048.79829	3056.86467	4682.4002	3222.685	3667.59424	3705.72759	3743.589258
	III-MS	2726.502913	2032.855882	5031.77592	1640.22326	11777.5815	3158.12076	1962.5351	3583.7266	82967.5268	7219.89112	12245.63926
	MS-OS	780.8407811	1332.413314	1792.1563	3180.810571	776.919804	1397.7213	1083.3581	711.07575	297.194937	122.747191	301.1779782
τ days	I-II	10.42989833	10.42989833	4.3487223	0.1726055	13.4587269	7.88386384	14.131751	8.2448605	6.46942817	12.3903423	10.01097656
	II-MS	9.722531963	28.98926685	11.419479	16.38751027	11.9277348	15.7399134	10.297302	14.873715	13.0348053	12.9847494	12.82657505
	III-MS	12.74234418	17.04421258	6.92966575	21.07079458	2.96790432	11.0127755	17.586887	9.694105	0.42189501	4.83281343	2.852694146
	MS-OS	33.23542477	19.56297472	14.5677925	8.224580507	33.401371	18.6543413	23.967448	36.323435	84.1954945	197.444583	83.85342858
ΔP $mol.m^2.d^{-1}$	I-II	-0.04705285	0.052633509	0.12713994	-15.4758453	-0.1106071	-0.0898238	0.0100368	0.1018165	-0.135324	0.04201564	0.015320227
	II-MS	-0.35480323	-0.04747238	-0.6797982	0.1212119	0.08321713	-0.1216728	-0.973267	0.100907	0.15993507	0.08662956	-0.10279586
	III-MS	-0.51487607	-0.196948598	1.14612554	0.486095682	-0.0240527	0.14999764	-0.1819388	0.5940895	24.0666725	0.25381459	1.23849088
	MS-OS	0.661276644	0.240115134	1.2483654	0.008325585	-0.4173088	0.33333639	0.780753	-0.1026716	-0.0543941	-0.01984432	0.016394839
ΔN $mol.m^2.d^{-1}$	I-II	0.168739686	-0.235502311	1.41466599	-7.29339164	0.08874608	0.13377683	-0.0283036	-0.3358296	-1.3769321	6.7245185	1.786889676
	II-MS	2.485454517	-1.518280545	-1.3613948	0.512089336	-0.9331898	-0.1450598	-3.3326325	0.9416219	1.69342145	-3.05012368	-0.72749271
	III-MS	3.318385396	-0.086305775	-1.5980296	0.335468162	0.19398186	0.68146718	0.2703243	8.8882093	38.9171762	-6.42535523	6.819781404
	MS-OS	-2.05311044	0.613317908	-2.0695353	-2.10699821	-0.111037	-0.7009136	0.9257054	0.1456428	-0.0097748	0.15947063	0.177806599
N(*fix-denit*) $mol.m^2.d^{-1}$	I-II	0.921585285	-1.077638453	-0.619573	240.3201333	1.85846016	1.57095746	-0.1888919	-7.68E-25	0.78825247	-4.45365807	1.541766041
	II-MS	8.162306127	0.051858263	10.2421983	-1.7006957	-1.7664518	1.87914954	14.018867	1.017E-25	-1.7696248	-9.18273316	1.305635312
	III-MS	11.55640257	3.064756497	-19.938173	-7.44161462	0.5790837	-1.7175847	3.181706	2.044E-23	-346.0976	-26.9043466	-12.9869624
	MS-OS	-12.6335368	-2.244561525	-25.363594	-5.62052248	6.3877642	-7.1587906	-10.081209	1.532E-23	0.84484881	2.1034976	0.200749168
NEM (p-r) $mol.m^2.d^{-1}$	I-II	4.987602092	-5.579151942	-13.476834	1640.439603	11.7243558	9.52132167	-1.0638976	-10.792546	14.3443476	-4.45365807	-1.62394409
	II-MS	37.60914191	5.032072284	72.0586057	-12.8484614	-8.8210156	12.8973161	103.1663	-10.696143	-16.953118	-9.18273316	10.89636063
	III-MS	54.57686375	20.87655136	-121.48931	-51.5261423	2.54958293	-15.89975	19.285511	-62.973487	-2551.0673	-26.9043466	-131.280033
	MS-OS	-70.0953243	-25.45220422	-132.32673	-0.88251196	44.2347327	-35.333657	-82.759823	10.883192	5.76577378	2.1034976	-1.73785295

Vx = Mixing volume

t = Residential time

ΔP = Nonconservative flux of P

ΔN = Nonconservative flux of N

N(*fix-denit*) =Difference between nitrogen fixation and denitrification

NEM (p-r) = Net Ecosystem Metabolism (production - respiration).

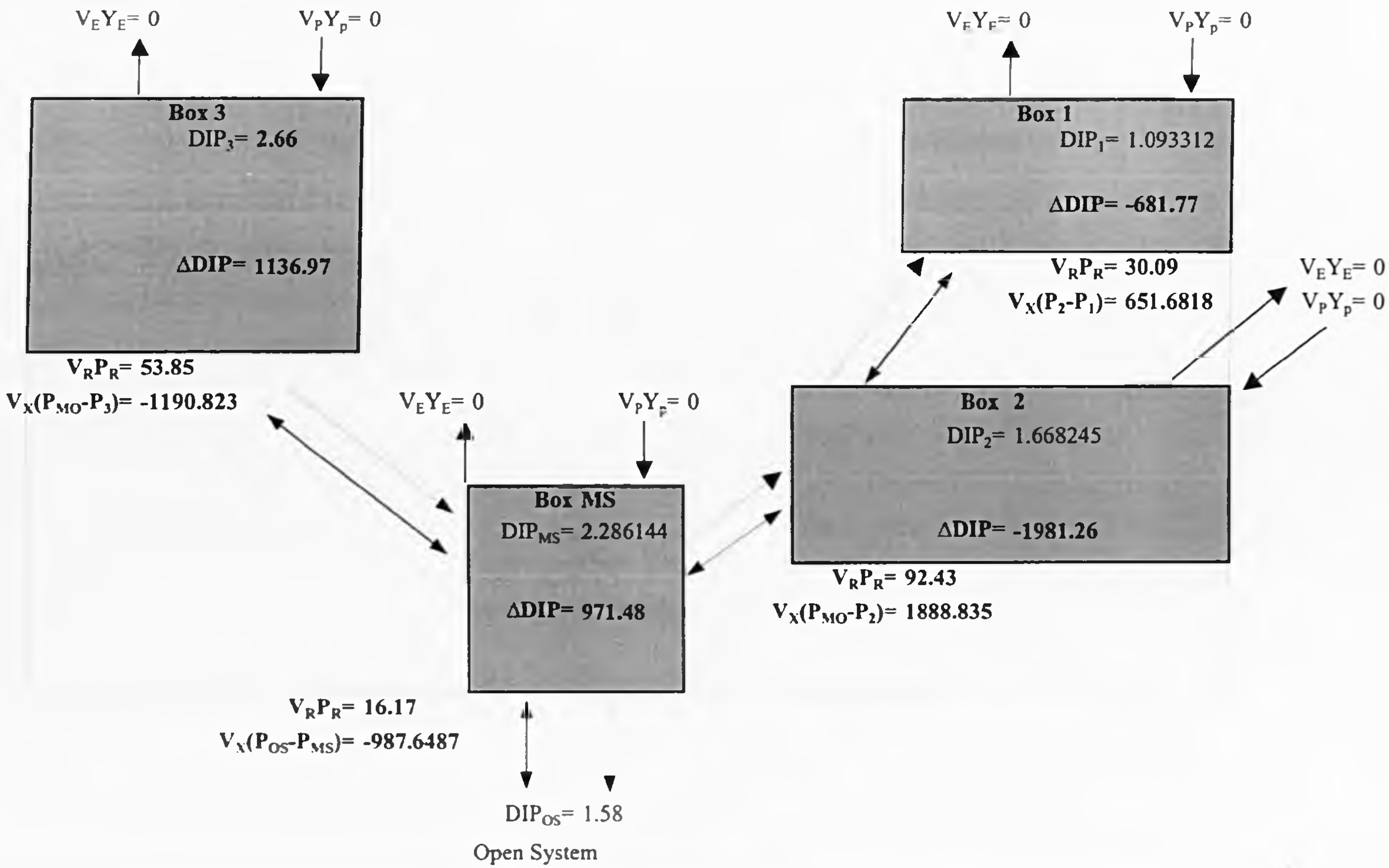

Figure 5.13a. Steady-state dissolved inorganic P budget for the Guaymas system, winter season. Phosphorus fluxes (ΔDIP) in mold^{-1}; $Vx.(S_{out}-S_{in})$ is given in $(10)^3$mmold^{-1}. Arrows at the top of the boxes represent inputs and outputs from atmospheric processes; the double head arrows represent the mixing between compartments; and, the dashed arrows indicate the combined entrainment (V_RY_R) and mixing ($V_X(Y_2-Y_1)$) fluxes.

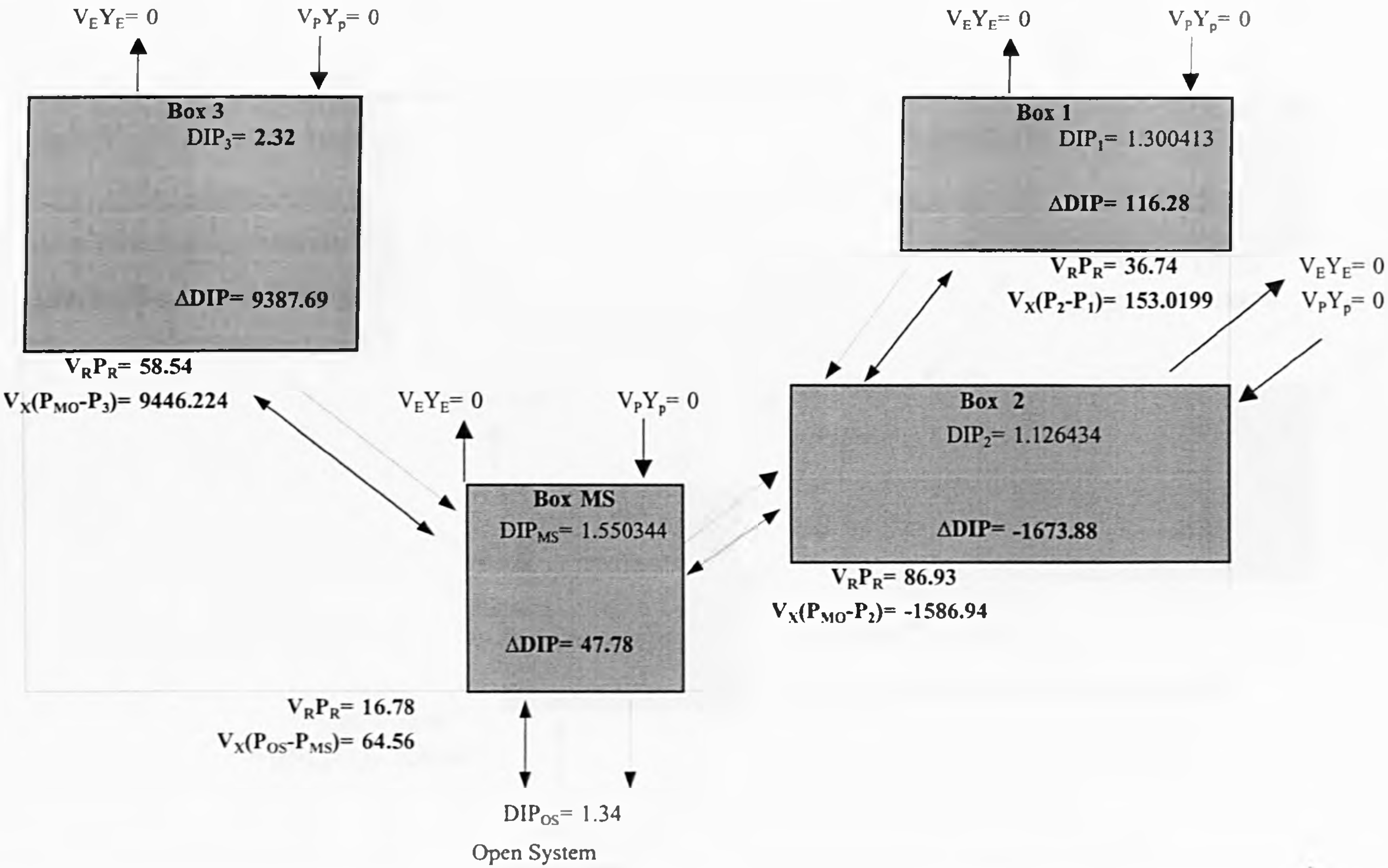

Figure 5.13b. Steady-state dissolved inorganic P budget for the Guaymas system, summer season. Phosphorus fluxes (ΔDIP) in $mold^{-1}$; $Vx.(S_{out}-S_{in})$ is given in $(10)^3 mmold^{-1}$. Arrows at the top of the boxes represent inputs and outputs from atmospheric processes; the double head arrows represent the mixing between compartments; and, the dashed arrows indicate the combined entrainment (V_RY_R) and mixing ($V_X(Y_2-Y_1)$) fluxes.

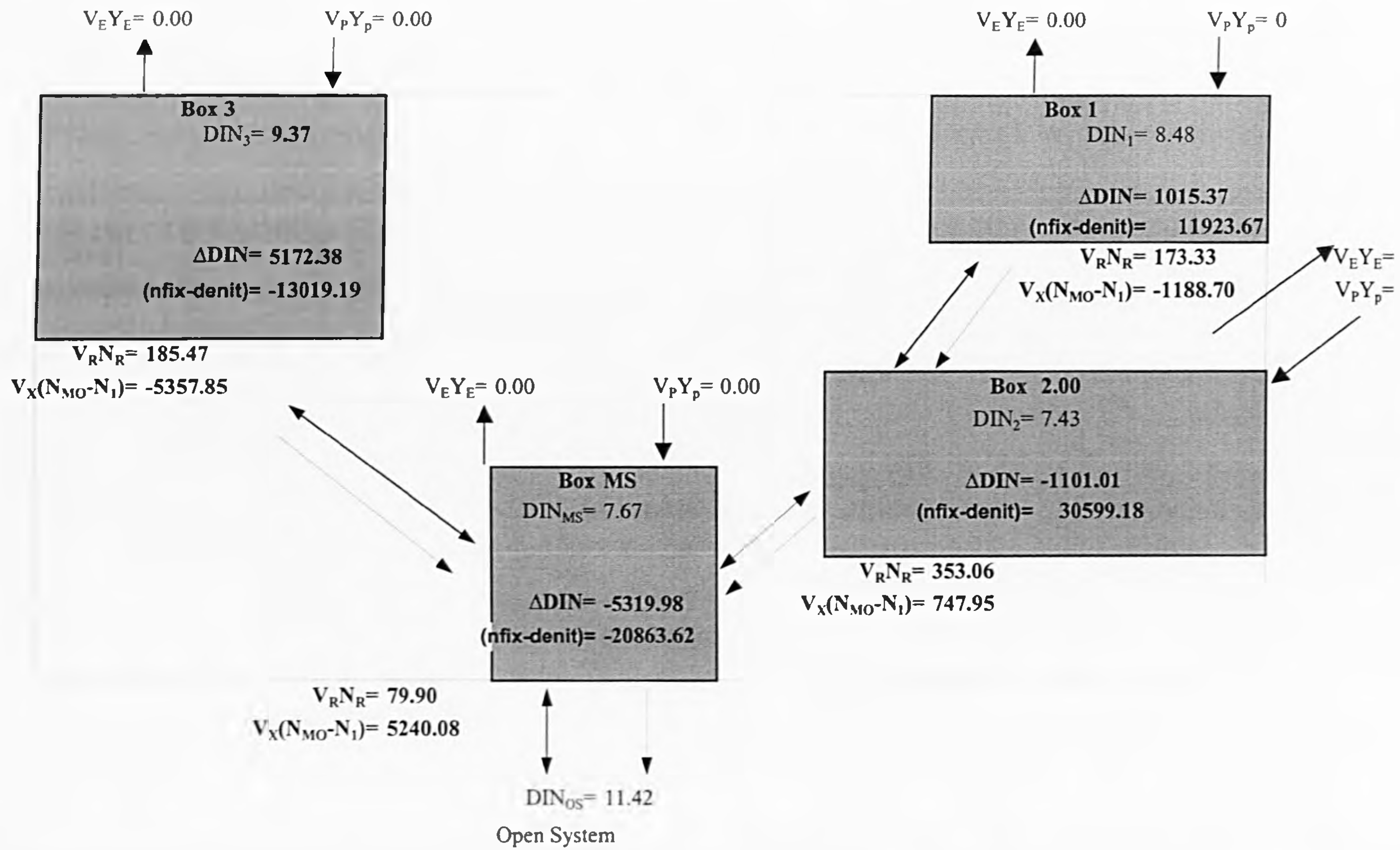

Figure 5.14a. Steady-state dissolved inorganic N budget for the Guaymas system, winter season. Nitrogen fluxes (ΔDIN) in mold^{-1}; Vx.(S_{out}-S_{in}) is given in $(10)^3$mmold^{-1}. Arrows at the top of the boxes represent input and outputs from atmospheric processes; the double head arrows represent the mixing between compartments; and, the dashed arrows indicate the combined entrainment (V_RY_R) and mixing ($V_X(Y_2-Y_1)$) fluxes.

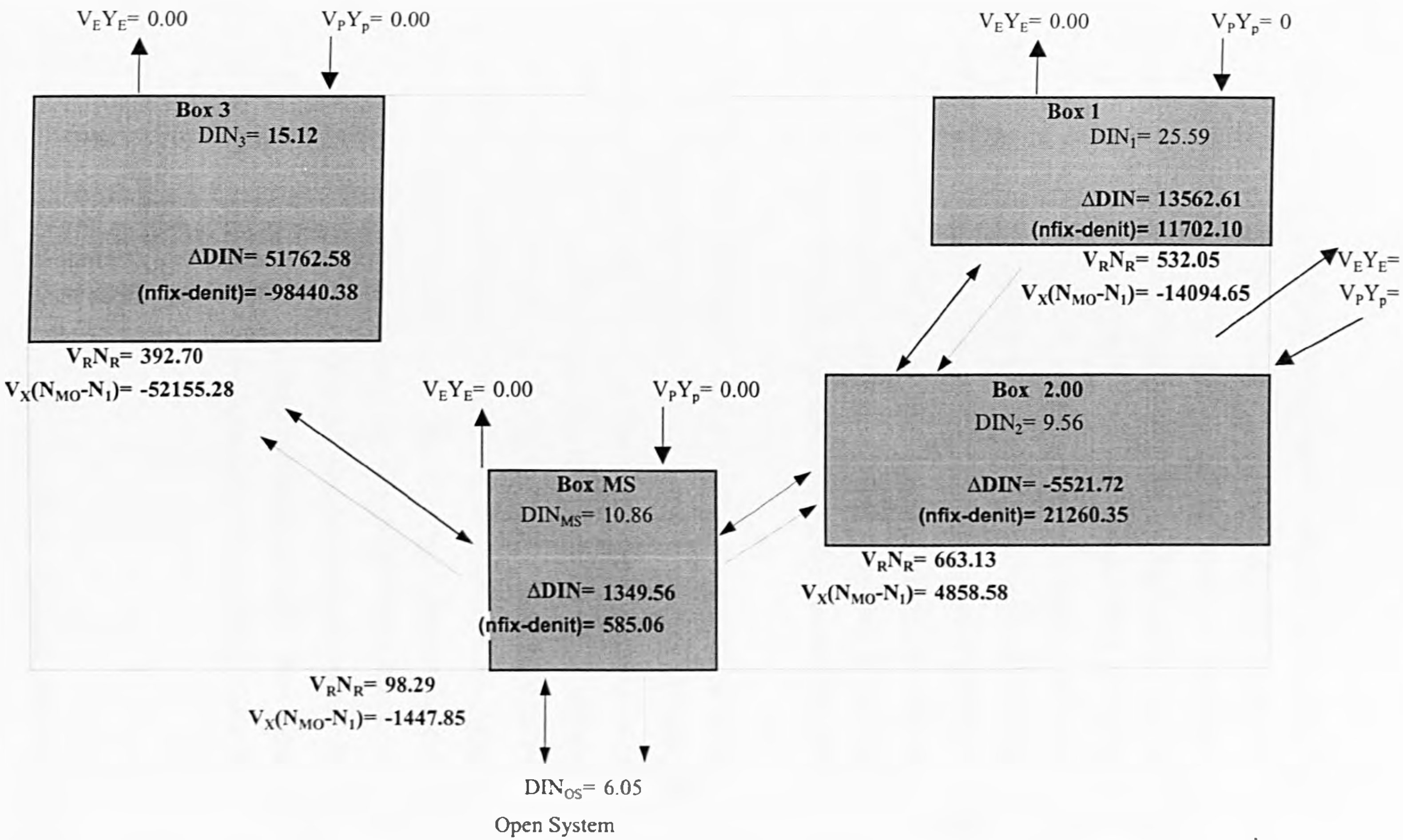

Figure 5.14b. Steady-state dissolved inorganic N budget for the Guaymas system, summer season. Nitrogen fluxes (ΔDIN) in $mold^{-1}$; $Vx.(S_{out}-S_{in})$ is given in $(10)^3 mmold^{-1}$. Arrows at the top of the boxes represent input and outputs from atmospheric processes; the double head arrows represent the mixing between compartments; and, the dashed arrows indicate the combined entrainment (V_RY_R) and mixing ($V_X(Y_2-Y_1)$) fluxes.

Nitrogen fixation-denitrification. Box 1 and Box 2 during winter and summer were characterised by nitrogen fixation, this means that there must be other sources than the expected nitrogen from the reacting organic matter of phytoplankton. Other sources of nitrogen may be related to organic matter decomposition, sediment fluxes enhanced by benthic activity, and dissolved inorganic nitrogen from terrestrial sources (Heip, 1995). However, the latter sources are unlikely to be a major contributor for this compartment, given the lack of discharges and runoff (Figures 5.14a and 5.14b). Especially for Box 2, organic matter decomposition may be important, since this material might be carried from the Guaymas basin and fishing industry areas through Box MS. In the case of Box 1, the same source of organic matter is unlikely to impact at the same intensity, given the distance from the Guaymas basin and the restricted connection with Box 2.

Net Ecosystem Metabolism. Boxes 1 and 2 were working as a net autotrophic system during winter, whereas, for summer, Box 1 became heterotrophic (Table 5.9). The dominance of the respiration processes was more intensive during summer mainly for compartment 1. The NEM under this approach is strongly linked to the P amount in the boxes, and hence variation in P loads from anthropogenic sources. Variation through the months showed a sinusoidal shape for both compartments, changing from heterotrophic values to autotrophic (Table 5.9). Box 1 during February showed a high positive value, this high autotrophic result is related to a small P concentration measured in Box 1 for this month, producing a large P gradient among compartments. The above highlights the sensitivity of this approach to the estimations of ΔDIP. Box 2 showed a slight variation, changing from heterotrophic to autotrophic and *viceversa* (Table 5.9).

5.3.4 Scenario 4.

Discussion of this scenario is focused on Guaymas basin, which is divided into Boxes 3 and 4 (Figure 5.4).

Salt and water budget. It is important to reiterate the influence of fresh water inputs through the Guaymas basin, and the assumption that these water inputs are regarded as negligible considering the size and volume of the compartments. As stated in previous scenarios, V_R is strongly dependent on the area represented. Box 3 is a small compartment that characterises the inner part of the Guaymas Bay. There is a net water flux toward this Box in order to balance water lost by evaporation processes, and a net salt flux toward Box 4, during both averaged seasons (Figures 5.15a and 5.15b). Box 4 shows a similar pattern for V_R during winter and summer with a net flux of seawater from Box MS. Salt fluxes during winter show a net export of salt material to the external compartment. However, during summer this pattern is inverted, when salt from Boxes 3 and MS is brought in order to balance dilution occurred in Box 4 (Figure 5.15b). Thus, it seems to be that, during summer, in spite of the high evaporation rate, compartment 4 is strongly influenced by freshwater inputs, as is reflected by negative Vx. The above may produce several issues: the most likely reason for these negative Vx values is related to the fact that some fixed stations are located near the freshwater discharges, for instance station 9, hence the dispersion plume has a strong effect which is magnified in the box. It was not possible to obtain data for fresh water input in to the system, therefore, the assumption of a low fresh water proportion in relation to the total volume of the compartment can be questioned. Finally, compartment-sizing may be important, as shown by scenario 2 in which fresh water inputs were not important when they are integrated to the whole sub-system, but became important for smaller compartments. Further subdivision may isolate areas heavily impacted by fresh water inputs.

In the monthly context, Boxes 3 and MS presented a salt mass delivery to Box 4 during the warmer months (Table 5.10). Thus, high salinity in Box 3 can be explained by the shallowness of the area and almost no freshwater input, while Box MS is influenced by high salinity from the Empalme basin (Figure 5.15b). Residence times were strictly determined by the salinity gradients, and hence also affected by the little freshwater inputs in to the sub-system.

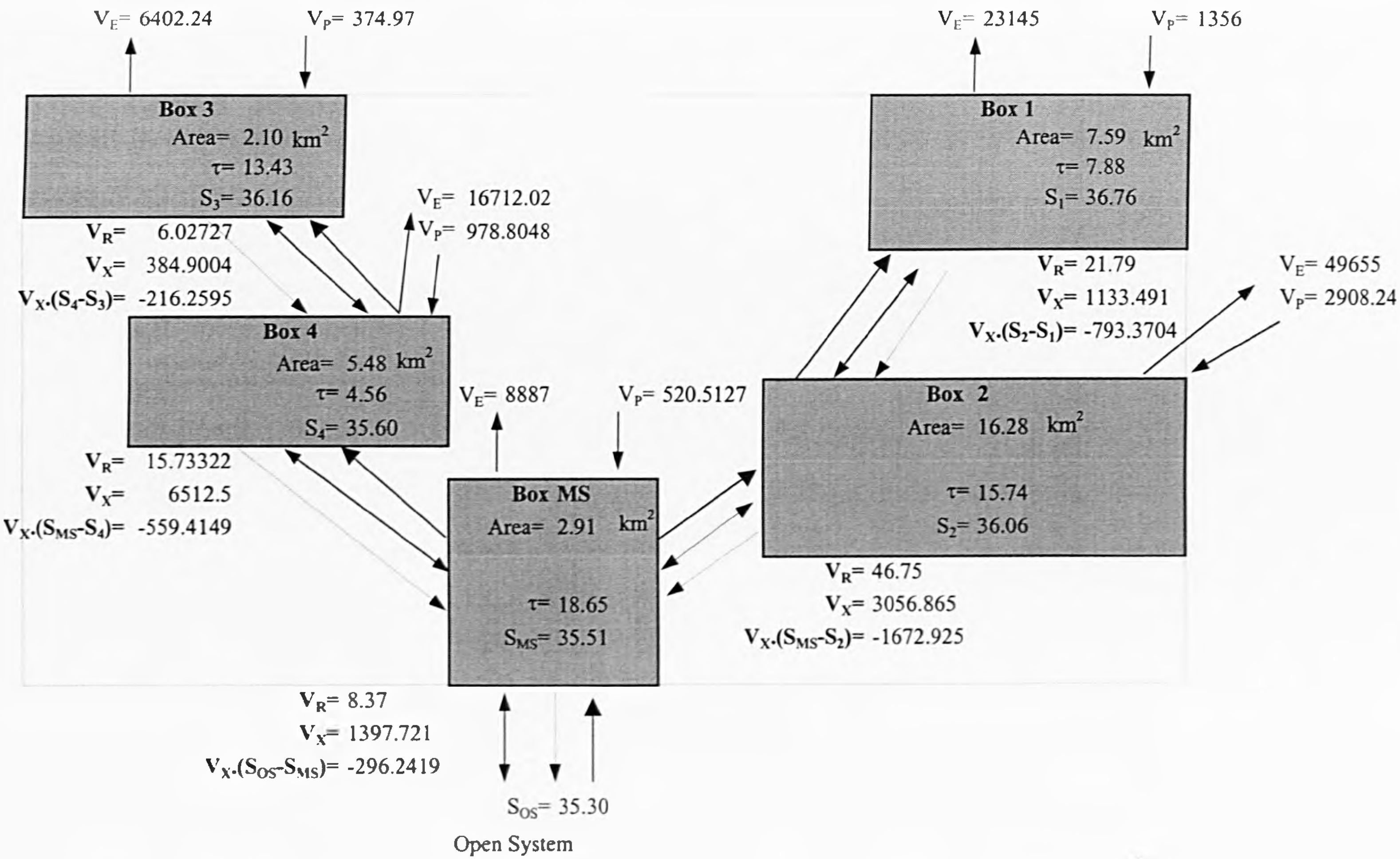

Figure 5.15a. Steady-state water and salt budgets for the Guaymas system, during winter season. Water fluxes in 10^3 m^3 d^{-1}, Salt fluxes in 10^3 kg d^{-1}. Arrows at the top of the boxes represent input and outputs by evaporation and precipitation processes; the wide head arrows represent the advective flows between compartments; the dashed arrows represent salt delivery; and, the double head arrows represent the mixing between compartments.

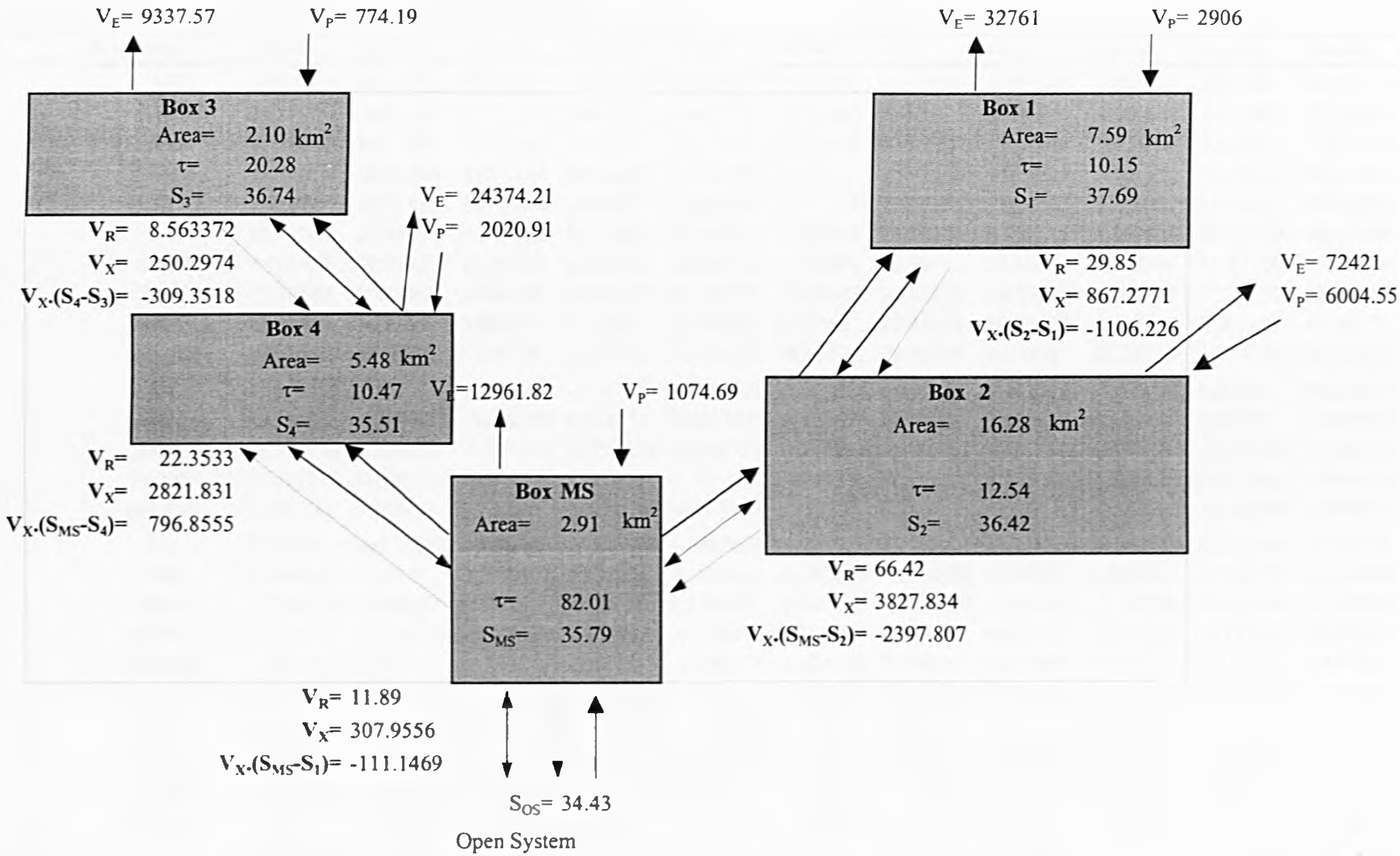

Figure 5.15b. Steady-state water and salt budgets for the Guaymas system, during summer season. Water fluxes in 10^3 m^3 d^{-1}, Salt fluxes in 10^3 kg d^{-1}. Arrows at the top of the boxes represent input and outputs by evaporation and precipitation processes; the wide head arrows represent the advective flows between compartments; the dashed arrows represent salt delivery; and, the double head arrows represent the mixing between compartments.

Table 5.10. Summary of budget properties for the Guaymas System.

	Box-linkages	Oct-Nov	December	January	February	March	Winter	April	May	Jun-Jul	Aug-Sep	Summer
Vx $(10)^3 m^3 d^{-1}$	I-II	851.4766	851.4766	2072.637	52746.39	654.9518	1133.491	615.7908	1075.005	1370.524	663.997	867.2771
	II-MS	4977.724	1638.38	4231.082	2934.217	4048.798	3056.865	4682.4	3219.851	3709.641	4032.987	3827.834
	III-IV	425.0528	841.7848	876.9047	243.8437	237.3231	384.9004	314.2787	191.2411	301.4595	222.9125	250.2974
	IV-MS	4867.954	1818.144	4954.143	2561.657	1715.678	6512.5	2830.368	940.4222	2603.392	3112.248	2821.831
	MS-OS	780.8408	1332.413	1792.156	3180.811	776.9198	1397.721	1083.358	710.4505	300.6021	133.5872	307.9556
τ days	I-II	10.4299	10.4299	4.348722	0.172606	13.45873	7.883864	14.13175	8.252116	6.469428	13.22629	10.15244
	II-MS	9.722532	28.98927	11.41948	16.38751	11.92773	15.73991	10.2973	14.8868	12.88706	11.93109	12.54428
	III-IV	12.17586	6.190962	5.944708	21.00593	21.56878	13.42645	16.28924	26.35116	16.82802	22.73872	20.27643
	IV-MS	6.095093	16.23147	5.98939	11.5491	17.19206	4.55966	10.44034	30.96937	11.31522	9.501225	10.46575
	MS-OS	33.23542	19.56297	14.56779	8.224581	33.40137	18.65434	23.96745	36.3554	83.24119	181.4228	82.00793
ΔP $mol.m^2.d^{-1}$	I-II	-0.047053	0.052634	0.12714	-15.47585	-0.110607	-0.089824	0.010037	0.101727	-0.421562	0.03936	-0.030337
	II-MS	-0.354803	-0.047472	-0.679798	0.121212	0.083217	-0.121673	-0.973267	0.100818	0.514158	0.09428	-0.013998
	III-IV	-0.173358	0.198513	-1.691261	-0.209279	-0.018727	-0.233932	-0.030814	-0.147841	-0.018319	-0.091256	-0.084163
	IV-MS	-1.019737	-0.290177	2.601693	1.287468	0.109374	0.949795	-0.331172	0.285896	1.037154	0.281568	0.480436
	MS-OS	0.661277	0.240115	1.251303	0.008326	-0.417309	0.333336	0.780753	-0.102581	-0.055018	-0.021597	0.016764
ΔN $mol.m^2.d^{-1}$	I-II	0.16874	-0.235502	1.414666	-7.293392	0.088746	0.133777	-0.028304	-0.335534	-1.395305	6.299506	1.730474
	II-MS	2.485455	-0.7077	-0.634572	0.238695	-0.434978	-0.067615	-1.553404	0.438522	0.807822	-1.547276	-0.344083
	III-IV	-1.236718	0.585877	-2.03115	-0.490966	0.190528	-0.447057	-1.404242	-2.435363	-2.212395	0.124286	-1.474981
	IV-MS	9.735847	-0.244913	-0.932101	1.288842	-0.129357	2.771341	1.924641	4.46038	3.672997	-4.112031	3.904857
	MS-OS	-2.05311	1.597281	-5.389747	-5.487313	-0.289177	-1.825408	2.41084	0.378968	-0.02524	0.451991	0.463684
N(*fix-denit*) $mol.m^2.d^{-1}$	I-II	0.921585	-1.077638	-0.619573	240.3201	1.85846	1.570957	-0.188892	-1.963166	5.349679	5.669744	2.215864
	II-MS	8.162306	0.051858	10.2422	-1.700696	-1.766452	1.87915	14.01887	-1.17457	-7.418713	-3.055755	-0.120108
	III-IV	1.537007	-2.590335	25.02902	2.857504	0.490167	3.295856	-0.911223	-0.069904	-1.919292	1.584381	-0.128372
	IV-MS	26.05163	4.397927	-42.55918	-19.31064	-1.879334	-12.42538	7.223388	-0.113963	-12.92147	-8.617116	-3.782123
	MS-OS	-12.63354	-2.244562	-25.41059	-5.620522	6.387764	-7.158791	-10.08121	2.02027	0.855043	0.79754	0.195463
NEM (*p-r*) $mol.m^2.d^{-1}$	I-II	4.987602	-5.579152	-13.47683	1640.44	11.72436	9.521322	-1.063898	-10.78306	44.68552	-4.172171	3.215706
	II-MS	37.60914	5.032072	72.05861	-12.84846	-8.821016	12.89732	103.1663	-10.68674	-54.50079	-9.993676	1.483832
	III-IV	18.37592	-21.0424	179.2736	22.18361	1.985108	24.7968	3.266247	15.67117	1.941809	9.673128	8.921288
	VI-MS	108.0921	30.75881	-275.7794	-136.4716	-11.5936	-100.6783	35.1042	-30.30502	-109.9383	-29.84619	-50.92625
	MS-OS	-70.09532	-25.4522	-132.6381	-0.882512	44.23473	-35.33366	-82.75982	10.87362	5.831875	2.289261	-1.776961

Vx = Mixing volume, τ = Residential time, ΔP = Nonconservative flux of P, ΔN = Nonconservative flux of N,

N(fix-denit) Difference between nitrogen fixation and denitrification, NEM (p-r) = Net Ecosystem Metabolism (production - respiration).

Non-conservative budgets. Box 3 works as a net sink for DIP, whereas Box 4 works as a net DIP producer, exporting to Box 3 and Box MS through winter and summer (Figure 5.16a and 5.16b). Certainly, fluxes of ΔDIP in the Guaymas basin seem to be determined by Box 4. Within this box are identified the main discharges from both industrial and urban sources for the Guaymas sub-system. On a monthly basis, Box 3 works as net sink of DIP through the whole year, except for December, during which Box 4 shows an unusual minimum value which allows a slight negative gradient with Box 3 (Table 5.10). In general for this compartment, P is likely to be assimilated by phytoplankton and benthic algae or buried into sediments. For Box 4, October-November, December and April were the months in which the compartment became a sink of P. This pattern may be related to a high DIP concentration in Box MS, these higher concentrations are associated with the fishing industry loads, which are located outside the system.

For both averaged seasons within the Guaymas sub-system, nitrogen is pumped from Box 4 to Boxes 3 and MS (Figures 5.17a. and 5.17b). As stated before, Box 4 is associated with anthropogenic organic matter discharges (Figure 1.3; Figures 5.17a. and 5.17b). A substantial proportion of this nitrogen is exported through advection fluxes as shown in Figures 5.17a and 5.17b, however, an important part may be fixed by phytoplankton. Thus, an important and persistent phytoplankton biomass has been associated with this area (Chapter 6).

Nitrogen fixation-denitrification. Nitrogen fixation was a dominant process for Box 3 during winter, whereas, in the summer, denitrification was dominant in this compartment (Figures 17a. and 17b). Denitrification bacteria capabilities may be increased with high temperatures during the warm months (Jansson, 1994). In spite of the high DIN measured for Box 4, the expected ΔDIN scaled through the Redfield ratio is higher than the ΔDIN observed, which indicates that denitrification processes were dominant during winter and summer. Thus, if the stoichiometric proportions used in this approach works, an important part of the produced N must be taken or buried within the system. However, it

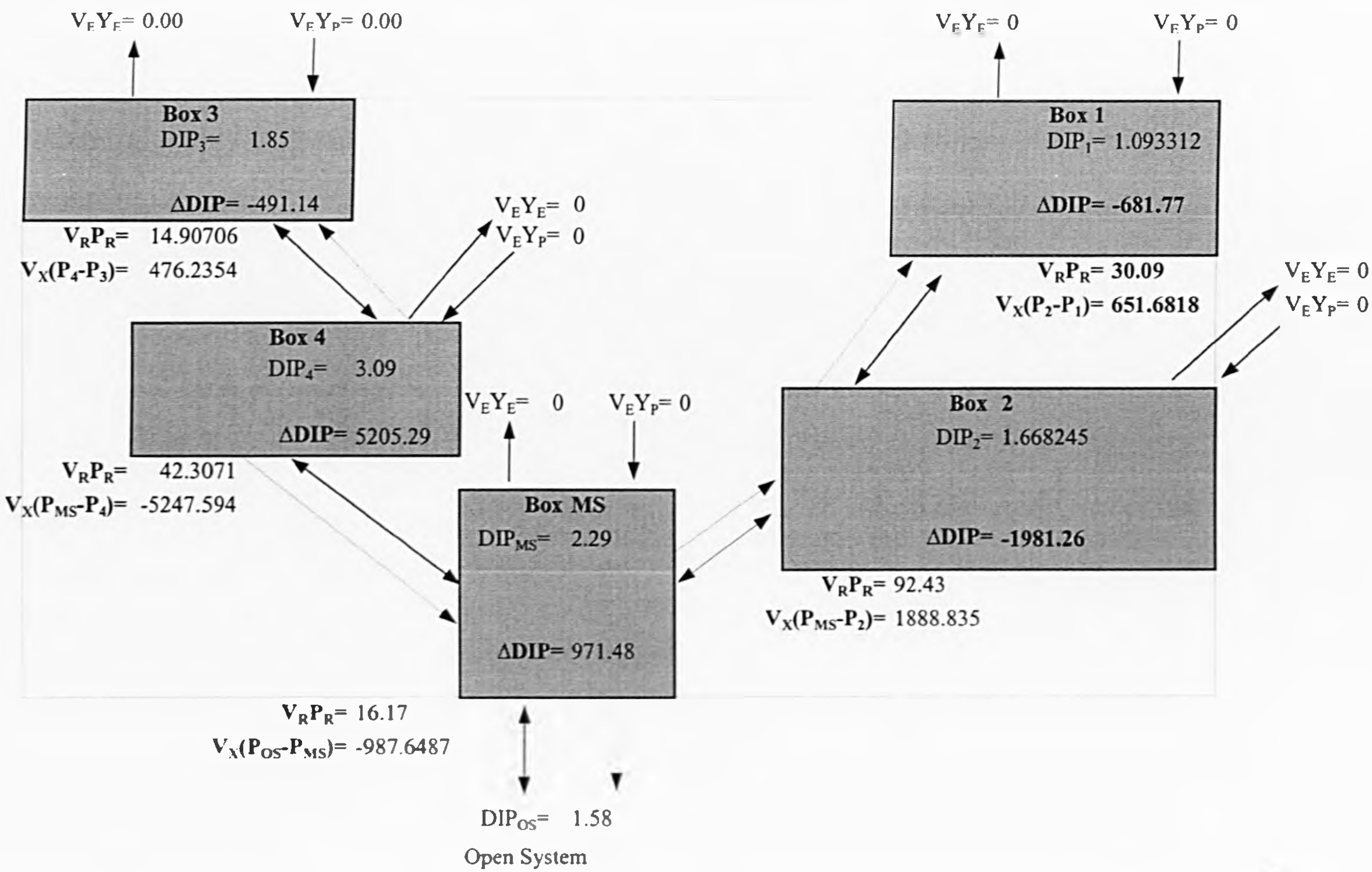

Figure 5.16a. Steady-state dissolved inorganic P budget for the Guaymas system, winter season. Phosphorus fluxes (ΔDIP) in mold^{-1}; Vx.(S_{out}-S_{in}) is given in $(10)^3$mmold^{-1}. Arrows at the top of the boxes represent inputs and outputs from atmospheric processes; the double head arrows represent the mixing between compartments; and, the dashed arrows indicate the combined entrainment (V_RY_R) and mixing ($V_X(Y_2-Y_1)$) fluxes.

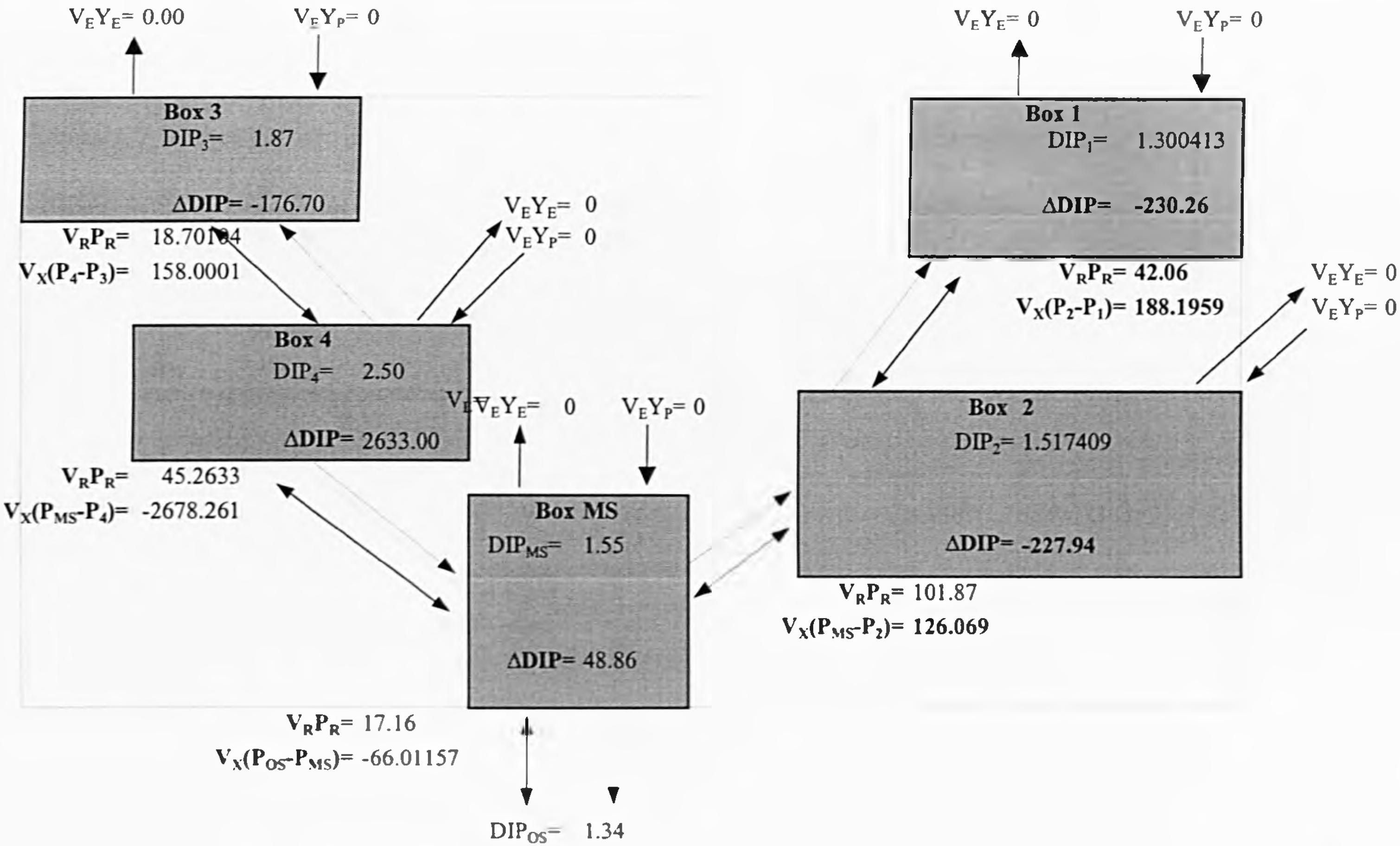

Figure 5.16b. Steady-state dissolved inorganic P budget for the Guaymas system, summer season. Phosphorus fluxes (ΔDIP) in mold^{-1}; Vx.(S_{out}-S_{in}) is given in $(10)^3$mmold^{-1}. Arrows at the top of the boxes represent inputs and outputs from atmospheric processes; the double head arrows represent the mixing between compartments; and, the dashed arrows indicate the combined entrainment ($V_R Y_R$) and mixing ($V_X(Y_2-Y_1)$) fluxes.

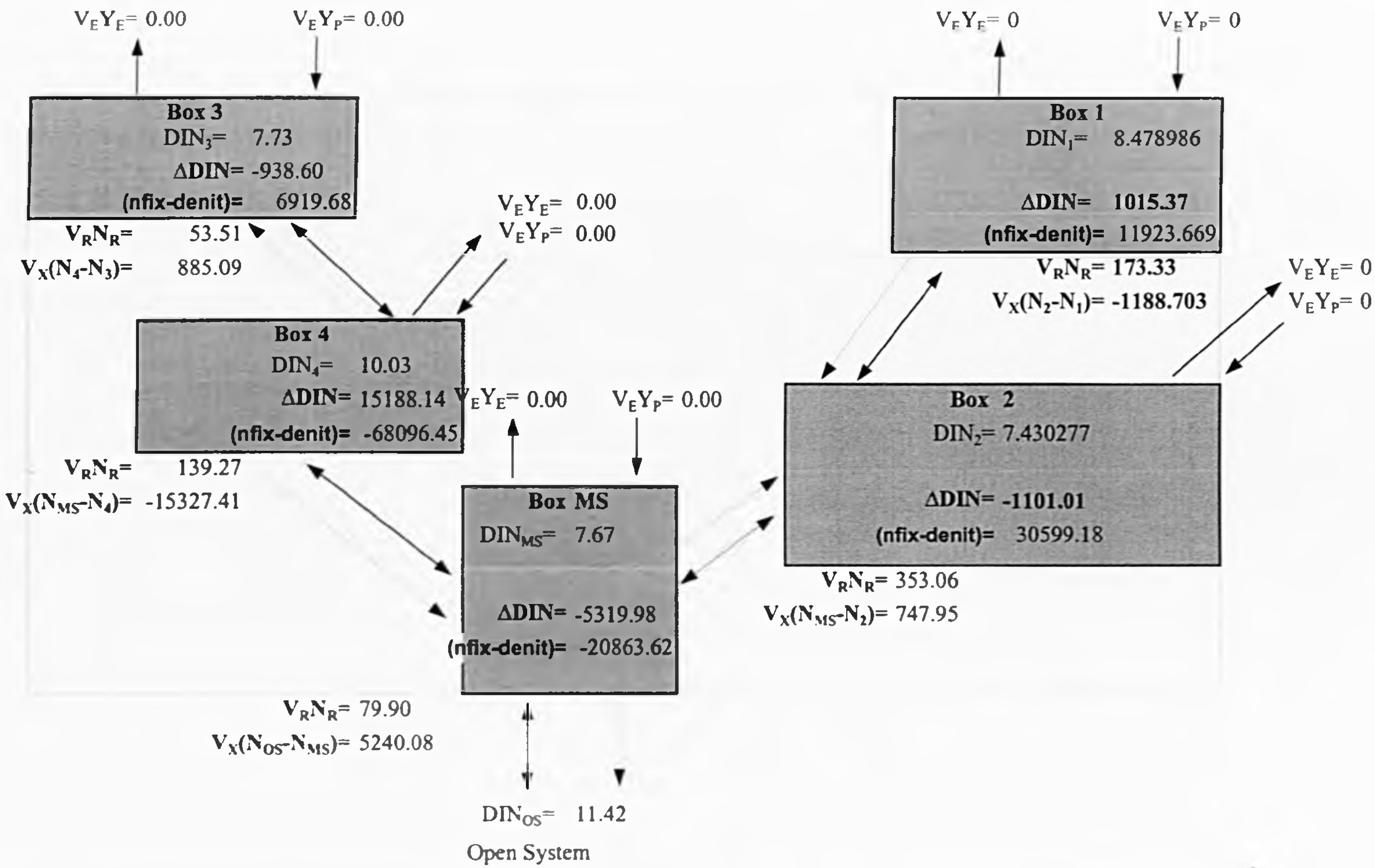

Figure 5.17a. Steady-state dissolved inorganic N budget for the Guaymas system, winter season. Nitrogen fluxes (ΔDIN) in $mold^{-1}$; $Vx.(S_{out}-S_{in})$ is given in $(10)^3 mmold^{-1}$. Arrows at the top of the boxes represent inputs and outputs from atmospheric processes; the double head arrows represent the mixing between compartments; and, the dashed arrows indicate the combined entrainment ($V_R Y_R$) and mixing ($V_X(Y_2-Y_1)$) fluxes.

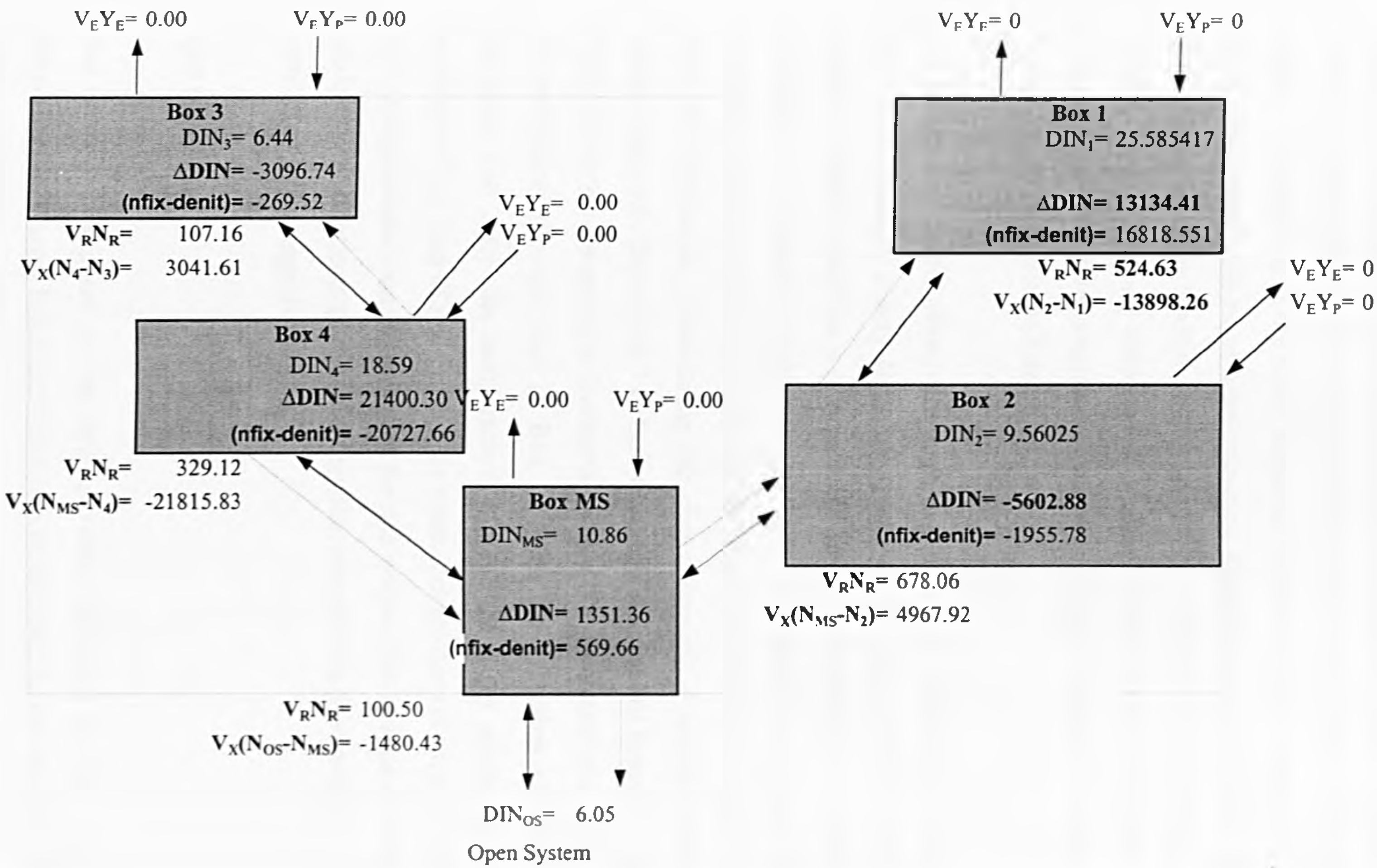

Figure 5.17b. Steady-state dissolved inorganic N budget for the Guaymas system, summer season. Nitrogen fluxes (ΔDIN) in $mol d^{-1}$; $Vx.(S_{out}-S_{in})$ is given in $(10)^3 mmol d^{-1}$. Arrows at the top of the boxes represent inputs and outputs from atmospheric processes; the double head arrows represent the mixing between compartments; and, the dashed arrows indicate the combined entrainment (V_RY_R) and mixing ($V_X(Y_2-Y_1)$) fluxes.

is important to highlight that, generally, in environments affected by industrial and urban discharges, Redfield proportions are likely to be modified, and hence there must be a slight over-estimation of the ΔDIN expected within the system (Jacinto, *et al.* 1998). The above observation may be of more relevance when the system has been fragmented and areas characterised by wastewater, isolated. At a monthly basis, nitrogen denitrification for Box 3 during January shows a relative high positive value, which accounts for large proportion of the winter season. For summer, nitrogen fixation is a dominant process during August-September (Table 5.10).

Net Ecosystem Metabolism. The high negative value observed in scenario 3 for the Guaymas-subsystem during June-July, tends to disappear when the former Box 3 is divided into Box 3 and Box 4 (Tables 9 and 10). This indicates the disadvantage of using mathematical averages within this approach. Averaged values tend to magnify or minimise some processes that occur in the computational domain, especially when large areas are represented. Considering the above, scenario 4 seems to represent a more realistic approach. Either Box 3 or Box 4 presents a sinusoidal behaviour through the year (Table 5.10). An exception is December, where the respiration processes dominate over the production through year in Box 3. With the exception of October-November, December and April the compartment 4 presented a net production throughout the remainder of the year (Table 5.10). This consistent production coincides with a persistent high phytoplankton biomass observed for this system (See chapter 6). This high biomass indicates persistent eutrophication symptoms related with phytoplankton blooms near to areas receiving sewage discharges.

5.3.5 Scenario 5.

This scenario is focused on the new boundary definition for the Guaymas sub-basin compartments. Former box 3 is divided into boxes 3 and 4, whiles box 4 is separated into boxes 5 and 6 (Figure 5.5).

Salt and water budget. Water fluxes within the new compartments follow the same patterns as in previous scenarios, where the box area defines V_R (Figures 5.18a and 5.18b).

There is a net salt delivery from Box 3 to Box 4, and from it to Box 6 which delivers to both Box 5 and Box MS. The above pattern is maintained during the two averaged seasons, where salt delivery is increased during summer as a response to evaporation and almost absent rainfall. Box 5 represents those fixed stations most closely situated to known urban and industrial discharges. Thus, low salinity from Box 5 must be the result of seawater dilution from fresh water sources (Figure 1.3). This produces a negative gradient against Box 6, implying a negative salt wedge in this compartment. In this case, box fragmentation allows segregating areas receiving wastewater into small and mostly realistic areas. Also, very low salinity gradients between Box 4 and Box 6 indicate the possibility of re-combining these two boxes.

Non-conservative budgets. During winter, there is a net transfer of DIP from Box 5 to Box 6, and a slight net transfer from Box 4 to Box 3 and Box 6 (Figure 5.19a). For summer, Box 3 became source of P and, together with Box 5, drives ΔDIP fluxes toward the mouth of the system (Figure 5.19b).

During winter, Box 3 works as a net sink of DIP, whereas in summer it became a net source of phosphate (Figures 5.19a and 5.19b). This small compartment is characterised as having a big proportion of mud flats, including a limited mangrove area. The compartment might work as small trap for domestic drainage discharges during most of the year. However, these kinds of traps often present pulsing releases which are dynamically-influenced by hydrological and hydrochemical conditions, and intensified by any increase in runoff (Arheimer and Wittgren, 1994; Sham, *et al.* 1995). Also, it is likely that phosphate releases from organic matter oxidation and sediment fluxes are boosted by high temperatures during summer season.

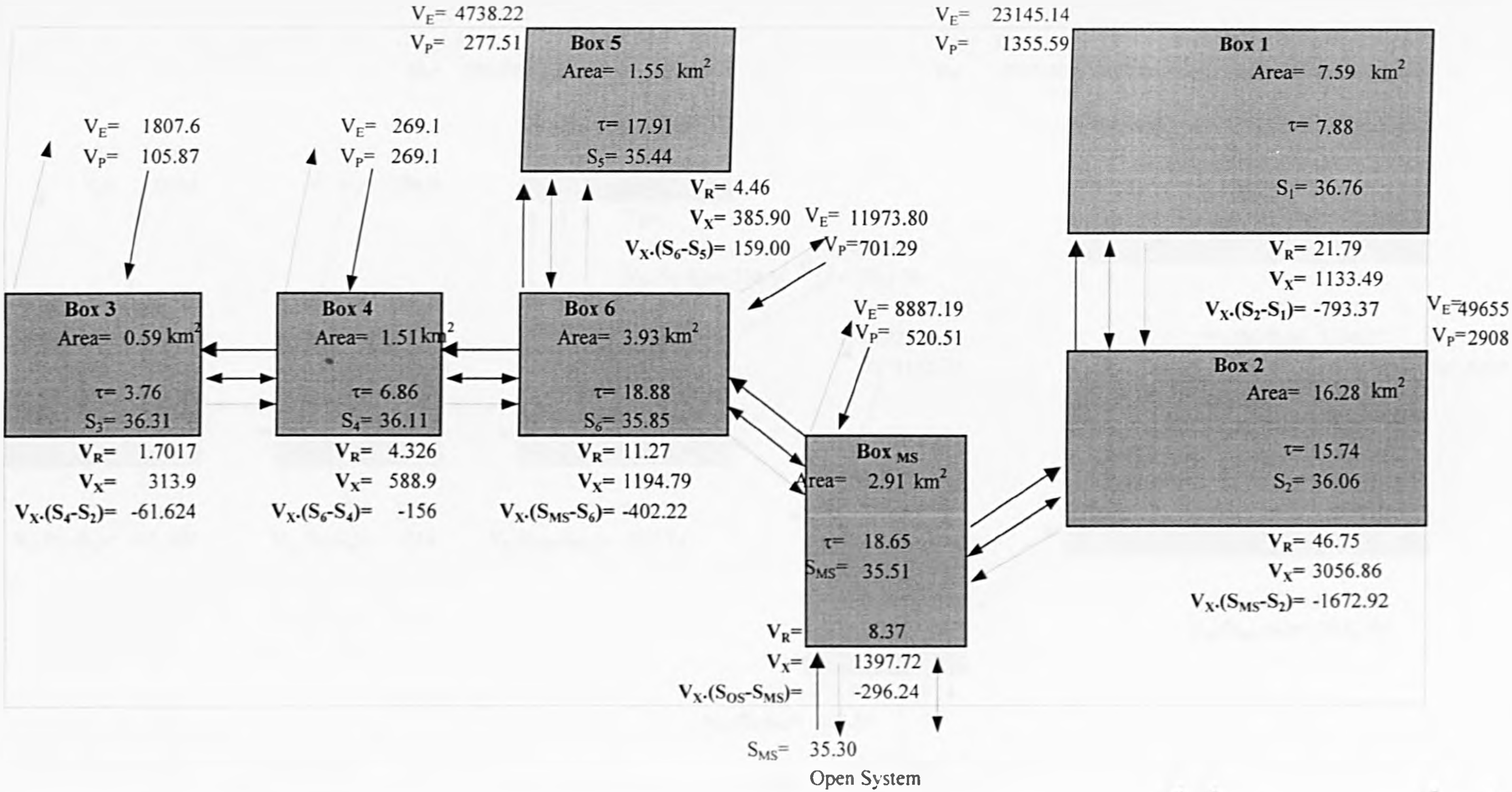

Figure 5.18a. Steady-state water and salt budgets for the Guaymas system, during winter season. Water fluxes in 10^3 m^3 d^{-1}, Salt fluxes in 10^3 kg d^{-1}. Arrows at the top of the boxes represent input and outputs by evaporation and precipitation processes; the wide head arrows represent the advective flo between compartments; the dashed arrows represent salt delivery; and, the double head arrows represent the mixing between compartments.

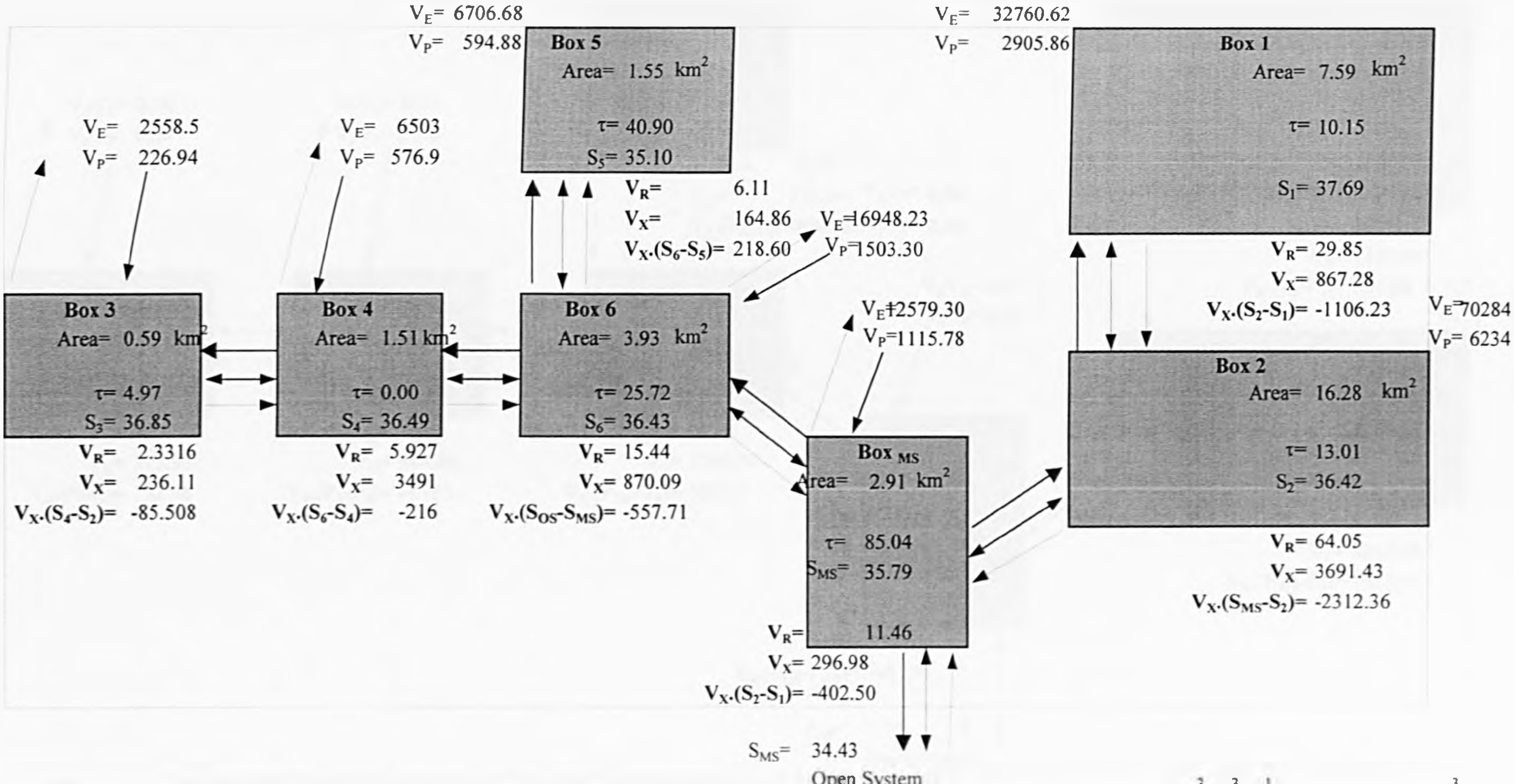

Figure 5.18b. Steady-state water and salt budgets for the Guaymas system, during summer season. Water fluxes in 10^3 m^3 d^{-1}. Salt fluxes in 10^3 kg d^{-1}. Arrows at the top of the boxes represent input and outputs by evaporation and precipitation processes; the wide head arrows represent the advective flo between compartments; the dashed arrows represent salt delivery; and, the double head arrows represent the mixing between compartments.

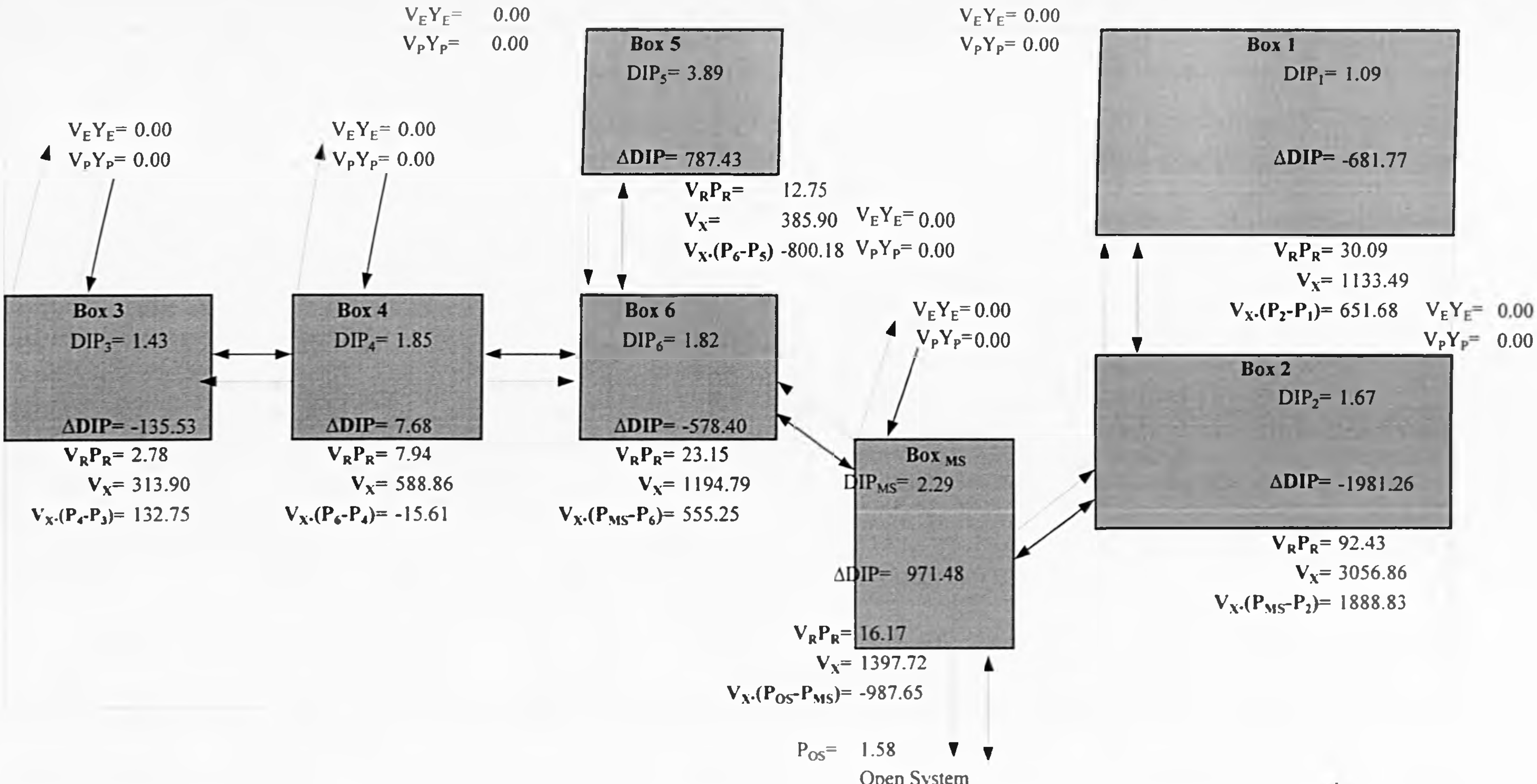

Figure 5.19a. Steady-state dissolved inorganic P budget for the Guaymas system, winter season. Phosphorus fluxes (ΔDIP) in mold^{-1}; $Vx.(S_{out}-S_{in})$ is given in $(10)^3$mmold^{-1}. Arrows at the top of the boxes represent inputs and outputs from atmospheric processes; the double head arrows represent the mixing between compartments; and, the dashed arrows indicate the combined entrainment (V_RY_R) and mixing ($V_X(Y_2-Y_1)$) fluxes.

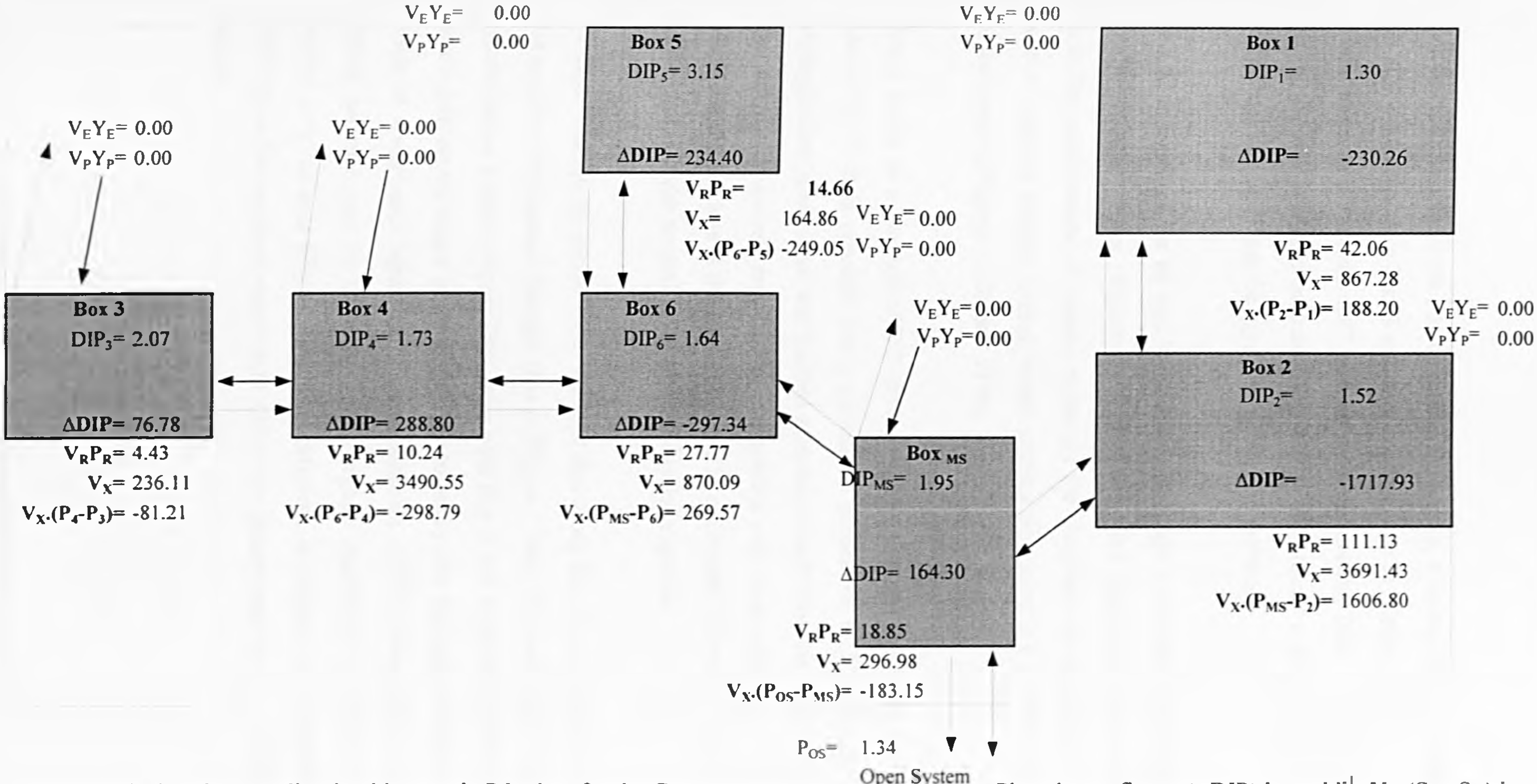

Figure 5.19b. Steady-state dissolved inorganic P budget for the Guaymas system, summer season. Phosphorus fluxes (ΔDIP) in $mold^{-1}$; $Vx.(S_{out}-S_{in})$ is given in $(10)^3 mmold^{-1}$. Arrows at the top of the boxes represent inputs and outputs from atmospheric processes; the double head arrows represent the mixing between compartments; and, the dashed arrows indicate the combined entrainment ($V_R Y_R$) and mixing ($V_X(Y_2-Y_1)$) fluxes.

Box 4 works as a weak net source during the winter, whereas, during summer, works as a net sink with respect to Box 3 and as a slight source in relation to Box 6. Thus, this Box works more as a "transitional" compartment connecting Box 3 with Box 6. Moreover, during the two averaged seasons, Box 4 does not present a strong gradient with Box 6, suggesting that both may be regarded as one compartment.

Box 5, as expected for an area located near drainage and wastewater discharges, showed the higher ΔDIP fluxes (Figures 1.3; 5.19a and 19b). Certainly, this compartment seems to be the major source of organic matter for the Guaymas sub-system and hence from the whole Guaymas system. During winter and summer there is a net flux toward the month of the system (Figures 5.19a and 519b).

Box 6 works as a net sink of DIP during winter, although it is necessary to question the fate of the P. It is possible that a substantial proportion of DIP can be assimilated by phytoplankton since there was located a persistent high biomass in Box 6 (Chapter 6). An alternative explanation may be the interactions with suspended material and sediments where substantial loss is the result of burial in sediments. However, further research must carried out in order to confirm or reject those assumptions.

Nitrogen budgets in winter show a ΔDIN flux from Box 4 to Box 3, and from Box 5 to the mouth of the system through Box 6 (Figure 5.20a). For summer, the inner part of the system Boxes 3 and 4 import DIN from both Box 5 and compartment MS (Figure 5.20b). Box 5 delivers the major input of nitrogen to the system through the whole year, which is result of wastewater inputs to this compartment. ΔDIN fluxes from compartment MS during summer may be associated with organic discharges from the fishing industry located near the area (Figure 1.3). This influence is evident during winter, but the high DIN inputs derived from wastewater within the system seem to drive ΔDIN fluxes for this season.

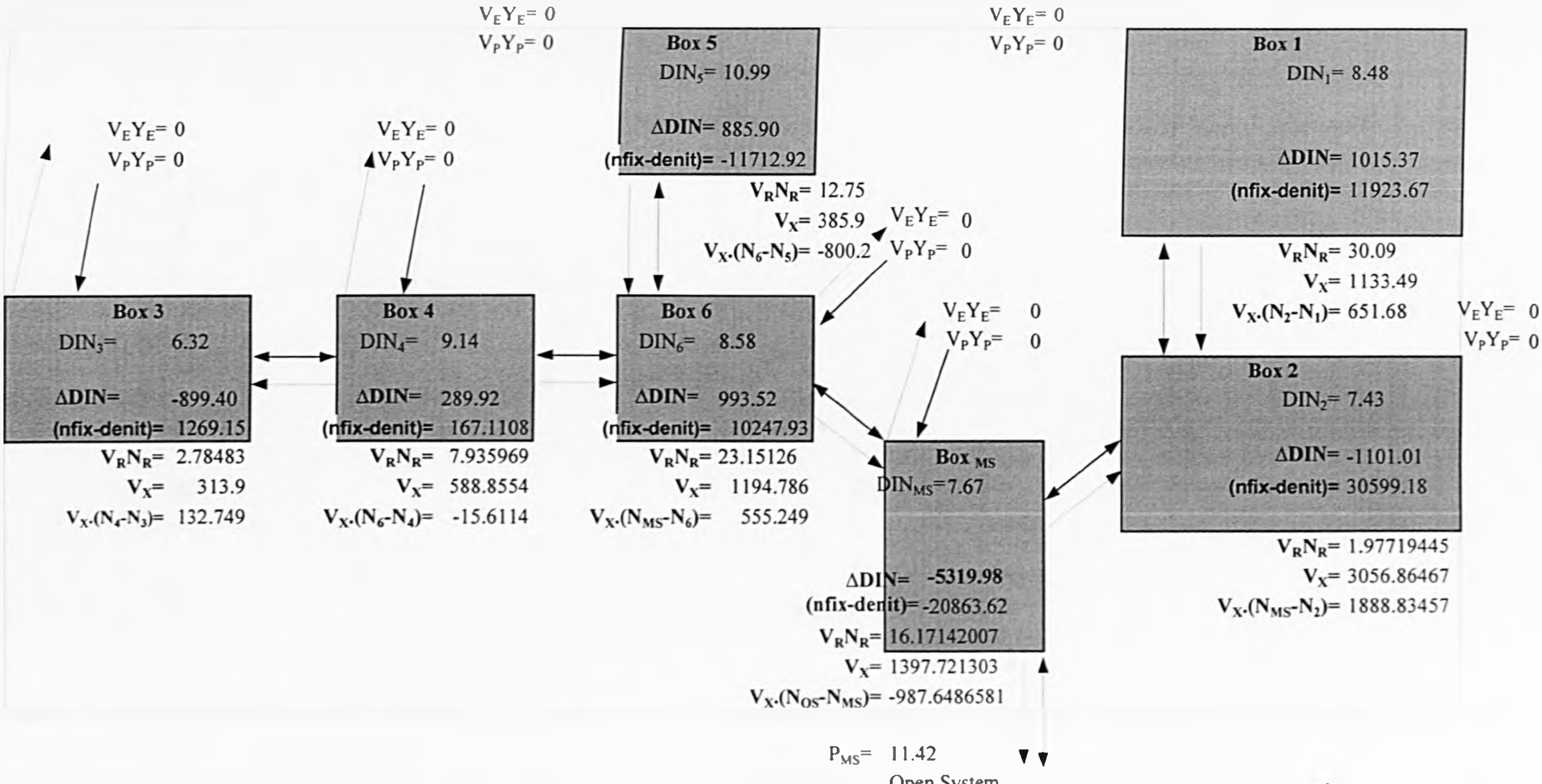

Figure 5.20a. Steady-state dissolved inorganic N budget for the Guaymas system, winter season. Nitrogen fluxes (ΔDIN) in mold^{-1}; Vx.(S_{out}-S_{in}) is given in $(10)^3$mmold^{-1}. Arrows at the top of the boxes represent inputs and outputs from atmospheric processes; the double head arrows represent the mixing between compartments; and, the dashed arrows indicate the combined entrainment (V_RY_R) and mixing ($V_X(Y_2-Y_1)$) fluxes.

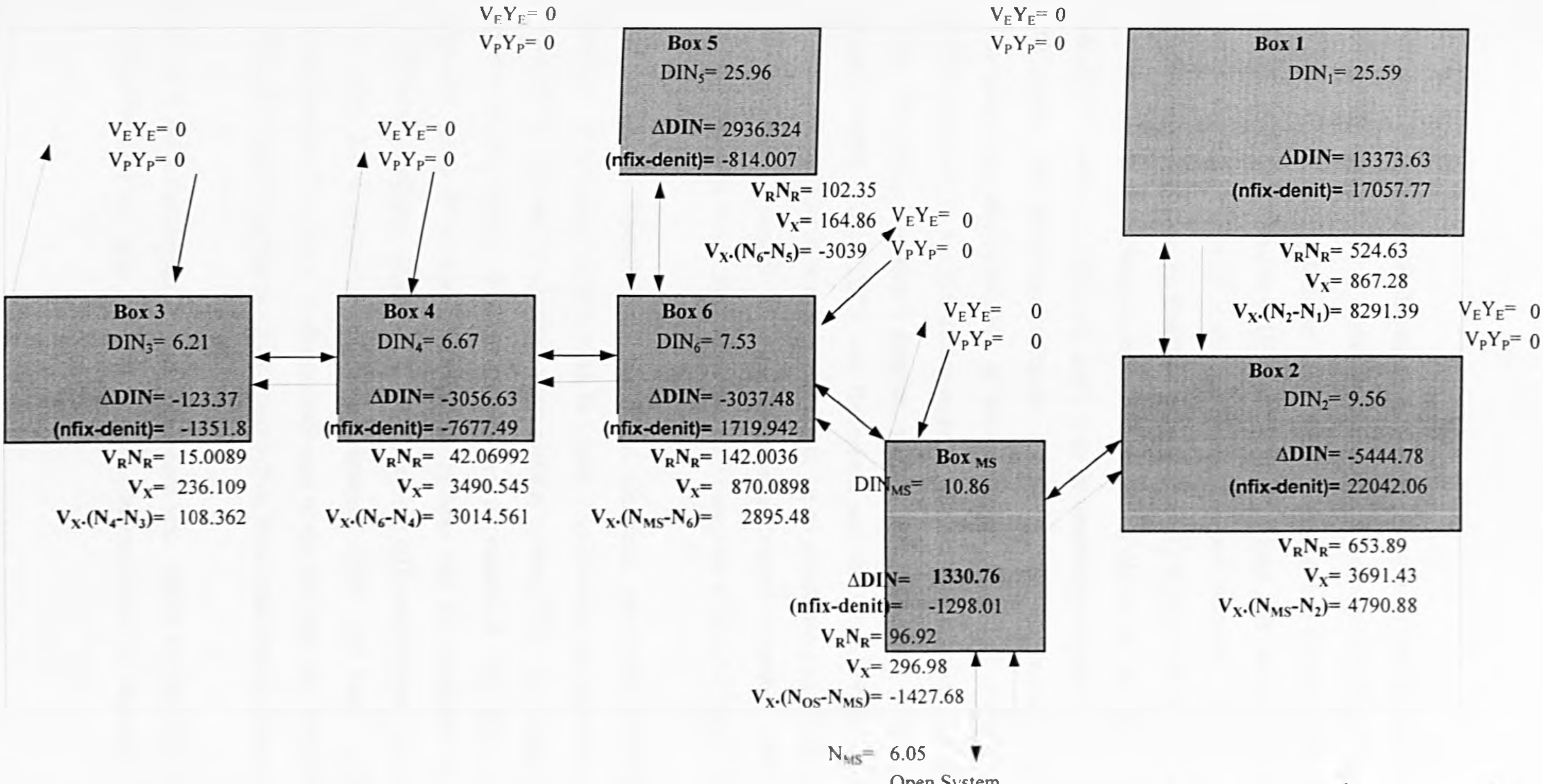

Figure 5.20b. Steady-state dissolved inorganic N budget for the Guaymas system, summer season. Nitrogen fluxes (ΔDIN) in mold^{-1}; Vx.(S_{out}-S_{in}) is given in $(10)^3$mmold^{-1}. Arrows at the top of the boxes represent inputs and outputs from atmospheric processes; the double head arrows represent the mixing between compartments; and, the dashed arrows indicate the combined entrainment (V_RY_R) and mixing ($V_X(Y_2-Y_1)$) fluxes.

Nitrogen fixation-denitrification. In winter, nitrogen denitrification was a dominant process for boxes 3 and 5, whiles for boxes 4 and 6 nitrogen fixation was a dominant one (Figure 5.20a). During summer in the whole Guaymas sub-system, denitrification became the most important processes (Figure 5.20b). However, it is known that the major organic matter reacting in Box 5 is sewage derived organic material, and for consistency, the present work assumes the Redfield ratio, N:P 16:1, which is similar to that proposed by Jacinto (1998) for sewage-material of N:P 15:1. However, the real N:P ratio and its temporal variation is unknown, and it may be responsible mainly for the ΔDIN expected, and hence N-fixation-denitrification. Assuming that the reacting organic matter is dominated by phytoplankton in compartments 3 and 5 during winter and for compartments 3, 4, 5 and 6 during summer, the nitrogen supplied may be insufficient to cover the primary producer demand, so that demand can be covered by turnover of organic matter (Heip, 1995; van Beusekom and de Jonge, 1998). Another important process to consider is that N burial might be an important part of the nitrogen lost by denitrification. Through the year there is a dynamic transition from N-fixation to denitrification in all the compartments, with exception of Box 5 (Table 5.11b).

Net Ecosystem Metabolism. The NEM Guaymas sub-system presented spatial and temporal differences (Table 5.11b). In winter, respiration is the dominant process for Box 3, whiles in summer it became a heterotrophic system. Box 4 is a slightly heterotrophic system during winter, whereas in summer it presents a very high production. This elevated value of production registered in May can be explained by the very little difference in salinity respect to Box 6. This little difference between boxes enhances the Vx value by a factor of 100, overestimating ΔDIP, and hence production in this compartment. The above, is also an indicator of the fact that Box 4 and Box 6 should be integrated, and it highlights a problem resulting from unnecessary fragmentation.

Box 5 is net heterotrophic through the whole year, except in December. In this case the use of the Redfield ratio C:P 106:1 may under-estimated the capacity of the system to

Table 5.11a. Summary of budget properties for the Guaymas System.

	Box	Oct-Nov	December	January	February	March	Winter	April	May	Jun-Jul	Aug-Sep	Summer
Vx $(10)^3 m^3 d^{-1}$	I-II	851.4766	851.4766	2072.637	52746.39	654.9518	1133.491	615.7908	1075.005	1370.524	663.997	867.2771
	II-MS	4977.724	1638.38	4231.082	2934.217	4048.798	3056.865	4682.4	3219.851	3667.594	3471.513	3691.426
	III-IV	2862.77	421.2327	119.0203	740.5331	282.7885	313.8997	147.6325	228.7682	399.7455	269.0931	236.1091
	IV-VI	377.882	666.5838	1074.94	257.4778	2066.742	588.8554	357.0957	351.1846	30342.62	695.7768	3490.545
	V-VI	1372.771	1981.981	938.4102	394.4874	108.4541	385.8985	2089.195	82.69345	147.5881	220.6854	164.8632
	IV-MS	1988.776	1543.654	1870.915	873.0977	736.4185	1194.786	1648.255	482.195	952.3258	1195.367	870.0898
	MS-OS	780.8408	1332.413	1792.156	3180.811	776.9198	1397.721	1083.358	710.4505	297.1949	114.9891	296.9814
τ days	I-II	10.4299	10.4299	4.348722	0.172606	13.45873	7.883864	14.13175	8.252116	6.469428	13.22629	10.15244
	II-MS	9.722532	28.98927	11.41948	16.38751	11.92773	15.73991	10.2973	14.8868	13.03481	13.8608	13.00783
	III-IV	0.413877	2.803125	9.820395	1.597255	4.167236	3.75644	7.910152	5.13195	2.944253	4.3744	4.972045
	IV-VI	10.64395	6.063708	3.769413	15.53913	1.9643	6.858275	11.21342	11.39915	0.134043	5.806174	1.163515
	V-VI	5.076993	3.519959	7.415856	17.52658	61.92451	17.91221	3.337444	78.94263	45.04343	30.97604	40.89599
	IV-MS	11.38689	14.64657	12.09993	25.75204	30.45955	18.88327	13.6938	45.81869	23.43899	18.85117	25.71817
	MS-OS	33.23542	19.56297	14.56779	8.224581	33.40137	18.65434	23.96745	36.3554	84.19549	210.7657	85.03835
ΔP $mol.m^2.d^{-1}$	I-II	-0.047053	0.052634	0.12714	-15.47585	-0.110607	-0.089824	0.010037	0.101727	-0.421562	0.03936	-0.030337
	II-MS	-0.354803	-0.047472	-0.679798	0.121212	0.083217	-0.121673	-0.973267	0.100818	0.141887	0.081154	-0.105501
	III-IV	-3.515739	-0.518872	-0.212214	-0.123153	0.213443	-0.228646	0.014837	0.100375	0.477241	0.121475	0.129523
	IV-VI	0.043006	-0.135787	0.235568	-0.041008	0.122025	0.005094	0.364379	-0.036465	-5.484433	-0.381305	0.191674
	V-VI	0.773122	-0.169829	3.857489	0.608925	0.048793	0.506768	3.918859	0.126561	0.017743	0.027179	0.150851
	IV-MS	-0.917017	-0.312346	-0.463647	0.281917	-0.019801	-0.147303	-1.004118	0.016621	0.131584	0.10811	-0.075724
	MS-OS	0.661277	0.240115	1.251303	0.008326	-0.417309	0.333336	0.780753	-0.102581	0.105762	-0.01859	0.056374

Vx = Mixing volume, τ = Residential time, ΔP = Nonconservative flux of P, ΔN = Nonconservative flux of N,

N(fix-denit) Difference between nitrogen fixation and denitrification, NEM (p-r) = Net Ecosystem Metabolism (production - respiration).

Table 5.11b. Summary of budget properties for the Guaymas System.

	Box	Oct-Nov	December	January	February	March	Winter	April	May	Jun-Jul	Aug-Sep	Summer
ΔN mol.m^2.d^{-1}	I-II	0.16874	-0.235502	1.414666	-7.293392	0.088746	-1.171348	-0.028304	-0.331301	-1.395305	6.299506	1.136149
	II-MS	2.485455	-0.7077	-0.634572	0.238695	-0.434978	0.18938	-1.553404	0.434149	0.798666	-1.331864	-0.413113
	III-IV	19.41677	-5.373369	-0.927971	-2.045725	-2.171662	1.779609	-1.004805	1.118799	0.218721	-0.588548	-0.063958
	IV-VI	-0.260334	0.126061	-1.688226	0.062985	7.183401	1.084777	0.417755	-0.933119	-36.01129	0.141694	-9.096241
	V-VI	10.26229	-10.4754	0.185782	1.558674	0.129604	0.332189	20.14302	1.914859	2.055714	-0.453912	5.914921
	IV-MS	2.004877	1.639582	-0.620699	-0.216446	-0.303536	0.500755	-2.213148	0.322061	-1.386187	-1.684047	-1.240331
	MS-OS	-2.05311	1.597281	-5.389747	-5.487313	-0.289177	-2.324413	2.41084	0.375941	-0.024954	0.389064	0.787723
N(*fix-denit*) mol.m^2.d^{-1}	I-II	0.921585	-1.077638	-0.619573	240.3201	1.85846	48.28059	-0.188892	-7.58E-25	5.349679	5.669744	2.707633
	II-MS	8.162306	0.051858	10.2422	-1.700696	-1.766452	2.997843	14.01887	1.01E-25	-1.471526	-2.630332	2.479252
	III-IV	75.6686	2.928587	2.467449	-0.075271	-5.586755	15.08052	-1.2422	5.37E-21	-7.417132	-2.532154	-2.797871
	IV-VI	-0.94843	2.298651	-5.45731	0.719107	5.231005	0.368605	-5.412311	-2.73E-22	51.73964	6.242572	13.14247
	V-VI	-2.10766	-7.758139	-61.53405	-8.184131	-0.651088	-16.04701	-42.55873	5.1E-22	1.771822	-0.888777	-10.41892
	IV-MS	16.67715	6.63712	6.797657	-4.727125	0.01328	5.079616	13.85274	5.32E-24	-3.491533	-3.41381	1.736849
	MS-OS	-12.63354	-2.244562	-25.41059	-5.620522	6.387764	-7.90429	-10.08121	1.52E-23	-1.717151	0.686506	-2.777963
NEM (*p-r*) mol.m^2.d^{-1}	I-II	4.987602	-5.579152	-13.47683	1640.44	11.72436	327.6191	-1.063898	-10.78306	44.68552	-4.172171	7.166599
	II-MS	37.60914	5.032072	72.05861	-12.84846	-8.821016	18.60607	103.1663	-10.68674	-15.04003	-8.602353	17.2093
	III-IV	372.6683	55.00046	22.49466	13.05426	-22.62499	88.11854	-1.572745	-10.6397	-50.58753	-12.87639	-18.91909
	IV-VI	-4.558635	14.39341	-24.97018	4.34681	-12.93462	-4.744644	-38.62419	3.865303	581.3499	40.41831	146.7523
	V-VI	-81.9509	18.00186	-408.8939	-64.54608	-5.172083	-108.5122	-415.3991	-13.41551	-1.880786	-2.880981	-108.3941
	IV-MS	97.20381	33.10869	49.14661	-29.88325	2.098909	30.33495	106.4365	-1.761875	-13.94792	-11.45967	19.81676
	MS-OS	-70.09532	-25.4522	-132.6381	-0.882512	44.23473	-36.96668	-82.75982	10.87362	-11.21081	1.970549	-20.28161

Vx = Mixing volume, τ = Residential time, ΔP = Nonconservative flux of P, ΔN = Nonconservative flux of N,
N(fix-denit) Difference between nitrogen fixation and denitrification, NEM (p-r) = Net Ecosystem Metabolism (production - respiration).

produce or consume organic matter. Other C:P ratios, used in systems dominated by sewage-derived organic material, imply the use of a 190:1 C:P ratio (Jacinto, *et al.* 1998). However, in order to be consistent, this work retains the Redfield ratio for this compartment. Also this indicates that segmentation of the system allows the use of different ratios depending upon the characteristics of the systems to be analysed.

Compartment 6 is characterised by a consistent production through winter and it is likely that this production is associated with phytoplankton, which maintains an elevated population in this compartment through the year. However, during the warm months from May to September, the system became net heterotrophic. As indicated, the system works as a pathway for ΔDIP fluxes from Box 3 and Box 5 to the open sea, therefore the positive ΔDIP flux provides a net heterotrophic characteristic.

5.3.6. General differences among scenarios.

The present work indicates that scenarios 1 and 2 are adequate to establish comparisons with other systems world-wide. In terms of management, scenarios 4 and 5 allow the qualitative isolation of areas that represent a source or sink of organic and inorganic matter, and fluxes among compartments indicate their influence in relation to neighbouring areas across space and time. The above provides a cost-effective tool for the management, since it provides the likely response of the system to the input of sewage discharges in specific areas.

A comparative exercise between scenarios provides an insight into which is the optimum box number and sizes for the system. Also indicated is which boxes better represent the area. Thus, in this case the increment in frequency affects in a positive way the representation of the model.

Finally, an important note for all these estimations is that estimations need to be taken with some degree of caution, as phytoplankton blooms may occur at time and scales of days and weeks, and the sampling interval for this work was set to months. Moreover, each sampling survey represents only a "snapshot" of the system metabolism.

5.4 Conclusion.

The salt budget approach (Gordon, *et al.* 1996), as limited to the present biochemical budgetary assessment, represents a good first approximation for the trophic status of the system. This highlights the areas that represent a net source or sink for nutrients and identifies those compartments that are net producers or consumers of organic matter.

The outcome of the present works shows that the system is net heterotrophic, with a value of -4811.72 $mmolm^{-2}y^{-1}$, which can be compared with other areas elsewhere assessed using budget analysis.

Although it is often recommended that robust budgets of systems should be developed at the larger scales than the smaller spatial scales, the analysis shows that fragmentation may help to identify and to isolate areas affected by anthropogenic activities. Also, the approach allows an indication of which compartments must be re-grouped in order to achieve better results.

The analysis also indicates the importance of the monitoring fixed stations in relation to the computational domain. The use of averaged stations in the representing big areas may under or over estimate the modelling outcomes.

The stoichiometric Redfield approach provides robust overviews of the nitrogen fixation-denitrification and NEM at large scale level (scenario 1 to 3). However, the analysis indicates that more appropriate relationships may be applied when fragmentation allows the identification of compartments characterised by the specific primary producer or sources of organic matter production.

The model produces a primary quantitative outcome of the eutrophic status for some areas affected by anthropogenic activities and an insight of their likely impact over the rest of the system. This above provides a valuable and cost-effective decision making-tool for the management of the Guaymas system.

5.5. Further work.

Another characteristic of the present budgetary approach is the raising of new questions about the NEM of the system. Thus, the present study identified that further research must be carried out in order to improve knowledge and satisfy the scientific and management interest of the system. The most important of these needs are listed below:

- Further studies are required to know the exact composition and variation of the discharges within the system. Also, their likely variation in the near and mid-term future. This above will allow better modelling with predictive purposes to be generated.

- The question needs answering of whether the metabolism of the Guaymas System is dominated by phytoplankton or another primary producer, including their temporal and spatial variation. Further research must be focused to characterise the proportion and contribution to the total primary production of the system.

- Regarding the above, analysis of the C:N:P ratios for wastewater in the systems and other be primary producers such as benthic and pelagic algae, will allow the refining of the present approach.

- It is important to characterise ground water rate, V_G, for the area. V_G can be represented in the Guaymas basis by percolation from the water and drainage.

- This approach relies very much on the consideration that phosphorus is a conservative material through the system. This hypothesis must be corroborated, since these may be an important loss of phosphorus as phosphine (PH_3). Also, other phosphate forms and their speciation must be considered.

- Organic nitrogen in some parts of the system may be highly important, mainly in those where denitrification process are important, and therefore must be included in further refined budgetary models for this system.

CHAPTER 6.

SEASONAL VARIATION OF BIOTIC AND ABIOTIC PARAMETERS IN RELATION TO THE POTENTIAL FOR EUTROPHICATION WITHIN THE GUAYMAS SYSTEM.

6.1 Introduction.

There is an increasing concern about the implications of water disposal, especially organic inputs, into marine coastal systems (e.g. Skogen *et al.* 1995). Generally, nutrient load discharges into coastal ecosystems leads to environmental problems such as the eutrophication process.

Eutrophication is defined by Nixon (1995) as, *the increase in the rate of supply of organic matter to an ecosystem.* Eutrophication effects include, in the first instance, an increase in biomass followed by decomposition and oxygen depletion, leading to species successions and/or mass mortality (Baretta-Bekker, *et al.* 1989; Rosenberg, *et al.* 1990; Rydberg, *et al.* 1990). Also, biomass increase can be characterised by opportunistic phytoplankton blooms, often represented by toxic species with undesirable effects in the ecosystem, thus eutrophication can be regarded as a set of symptoms or adverse effects (Rosenberg, *et al.* 1990; Chapelle, *et al.* 1994; Skogen, *et al.* 1995). Ecological models can be used to predict the potential for eutrophication and help to study the likelihood that detrimental characteristics will develop if nutrients inputs are not controlled in specific coastal systems such as the Guaymas system. The characterisation of trophic conditions represents an invaluable tool for the assessment and management of coastal systems. (Elliott, *et al.* 1994) In order to characterise trophic conditions and to provide an assessment of the ecosystems data gathered must include, if possible, information about pristine and normal situations in the ecosystem and what are the expected limits of variability. Also, where possible, information must indicate the change from the normal situation, the best quantification and statistical representation of these changes, and the significance of the influence of present developments on those changes, establishing their differences with respect to general environmental perturbations. Finally, information must help to establish if these changes affect the present and future developments.

In order to generate this information, there is a pool of methodological approaches to model eutrophication, and hence the trophic status of the system: Empirical models are those based on statistical analysis of observed trends (Forsberg, 1994; Botello-Ruvalcaba 1995; de Jonge and Raaphorst, 1995; Pan and Subba, 1997). Analytical or stochastic models are those based on theoretical expressions of the effect of each factor affecting the rate of the represented processes independently (Strain, *et al.* 1995; Cloern, 1996; Gordon, *et al.* 1996), and; Conceptual models (numerical) highlight those aspects of the ecosystem that are considered to be most significant in relation to the question asked. Through these models, it is possible to identify those process to be modelled mathematically (Engqvist, 1996; Rene-Flindt and Kamp-Nielsen, 1997; Yanagi, *et al.* 1997;)

6.2 Aims.

The present chapter characterises the variation of biotic and abiotic parameters, and aims to produce empirical models based on statistical analysis of observed trends. Also, using information derived from previous chapters, it evaluates the potential for eutrophication within the Guaymas system

6.3 Materials and Methods.

The study examines the variation of phytoplankton biomass (chlorophyll-*a*) and associated physico-chemical parameters. Described trends are discussed and further incorporated in to the modelling section. Data were obtained from a seasonal survey programme performed on 13 fixed stations in Guaymas system and adjacent sea (Chapter 2).

Statistical analysis:

Spatial and temporal differences for the observed trends were assessed through a two-way ANOVA. An *a-posteriori* test was performed to assess the cause of significant differences in the variables (Jongman *et al.*, 1987).

The non-parametric Spearman's rank correlation analysis was performed to determine the statistical significance of the observed trends. Those variables that present significant correlation were further quantified and assessed through multiple regression analysis (MRA). The method used for MRA was stepwise after retaining those variables with a contribution > than 10 % to explain the overall variability.

6.4 Results and Discussions.

Spatial and seasonal trends for environmental parameters for the Guaymas system are shown in figures 6.1 to 6.16. Statistically, data showed a normal tendency and a significant homogeneity in their variance.

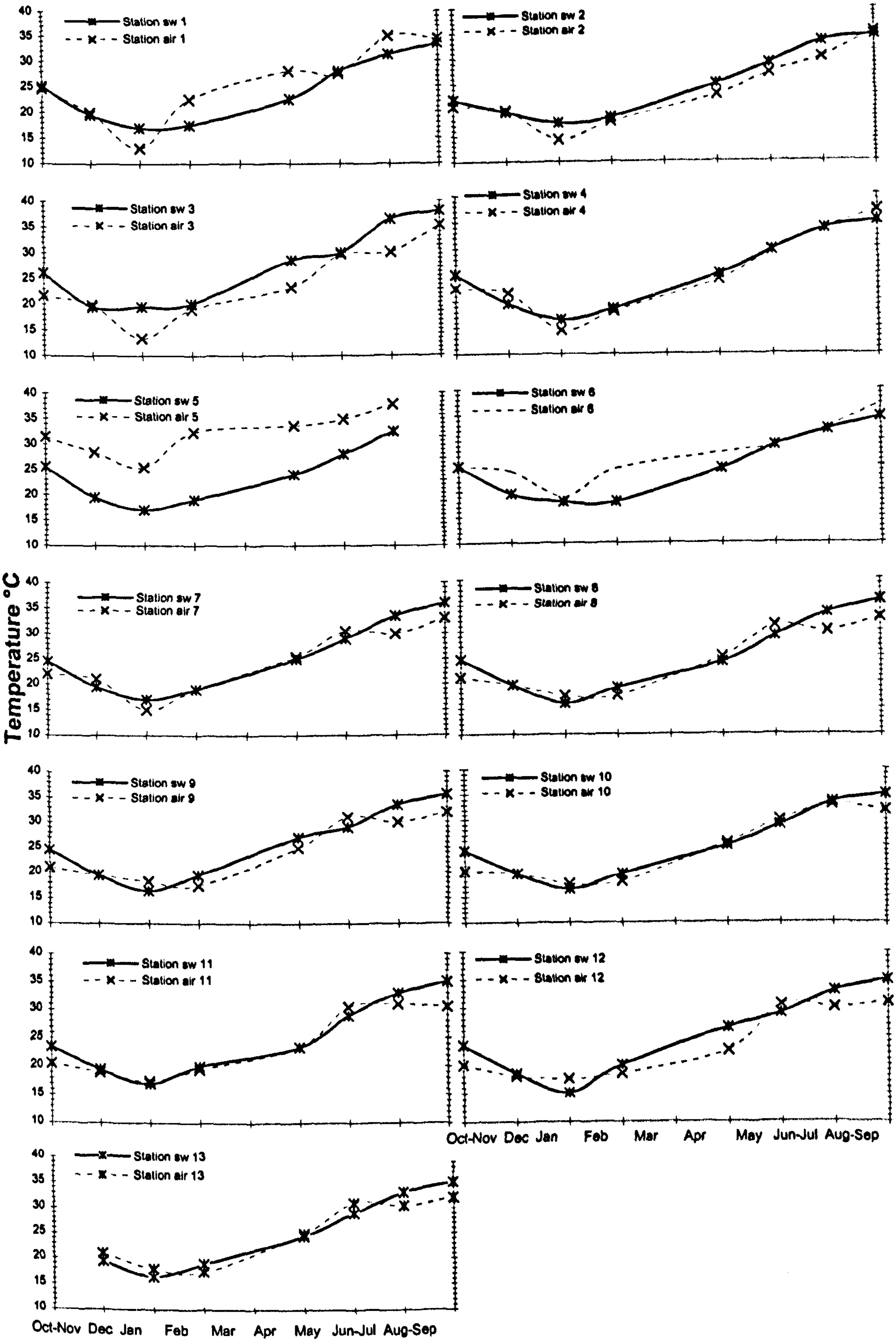

Figure 6.1. Seasonal trend in Temperature for the Guaymas System. Dashed lines represent bottom level.

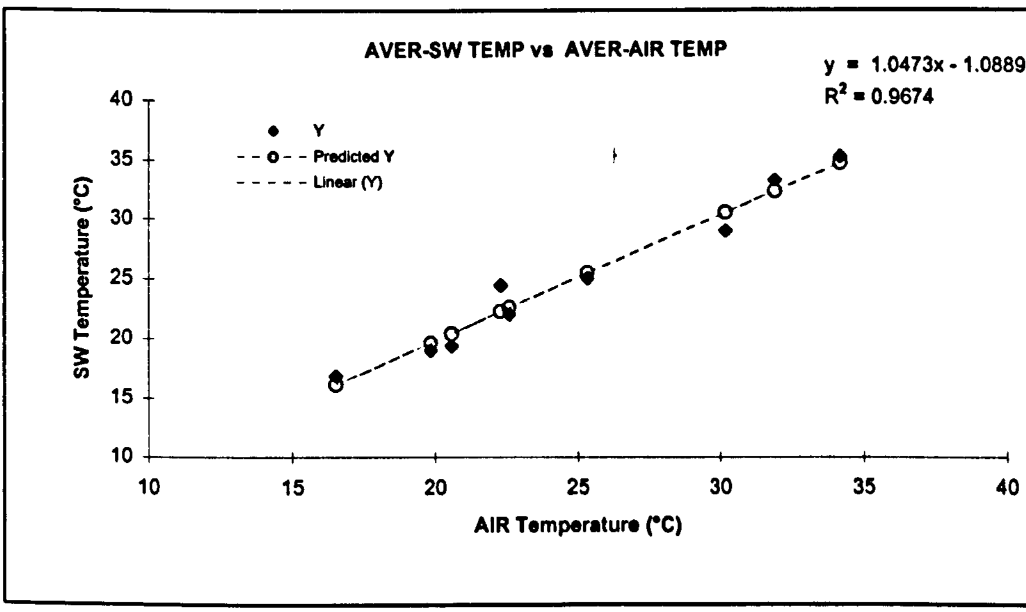

Figure 6.2. Mean monthly sea water temperature (SW) versus monthly mean air temperature (Air). Regression equation is also shown.

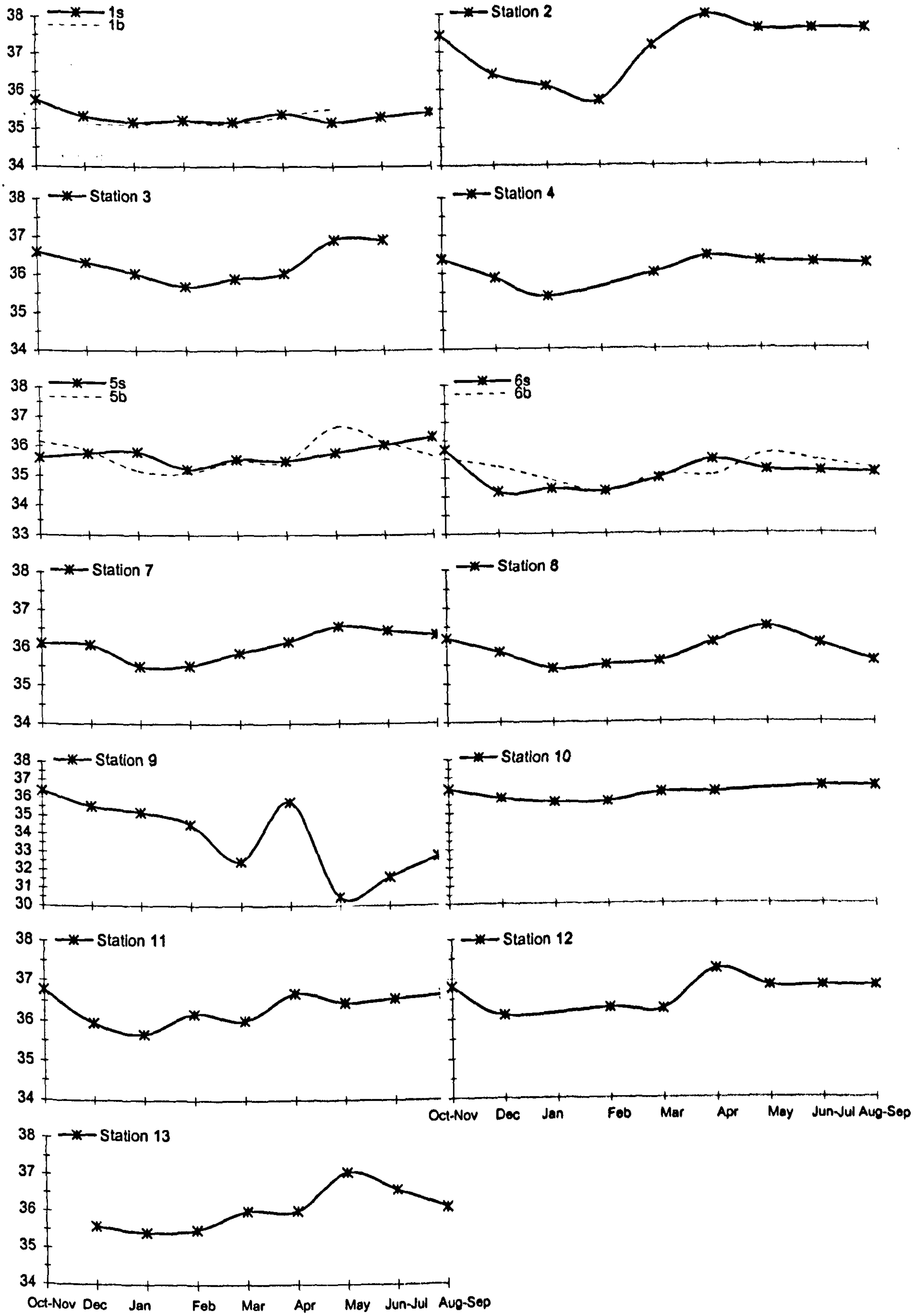

Figure 6.3. Seasonal trend in Salinity for the Guaymas System. Dashed lines represent bottom level.

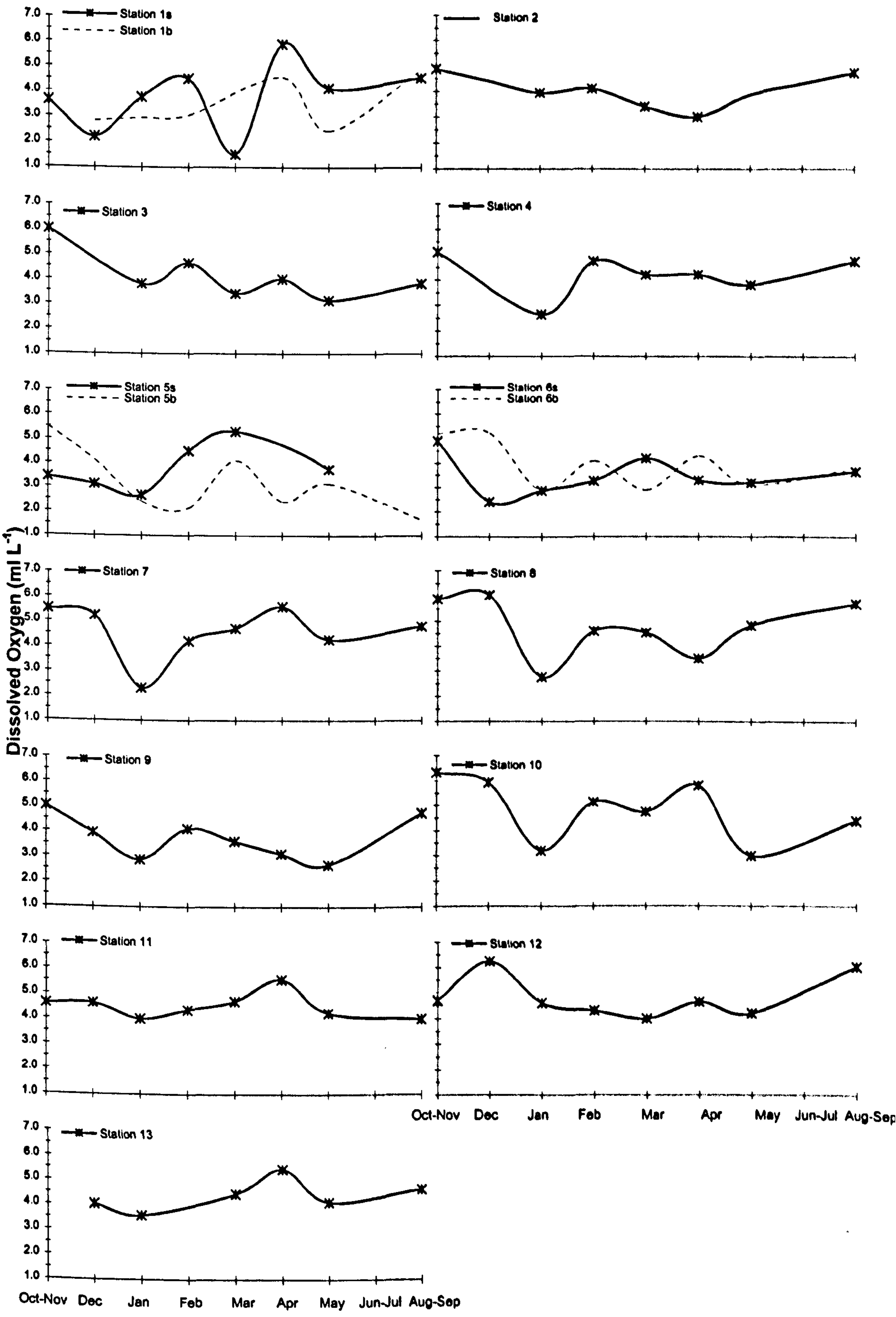

Figure 6.4. Seasonal trend in Dissolved Oxygen for the Guaymas System. Dashed lines represent bottom level.

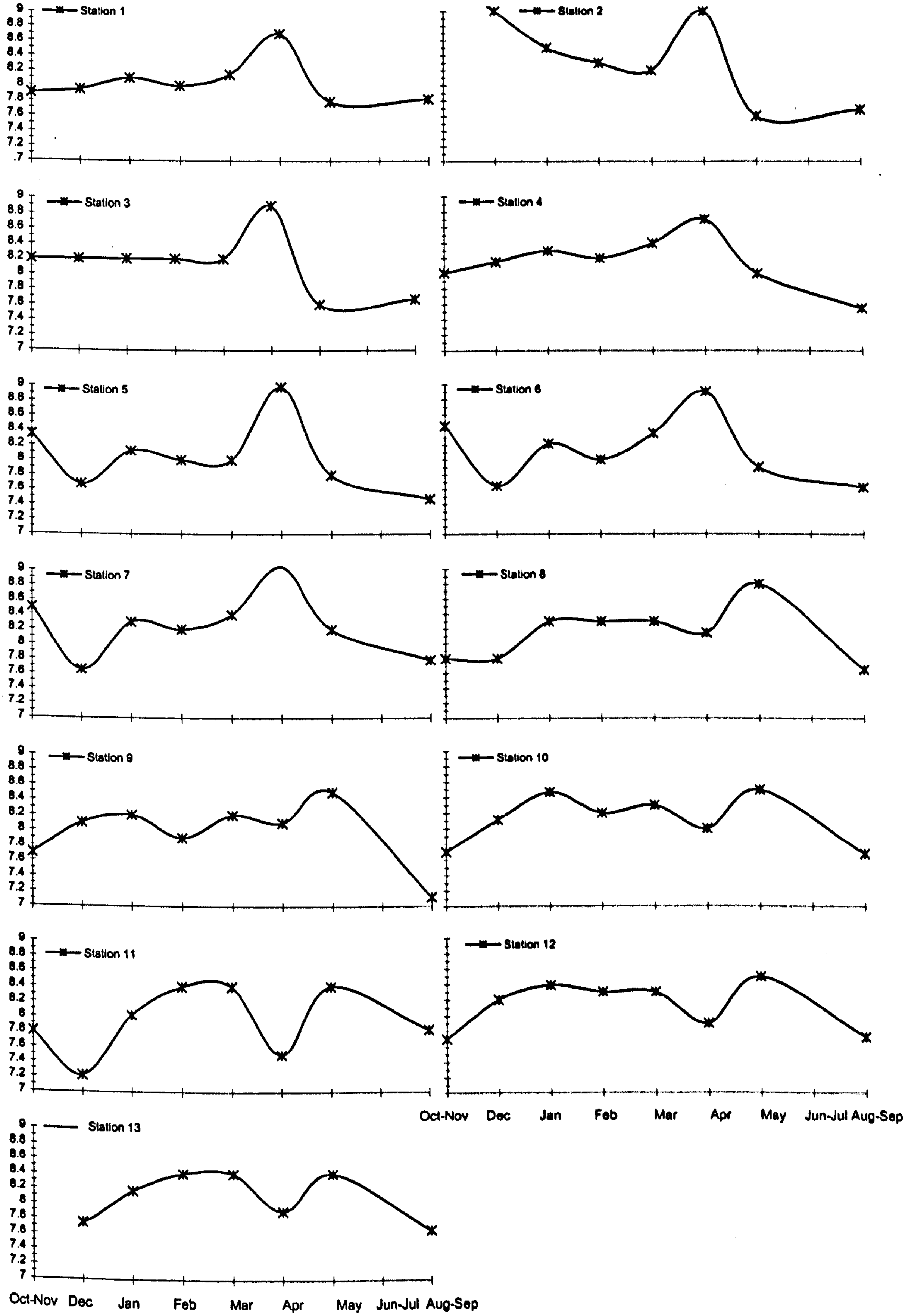

Figure 6.5. Seasonal trend in pH for the Guaymas System.

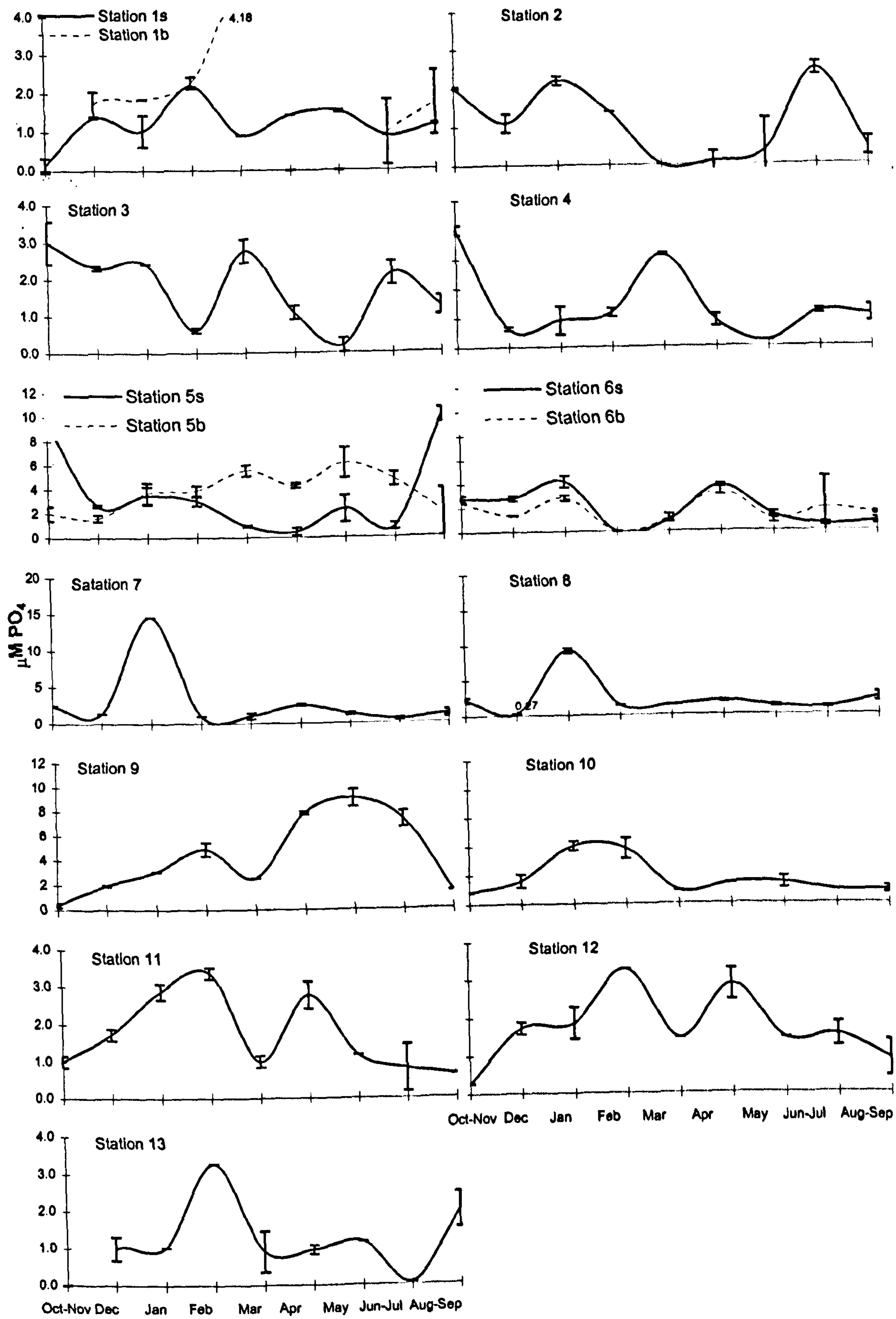

Figure 6.6. Seasonal trend in Dissolved Inorganic Phosphate (μM PO_4) for the Guaymas system. The bar represents standard deviation.

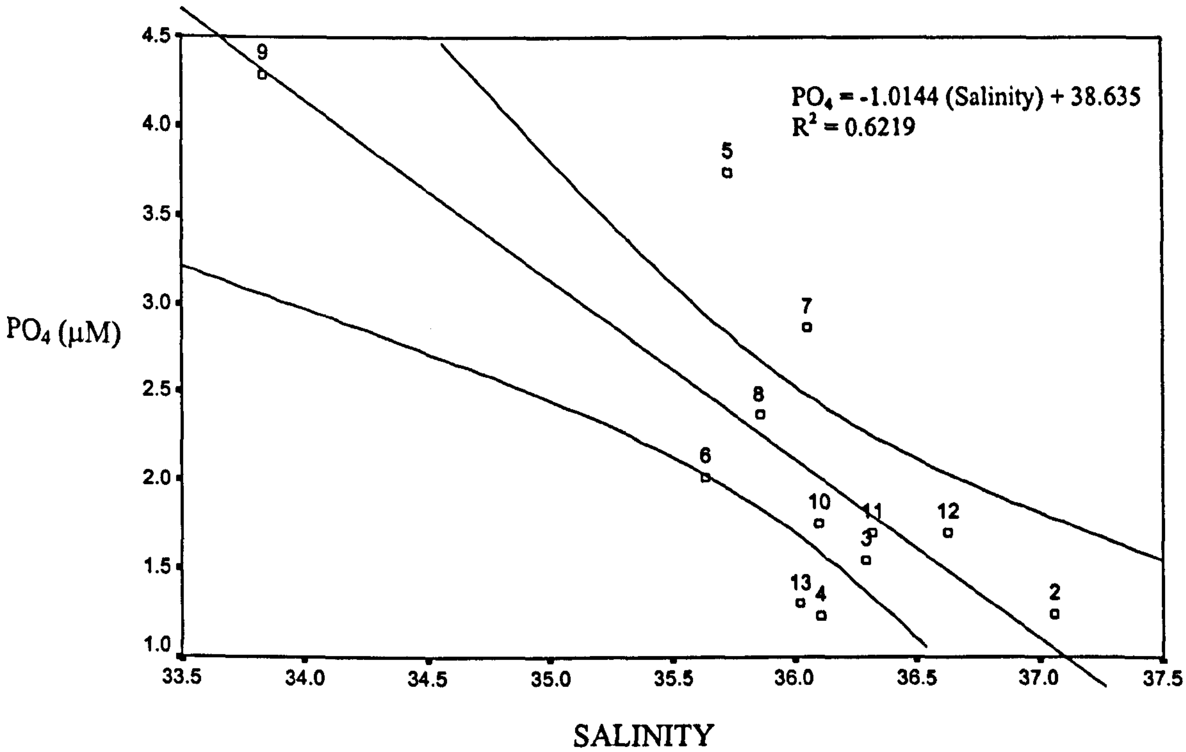

Figure 6.7. Mean averaged PO_4 versus averaged salinity. The numbers represent the fixed stations. Regression analysis and 95% confidence level are shown.

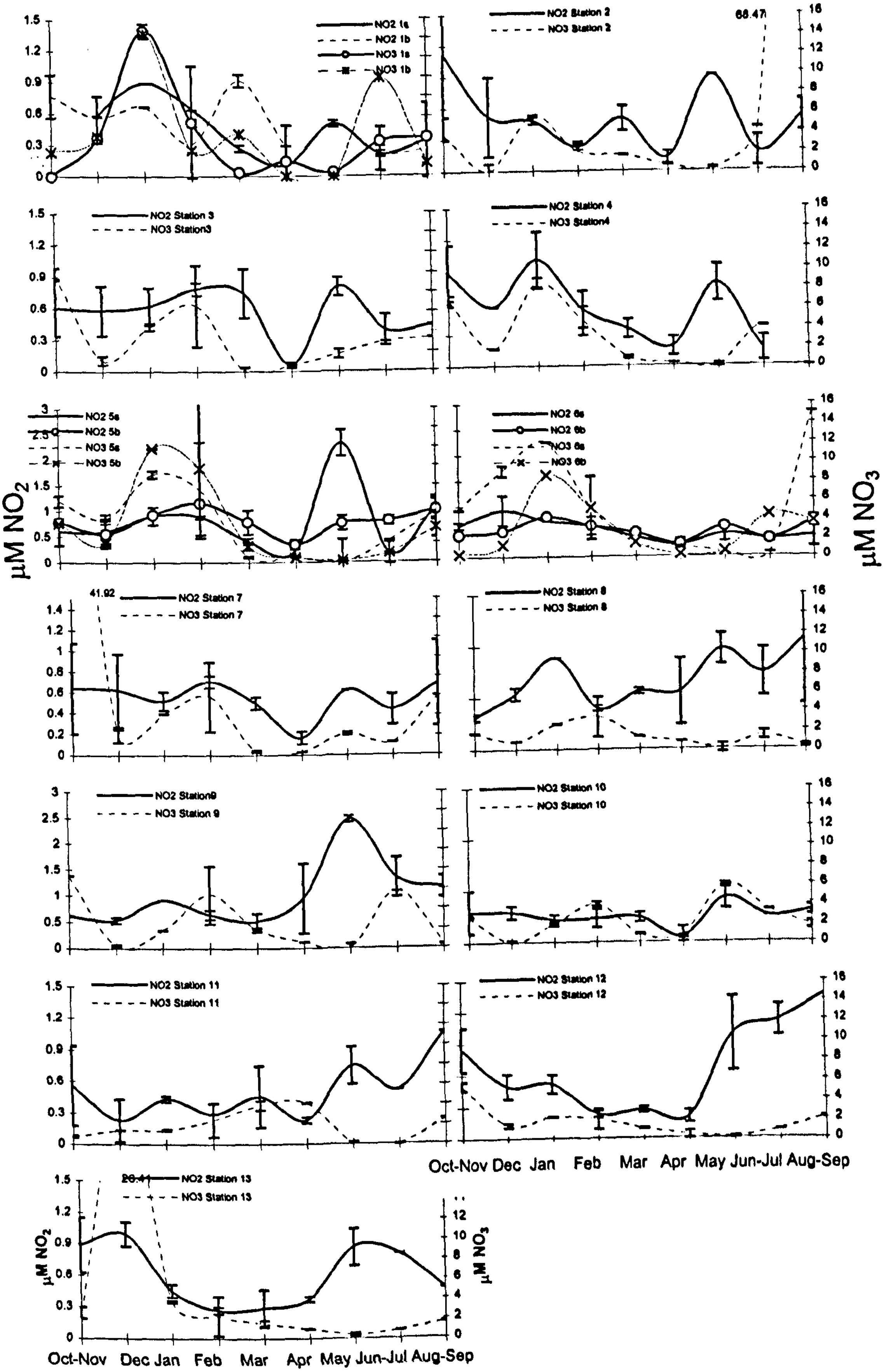

Figure 6.8. Seasonal trend in Nitrite and Nitrate (μM N) for the Guaymas system. The bars represent standard deviation.

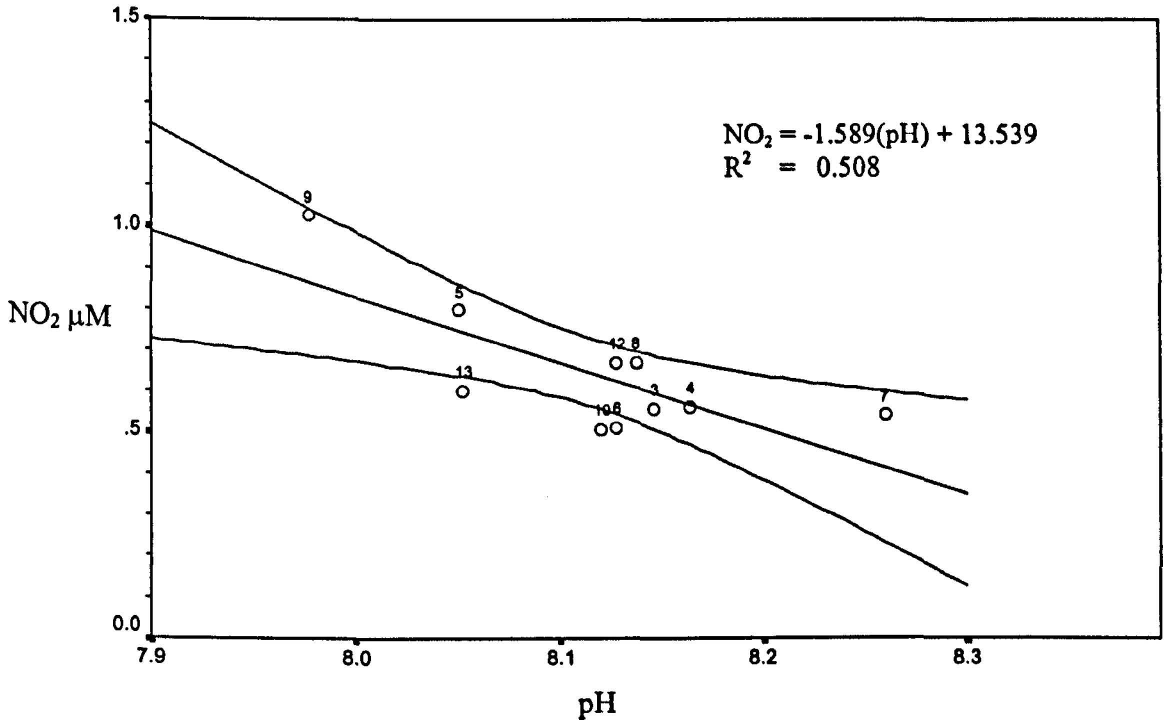

Figure 6.9. Monthly averaged NO_2 versus pH. The Numbers represent fixed stations. Regression analysis and 95% confidence level are shown.

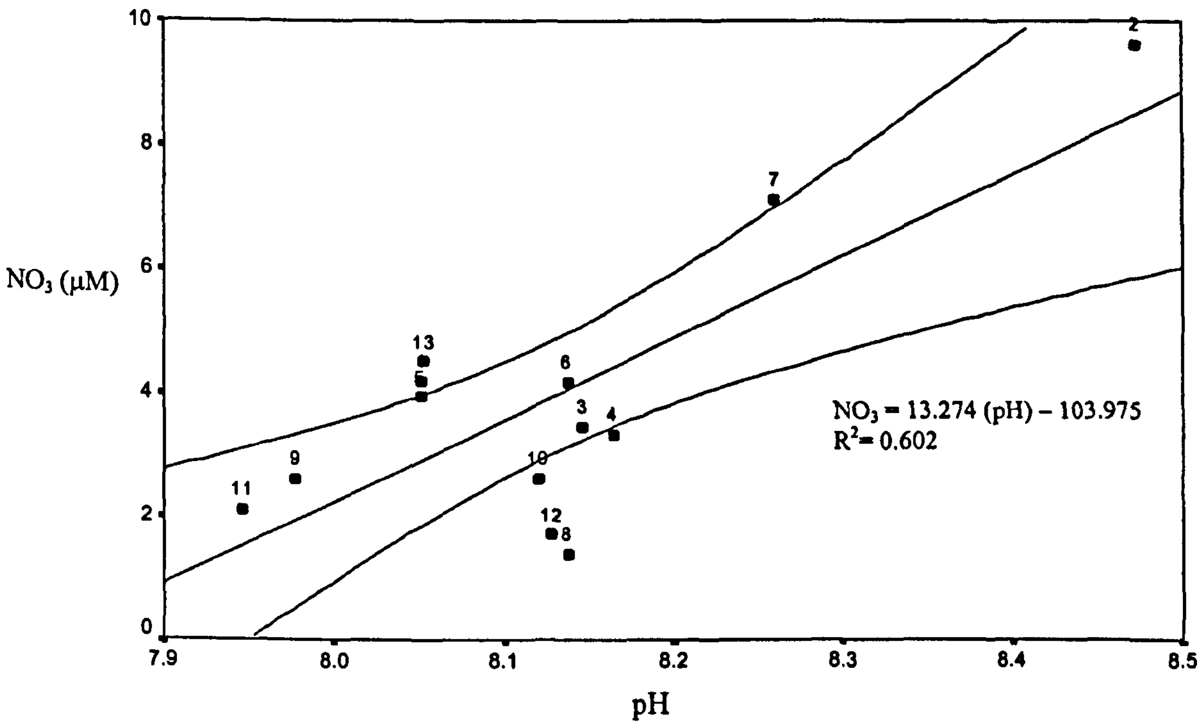

Figure 6.10. Monthly averaged NO_2 versus pH. The numbers represent fixed stations. Regression analysis and 95% confidence level are also shown.

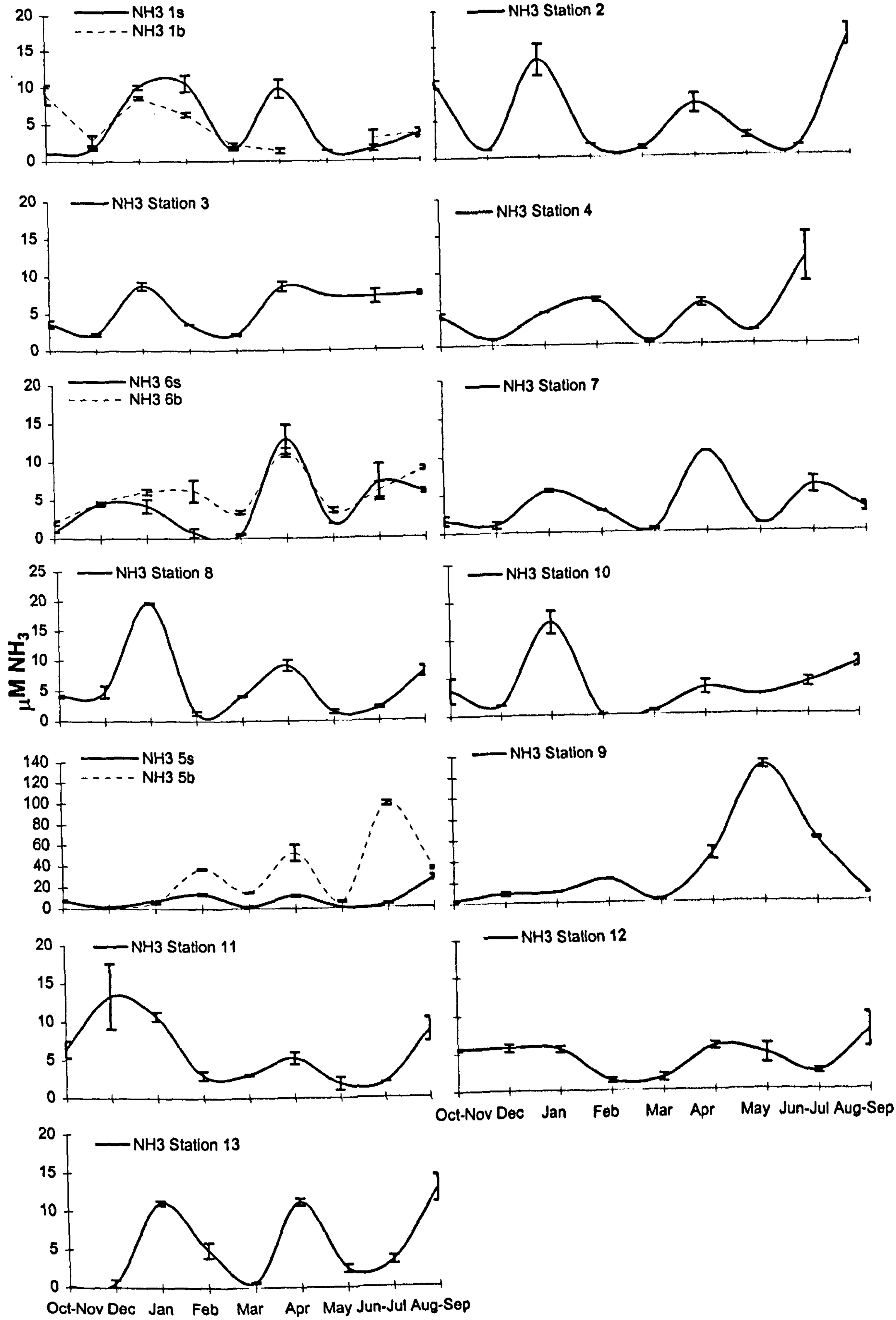

Figure 6.11. Seasonal trend in Ammonia (μM NH_3) for the Guaymas system. The bars represent standard deviation.

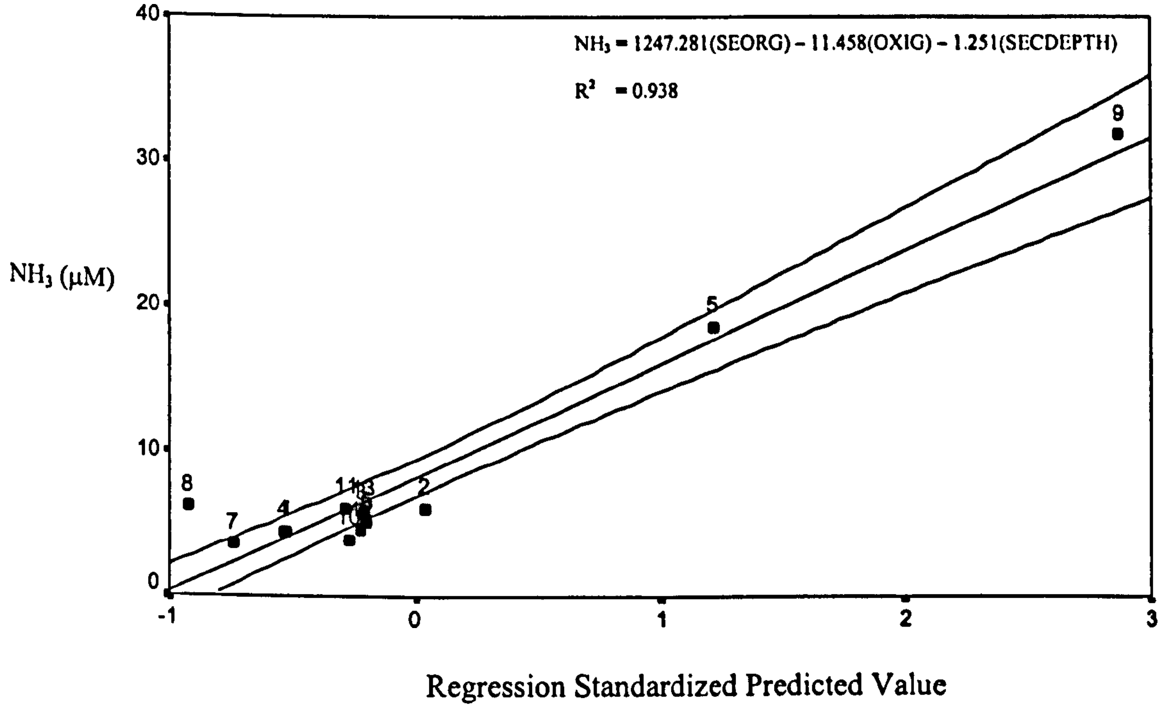

Figure 6.12.Monthly averaged NH_3 versus standardized predicted value. The numbers represent fixed stations. Regression model and 95% confidence level are shown.

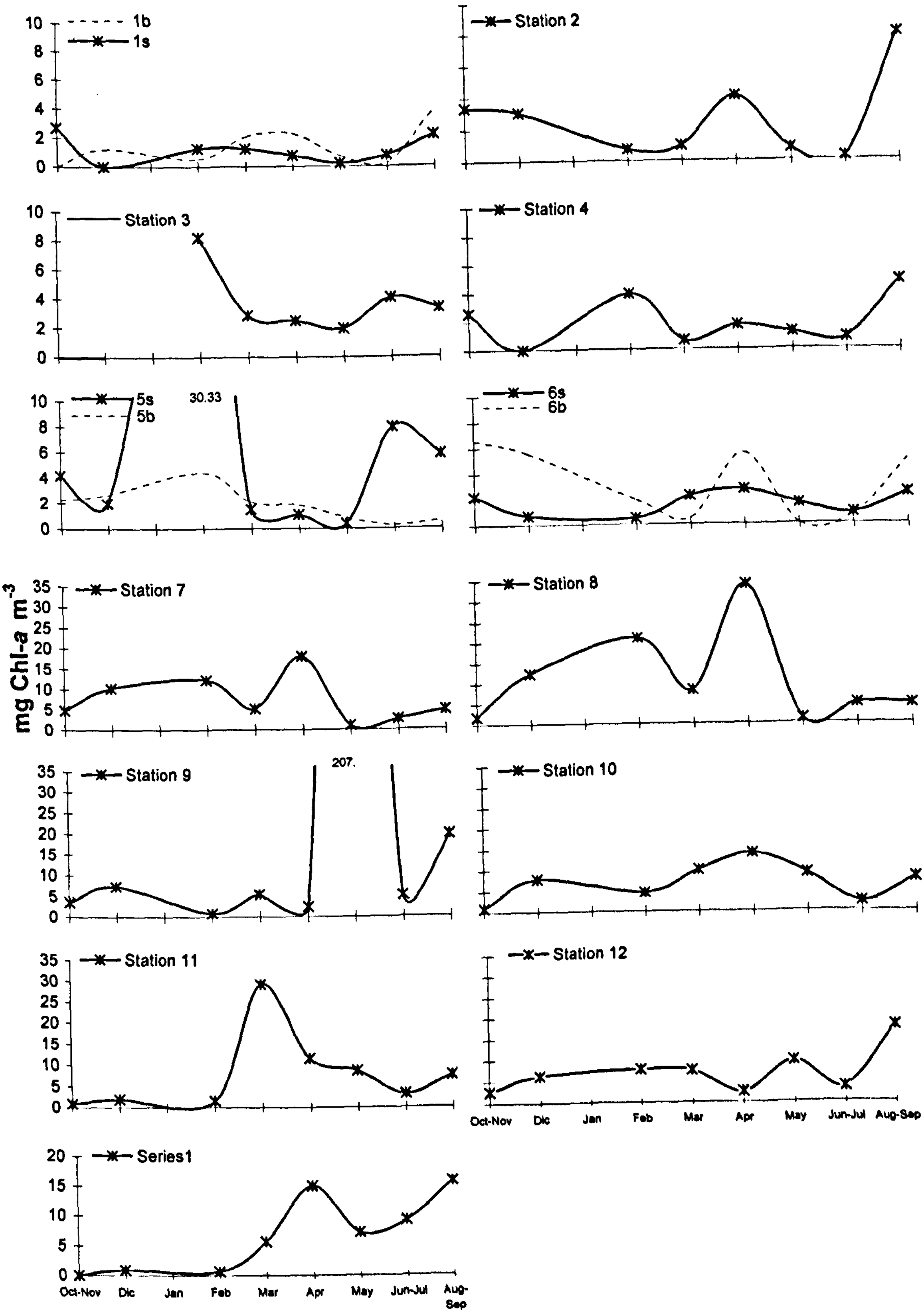

Figure 6.13. Seasonal trend in Chlorophyll-a (mg Chl-a m^{-3}) for the Guaymas System. Dashed lines represent bottom level.

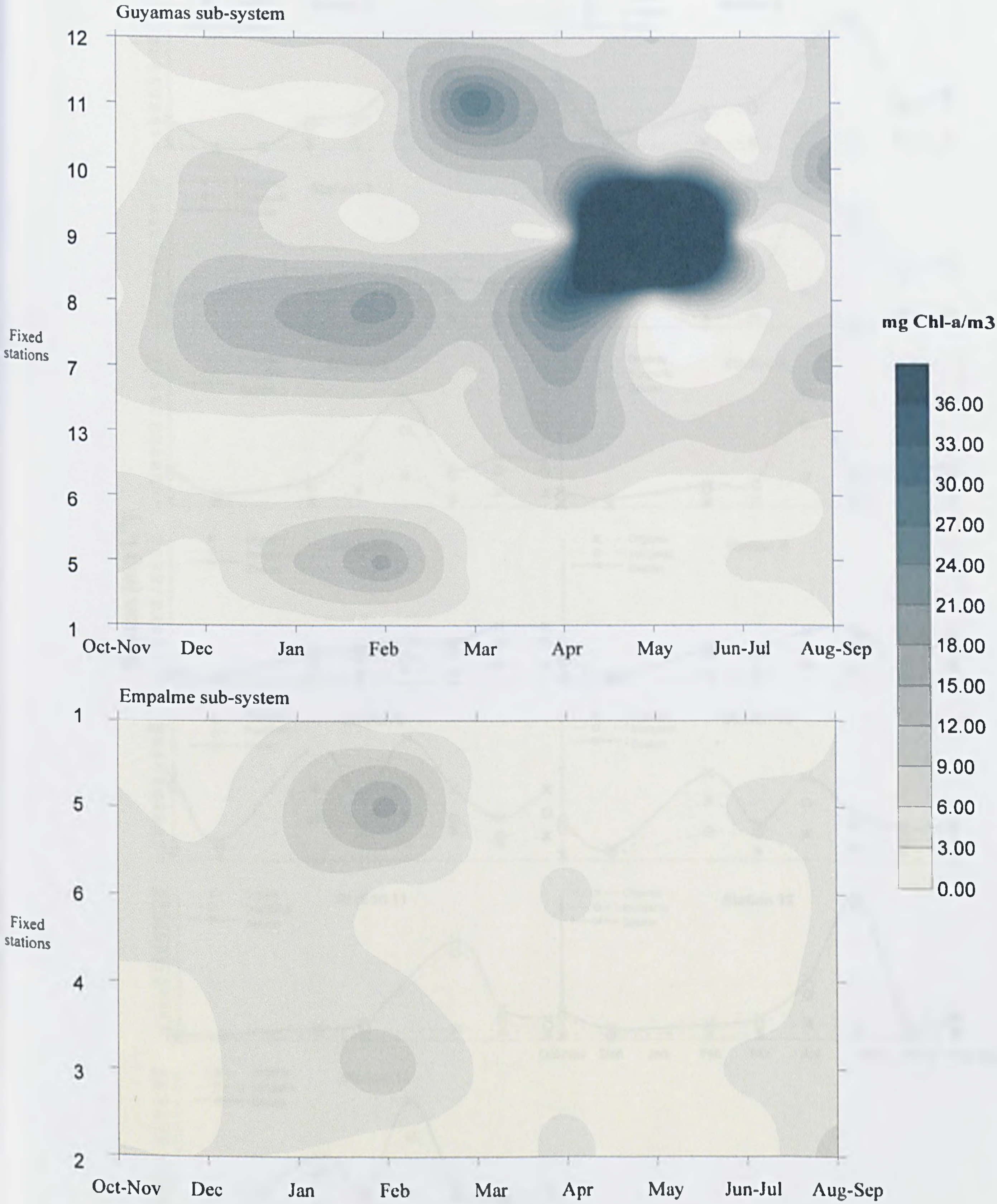

Figure 6.14 . Seasonal trend in Chlorphyll-a for the Guaymas System.

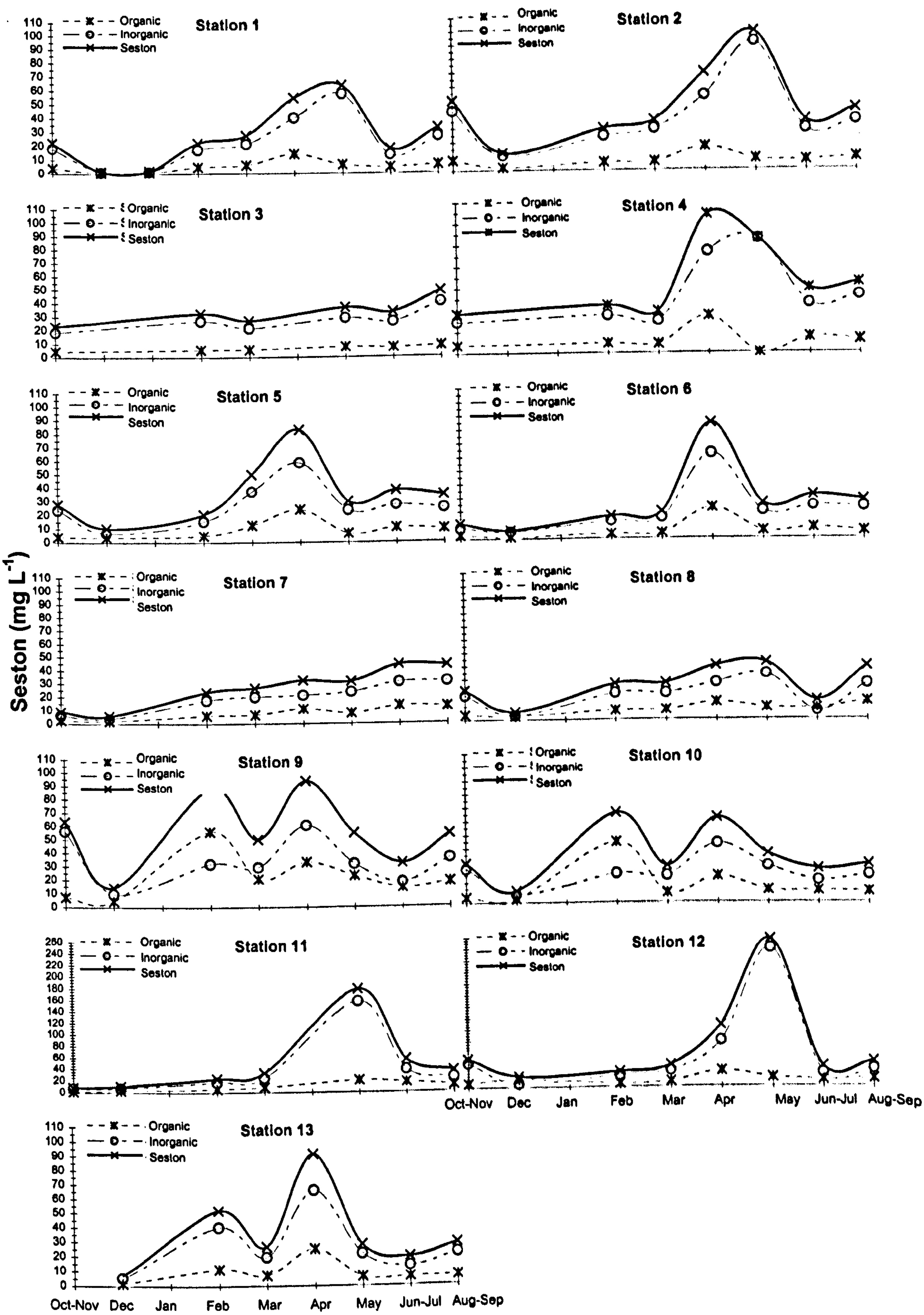

Figure 6.15. Seasonal trend in Seston for the Guaymas System.

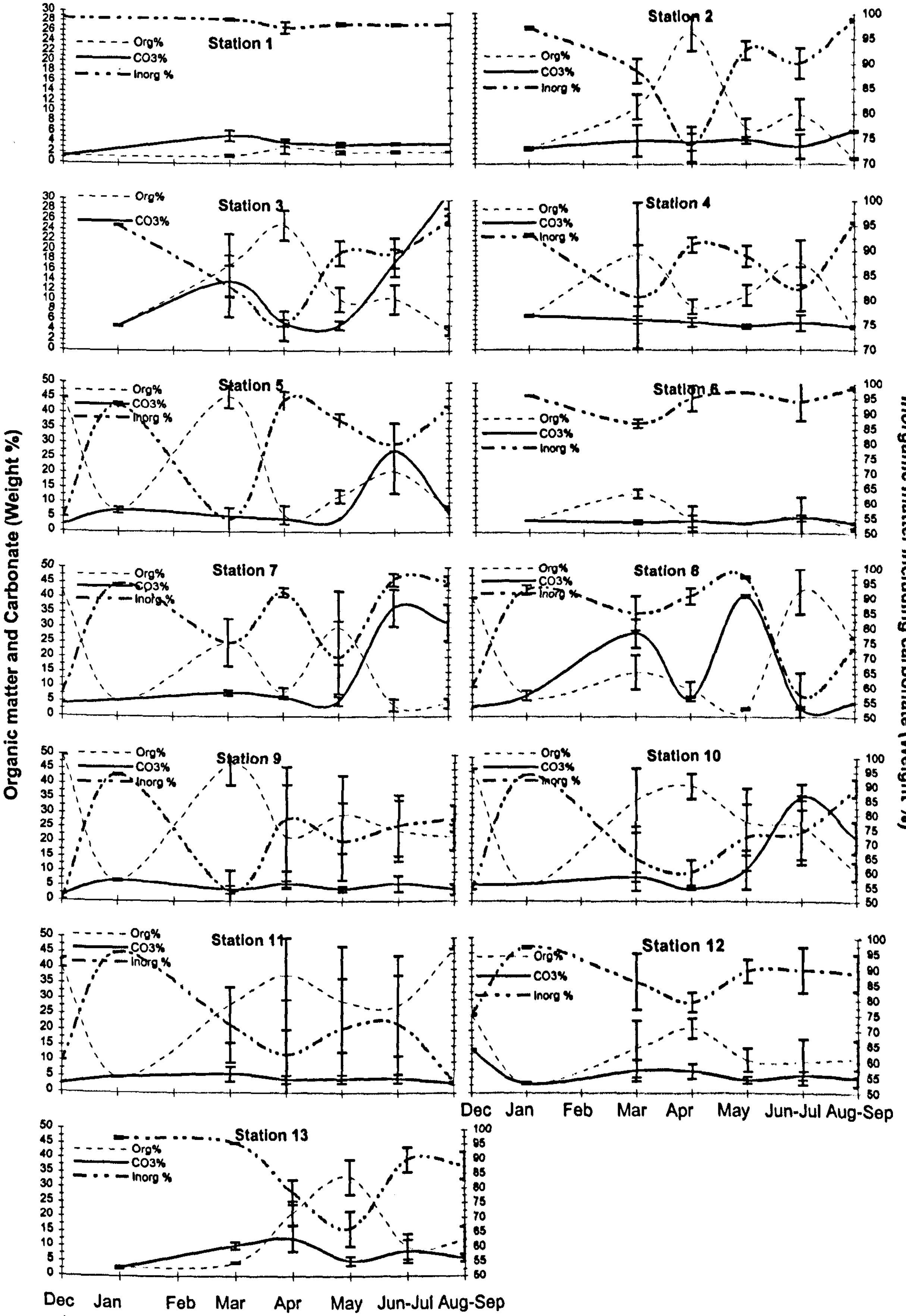

Figure 6.16. Seasonal trend in sediment composition for the Guaymas System. The bars represent the standard deviation. Carbonate percentage is expressed as part of the whole sample.

6.4.1 Main Physico-Chemical parameters.

Temperature. Water temperature in the Guaymas system had a maximum and minimum values of 38 °C (August-September, station 3) and 15.1°C (January station 12) respectively, and a mean annual value of 25.5 °C (Table 6.1). Temperature showed a marked seasonal variation ($p < 0.5$), although there were no significant differences at the spatial scale when the whole seasonal data set is used (Tables 6.2 and 6.3). However, Ramirez-Siqueiros (1999), grouping data from the inner part (head) and outer (mount of the system) on a monthly basis, during winter and spring, found spatial and temporal significant differences. This feature highlights the importance of proper scale definition in the characterisation of environmental parameters. This section, regarding the information from Ramirez-Siqueiros (1999) and Tejeda-Valenzuela (1999) which provides an insight of the likely variation of physical and chemical parameters at monthly basis, focuses attention at a seasonal level. Seasonal variations are typical for semi-temperate coastal systems within the Gulf of California (Badan-Dagon, 1985; Botello-Ruvalcaba, 1995; Delgadillo-Hinojosa, *et al.*, 1997), which are sometimes disrupted by oceanographic anomalies such as El Niño with strong effects for the coastal systems (Valdez-Holguin and Lara-Lara, 1987). For the present study, the monitoring period from (October 1996 to September 1997) was just before a strong El Niño anomaly, and therefore was not affected by it.

Seawater temperature shows significant correlation with Air temperature (Figure 6.1; correlation coefficient, r_s= 0.9), Oxygen (r_s= 0.2), pH (r_s= -0.261), PO_4 (r_s= -0.2760), Salinity (r_s= 0.492), and Seston (e= 0.4; Table 6.4). The monthly-averaged air temperature explains 96 % of the variation in mean seawater temperature when a regression analysis is performed (Figure 6.2). This is consistent with the findings reported by Ramirez-Siqueiros (1996) on a monthly basis, which indicate that heat exchange is greatest in shallow areas where, during cold months, heat exchange is from the sea to the atmosphere, and *vice versa* during warmest months.

Table 6.1. Descriptive statistics for biotic and abiotic parameters in the Guaymas system.

Descriptive Statistics

	N	Range	Minimum	Maximum	Mean	Std. Deviation	Variance
AIRTEMP	117	26.50	13.00	39.50	24.8188	5.9878	35.854
AMONIA	115	129.26	.10	129.36	8.2142	14.7404	217.281
BOTTIRRA	39	503.00	.00	503.00	130.0651	124.1092	15403.085
CHLOROPH	100	206.92	.19	207.12	7.5537	21.0377	442.584
DEPTH	39	9.10	.40	9.50	2.0167	1.9746	3.899
NO2	116	2.42	.06	2.48	.6076	.3382	.114
NO3	114	68.45	.02	68.47	3.9310	7.9087	62.548
OXYGEN	101	4.83	1.50	6.33	4.1830	.9967	.993
PH	104	2.38	7.12	9.50	8.1264	.4076	.166
PO4	114	14.46	.07	14.53	2.1101	2.0446	4.180
SALINITY	112	7.51	30.46	37.97	35.9081	1.0134	1.027
SECCHI	111	11.90	.40	12.30	2.0099	1.9996	3.998
SECLIGHT	39	925.00	100.00	1025.00	581.6667	192.9133	37215.544
SEDCO3	85	39.34	1.36	40.70	8.0427	8.3161	69.157
SEDINORG	85	48.60	50.26	98.86	83.0865	14.0361	197.013
SEDORG	85	48.60	1.14	49.74	16.9135	14.0361	197.013
SESINMG	101	240.16	.00	240.16	29.2814	29.9556	897.337
SESINORG	99	.23919	.00097	.24016	2.83E-02	2.72E-02	7.381E-04
SESORG	100	.05602	.00000	.05602	9.56E-03	8.62E-03	7.423E-05
SESTONTO	100	.25398	.00168	.25566	3.91E-02	3.41E-02	1.162E-03
SOLARIRR	39	1913.00	999.00	2912.00	1868.0256	466.9499	218042.2
SURFIRRA	37	1978.00	482.00	2460.00	1451.6486	503.5959	253608.8
WATEMP	117	22.89	15.11	38.00	24.8885	6.0936	37.132
Valid N (listwise)	21						

Table 6.2. Analysis of variance by month.

ANOVA

		Sum of Squares	df	Mean Square	F	Sig.
AIRTEMP	Between Groups	3660 594	8	457 574	99 143	000
	Within Groups	498 454	108	4 615		
	Total	4159 049	116			
AMONIA	Between Groups	1678 344	8	209 793	963	469
	Within Groups	23091 666	106	217 846		
	Total	24770 010	114			
CHLOROPH	Between Groups	2389 364	7	341 338	758	624
	Within Groups	41426 404	92	450 287		
	Total	43815 767	99			
DEPTH	Between Groups	1 686	2	843	207	814
	Within Groups	146 470	36	4 069		
	Total	148 157	38			
NO2	Between Groups	3 713	8	464	5 263	000
	Within Groups	9 437	107	8 819E-02		
	Total	13 150	115			
NO3	Between Groups	759 068	8	94 883	1 579	140
	Within Groups	6308 877	105	60 085		
	Total	7067 945	113			
OXYGEN	Between Groups	27 663	8	3 458	4 438	000
	Within Groups	71 685	92	779		
	Total	99 348	100			
PH	Between Groups	5 388	7	770	6 306	000
	Within Groups	11 720	96	122		
	Total	17 108	103			
PO4	Between Groups	60 392	8	7 549	1 924	064
	Within Groups	411 989	105	3 924		
	Total	472 381	113			
SALINITY	Between Groups	9 394	8	1 174	1 156	333
	Within Groups	104 602	103	1 016		
	Total	113 996	111			
SECCHI	Between Groups	61 876	8	7 734	2 087	044
	Within Groups	377 944	102	3 705		
	Total	439 819	110			
SEDCO3	Between Groups	606 944	6	101 157	1 517	184
	Within Groups	5202 218	78	66 695		
	Total	5809 162	84			
SEDINORG	Between Groups	5181 185	6	863 531	5 926	000
	Within Groups	11367 877	78	145 742		
	Total	16549 061	84			
SEDORG	Between Groups	5181 185	6	863 531	5 926	000
	Within Groups	11367 877	78	145 742		
	Total	16549 061	84			
SESINMG	Between Groups	28646 642	8	3580 830	5 393	000
	Within Groups	61087 035	92	663 990		
	Total	89733 677	100			
SESINORG	Between Groups	2 158E-02	8	2 698E-03	4 784	000
	Within Groups	5 076E-02	90	5 639E-04		
	Total	7 234E-02	98			
SESORG	Between Groups	2 208E-03	8	2 760E-04	4 885	000
	Within Groups	5 141E-03	91	5 649E-05		
	Total	7 349E-03	99			
WATEMP	Between Groups	4150 605	8	518 826	357 523	000
	Within Groups	156 726	108	1 451		
	Total	4307 331	116			

Table 6.3. Analysis of variance by fixed stations.

ANOVA

		Sum of Squares	df	Mean Square	F	Sig
AIRTEMP	Between Groups	141.949	12	11 829	.306	.987
	Within Groups	4017 099	104	38 626		
	Total	4159 049	116			
AMONIA	Between Groups	7084.357	12	590.363	3.405	.000
	Within Groups	17685 653	102	173 389		
	Total	24770.010	114			
CHLOROPH	Between Groups	5731.073	12	477.589	1 091	.378
	Within Groups	38084 694	87	437.755		
	Total	43815.767	99			
DEPTH	Between Groups	135.025	12	11 252	22 279	000
	Within Groups	13 132	26	.505		
	Total	148.157	38			
NO2	Between Groups	2.561	12	213	2 076	.025
	Within Groups	10.589	103	103		
	Total	13 150	115			
NO3	Between Groups	551.214	12	45 935	.712	.737
	Within Groups	6516 731	101	64 522		
	Total	7067.945	113			
OXYGEN	Between Groups	25.300	12	2.108	2 506	.007
	Within Groups	74.049	88	.841		
	Total	99.348	100			
PH	Between Groups	1 690	12	.141	831	.619
	Within Groups	15.419	91	.169		
	Total	17.108	103			
PO4	Between Groups	101.462	12	8 455	2.302	.012
	Within Groups	370.919	101	3.672		
	Total	472.381	113			
SALINITY	Between Groups	62 387	12	5.199	9 973	.000
	Within Groups	51.609	99	.521		
	Total	113.996	111			
SECCHI	Between Groups	320.290	12	26.691	21 883	000
	Within Groups	119 529	98	1.220		
	Total	439 819	110			
SEDCO3	Between Groups	1332.051	12	111.004	1.785	067
	Within Groups	4477 111	72	62 182		
	Total	5809 162	84			
SEDINORG	Between Groups	6099.183	12	508 265	3.502	.000
	Within Groups	10449 878	72	145.137		
	Total	16549 061	84			
SEDORG	Between Groups	6099.183	12	508 265	3.502	000
	Within Groups	10449 878	72	145.137		
	Total	16549 061	84			
SESINMG	Between Groups	12136 933	12	1011.411	1.147	.334
	Within Groups	77596 744	88	881.781		
	Total	89733 677	100			
SESINORG	Between Groups	1.154E-02	12	9.619E-04	1.361	.201
	Within Groups	6.079E-02	86	7.069E-04		
	Total	7.234E-02	98			
SESORG	Between Groups	1.911E-03	12	1.593E-04	2 548	006
	Within Groups	5.438E-03	87	6.250E-05		
	Total	7.349E-03	99			
WATEMP	Between Groups	59 603	12	4 967	122	1 000
	Within Groups	4247 728	104	40 844		
	Total	4307.331	116			

Table 6.4. Non parametric Sperman correlation test for biotic and abiotic parameters in the Guaymas system.

Correlations

			AIRTEMP	AMONIA	BOTTIRRA	CHLOROPH	DEPTH	NO2	NO3	OXYGEN	PH	PO4	SALINITY	SECCHI	SEDCO3	SEDORG	SEDINORG	SESORG	SESINORG	SESTONTO	WATEMP
Spearman's rho	Correlation Coefficient	AIRTEMP	1.000	.076	-.259	-.003	-.050	.081	-.219*	.055	-.234**	-.195*	.334**	.026	.085	-.074	.074	.303**	.354**	.337**	.903**
		AMONIA		1.000	.090	.159	-.098	.079	.080	-.205*	-.127	.299**	-.176*	-.114	.030	-.117	.117	.348**	.266**	.266**	.057
		BOTTIRRA			1.000	.021	-.433**	.139	-.202	-.080	-.246	.087	.252	-.423**	-.059	.238	-.238	.139	.224	.223	-.183
		CHLOROPH				1.000	-.278*	.182*	-.015	.321**	.053	.051	.023	-.264**	.174	.369**	-.369**	.245**	-.050	.033	.059
		DEPTH					1.000	-.364*	.055	.120	-.002	-.080	-.458**	.996**	-.244	-.411**	.411**	-.360*	-.217	-.323*	-.235
		NO2						1.000	.136	-.179*	-.254**	.123	-.052	-.156	.068	.129	-.129	-.052	-.065	-.031	.086
		NO3							1.000	-.015	-.197*	.061	-.205*	.084	.020	-.271**	.271**	-.304**	-.299**	-.322**	-.229*
		OXYGEN								1.000	-.107	-.211*	.412**	-.157	.103	.292**	-.292**	.003	-.089	-.071	.206*
		PH									1.000	.049	-.021	-.012	.149	-.050	.050	.183*	.051	.100	-.261**
		PO4										1.000	-.393**	-.028	-.020	-.069	.069	.134	.032	.085	-.276**
		SALINITY											1.000	-.335**	.230*	.168	-.168	.104	.264**	.220*	.492**
		SECCHI												1.000	-.238*	-.168	.168	-.488**	-.421**	-.467**	-.177*
		SEDCO3													1.000	-.041	.041	.234*	.082	.081	.151
		SEDORG														1.000	-1.000**	.089	-.241*	-.153	.005
		SEDINORG															1.000	-.089	.241*	.153	-.005
		SESORG																1.000	.708**	.826**	.366**
		SESINORG																	1.000	.968**	.412**
		SESTONTO																		1.000	.404**
		WATEMP																			1.000
	Sig. (1-tailed)	AIRTEMP	.	.209	.056	.486	.382	.195	.010	.292	.008	.019	.000	.394	.220	.251	.251	.001	.000	.000	.000
		AMONIA		.	.293	.058	.277	.201	.200	.020	.102	.001	.032	.117	.395	.145	.145	.000	.004	.004	.273
		BOTTIRRA			.	.450	.003	.199	.112	.346	.113	.299	.064	.004	.360	.072	.072	.206	.095	.092	.132
		CHLOROPH				.	.043	.036	.444	.001	.314	.310	.413	.005	.070	.001	.001	.008	.315	.372	.280
		DEPTH					.	.011	.371	.275	.497	.314	.002	.000	.067	.005	.005	.014	.102	.026	.075
		NO2						.	.074	.037	.005	.097	.295	.051	.269	.122	.122	.305	.263	.380	.180
		NO3							.	.442	.024	.263	.016	.194	.428	.007	.007	.001	.002	.001	.008
		OXYGEN								.	.144	.018	.000	.061	.193	.006	.006	.490	.208	.257	.019
		PH									.	.313	.417	.452	.106	.338	.338	.045	.320	.179	.004
		PO4										.	.000	.386	.429	.267	.267	.095	.377	.203	.001
		SALINITY											.	.000	.019	.066	.066	.156	.005	.015	.000
		SECCHI												.	.015	.064	.064	.000	.000	.000	.032
		SEDCO3													.	.355	.355	.025	.250	.252	.083
		SEDORG														.	.000	.230	.022	.102	.482
		SEDINORG															.	.230	.022	.102	.482
		SESORG																.	.000	.000	.000
		SESINORG																	.	.000	.000
		SESTONTO																		.	.000
		WATEMP																			.
	N	AIRTEMP	117	115	39	100	39	116	114	101	104	114	112	111	85	85	85	100	99	100	117
		AMONIA		115	39	99	39	115	113	100	102	113	111	111	84	84	84	99	98	99	115
		BOTTIRRA			39	39	39	39	38	27	26	39	38	39	39	39	39	37	36	37	39
		CHLOROPH				100	39	99	97	87	87	98	97	97	73	73	73	98	97	98	100
		DEPTH					39	39	38	27	26	39	38	39	39	39	39	37	36	37	39
		NO2						116	114	100	103	113	111	111	84	84	84	99	98	99	116
		NO3							114	99	102	111	109	109	82	82	82	97	96	97	114
		OXYGEN								101	100	99	97	98	73	73	73	87	86	87	101
		PH									104	101	99	98	72	72	72	87	86	87	104
		PO4										114	110	109	85	85	85	98	97	98	114
		SALINITY											112	107	82	82	82	97	96	97	112
		SECCHI												111	83	83	83	97	96	97	111
		SEDCO3													85	85	85	71	70	71	85
		SEDORG														85	85	71	70	71	85
		SEDINORG															85	71	70	71	85
		SESORG																100	99	100	100
		SESINORG																	99	99	99
		SESTONTO																		100	100
		WATEMP																			117

**. Correlation is significant at the .01 level (1-tailed).

*. Correlation is significant at the .05 level (1-tailed).

Salinity. Maximum values for salinity were found in April for station 2 with 37.97 and the minimum values were measured in May for station 9 with 30.46, the mean annual value was 35.9 (Table 6.1). This parameter did not present a significant temporal variation throughout the survey programme period, and shows a highly significant spatial difference (Tables 6.2 and 6.3; Figure 6.3). The *a-posteriori* analysis shows significant differences between those stations located at the head of the system (stations 2 and 12), those heavily influenced by urban discharges (station 9) and those represented by the mouth of the system (stations 5 and 6) and the adjacent sea (station 1). The above indicate that salinity in the interior of the system is influenced by local processes such as water exchange and evaporation rate, and human activities within the area.

Salinity presented a highly significant correlation ($p < 0.01$) with air temperature, water temperature, depth, Oxygen, PO_4, Secchi depth, Seston organic and inorganic, and a significant correlation ($p < 0.05$) with NO_3+NO_2 (Table 6.4). Thus, high salinity areas are associated with low exchange rates, shallow depths ($r_s = -0.458$), higher temperature ($r_s = 0.492$), often with low transparency (Sd; e= -0.335) as the product the suspension of organic ($r_s = 0.264$) and Inorganic ($r_s = 0.276$) particles. Low salinity is more likely to be associated with areas affected by wastewater discharges characterised by high nutrient concentration (PO_4, $r_s = -0.393$; NO_3+NO_2, $r_s = -0.205$), and relatively low oxygen concentrations ($r_s = 0.412$).

Dissolved Oxygen. Dissolved oxygen maximum values were encountered in December for stations 12 and 8 with a value of 6.33 $ml.L^{-1}$, and the minimum was registered in March for station 1 with 1.5 $ml.L^{-1}$, the mean annual value was 4.18 $ml.L^{-1}$ (Table 6.1). This parameter did not present a significant temporal difference, although there was a highly significant spatial variation (Tables 6.2 and 6.3; Figure 6.4). The analysis *a posterior* did not show any distinction between stations or group of stations. It is of note that dissolved oxygen was taken at surface (1 m below water) and this area is heavily influenced by turbulence induced by local waves and wind.

Dissolved oxygen presented a highly significant correlation ($p < 0.01$) with salinity and chlorophyll-a, and a significant correlation ($p < 0.05$) with water temperature, ammonia and PO_4 and the organic fraction of seston. This parameter seems to be more strongly influenced by biological conditions such as phytoplankton biomass ($r_s = 0.280$) and does not strictly follows gas solubility laws, since it increases with temperature ($r_s = 0.206$) and salinity ($r_s = 0.412$). Dissolved oxygen correlates positively with salinity and temperature, and hence must increase in areas characterised by those conditions, such as shallow areas at the head of the system. In those areas at surface level, as indicated before, other processes such as turbulence by tide and wind may determine the oxygen concentration. It is important to highlight that dissolved oxygen was taken at surface (1 m below water) and this area is heavily influenced by turbulence induced by local waves, and wind. Low concentrations were associated with parameters that characterise areas affected by wastewater discharges (Figure 6.4; Station 9).

Nutrients:

Dissolved Inorganic Phosphorus (DIP). This work assumes that PO_4 represents the major percentage of the DIP in the system. DIP shows maximum values during January for station 7 with 14.53 μM, and a minimum value of 0.07 μM in June-July for station 13 (Figure 6.6). The mean annual value was 2.11 μM (Table 6.1). DIP did not shows a significant temporal variation ($p<0.05$). However, February presented the maximum averaged value with 3.71 μM, which was not quite significantly different from the rest of the months (p level of 0.065). Spatially, DIP shows a significant variation (Table 3). The *a-posteriori* analysis indicates the segregation of those stations associated with urban and industrial discharges (Stations 5 and 9) from the remainder of the stations. Station 9 was significantly different from the remaining stations, whereas station 5 was significantly different from those stations located mainly in the Empalme sub-system (stations 2, 3 and 4) and adjacent sea (station 1). This highlights the influence of the industrial area located near the mouth of the system; that influence is higher for the Guaymas sub-system given the major exchange characteristics (Figure 1.3; Chapter 3).

DIP showed a highly significant correlation with ammonia, salinity and seawater temperature, and also significant correlation with dissolved oxygen. DIP thus appeared to be associated with areas receiving wastewater discharges, characterised by low salinity (r_s -0.393) and reduced nitrogen forms such as ammonia (r_s = 0.299) and poor oxygen conditions (r_s -0.211). The best-fitted multiple regression model applied to DIP shows that salinity explain the major contribution to the DIP variance (62%; Figure 6.7). Also, the highly significant correlation with temperature (r_s -0.276) and significant with oxygen may indicate the importance of these parameters in the speciation, phosphorus turnover, and desorption/absorption from sediments and organic matter (Organza-Gonzales and Statham, 1991; Chapelle, *et al.* 1994; de Jonge 1995;).

Nitrogen species. Dissolved Inorganic Nitrogen (DIN) here was determined as the sum of NO2, NO3 and NH3.

Nitrite. Maximum values for nitrite were detected in May at stations 5 and 9 with 1.55 μM and 2.48 μM respectively. The minimum values were in April for station 3 with 0.06 μM, the mean annual average was 0.607μM (Table 6.1, Figure 6.8). The NO_2 did not present a significant temporal variation through the period sampled. However, this nitrogen species shows spatial differences among survey stations (Table 6.3). The *a-posteriori* test separates station 9 from the remainders with the exception of station 5. Nitrite was highly significantly correlated with pH (r_s = -0.254) and significantly with depth (r_s = -0.364; Table 6.4). The multiple regression model shows that 50% of NO_2 variance can be explained by changes in pH (Figure 6.8). Station 5 and 9 appeared to be strongly related with wastewater discharges, hence low pH conditions that favour nitrogen reduction forms. The significance with depth may associate the shallow location of wastewater sources.

Nitrate. The higher oxidised form of nitrogen analysed in the present work, NO_3, shows an extreme maximum value of 68.47 μM for June-July in station 2 and a minimum value of 0.02μM for March in station 9. The annual average value was 3.93μM (Figure 6.8). As in the case of NO_2, nitrate did not show a temporal significant difference. Spatially, nitrate shows a scattered distribution through the system without significant differences among stations.

Nitrate shows highly significant correlation with organic (r_s = -0.304) and inorganic (r_s = -0.321) seston, and significant correlation with pH (r_s = -0.195), salinity (r_s = 0.205), and organic (r_s = -0.271) and inorganic (r_s = 0.271) sediment (Table 6.4). The MRA performed for Nitrate, as with nitrite, only retained the independent variable pH, which explained 60 % of the Nitrate variance (Figure 6.10). These findings reflect the importance of the redox condition in the speciation of nitrogen. They also indicate that NO_3 concentration characterises those areas with relative high pH and hence are separated from wastewater discharges (Enoksson, *et al.* 1990; Jansson, *et al.* 1994).

Ammonia. The most reduced form of nitrogen determined in the present study, NH_3, showed an extreme maximum values of 129.36 μM at station 9 for May, and a minimum value of 0.1 μM at station 10 during March. The mean annual value was 8.21 μM (Table 6.1; Figure 6.11). During the survey programme period, ammonia did not show significant difference between months. However it presented a highly significant difference ($p < 0.000$) at the spatial scale (Table 6.3). The *a-posteriori* test shows that those stations related to wastewater discharges (stations 5 and 9) were significantly different from the rest, and therefore were segregated.

The non-parametric Spearman correlation analysis shows a highly significant correlation between NH_3 and DIP (r_s = 0.299), organic (r_s = 0.348) and inorganic (r_s = 0.266) seston, and significant with secchi depth and dissolved oxygen (Table 6.4). The best MRA model retains organic seston, oxygen and secchi depth. This model explains 93% of the NH_3 variance from which organic seston defines the major percentage (Figure 6.12). This complex relation between organic matter, oxygen and light, can be explained in terms of nitrogen denitrification, where the reduction of organic compounds and nitrogen forms (NO_3 and NO_2) is carried out in the absence of oxygen (r_s = -0.205) and light (r_s = -0.117). Thus, heterotrophic facultative aerobic bacteria tend to reduce organic compounds to obtain energy and they can use either oxygen or nitrate (Rosenberg, *et al.* 1990; Jansson, *et al.* 1994).

In general it was observed that nutrient speciation was related to physical and chemical conditions induced in the system by anthropogenic developments. Thus, local anthropogenic effects in the Guaymas system seems to exceed natural seasonal environmental changes reported for coastal lagoons in the Gulf of California (Valdez-Hoguin, 1994; Botello-Ruvalcaba, 1995; Delgadillo-Hinojosa, et al, 1997). Local wastewater input strongly determines nutrient distribution and speciation. Areas impacted by organic matter discharges were associated with low water quality conditions, which, in turn, strongly determined the nitrification or denitrification state for the Guaymas system.

Phytoplankton biomass. The phytoplankton biomass, measured as chlorophyll-*a* presented an extreme maximum value of 102.00 mg chl-*a* m^{-3} during May in station 9, and a minimum of 0.19 mg chl-*a* m^{-3} for June-July in station 2. The annual average value was 7.55 mg chl-*a* m^{-3} (Table 6.1; Figure 6.13). Chlorophyll-*a* did not show a significant difference, either on the temporal or spatial scale. However, spatially, the *a-posteriori* test indicates that station 9 differed from the remainders when a significant level of 0.06 occurs.

The highly variability for chlorophyll-*a* can be explained by considering that phytoplankton biomass, in contrast to other environmental parameters, is subject to the influence of variables such as temperature, light penetration, nutrient level, species composition and prehistory of the cells (Curl and Small, 1969; Aksnes, *et al.*, 1995). In addition, effects of dilution and transport experienced by the phytoplankton cells (Aksnes, *et al.*, 1995; Skogen, *et al.*, 1995; Yanagi, *et al.*, 1997).

Phytoplankton biomass showed a highly significant correlation with dissolved oxygen, organic (r_s = -0.369) and inorganic (r_s = -0.369) sediment, and significant correlation with secchi depth and organic seston (Table 6.4). This suggests that phytoplankton biomass is an important regulator, together with other physical variables, of the oxygen concentration within the system. Thus, a proportion of the dissolved oxygen production in the water column is determined by the photosynthetic activity of the phytoplankton biomass (r_s = 0.280), which in turn is affected by light penetration in the water column (r_s = -0.249), and other phytoplankton physiological adaptations, including photoadaptation, and photoinhibition (Curl and Small, 1969; Wofsy, 1983; Baumert, 1996). The relationship between suspended organic matter, represented by organic seston and chlorophyll-*a,* indicates the significant contribution of the phytoplankton biomass (r_s = 0.257) to the total suspended matter. The distribution of chlorophyll-*a* was not directly associated with areas receiving sewage discharges (except for February at station 5 and May at station 9) in which seston was highly significantly associated. However, for those areas not directly associated with wastewater discharges, organic seston closely follows phytoplankton blooms, as can be seen for instance, in the phytoplankton blooms located in April in stations 13, 8, 10 and 11, which coincide with high values of seston (Figures 6.13, 6.14 and 6.15). Finally, the highly significant correlation with organic sediment questions whether or not microphytobenthos biomass is an important contributor of the total phytoplankton biomass for the system. Although, chlorophyll-*a* samples were taken from the water column, these samples did not discriminate chlorophyll-*a* from microphytobenthos, which may use suspended sediment as a substratum. Thus, chlorophyll-*a* and organic sediment content show a similar pattern mainly in those stations not directly associated with sewage discharges (e.g. Station 8 in Figures 6.13 and 6.16). There are no previous studies considering microphytobenthos contributions in these semi-temperate systems within the Gulf of California. However, another important contributor for the total biomass of the system is represented by benthic macroalgae such as *Ulva* sp. Most studies of microphytobenthos refer to high latitude temperate systems where microphytobenthos contributes a high percentage of the total phytoplankton biomass (Colijn and de Jonge, 1984; de Jonge and Raaphorst, 1995). In contrast, in semi-temperate and temperate potential eutrophic systems, macro-algae may dominate a large proportion of vegetable biomass (Caderwall and Elmgren, 1990; Peckol and Rivers, 1996). The correlation between chlorophyll-*a* and sediment may also reflect the fact that phytoplankton blooms may remain sufficiently long to allow phytoplankton to sink into the sediment, which is likely to occur during calm periods in some areas, especially given the high residence time (Chapter 2). These findings highlight the importance of further research to evaluate the microphytobenthos and macroalgae biomass contribution for the system.

The significantly associated parameters with chlorophyll-*a* were further analysed through a multiple regression analysis. Three multiple regression models were generated: For the first model, as in former MRA, the method used was step-wise and retaining those variables that explain more than 10% of the dependent variable. The model only retained organic seston, explaining 80% of phytoplankton variance (Figure 6.17). No further significant improvements were achieved when the rejected variables were entered. As described above, phytoplankton biomass may represent an important percentage of the total organic seston and, therefore, their correlation with chlorophyll-*a*. Also, it is important to emphasis that organic matter from seston may be an important precursor for organic and inorganic nutrients, and therefore can be associated with phytoplankton biomass (Villate, *et al.*, 1991). Moreover, there is not a straight pathway from organic matter to nutrients and phytoplankton biomass, as shown by the poor correlation between these variables.

A second multiple regression model was created forcing those variables known to regulate phytoplankton biomass in coastal systems (Curl and Small, 1969; Wolfy, 1983; Capelle, *et al.*,1994). Thus, the variable water temperature, salinity, NH_3, NO_2, NO_3, PO_4 and secchi depth were used. The resulting model explained 91% of the phytoplankton biomass variability where the variables light penetration and salinity were retained.

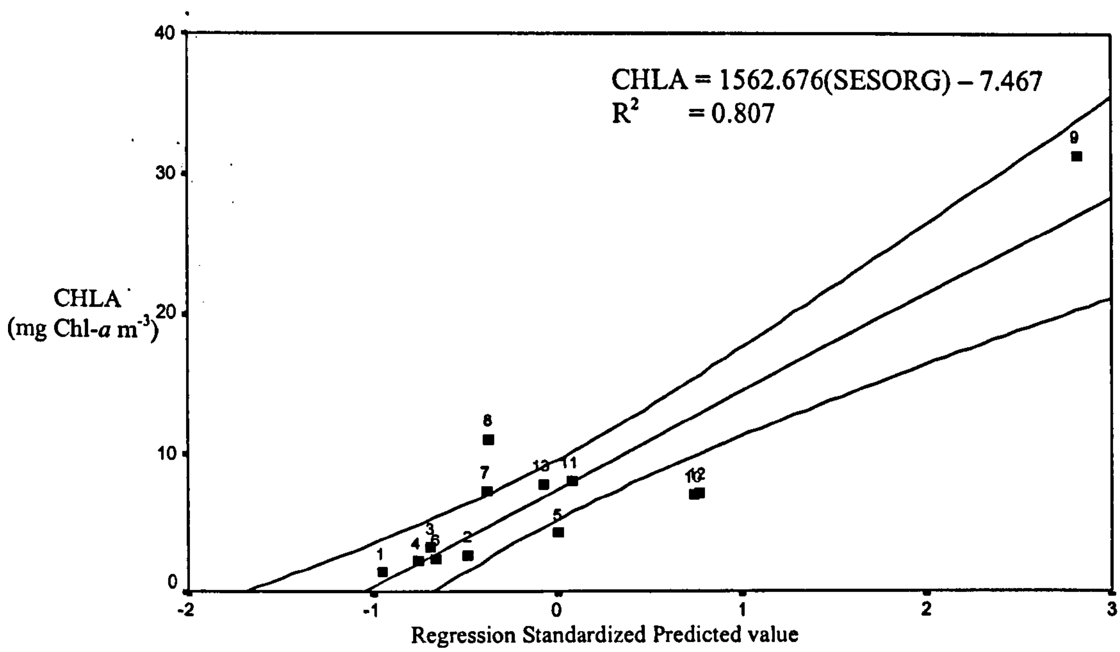

Figure 6.17. Monthly averaged chlorophyll-a versus standardized predicted value. The numbers represent fixed stations. Regression model and 95% confidence level are shown.

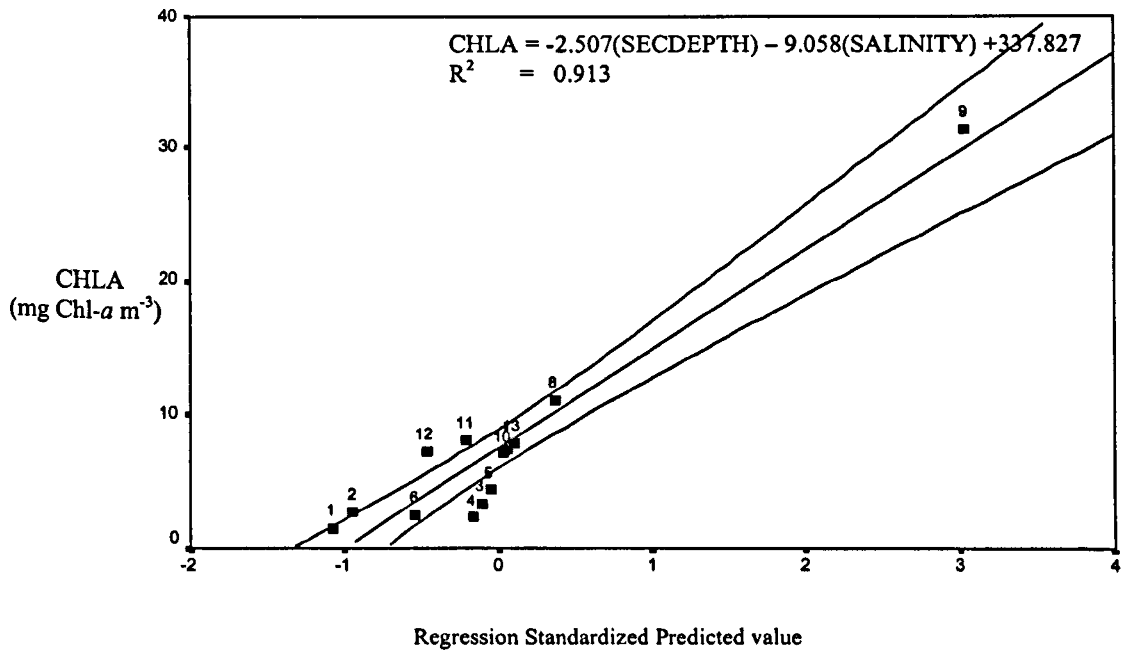

Figure 6.18 Monthly averaged chlorophyll-a versus standardized predicted value. The numbers represent fixed stations. Regression model and 95% confidence level are shown.

Salinity defined the major percentage of this variance (Figure 6.18). The inclusion of the other parameters did not improve significantly phytoplankton biomass variance predictions. The relation between chlorophyll-*a* and salinity appears to be strongly-related to areas receiving wastewater, especially station 9. Thus, for either model one or two, the strong influence of station 9 defines the regression coefficient, but, this station can not be considered as an outliner since it has influence on the whole Guaymas sub-system. Figure 6.19 shows that the two models predictions for the annual averaged chlorophyll-*a* by stations perform well in the spatial scale. On the temporal scale, using the best-fitted model (model two), it works satisfactorily within the Guaymas sub-system, although the model fails to predict the peak presented during May (Figure 6.20). For the Empalme sub-system, model two follows the same patterns as the measured chlorophyll-*a*. However, the model overestimates phytoplankton biomass from December to March and then underestimates chlorophyll-*a* until the end of the simulation (Figure 6.20).

The purpose of the third model was to improve the seasonal simulation for of the whole system. The variables used were the same as those in the second model, with the exception of light penetration, which was removed without decreasing R^2. The model showed a very good representation of the mean-monthly phytoplankton biomass variability in the Guaymas System (Figure 6.21). Further attempts to reduce the number of variables defining chlorophyll-*a*, resulted in a significant decrease (>0.1) of R^2 in the predicted model. The model follows the chlorophyll-*a* measurements, during the phytoplankton maximum during May, and predicts a the value for January where phytoplankton was not reported (samples accidentally lost). Although ecological models require detailed information on processes, the study of eutrophication on large-scale (whole system) provides important and valuable information for management purposes. Thus, the large spatial scales supersede local high variation in environmental and biotic parameters, and hence produce a better representation of the ecosystem performance through the annual cycle. Management decisions often must be based at this level, since the factors that produce eutrophication have a wide scope in nature as well as temporal and spatial scales

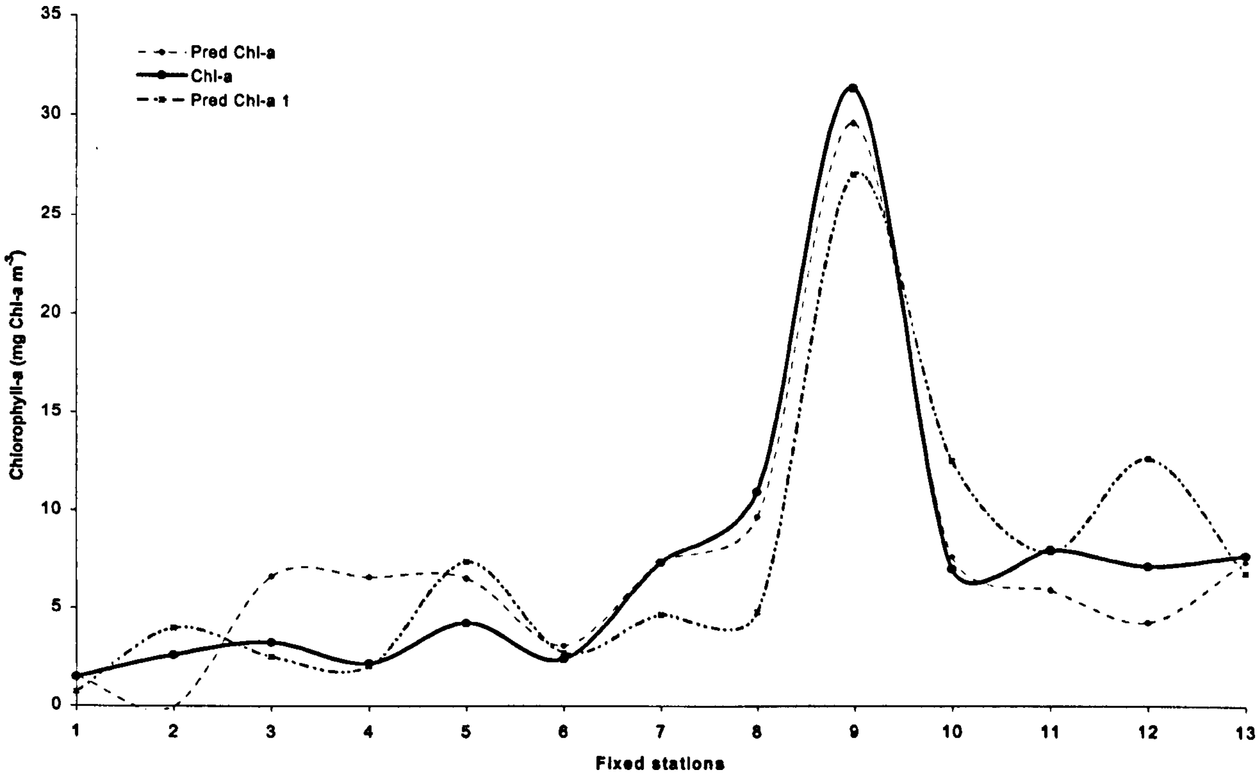

Figure 6.19. Annual averaged model predicted and measured chlorophyll-*a* for the Guaymas system.

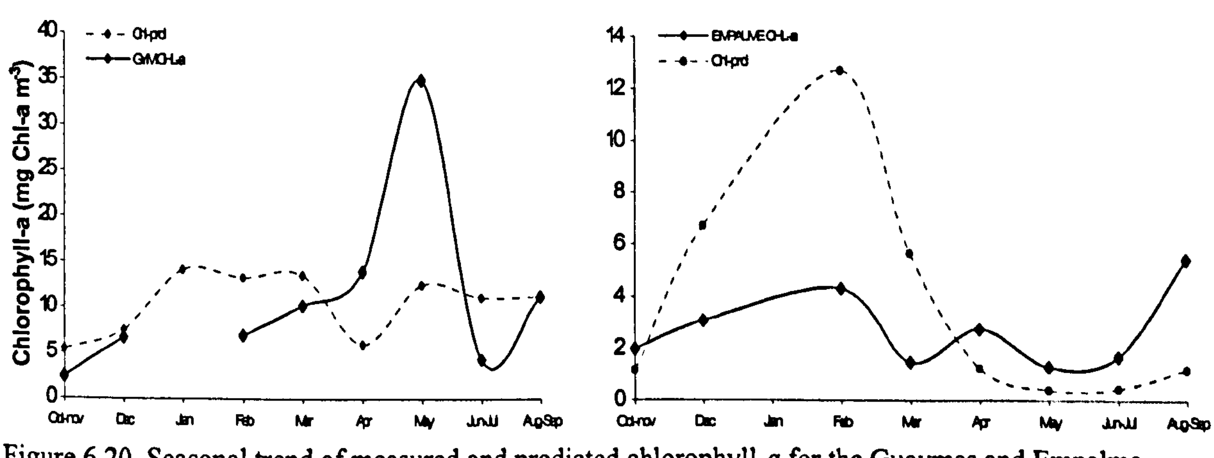

Figure 6.20. Seasonal trend of measured and predicted chlorophyll-*a* for the Guaymas and Empalme sub-systems.

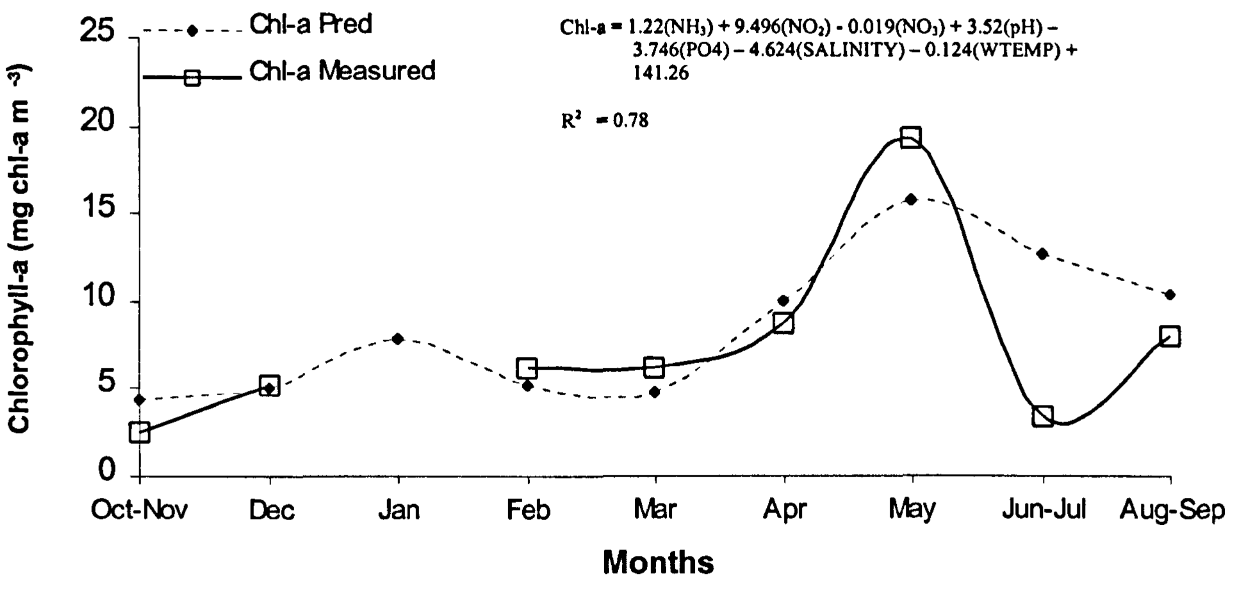

Figure 6.21. Annual averaged model predicted and measured chlorophyll-*a* for the Guaymas system.

(Rosenberg, *et al.*, 1990; Wulff, *et al.* 1990; Aknes, *et al.*, 1995; Gordon, *et al.*, 1996).

In general, phytoplankton biomass in the Guaymas system is determined by the direct and indirect influence of anthropogenic activities over the system. Thus, the anthropogenic induced changes in physical and chemical variables define nearly all the changes in phytoplankton biomass within the system. Chlorophyll-*a* was often associated with those stations that were not adjacent to wastewater discharges. MRA is appropriate for this system as a reliable technique to represent mathematically the averaged phytoplankton biomass according to known environmental parameters. Thus, the best fitted MRA model mimics the measured phytoplankton biomass when applied at seasonal level for the whole system.

6.4.2. Nutrients Limitation.

In the study of eutrophication, the question of which nutrient is most limiting for the phytoplankton is of central importance in order to reverse or manage the process. The most common approach to determine nutrient limitation in marine phytoplankton growth includes the inference of N:P ratios (Redfield, *et al.* 1963). Redfield approximation has been the most widely-used approach to compare nutrient limitations in oceans, world-wide (Graneli, *et al.*, 1990; Botello-Ruvalcaba, 1995). In the present Guaymas system study, using the Redfield approach for nutrient limitation, both nitrogen and phosphorus at different times were limiting factors of phytoplankton biomass. Certainly, molar N/P ratios were generally lower than 16 through the year, indicating a predominant nitrogen limitation with the exception of the fall (October–November and August-September) and April, when phosphorus became dominant (Figures 6.22 and 6.23).

A comparison between the two main hydrographic sub-systems, reveals the importance of wastewater inputs for the Guaymas sub-system. Thus, values below 16 were consistent through the annual cycle (except October-November), indicating nitrogen limitation (Figure 6.22). Nitrogen limitation under the Redfield approach may be connected to high

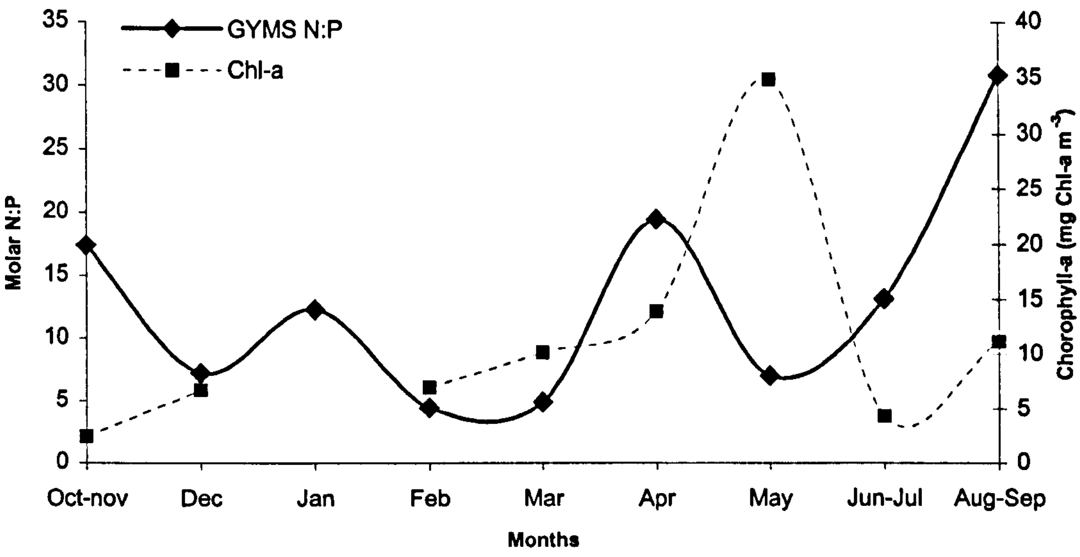

Figure 6.22. Seasonal trend in N:P molar ratios and phytoplankton biomass for the Guaymas system.

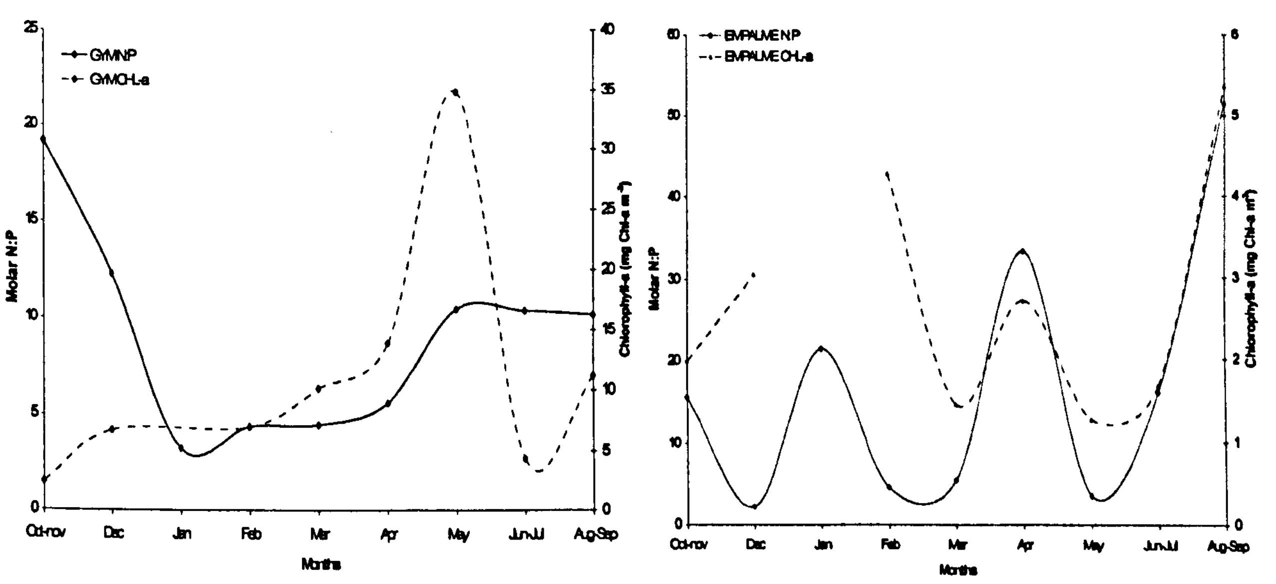

Figure 6.23. Seasonal trend in N:P molar ratios and phytoplankton biomass in the Guaymas and Empalme sub-systems.

amounts of phosphorus a loading from wastewater sources. There is no apparent relationship between nutrients and the biomass of phytoplankton, but the data shown in Figure 6.22 indicates that the phytoplankton bloom developed in May will be nitrogen limited, whereas the low phytoplankton biomass in October-November must be influenced by phosphorus limitation.

For the Empalme sub-system, N:P ratios presented a different pattern through the year (Figure 6.22). This sinusoidal pattern which alternates between nitrogen and phosphorus limitations, seems to be followed by increases and decreases of phytoplankton biomass, indicating that phytoplankton is potentially sensitive to nitrogen limitation. The sinusoidal shape of the seasonal trend can be partially-explained by considering the hydrodynamics of this semi-enclosed sub-system. Circulation for the sub-system is restricted at the mouth of the system and in the connection between the Laguna and Estero el Rancho (Figures 1.2 and 1.3). The above features enhance inward residual dominance during spring tides and oceanward residual dominance during neap tides (Chapter 3). This is consistent with the fact that those months showing a phosphorus limitation (N:P values > 16) were sampled during spring tides periods (14 days; Chapter 3) and the months where nitrogen was limiting (N:P values < 16) were sampled during neap tides (December and May) or periods of low difference between ebb and flood conditions, called relaxation periods (February and March). This indicates that nutrients (TDIN) may be pumped inside the system from either the adjacent sea or the Guaymas sub-system, alleviating phytoplankton deficiencies (Chapter 5). During low exchange periods (relaxation periods) and neap periods when the system is a net exporter of materials toward the adjacent sea and Guaymas sub-system (Chapter 3), there is not an important residual input of nutrients (TDIN), potentially-limiting phytoplankton biomass. As indicated previously, in the Empalme sub-system there is not another important source of nutrients other than the adjacent sea, therefore increases in N:P correspond to external TDIN supplied to the system, whereas low N:P ratios correspond to reductions in TDIN either by phytoplankton fixation and advected dilution or by the denitrification processes (Chapter 5).

In general, nitrogen is a limiting factor of the phytoplankton biomass in the Guaymas system when other factors such as light, sinking, grazing, temperature and salinity gradients are not. The analysis of the two main sub-basins indicates that the Guaymas sub-system is nitrogen-limiting through the year. Nutrients limiting in this sub-system are closely related to phosphorus loads from wastewater sources. For the Empalme sub-system, nutrient limitations were alternated between nitrogen and phosphorus. Thus, nutrient limitation is likely to be controlled by external nitrogen supplied from the adjacent sea and Guaymas sub-system. In terms of management it means that controlling phosphorus inputs in the Guaymas sub-system will reduce the potential for eutrophication and eutrophication problems. In the Empalme sub-system, management of nitrogen may prevent eutrophication occurrence.

6.4.3. Modelling potential for eutrophication: A simple Box model.

There is a wide range in the literature of numerical models aiming to predict eutrophication either at mesoscale or in small coastal systems (Chapelle, *et al.*, 1994; Aksnes, *et al.*, 1995; Kuusisto, *et al.*, 1997; Varela, *et al.* 1997). At the mesoscale level, acceptable resolution has been achieved in large ecosystems such as the North Sea and the Baltic Sea (Caderwall and Elmgren, 1990; Baretta-Bekker, *et al.*, 1997; Blackford, 1997). At finer scales, such as coastal lagoons, the large variety and complexity of the processes within these systems largely limit progress in developing ecosystem models in order to provide detailed answers of the ecosystem performance. However, general but valuable representation of the studied systems can be obtained (Chapelle, *et al.*, 1994; Skogen, *et al.*, 1995; Yanagi, *et al.*, 1997). The inclusion of large numbers of relevant parameters, complex algorithms to solve for their relationships and difficulties in obtaining reliable measurements, still represents a challenge for ecological models. Although research efforts seems to be the correct direction, at present the *state of the art* does not allow model-resolution at species level or the finer scales in time and space required for some specific management purposes. Certainly, highly-expensive and complex numerical models do not necessarily guarantee significant improvement in predictability or reducing uncertainty (Gordon *et al.*, 1996).

Phytoplankton blooms can be represented as simple population budgets, describing biomass for a fixed species and geographic area. From a pragmatic, management point of view, eutrophication models may not require the spatial and temporal resolution needed, for instance, in hydrodynamic models. Because of this, in this study a simple box model has been performed for the Guaymas system. Hydrodynamic, biological and chemical features, highlighted in previous chapters, were taken into account in order to choose the physiographic units in which the model was applied. In particular, the model assesses the two major sub-systems, the Guaymas and the Empalme sub-system (Figure 6.24).

This simple approach has been applied to well-mixed coastal system (Lee, 1995; Nadiarti, 1995). Phytoplankton biomass is given by the balance between phytoplankton growth rate, and losses from horizontal biomass exchange (well mixed systems), grazing and sinking of phytoplankton cells. The model simplifies the above considerations, assuming that Maximum Phytoplankton Biomass (MPB), as chlorophyll-*a* concentration is totally dependent on nutrient-enrichment and that all available nutrients are potentially assimilated by phytoplankton, and also that other factors are not limiting. This MPB will occur only if the specific growth rate (μ) overcame the phytoplankton dilution rate by horizontal exchange (Lee, 1995). Thus, MPB can be predicted from:

$$MPB = IPB + PLY_{(N,P)}.(S_{(N,P)} <S_{(N,P)}>/(E \,.\, V)) \qquad \text{mg chl.m}^{-3} \qquad (6.1)$$

where:

IPB = mg chlorophyll in m^{-3} entering in the box;

$PLY_{(N,P)}$.= Yield of phytoplankton from nutrient in mg Chl-a . $mmol^{-1}$;

$S_{(N,P)}$ = limiting nutrient in adjacent waters entering the box in mmol m^{-3};

$<S_{(N,P)}>$ = Total land derived flux of limiting nutrient in mmol day $^{-1}$;

V = Well mixed, box volume m^3;

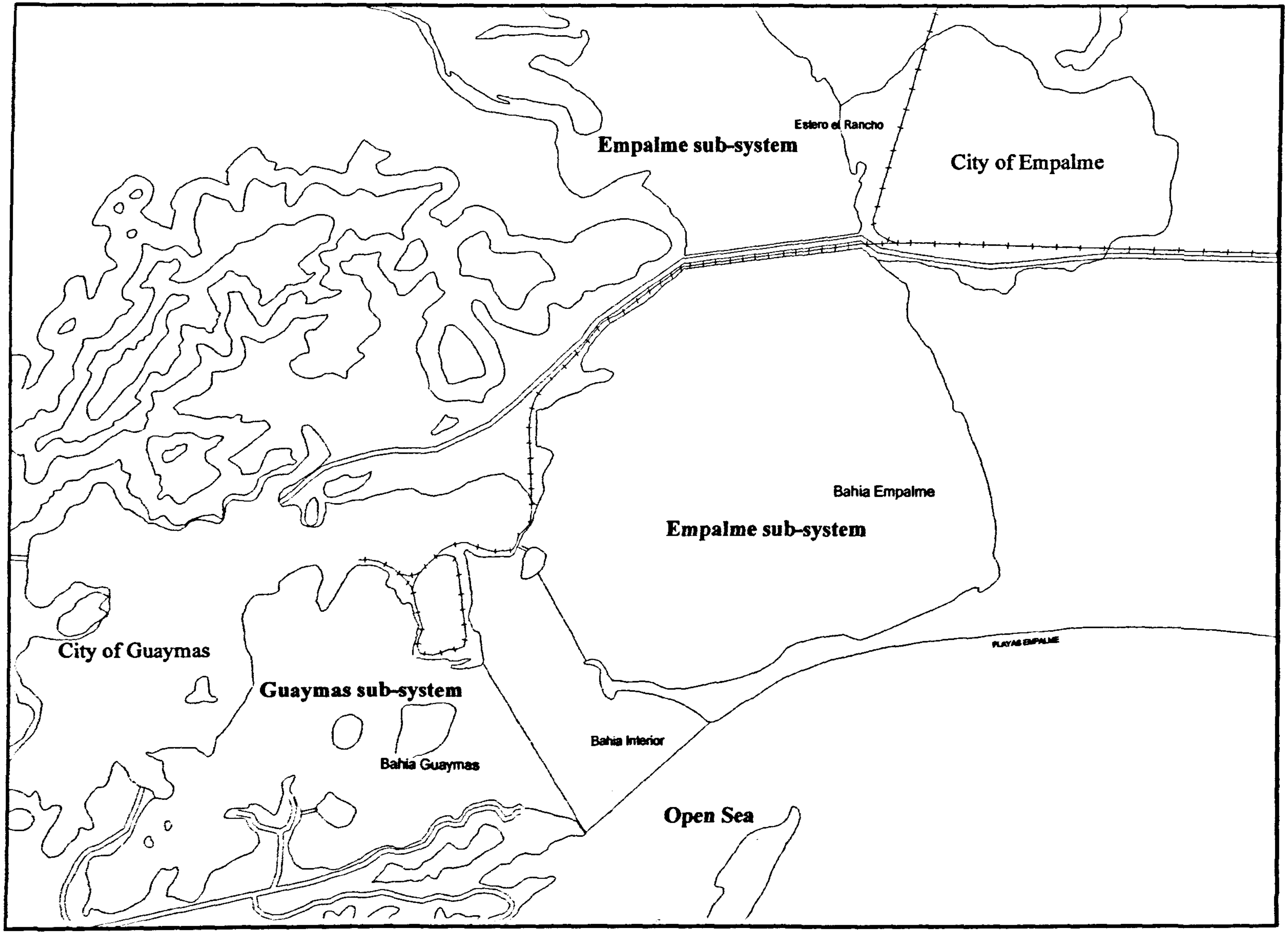

Figure 6.24. Map showing the Guaymas and Empalme physiographic units

E = Exchanging with the sea at relative rate day^{-1}.

The maximum chlorophyll-*a* predicted by equation 1 will occur only if:

$$\mu > E\,.\,(MPB - IPB)/MPB \qquad \text{day}^{-1} \qquad (6.2)$$

Where phytoplankton specific growth rate (μ) is given by:

$$\mu = \alpha\,.\,(m_2.\ I_0/K.h)\text{-}L_o \qquad \text{day}^{-1} \qquad (6.3)$$

Where:

α = phytoplankton photosynthetic efficiency under nutrient-sufficiency, in units of day-1, (μEm-2.s^{-1});

m_2 = factor correcting for extra losses of Photosynthetic Available Radiation (PAR) near sea surface;

I_0 = typical sea-surface (PAR) irradiance, mean over 24 hours, in $\mu Em^{-2}.s^{-1}$;

h = mean depth of defined area within the box in m;

L_o = Biomass-related respiration of phytoplankton and related organisms in units of day^{-1}

Table 6.5 gives a detailed description of the forcing variables, values and literature-reference used in the computations.

Light. The Light parameter was obtained from simultaneous *in-situ* Secchi disc readings (Sd, m) and PAR measurements performed with an underwater quantum sensor (LI-192SA), which has an output in units of moles where 1 $\mu molm^{-2}.s^{-1}$ = 1 $\mu Em^{-2}.s^{-1}$.

The light attenuation coefficient K is assumed constant with depth and was obtained from two underwater light measurements as follows:

$$K = -(\ln I/I_0)/z \qquad (6.4)$$

Table 6.5. Variables, definitions, values unites used in the eutrophication box model.

Variable	Definition	Value	Unites	Source
α	Maximum photosynthetic efficiency	0.015	Day-1/mE m-2 s-1	Nadiarty, 1995
m_2	Factor correction of extra loss PAR near sea-surface	0.37		Nadiarty, 1995
Io	24-hr mean subsurface PAR	Measured	$\mu Em^{-1}\ s^{-1}$	This work
K	Light attenuation coefficient	Computed		This Work
h	Average depth: Guaymas Empalme	4.62 2.43	m	This work
Lo	Biomass related to respiration of phytoplankton and other organisms	12	Day^{-1}	Lee, 1995
IPB	Initial Phytoplankton Biomass	Measured	mg Chl-*a* m^{-3}	This work
MPB	Maximum Phytoplankton Biomass	Computed	mg Chl-*a* m^{-3}	This work
PLY_N	Yield of phytoplankton from limiting Nitrogen	1.8		Lee, 1995
PLY_P	Yield of phytoplankton from limiting Phosphorus	50		Lee, 1995
S_N	Limiting Nitrogen entering to the box	Measured	m mol m^{-3}	This work
S_P	Limiting Phosphorus entering to the box	Measured	m mol m^{-3}	This work
E_{GYM}	Exchange Guaymas box with the adjacent sea	0.0833	Day^{-1}	This work
E_{EMP}	Exchange Empalme box with the adjacent sea	0.0653	Day^{-1}	This work
V_{GYM}	Volume Guaymas Box	35020263	m^3	This work
V_{EMP}	Volume Empalme Box	57958673	m^3	This work

Where I is PAR at depth z. A total of 52 determinations were performed, which were further related to Sd depth in a regression. Thus, K in the present work was determined either from vertical PAR profiles or from Secchi depths for those cases where PAR readings were not available, using the relation K=-0.1687(Sd) + 0.957 ($r^2 = 0.82$).

Nutrients. Limiting nutrient ($S_{(N,P)}$) levels, calculated in this work, were used for the simulation (Figure 6.23). Thus, the model was fed according to the seasonal trend in N:P ratios for the Guaymas and Empalme sub-systems.

Chlorophyll-*a*. Phytoplankton biomass values were fed into the model as chlorophyll-*a*. Missing values were replaced using the predicted chlorophyll-*a*, indicated in Figure 6.20.

Simulation.

With regard to the initial condition set-up in equation 6.2, Table 6.6 shows that, with the exception of June-July, in the Guaymas sub-system μ is greater than E . (MPB – IPB)/MPB, and hence is consider potentially eutrophic. Also, for the Empalme sub system, μ was < E.(MPB – IPB)/MPB only during June-July.

Three scenarios were simulated for each system. The first simulation was run using the limiting nutrients accord to the seasonal trend observed in each sub-system. This simulation represents a scenario base, where there is not a nutrient-reduction management in the system. For the second model, the phytoplankton response after reducing nutrient levels by 50%. The third scenario was performed by simulating reduction in nutrients of 75%.

Figures 6.25 and 6.26 summarise the model outcomes for both sub-systems. For the Guaymas system under the simulation, the potentially Maximum Phytoplankton Biomass represents an average increase of the phytoplankton biomass of 77.5%. This indicates that

Table 6.6. Comparison between phytoplankton specific growth (μ) and exchange and other losses (Equation 2).

MONTH	E*(MPB-IPB)/MPB	μ		E*(MPB-IPB)/MPB	μ	
October-Nove	0.072633	1.853305	Yes	0.030606	3.642547	Yes
December	0.046851	7.121061	Yes	0.003261	3.523305	Yes
January	0.030748	1.976833	Yes	0.015346	3.523305	Yes
February	0.040872	1.643153	Yes	0.00745	1.742434	Yes
March	0.019096	2.672097	Yes	0.006094	3.063981	Yes
April	0.031174	8.327097	Yes	0.006074	9.403069	Yes
May	0.022402	1.459288	Yes	0.011796	1.282097	Yes
June-July	0.056682	-2.42453	NO	0.017734	-1.19566	NO
August-Septem	0.031985	1.683989	Yes	0.017326	2.222322	Yes

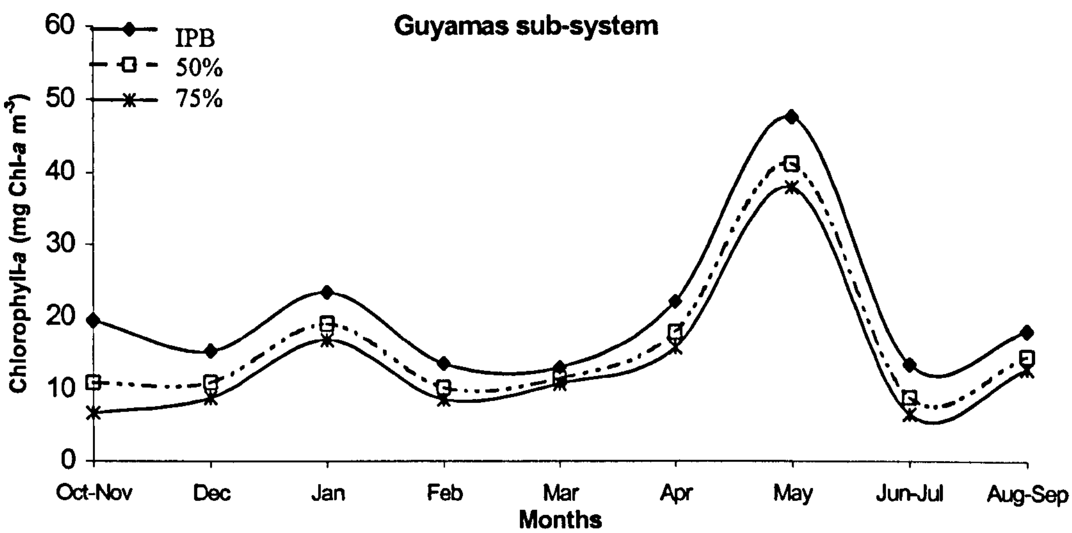

Figure 6.25. Seasonal trend of simulated Maximum Phytoplankton Biomass (MPB), and MPB under 50 and 75% nutrient limiting reduction for the Guaymas sub-system.

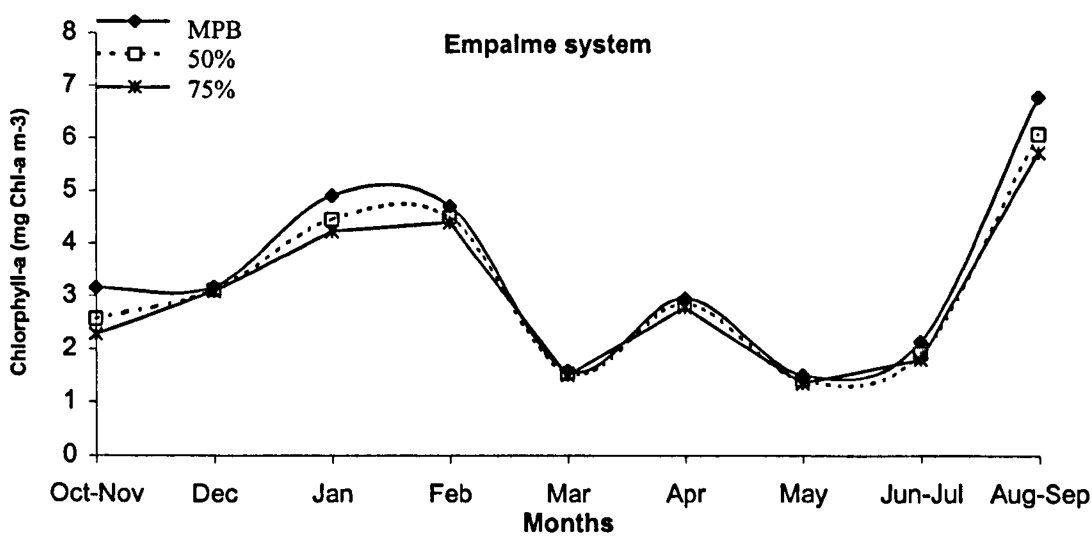

Figure 6.26. Seasonal trend of simulated Maximum Phytoplankton Biomass (MPB), and MPB under 50 and 75% nutrient limiting reduction for the Empalme sub-system.

biomass in the system potentially can increase significantly. This implies that there are limiting factors, other than nutrients, that limit phytoplankton biomass. This is consistent with the findings reported previously in this chapter, where chlorophyll-*a* shows a significant correlation with environmental variables other than nutrients. Assuming that the major proportion of the nutrient content in the Guaymas Bay came from industrial and urban wastewater, a reduction of the 50% of the nutrient availability in the bay will produce a reduction of 33% in MPB with respect to the scenario base (no nutrient reduction). A further reduction in nutrients of 75%, will reduce MPB by 58 % respect to the scenario base (Figure 6.25).

For the Empalme sub-system, the potential MPB represent an increase of only 19.5% in the biomass entering into the sub-system. It is unlikely in the Empalme sub-system, that an increase approximately to 20% represents any threat of eutrophication. Thus the low values of chlorophyll-*a* measured in the system will be increased below the present levels of chlorophyll-*a* measured in the Guaymas sub-system. In this case, an increase in phytoplankton may even benefit productivity of the sub-system. The model shows that a 50% reduction in nutrient entering the system will represent a decrease of approximately 10% in the 19.47% observed in the scenario base (no reduction in nutrients). A further nutrient reduction of 75% will represents a decrease of 14% of the 19.47% reported for the scenario base (Figure 6.26).

In general, the model provides an insight into the potential for eutrophication within the Guaymas system. The approach shows that the Guaymas sub-system is potentially a highly-eutrophic system, whereas in the Empalme system the potential for eutrophication will produce a lower phytoplankton biomass than that measured in the Guaymas system ($IPB_{Guaymas}$). In terms of management, the question of what effect different nutrient management strategies will have on the Guaymas System can be partially answered. The model shows that a reduction of the limiting nutrients presents an important decrease in potential phytoplankton biomass in the Guaymas sub-system, and a moderate one for the Empalme sub-system. The Guaymas sub-system is phosphorus-limited, hence a decrease in the phosphorus loads will improve water quality. Local policies must encourage P control in sewage facilities and in contrast to nitrogen, the control of phosphorus in sewage is technically straightforward (Caderwall and Elmgren, 1990).

The Empalme sub-system does not present a high potential for eutrophication. The MPB values and the alternation of limiting nutrients (nitrogen and phosphorous) through the year, suggest that a nutrient reduction programme in this sub-system may be low cost-effective. Despite this, it is likely that a nutrient reduction in the Guaymas sub-system will imply further reductions in the Empalme system.

Although the model provides a general picture of the potential for eutrophication, this approach relies greatly on assumptions inherent in the model. Certainly, the model is sensitive to factors such as $PLY_{(N,P)}$, E, and α, which are given as a constants. For the present work, the values used in these constants are the result of the review from the works produced by Lee (1995) and Nadiarty (1995), who assess the model's performance.

6.5 Conclusions.

In the present work, characterising the biotic and abiotic parameters influencing phytoplankton biomass allows the production of empirical models based on the statistical analysis of observed trends. Also, using information presented in previous chapters and a simple box model, the work assesses the potential for eutrophication within the Guaymas system.

The present study shows that nutrient speciation was related to physical and chemical conditions induced by anthropogenic developments. Thus, local anthropogenic effects in the Guaymas systems dominate seasonal environmental changes reported for coastal lagoons in the Gulf of California.

Local wastewater inputs strongly determine the nutrient distribution and speciation, and the nitrification or denitrification state of the system. In turn, anthropogenic-induced changes in physical and chemical variables account for a large percentage of the changes in phytoplankton biomass within the system.

The multiple regression analysis for this system gives a reliable predictive technique to represent mathematically the averaged phytoplankton biomass according to known environmental parameters. Thus, the best fitted MRA model follows the measured phytoplankton biomass when is applied at a seasonal level for the whole system, and explains a high percentage of its variance.

The stoichiometric Redfield approach indicates that nitrogen is a limiting factor of the phytoplankton biomass growth in the Guaymas system, when other factors such as light, sinking, grazing, temperature and salinity gradients are not.

Nutrient limitation in the Guaymas sub-system is closely related to phosphorus loads from wastewater sources. For the Empalme sub-system, nutrient limitation was alternately by nitrogen and phosphorus. In this sub-system nutrient ratio trends were associated with residual transport of spring and neap tides.

A simple box model approach allowed the characterisation of the potential hyper-trophic conditions for the Guaymas sub-system, and shows that phosphorus reduction in the system will be accompanied by an improvement in water quality. Furthermore, the results suggest that management strategies must encourage P control from wastewater discharges into the sub-system.

The same approach applied to the Empalme sub-system, indicates that the potential for eutrophication in the sub-system does not represent a threat for the ecosystem health. Therefore, a nutrient reduction strategy may be a low cost-effective option.

6.6 Further Work.

- The present box model provides a valuable general picture of the trophic status of the system, encouraging management strategies. However, the work recognise that better results may be obtained with effort towards model prediction improvement. Thus, model findings produce new questions, suggesting that further research must conducted in order to incorporate further forcing variables without reducing the cost-benefit of the approach. The most important of these needs are listed below:

- Eutrophication prediction should be built-up from hydrodynamic model outputs, including turbulent mixing induced by wind and tide.

- Potential for eutrophication models also must incorporate other physical and chemical state variables such as temperature, salinity, pH, oxygen and nutrients, and biological variables should be represented by the two phytoplankton major groups characterised at local level.

- Biological plankton processes such as grazing, mortality, and sinking rate, respiration and decomposition should be estimated from local conditions.

- A further quantification of the light parameter, including better and more local validated self-shading correction factors, is required for this system.

- Other important components of the index of the eutrophication processes such as macroalgae and microphytobenthos must be characterised and their contribution included in further modelling.

- Further studies are required to characterise the exact location and composition of the waste discharges along the Guaymas and Empalme basis. The study must include the effect of the projected improvements in sewage facilities and the likely industrial and urban future growth.

CHAPTER 7

GENERAL DISCUSSION AND CONCLUSIONS

7.1. General Conclusion.

The present study has encompassed a series of field observations and theoretical considerations related to physical, chemical, and biological factors defining the process of eutrophication in the Guaymas system. Additionally, the work has produced the basic ecosystem model of the system through the modelling of the hydrodynamics, sediment dynamics, budget dynamics, net ecosystem metabolism and the potential for eutrophication. These findings produce an overall assessment of the system, which together with the environmental legislation and socio-economic concerns allows those factors influencing decision making to be highlighted. Finally, the work introduces further discussion against the background of the repercussions of the Mexican environmental policy and legislation and their likely implications at international level.

The Guaymas system historically has been systematically impacted by anthropogenic activities that include land reclamation, restriction of circulation by engineering works, dredging for navigation purposes, unregulated and regulated industrial and human settlements, and urban and industrial discharges. All of these modification and inputs to the systems have transformed the natural conditions, including hydrodynamics and other physical, chemical and biological conditions that define the status of the system. In this context the present chapter provides a synthesis of the assessment of the Guaymas system.

7.1.1. Hydrodynamic and sediment dynamics.

Hydrodynamic modelling was performed, to describe hydrodynamic features for the Guaymas system. Also, it is used as the primary framework for the development of sediment transport, water quality, geochemical and ecosystem models. There is a strong influence of tide and probably wind-generated water currents. Circulation patterns within the system follows topographic and bathymetric features, where strong currents were associated to channel depths and local hydraulic pressure gradients. This circulation feature indicates that the Empalme sub-system was an ebb dominant system, as showed by the simulated period. The difference in ebb and flood characteristics of both systems produces a residual water movement towards the Guaymas sub-system.

Circulation patterns as shown by residual currents characterised through particles tracking, indicates high residence times, which in turn may produce phytoplankton blooms and low dispersion rates for materials discharged into the system. Major residence times are present at the head of the system in both sub-systems, Guaymas and Empalme.

Simulation of the trends for potential net transport of sediment indicates that bedload transport is likely to occur toward the head of the Guaymas sub-system. For the Empalme sub-system, there was a net bedload displacement toward the mouth. The study strongly suggests that the model requires further validation and calibration before it can be used as quantitative management tool.

In general the knowledge of the hydrodynamic features indicates that the flushing capacity of the system may be insufficient to remove pollution discharged into the Guaymas sub-system. This in turn indicates that the sub-system may be a pollutant sink thus provides the conditions for phytoplankton blooms to occur. The same hydrodynamic conditions occur in the Estero El Rancho although there is no major pollution discharges in that area. Finally, the hydrodynamics of the system indicates that there is a residual mass of water that exchanges from the Empalme sub-system to the Guaymas sub-system. This is particularly important if there were oil spills, since oil reception facilities are located at the mouth of the Empalme subsystem.

7.1.2 Biotic and environmental parameters.

The characterisation of biotic and abiotic parameters influencing phytoplankton biomass shows that nutrient speciation was related to physical and chemical conditions induced by anthropogenic developments. Thus, local anthropogenic effects in the Guaymas systems are greater than seasonal environmental changes reported for coastal lagoons in the Gulf of California. In this context, the local wastewater input strongly determines nutrient distribution and speciation, together with the nitrification or denitrification state of the system. In turn, anthropogenically induced changes in physical and chemical variables explain much of the variation in phytoplankton biomass within the system.

Empirical models based on statistical analysis of observed trends.

Attempts to describe mathematically the interrelationships between the biotic and environmental parameters in the Guaymas system succeed in to represent the averaged phytoplankton biomass. Thus, the best fitted MRA model predicts the measured phytoplankton biomass when applied at seasonal level for the whole system, and explain nearly 0.78 of its variance. This model highlights the importance of nutrients, pH, temperature and salinity determining phytoplankton biomass, and hence indicates that a control in at least one of those variables will affect phytoplankton biomass.

Nutrient limitation.

The stoichiometric Redfield approach indicates that nitrogen is a limiting factor of the phytoplankton biomass growth in the Guaymas system, when other factors such as light, sinking, grazing, temperature and salinity gradients are not. However, an analysis of the different compartments in the system shows that nutrients limiting in the Guaymas sub-system are closely related to phosphorus loads from wastewater sources, whereas for the

Empalme sub-system, nutrient limitation was alternately by nitrogen and phosphorus. In this sub-system, nutrient ratio trends were associated with residual transport of spring and neap tides.

Trophic status.

Using simple box models, the present work assessed nutrient budget dynamics, and net ecosystem metabolism within the Guaymas system. The presented biochemical budgetary assessment (Gordon, *et al.* 1996) represents a good approximation for the trophic status of the system. The study also explored the model through box fragmentation, indicating that the stoichiometric Redfield approach provides robust overviews of the nitrogen fixation-denitrification and net ecosystem metabolism at a large scale level such as the whole Guaymas system, the Guaymas and Empalme Sub-system, and when the Empalme sub-system is divided into the Rancho and the Laguna.

This approach indicates that the Guaymas system is a net heterotrophic system, with a value of -4811.72 $mmol.C.m^{-2}.y^{-1}$, which can be compared with other areas elsewhere assessed using budget analysis. This indicates that a high percentage of organic matter produced in the system is retained by different processes including phytoplankton blooms and benthic algal mats, which in turn may pose eutrophication risks for the system. Thus, the model produces a primary quantitative outcome of the eutrophic status for areas heavily affected by anthropogenic activities and an insight of their likely impact over the rest of the system. Also, the likely pathway of nutrients through compartments is shown, illustrating qualitatively the impacts in areas receiving direct sewage discharges.

7.1.3 Potential for eutrophication.

A simple box model approach allows the characterisation of potential hyper-trophic conditions for the Guaymas sub-system, and suggests that phosphorus reduction in the system is accompanied by an improvement in water quality. Further more, the results suggest that management strategies must encourage P control from wastewater discharges into the sub-system. The same approach applied to the Empalme sub-system indicates that the potential for eutrophication in the Empalme sub-system does not represent a threat for the ecosystem health. Therefore, a nutrient reduction strategy for this sub-system may result in a low cost-effective option.

7.1.4 Background of the repercussions of the Mexican environmental legislation.

The Guaymas system has been reported to be impacted by pollutants such as: heavy metals (Hosch, 1997); hydrocarbons; organic matter, suspended solids; fats and oils, and; faecal coliforms (SMAM, 1991). However, the present section is limited to those parameters related to the potential for eutrophication in the context of the Mexican environmental legislation.

The Secretariat of Environment, Natural Resources and Fisheries (SEMARNAP), is the governmental body in charge of developing, verifying and, together with the Secretariat of Marine, enforcement of environmental standards. The General Law of Ecological Balance and Environmental Protection (LGEEPA) is the primary legislation for environment. The prevention and control of pollution in water and aquatic ecosystems is undertaken in Chapter III of LGEEPA, and Article 117 presents the prevention and control criteria of pollution in national waters. Among these criteria it states that "the prevention and control of pollution in water is fundamental, in order to avoid reduction in its availability and to protect the national ecosystems", and that the utilisation of water for development activities must include the responsibility for its treatment in order to guarantee other activities and to maintain the ecosystem balance. Furthermore Article 118 indicates several considerations in relation to the criteria for prevention and control of pollution in water, and considers, that the quality classification of the systems receiving residual waters is a function of their assimilation or dilution capacity, and the amount of pollutant that these systems can absorb. Article 122 highlights that urban and industrial discharges must have the necessary quality to prevent pollution in the receiving water body. Article 130 is related to the waste discharges in marine environments, and Article

131 indicates that for the protection of the marine environment the secretariat must create the official standards for the administration, exploitation and preservation of the marine resources.

In the present context, the most appropriate legislation applied to the Guaymas system regards the official Mexican standards through the *Norma Oficial Mexicana*-NOM-001-ECOL-1996. This standard states the maximum permissible limits of pollutants in wastewater discharged in to national waters (rivers, natural and artificial lakes, including dams, coastal waters and wetlands). Although this does not give the limits of pollutants in side the coastal waters, it indicates the maximum allowed into the system. The norm separates wetlands of coastal waters, making three categories of coastal waters, the first includes those for fishing exploitation, navigation and other uses, the second category include recreation uses, and the last categorises estuaries. The norm is comprehensive in setting a large number of water quality parameters including pH, temperature, total nitrogen and total phosphorus of relevance in the present study. However, establishing a comparisons with the parameters studied in this work, temperature and pH apply to wetlands and coastal waters, the maximum allowed values in these systems are 40°C for temperature and a range of 5 to 10 in pH. Total nitrogen and phosphorus only apply to coastal waters in the category of estuaries where the standard for total nitrogen are 15 $mg.L^{-1}$ as a monthly mean and 25 mg.L-1 as daily mean, and for total phosphorus the standards are 5 $mg.L^{-1}$ as a monthly mean and 10 mg.L-1 as daily mean.

It is of importance that the standard does not consider nitrogen and phosphorus enrichment in coastal environments, and hence eutrophication risks poses over the system. There is a complex set of standards and regulations regarding issues in coastal areas, for example the designation of bathing or recreation areas, and the designation of zones for bivalve molluscs culture. None of these regulations cover nutrient concentrations in the receiving water body as potential threat for the ecosystem. Moreover, for the specific case of the Guaymas systems, the multi-use characteristics of the system makes designation more difficult. However, the eutrophication process together with other pollution processes is covered by articles 117, 118, 122 and 130 of the LGEEPA. Finally, it is important to highlight that the production of environmental standards in Mexico is an ongoing process. In this context, the present work emphasises an area in which further standards should be produced.

Relation with other international legislation.

Mexican environmental legislation is enacted through general environmental objectives included in the LGEEPA articles, e.g. articles 117 and 118. At a practical level, the objectives are achieved through the official environmental standards. This may be similar to the concept of Environmental Quality Objectives (EQO) and Environmental Quality Standards applied in several countries such as those of the European Community (EC; e.g. Ellitott *et al.*, 1995).

In relation to the degree of agreement between Mexican environmental standards and international standards, the Mexican Legislation clearly states that Mexican environmental standards can not be equivalents to those proposed by other countries, since they are not compatible with the technical and juridical elements integrated in the Mexican official standards, which are produced regarding national and international well recognised technical and scientific knowledge. This precept is closely related with the principle of national sovereignty and national security practised by the Mexican state. Thus, there is not direct comparison between the effectiveness of the Mexican environmental legislation and that of other countries.

Nevertheless, since pollution is an international issue, Mexico has accepted the challenge toward better environmental enforceability and quality standards posed by international agreements and conventions. This, together with economic improvements will allows the diminishing of the environmental gap with respect to those countries with the better environmental standards.

In the particular case of the Guaymas system, the quality standards set for the system will depend very much upon the designation ultimately used for the system. For instance, if some areas of the Guaymas sub-basin are designated for industrial use, a polluted influenced is likely to occur in an area near the development. However, the areas influenced by this development must not pose a treat for the people living the Guaymas basin as stated in the LGEEPA.

There are some external factors that may improve water quality in the Guaymas system, for example:

- better enforceability of the environmental legislation set up by the national environmental plan 1995-2000, including integral environmental plans;
- better industrial environmental culture, including the cost-benefit of clean technologies;
- open market economy, mainly new international and developing export enterprises to improve quality standards (voluntary environmental standards) in order to obtain preferential opportunities in foreign countries. In this aspect, voluntary standards together with other instruments (e.g. fiscal policies; preferential access to credit) considered in the national environmental plan may encourage the use of clean technologies.
- The role of the Non-Governmental Organisations is vital in order to raise environmental issues in public opinion.
- The comparison and enactment of international agreements, which at the present are limited.
- The possibility of developing an Integral Coastal Zone Management Plan for the system which will boost those initiatives set up by the environmental plan 1995-2000.

7.1.5 Final remarks.

Environmental modelling has been shown here to be an important tool for coastal zone management. This helps to integrate a large number of environmental variables in order to explain and to analyse the complexity of some processes within the studied ecosystem. Ecosystem modelling is similar to Coastal Zone Management since it is characterised by an interdisciplinary approach. The present work has produced the basic ecosystem model of the Guaymas system, allowing characterisation, for example of the potential for eutrophication of the system, and showing their value deriving procedures for coastal management. Finally, it is important to highlight that environmental modelling outcomes are as good as the understanding of the system and the data obtained for deviates and validates. Further more, as indicated through this work, modelling still relay in may theoretical assumptions that must be undertaken by further research, in order to improve models predictability.

7.2. Suggestion for further work.

Knowledge and characterisation of a coastal ecosystem is a long ongoing process. Thus, the present study has identified that further research must be carried out in other to improve knowledge and satisfy the scientific and management interest of the system. The most important of these needs are listed below:

7.2.1 Survey programme.

It is necessary to continue fieldwork through a comprehensive survey programme that allows the validation and further calibration of the produced models. The survey campaigns should produce data for:

Hydrodynamics.

- Simultaneous tide amplitude and current velocity measurements within the two main sub-systems, in order to identify tide constituents, phase, the ratio of semidiurnal to diurnal constituents (F), and current velocities. These measurements should be obtained for at least two encompassed spring and neap tide periods, and if possible, to obtain information of how these vary seasonally within the Guaymas System.

- Dye releases and tracking particles through fluororimtric techniques, to provide a good feedback to the model, allowing validation for the field current model and further calibration in the Lagrangian transport model.

Sediment dynamics.

- A temporal variation including spring and neap tides, and a well spread spatial variation, including channels and shallow waters, ensuring an adequate representation of the data with respect to the system.
- Simultaneous measurements of both bed sediments and suspended sediments, including a complete profile through the water column, particularly near to the bed.

Other physical, chemical and biological parameters.

- To extend the present survey programme in order to encompass at least two seasonal periods, including primary productivity measurements from both the water column and sediment.
- The exact composition and temporal variation of the discharges within the system.

7.2.2 Coastal research studies.

Further investigations should be conducted in the following areas:

Hydrodynamics and sediment dynamics studies.

- The identification and characterisation of fine grid cells for sediment circulation will produce a better framework for shoreline management.

- Washout load is an important fraction of total sediment displacement in some areas, in which direct research efforts must be addressed.

Net ecosystem metabolism and nutrient dynamics studies.

- Further research must be focused on characterising primary producers for the system, and their contribution to the total primary production.

- Research defining the C:N:P ratios from: wastewater, benthic primary producers, and pelagic algae, will allow the refining of the present approach.

- Characterisation of ground water, VG, for the area. VG can be represented in the Guaymas basis by percolation from drainage.

- Other phosphate and nitrogen forms and their speciation must be considered.

Eutrophication studies.

- Eutrophication prediction should be built-up further from hydrodynamic model outputs, including turbulent mixing induced by wind and tide.

- Consideration of other physical and chemical state variables such as temperature, salinity, pH, oxygen and nutrients, and the biological variables should be represented for the two phytoplankton major groups characterised at local levels. The light parameter must include a better and local validated self-shading correction factors, for this system.

- Biological processes such as grazing, mortality, and sinking rate, respiration, and organic breakdown must be estimated from local conditions.

- Other important components showing eutrophication response such as macroalgae and microphytobenthos must be characterised and their contribution included in further modelling.

- Further studies characterising the exact location and composition of the waste discharges along the Guaymas and Empalme basis. The study must include the projected improvements in sewage facilities and the likely industrial and urban future growth.

References.

Ackers P. and W.R. White. 1973. Sediment Transport: new approach and analysis. Journal of Hydraulics. Div. ASCE, 99, HY11, 2041-2060.

Aksnes, D. L., Ulvestand K. B., Balino B. M., Berntsen J., Egge J. K., and E. Svendsen. 1995. Ecological modelling in coastal waters: towards predictive physical-chemical-biological simulation models. In: Proceedings of the International Symposium on Nutrient Dynamics in Coastal and Estuarine Environments. International Journal of Marine Biology (OPHELIA).Vol. 41, pp. 5-37.

Altamirano-Cortez, R. 1987. Observations of Red Tide in the Mazatlán Bay, Sinaloa, México. Ciencias Marinas. Vol. 13, No. 4, pp 1-19.

Alvarez,L,G; Badan-Dagon,A; Valle,A 1989. On Coastal Currents off Tehuantepec. Estuarine, Coastal and Shelf Sciences. No. 29, pp. 89-96.

Arheimer B. and H.B. Wittgren. 1994. Modelling the Effect of Wetlands on regional Nitrogen Transport. In Wetlands and Lakes as Nitrogen Traps. AMBIO, Vol.23, No. 6, p. 378-386.

Atkinson, M.J. and S.V. Smith. 1983. C:N:P ratios of benthic marine plants. Limnology and Oceanography 28:568-572.

Aubrey, D. G. 1986. Hydrodynami Controls on Sediment Transport in Well-Mixed Bays and Estuaries Lecture Notes on Coastal and Estuarine Studies: Physics of Shallow Estuaries and Bays. Edited by J. van de Kreeke. Berlin. No. 9, Vol 16, pp.245-259.

Aubrey, D. G. and P. E. Speer. 1985. A Study of Non-linear Tidal Propagation in shallows Inlet/Estuarine Systems Part I: Observations. Estuarine, Coastal and Shelf Science. 21, pp 185-205.

Badan-Dagon A., C.J. Koblinsky, and T. Boumgartner. 1985. Spring and Summer in the Gulf of California: Observations of surface thermal patterns. Ocenologica Acta. Vol. 8, No. 1,. pp 13-22.

Bagnold, R.A. 1966. An approach to the sediment transport problem from general physics. US Geological Survey. Prof. pap. No. 422-1.

Baretta-Bekker J. G., Duursma E.K. and B.R. Kuipcrst al. 1989. Encyclopedia of Marine Sciences. Springer-Verlag. Berlin. pp.357.

Baretta-Bakker,JG; Baretta,JW; Ebenhoh,W 1997. Microbial dynamics in the marine ecosystem model ERSEM II with decoupled carbon assimilation and nutrient uptake. J. of Sea Res. 38, 195-211.

Baumert Helmut 1996. On the theory of photosynthesis and growth in phytoplankton. Part I: light limitation and constant temperature. Int. Revue ges. Hydrobiol. 81(1), 109-139.

Bearman G., Brown J., Colling A., Park D., Phyllips J., Rothery D., and J. Wright. 1993. Waves, Tides and Shallow-Water Processes. Pergamon press Oxford. pp.187.

Beckman RS10. 1986. Instruction Manual. Portable induction salinometer, Model RS10. Beckman ind. Corp. New Yersy, U.S.A.

Blackford, J.C. 1997An analysis of benthic biological dynamics in a North Sea ecosystem model. Journal of Sea Research. No. 38, pp.231-230.

Botello-Ruvalcaba 1995. Nutrients and primary productivity in relation to the potential for eutrophication and management, in the central region of the Gulf of California, Mexico. MSc. Thesis. The University of Hull, United Kingdom. pp. 84.

Botello-Ruvalcaba M.A. and J.E. Valdez-Holguin, 1997. Budgets analysis in Estero La Cruz, Sonora. in: Compressions of Carbon, Nitrogen and Phosphorus Fluxes in Mexican Coastal Lagoons. Smith, *et al.* ed. LOICZ Report & Studies No. 10, ii + 84 pp. LOICZ, Texel, The Netherlands.

Carter R.W.G.1988. Coastal Environments: An Introduction to Physical, Ecological and Cultural Systems of Coastlines. Academic press. pp. 611. London.

Cederwall, H. and R. Elmgren. 1990. Biological effects of Eutrophication on Benthic Communities including Fish: Swedish West Coast. In Marine Eutrophication, AMBIO, A Journal of the Human environment. Vol. XIX, No.3, pp. 109-112.

Chapelle, A. Lazure, P. and A. Menesguen. 1994. Modelling Eutrophication Events in a Coastal Ecosystem. Sensitivity Analysis. Estuarine, Coastal and Shelf Science. No. 39, pp.529-548.

Cheng R.T. and J.W. Gartner. 1985. Harmonic Analysis on Tides and Tidal Currents in South San Francisco Bay, California. Estuarine, Coastal and Shelf Science. Vol. 21, pp. 57-74.

Cheng R. T., Shizou F. and Xi Pangen. 1986. On Lagrangian Residual Ellipse. Lecture Notes on Coastal and Estuarine Studies: Physics of Shallow Estuaries and Bays. Edited by J. van de Kreeke. Berlin. Vol 16, No. 9, pp.102-114.

CICESE. 1995. Programa PREDOB, Departamento de Mareografia. Centro de Investigación y Enseñanza Superior de Ensenada. Carretera Ensenada-Tijuana. Ensenada, Baja California, México.

Clinch, J.R., Worsfold, P.J. and Sweeting, F.W. 1988. An automated spectrophotometric field monitor for quality parameters: Determination of ammonia. Analytica Chim. Acta. 214, pp.401-407.

Cloern, J. 1991. Annual variations in river flow and primary production in the South San Francisco Bay. In Estuaries and Coasts: Spatial and Temporal Intercomparations. Ed. Elliott M. and Jean-Paul Ducrotoy. ECSA 19 Symposium. Olsen & Olsen, Denmark. pp 91-96.

Cloern, J. 1996. Phytoplankton Bloom Dynamics in Coastal Ecosystems: A Review with some General Lessons from Sustained Investigation of San Francisco Bay, California. Reviews of Geophysics. Vol. 34, No. 2, pp. 127-168.

COAPAES, 1996. Delegacion Guaymas de COAPAES. Guaymas, Sonora México.

Colijn,F; de Jonge,VN 1984. Primary production of microphitobenthos in the Ems Estuary, 97-110.

Comision Nacional del Agua. 1998. Reporte interno. Secretaria de Medio Ambiente Recursos Naturales y de la Pesca. Empalme, Sonora, México.

Connell, Des W. 1995. Prediction of Bioconcentration and Related Lethal and Sublethal Effects with Aquatic Organisms. Marine Pollution Bulletin. Vol. 31, Nos. 4-21, pp. 201-205.

CSTT. 1994. Comprehensive studies for the purpose of Article 6 of Directive 91/271/EEC, the urban waste water treatment directive. Comprehensive

Studies task Team, Marine Pollution Monitoring Management Group. FRPB Edinburg.

Curl, Herbert Jr; Small,Lawrence F. 1969. Variations in photosynthetic assimilation ratios in natural marine phytoplankton communities. Limnology and Oceanography. R67-R73.

Daling P.S. and T. Strom. 1998.Weathering of oils at sea: Model/field data comparisons. Second International Marine Modelling Seminar. Norway.

de Jonge,V.N.1995. The Ems Estuary, The Netherlands. In: Eutrophic Shallow Estuaries and Lagoons. McComb, Arthur. J. ed. CRC Prss, Boca Raton-Londo-Tokyo. pp. 81-105.

de Jonge, V.N. and W. van Raaphorst. 1995. Eutrophication of the Ducth Wadden Sea (western Europe), an estuarine area controlled by the River Rhine. Eutrophic Shallow Estuaries and Lagoons. McComb, Arthur. J. ed. CRC Press, Boca Raton-London-Tokyo. pp.129-149.

de Jonge V.N. 1990. Response of the Dutch Wadden Sea ecosystem to phosphorus discharges from the River Rhine. Hydrobiologia. 195:46-62.

de Jonge, N.V and K. Essink. 1991. Long-term changes in nutrient loads and primary and secondary producers in the Dutch Wadden Sea. In Estuaries and Coasts: Spatial and Temporal Intercomparations. Ed. Elliott M. and Jean-Paul Ducrotoy. ECSA 19 Symposium. Olsen & Olsen, Denmark. pp 307-316.

de Silva, Samarasinghe J. R. 1989. Transient Salt-Wedges in a Tidal Gulf: A Criterion for Their Formation. Estuarine, Coastal and Shelf Science. Vol. 28, pp. 129-148.

Delgadillo-Hinojosa F. 1992. Productividad Organica Primaria y su Relacion con Variables Ambientales de Bahía de los Angeles Baja California. Msc. Thesis Universidad Autonoma de Baja California. Baja California México.

Delgadillo-Hinojosa F. and J.A. Segovia-Zavala. 1997. Budgets analysis in Bahía San Luis Gonzaga, Baja California. In Comparations of Carbon, Nitrogen and Phosphorus Fluxes in Mexican Coastal Lagoons. Smith, *et al.* ed. LOICZ Report & Studies No. 10, ii + 84 pp. LOICZ, Texel, The Netherlands.

Dyer Keith R. 1973. Estuaries: A Physical Introduction. Wiley & Sons ed. Chichester England. pp. 195.

Dyer Keith R. 1986. Coastal and Estuarine Sediment Dynamics. Wile & Sons ed. Chichester England. pp. 342.

Dyer Keith R. 1997. Estuaries: A Physical Introduction. Second Edition. John Wiley & Song Ed. Chichester, England. 195p.

Einstein, H.A. 1950. The bedload function for sediment transportation in open channel flows. Soil Cons. Serv. U.S. Department of Agriculture. Technical bulletin. No. 1026, pp 78.

Elliott M., de Jonge V.N., Burrell G.K., Johnson M.W., Phillips G.L. and T.M. Tuner. 1994. Trophic status of the Ore/Alde, Deben, Stour and Colne estuaries. Reports in Applied Marine Biology. The University of Hull, United Kingdom.

Engqvist Anders. 1996. Long-term Nutrient Balances in the Eutrophication of the Himmerfjarden Estuary. Estuarine, Coastal and Shelf Science. No. 42. pp. 483-507.

Enoksson, V., Sorensson, F., and W. Graneli. 1990. Nitrogen Transformation in the Kattegatt. In Marine Eutrophication, especial issue. AMBIO A Journal of the Human Environment. Vol. XIX, No. 3, pp.159-166.

Eppley R. 1969. An Incubation method for estimating the carbon content of phytoplankton in natural samples. Limnology and Oceanogaphy. Vol. 13, pp.574-582.

Fingas M. F. 1998. The Evaporation of Oil Spills: Development and Implementation of New Prediction Methodology. Second International Marine Environmental Modelling Seminar. Norway.

Flores-Verdugod F.J. and G. de la Lanza-Espino. 1997. Bahía de Altata-Ensenada del Pabellon, Sonora. In Comparations of Carbon, Nitrogen and Phosphorus Fluxes in Mexican Coastal Lagoons. Smith, *et al.* ed. LOICZ Report & Studies No. 10, ii + 84 pp. LOICZ, Texel, The Netherlands.

Forsberg Curt. 1994. The Large-Scale Flux of Nutrients from Land to Water and the Eutrophication of Lakes and Marine Waters. Marine Pollution Bulletin. Vol. 29, Nos. 6-12, pp.409-413.

French W. P. 1997. Coastal and Estuarine Management. Routledge Environmental Management Series. Routled ed. 251 p. London.

Friedrichs, C.T. and D.G. Aubrey. 1988. Non-linear tidal distortion in shallow well-mixed estuaries: a synthesis. Estuarine, Coastal and Shelf Science. No. 38, pp. 157-172.

Garcia, R.and R. Kahawita. 1986. Numerical Solution of the St. Venat Equation with the MacCormack Finite-Difference Scheme. International Journal for Numerical Methodos in Fluids. Vol. 6, pp. 259-274.

Garcia-Martinez, R. and H. Flores-Tovar. 1999. Computer modelling of oil spill trajectories with a high accuracy method. Spill Science and Technology Bulletin. In preens.

Gaxiola-Castro G., Garcia-Cordova J., Valdez-Holguin J. E., and M. Botello-Ruvalcaba. 1995. Spatial distribution of chlorophyll a and primary production in relation to winter physical structure in the Gulf of California. Continental Shelf Research, Vol. 5, No. 9, pp. 1043-1059. United Kingdom.

GESAMP. 1990. The State of the marine environment. UNEP Regional Seas Report and Studies No. 115. -(IMO/FAO/UNESCO/WMO/ WHO/ IAEA/UN/UNEP, Joint group of experts on the scientific aspects of marine pollution). UNEP 1990.

Gobierno de Sonora. 1998. Secretaria de Desarrollo Economico y Productividad, Centro de Gobierno. Hermosillo, Sonora, México.

Gomez-Jimenez S. 1998. Some physiological and immunological responses of the spiny lobster, Panulirus interruptus (Randall, 1840), to practices used in its live marketing in the Baja California. PhD thesis. University of Hull, Hull, United Kingdom..

Gordon, D.C., P.R. Boudreau, K.H. Mann, J.-E. Ong, W.L. Silvert, S.V. Smith, G. Wattayakorn, F. Wullff and T. Yanagi. 1996. LOICZ Biochemical Modelling

Guidelines. LOICZ Reports & Studies No. %. Second Edition, vi +96 pp. LOICZ, Texel, The Netherlands.GESAMP. 1990.

Graneli, E., Walldstrom, K., Larsson, U., Graneli, W., and R. Elmgren. 1990. Nutrient limitation of primary production in the Baltic Sea. In Marine Eutrophication special issue. AMBIO A Journal of the Human Environment. Vol. XIX, No. 3, pp. 142-151.

Grasshoff K., Ehrhardt M., and K. Kremling. 1983. Methods of Seawater Analysis. Second edition. pp 420.

Harris, J.R.W., Bale, A.J., Bayne, B.J., Mantoura, R.F.C., Morris, A.W., Nelson, L.A., Radford, P.J., Uncles, R.J., Weston, S.A. and J., Widdows. 1984. A preliminary model of dispersal and biological effects of toxins in Tamar estuary, England. Ecol. Modelling. Vol. 22, pp. 253-284.

Heip, C. 1995. Eutrophication and zoobenthos dynamics. In Proceedings of the International Symposium on Nutrient Dynamics in Coastal and Estuarine Environments. International Journal of Marine Biology. Ophelia Vol. 41, pp 113-136.

Heip, C. H. R., N. K. Goosen, P. M. J. Herman, J. Jromkamp, J.J. Middlelburg, and K. Soetaerd. 1995. Production and consumption of biological particles in temperate tidal estuaries. Oceanography and Marine Biology: An Annual Review. Vol. 33, pp. 1-149.

Hencly and Henzel.1980. Physiological indication of nutrient deficiency in lake phytoplankton. Can. J. Fish Aquat. Sci. Canada. No. 37, pp 442-453.

Hooke, J.M., Bray M.J. and D.J. Carter. 1996. Sediment transport analysis as a component of coastal management a UK example. Environmental Geology. Vol. 27, pp. 324-357.

Hosch, G. 1997. Prospective mapping of total cadmium, copper, zinc and lead contamination in water, sediment and clams (Chione gnidia) of Guaymas Bay, Sonora, Mexico. Msc. Thesis The University of Hull. Hull, United Kingdom.

Howarth M.J. and D.T. Pugh. 1983. Observations of tides over the continental shelf of north west Europe. In: Physical Oceanography of Coastal and Shelf Seas. B.

Johns editor. Elsevier Oceanographyc Series. Amsterdam, The Netherlands. pp.135-188.

Huang Po-Shu, Wang D. P. and Najarian T. O. 1986. Analysis of Residual Currents Using a two-dimensional Model. Lecture Notes on Coastal and Estuarine Studies: Physics of Shallow Estuaries and Bays. Edited by J. van de Kreeke. Berlin. No. 9, Vol 16, pp. 71-81.

Hunter, D.A., Uglow,R.F. 1993. A technique for the measurement of total ammonia in small volumes of seawater and haemolymph. Ophelia Vol. 37, No.1, pp. 31-40.

INEGI. 1998. Anuario estadistico del Instituto Nacional de Geografia e Informatica. Delegacion Sonora. Hermosillo Sonora México.

Ip J.T.C., Lynch D.R. and C.T. Friedrichs. 1998. Simulation of Estuarine Flooding and Dewatering with Application to Great Bay, New Hampshire. Estuarine, Coastal and Shelf Science. Vol. 47, pp.119-141.

Jacinto G. S., M. L. San Diego-McGlone, I. B. Velasquez, and S. V. Smith. 1998. N and P Budget of Manila Bay, Philippines. LOICZ Repot & Studies. LOICZ, Texel, The Netherlands.

Jansson, M., Andersson, R., Berggren, H. and L. Leonardson. 1994. Wetlands and Lakes as Nitrogen Tramps. AMBIO, Journal of the Human Environment. Sweden. Vol.23, No. 6.

Jing-Wen C. and L. Chin-Yuh. 1997. Representing Grain Size of Bed Material. Ocean Engineering. Vol. 24, No. 1, pp. 1-18.

Johnson, M.P., Costello, M. J. and D. O'Donnell. 1995. The nutrient economy of a marine inlet: Lough Hyne, South West Ireland. OPHELIA International Jounal of Marine Biology. Vol 41, pp. 137-152.

Kenneth, S.J. and L. Petty. 1982. Determination of Phosphate in Seawater by Flow Injection Analysis with Injection of Reagent. Anal. Che. No. 54, pp. 1185-1187.

Kildow, J. 1997. The Roots and Context of the Coastal Zone Movement. Coastal Management, Vol. 25, pp. 230-261.

Kjerfve, B. 1986. Circulation and Salt Flux in Well Mixed Estuary. Lecture Notes on Coastal and Estuarine Studies: Physics of Shallow Estuaries and Bays. Edited by J. van de Kreeke. Berlin. Vol 16, No. 9, pp. 22-30.

Knauss, J. A. 1978. Introduction to Physical Oceanography. Prentice-Hell ed. Englewood N.J. pp 335.

Kuusisto M., Koponen J. and J. Sarkkula. 1998. Modelling Phytoplankton Dynamics in the Gulf of Finland. Marine Environmental Modelling Seminar '98. Lilliehammer, Norway.

Lechuga-Deveze, C. 1997. Budgets analysis in Bahía Concepcion, Baja California Sur. in: Comparisons of Carbon, Nitrogen and Phosphorus Fluxes in Mexican Coastal Lagoons. Smith, *et al.* ed. LOICZ Report & Studies No. 10, ii + 84 pp. LOICZ, Texel, The Netherlands.

Lee, J. Y. 1995. Estimating Eutrophication Potential and its seasonal change in Milford Heven using a three-box model. Msc. Thesis University of Wales, Bangor. Bangor, United Kingdom.

Lin B. and R Falconer. 1997. Numerical modelling of three-dimensional suspended sediment for estuarine and coastal waters. Journal of Hydraulic Research. Vol.3, No. 4.

Makrama A. Gerges. 1994. Marine Pollution Monitoring Assessment and Control:UNEP's Approach and Strategy. Marine Pollution Bulletin, Vol. 28. No. 4, pp. 199-210.

Nadiarti. 1995. A Simple Model to Test for Eutrophication. Msc. Thesis. University of Wales, Bangor. Bangor, United Kingdom.

Nixon Scott W. 1995. Coastal Marine Eutrophication: A definition, Social Causes, and Future Concerns. OPHELIA, International Journal of Marine Biology. Vol. 41, pp. 119-219.

Officer, C.B. 1976. Physical Oceanography of Estuaries (And Associated Coastal Waters). Wiley-Interscience Publication. New York, U.S.A.

Organza-Gonzales, F.I. and P.J. Statham. 1991. The occurrence and behaviour of different forms of phosphate in the waters of four English estuaries. In

Estuaries and Coasts: Spatial and Temporal Intercomparations. Elliot M. and J.P. Ducrotoy eds. Olsen and Olsen. pp. 77-83.

Owens, P.H. 1986. Mathematical Modeling of Sediment Transport in Estuaries. PhD. Thesis. University of Birmingham. Birmingham United Kingdom.

Pan Youlian and D.V. Subba-Rao. 1997. Impact of Domestic Sewage effluent on phytoplankton from Bedford basin, Eastern Canada. Marine Pollution Bulletin, Vol. 34, No. 12, pp. 1001-1005.

Peckol, P. and J.S. Rivers. 1996. Contribution by Macroalgal Mats to Primary Production of a Shallow Embayment Under High and Low Nitrogen-loading Rates. Estuarine, Coastal and Shelf Sciences. Vol.43, pp. 311-325.

Person, T.R., Maita, Y. and Lalli, C.M. 1984. A Manual of Chemical and Biological Methods for Seawater Analysis. Pergamon Press. Vancouver Canada. p.p. 174.

Pethick, J. 1984. An Introduction to Coastal Geomorphology. Arnold ed. London. pp. 260.

Pingree, R.D. and L. Maddock. 1977. Tidal eddies and coastal discharge. Journal of Marine Biology Association United Kingdom. No. 57, 867-875.

Prandle, D. 1986. Generalised Theory of Estuarine Dynamics. In Physics of Shallow Estuaries and Bays. J. ven de Kreeke ed. Springer-Verlag. Berlin.

Rainbow Philip S. 1995. Biomonitoring of Heavy Metal Availability in the Marine Environment. Marine Pollution Bulletin, Vol. 31, No. 4-12, pp. 183-192.

Ramirez-Siqueiros G. 1999. Evaluacion del impacto de los aportes de nutrientes y materia organica en la biomasa fitoplanctonica de la sistema de Guaymas. Thesis de Licenciatura. Universidad de Sonora. Hermosillo, Sonora, México.,

Redfield A. C., Ketchum B. H. and F. A. Richards 1963. The influence of organisms on the composition of sea-water. In: The Sea. Hill ed. New York. Vol. 2, pp.26-77.

Reley, J.P. and R. Chester. 1971. Introduction to Marine Chemistry. Academic Press. London, U.K.

Rene-Flindt M. and L. Kamp-Nielsen. 1997. Modelling of an estuarine eutrophication gradient. Ecological Modelling Vol.102, pp. 143-153.

Rodríguez-Molina J. and R. García-Martínez. 1998. HydroTrack: A Graphical Software System for the Simulation of Pollutant Discharges in Water. To appear in Environmental Modelling and Software.

Rosales-Grano, P., Burrola-Sanchez, M. and S.O. Reyna-Espino. 1996. Estudio de la Hidrodinámica de la Bahía de Guaymas, Sonora. Reporte UR690. Unidad de Educación en Ciencia y Tecnología del Mar. Instituto Tecnológico del Mar, Centro de Investiaciones y Graduados del Mar. Guaymas, Sonora, México.

Rosenberg, R., Elmgren R., Fleischer S., Jonsson P., Persson G. and H. Dahlin. 1990. Marine Eutrophication in Sweden: Marine Eutrophication Case Studies in Sweden. AMBIO, Journal of the Human Environment. Vol. 10, No.3. pp 102-108.

Rydberg, L., Edler L., Floderus S., and W. Graneli. Eutrophication mechanisms. 1990. Marine Eutrophication in Sweden: Marine Eutrophication Case Studies in Sweden. AMBIO, Journal of the Human Environment. Vol. 10, No.3. pp 134-141..

SEMARNAP, 1998. Secretaria de Medio Ambiente Recursos Naturales y Pesca. México Distrito Federal. México.

Sham, C.H., Brawley, J.W. and M.A. Moritz. 1995. Quantifying septic nitrogen loading to receiving waters: Waquoit Bay, Massachusetts. International Journal of Geographical Information Systems. Vol. 9, No. 4, pp. 463-473.

Shin-ichi Sugioka, Takashi-Kojima, Nakatad K. and H. Fumio. 1998. A Numerical Simulation of a Oil Spill in Tokio Bay. Second International Marine Modelling Seminar. Norway.

Skogen, M.D., Svenden, E., Berntsen, J., Akses, D. and K.B. Ulvestad. 1995. Modelling the Primary Production in the North Sea using a Coupled Three-dimensional Physical-Chemical-Biological Ocean Model. Estuarine, Coastal and Shelf Science. Vol. 41, pp. 545-565.

Sleath, J. F.A. 1995. Sediment transport by waves and currents. Journal of Geophysical Research, Vol. 100, No. C6, pp.10,977-10,986.

SMAM. 1991. Secretaria de Marina, Armanda de México. Estudio de la Calidad del Agua de la Bahía de Guyamas, Sonora y Proximidades. Guaymas, Sonora, México.

Smith Ned P. 1990. Longitudinal Transport in a Coastal Lagoon. Estuarine, Coastal and Shelf Science. 31, 835-849.

Smith, S.V. and M.J. Atkinson. 1980. Mass balance of carbon and phosphorus in Shark Bay, Western Australia. Limnology and Oceanography. Vol. 28, No. 4, pp.1983, 625-639.

Smith, S.V., J.T. Hollibaugh, S.J. Dollar and S. Vink. 1991. Tomales Bay Metabolism: C-N-P Stoichiometry and Ecosystem Heterotrophy at the Land-Sea Interface. Estuarine, Coastal and Shelf Science. Vol. 33, pp. 223-257.

Smith, S.V., S. Ibarra-Obando, P.R. Boudreau and V.F. Camacho-Ibarra. 1997. Comparation of Carbon, Nitrogen and Phosphorus Fluxes in Mexican Coastal Lagoons, LOICZ Report & Studies No. 10, ii + 84 pp. LOICZ, Texel, The Netherlands.

Sorensen Jens. 1997. National and International Efforts at Integrated Coastal Management: Definitions, Achievements, and Lessons. Coastal Management. Vol. 25, pp. 3-41.

Strain P.M., Wildish D.J. and P.A. Yeats. 1995. The application of Simple Models of Nutrient Loading and Oxygen Demand to the Management of a Marine Tidal Inlet. Marine Pollution Bulletin. Vol. 30, No. 4, pp. 253-261.

Strickland J. D. and T. D. Parsons. 1972. A practical handbook of seawater analysis. Bull. Fish. Res. Bd. Canada. Ottawa.

Tejeda-Valenzuela, L.G. 1999. Variabilidad espacial de la materia organica y su posible efecto sobre el macrobentos de la Bahía de Guaymas, Sonora. Tesis de Licenciatura, Universidad de Sonora. Hermosillo, Sonora, México.

Thomann, R.V. 1983. Physico-Chemical and Ecological Modelling the fate of toxic substances in natural water systems. Ecological Modelling. Vol. 22, pp.145-170.

Uncles R. J., Elliot R. C. A., Weston S. A., Pilgrim D. A., Ackroyd D. R., McMillan D. J. and N.M. Lynn. 1986. Synoptic Observations of Salinity, Suspended Sediment and Vertical Current Structure in a Partly Mixed Estuary. Lecture Notes on Coastal and Estuarine Studies: Physics of Shallow Estuaries and Bays. Edited by J. van de Kreeke. Berlin. No. 9, Vol.16, 58-71 pp.

Valdez-Holguin,J.E. 1994. Daily Variations of temperature, salinity, dissolved oxygen and chlorophyll a, in a hypersaline lagoon of the Gulf of California. Ciencias Marinas Vol. 20, No. 2, pp.123-137.

Valdez-Holguin, J.E. and J.R. Lara-Lara. 1987. Primary productivity in the Gulf of California effects of EL NINO 1982-1983 event. Ciencias Marinas, Vol.13, pp.34-50.

Van Beusekom J.E.E. and V.N. de Jonge. 1998. Retention of Phosphorus and Nitrogen in the Ems estuary. Estuaries Vol. 21 No.4A, pp 527-540.

Van de Kreeke, J. 1986. Lecture Notes on Coastal and Estuarine Studies: Physics of shallow Estuaries and Bays. Spriner-Verlag. Berlin. No. 9, Vol 16, 280p.

van de Kreeke, J. 1986. Towards a Sustainable Future. Marine Pollution Bulletin. Vol. 31, Nos. 4-12, pp. 159-166.

Vant W.N., M. M. Gibbs, K.A. Safi and S.F. Thrush. 1998. Fluxes of Organic Carbon in Manukau Harbour, New Sealand. Estuaries Vol. 21 NO. 4a, p. 560-570.

Varela,Ramiro A; Cruzado,Antonio; Babaldon,Jesus E (1995 1997?): Modelling primary production in the North Sea using the European Regional Seas Ecosystem Model. J. of Sea Res. Vol.33, No.3/3, pp.337-361.

Villate, F., J. Franco, L. Gonzalez, I. de Madariaga, A.Ruiz and E. Orive. 1991. A comparative study of hydrography and seston in five estuarine systems of Basque Country. In Estuaries and Coasts: Spatial and Temporal Intercomparations. M. Ellott and J.P. Ducrotoy Eds. pp. 97-105.

Walter, E.D. 1974. Determination of carbonate and organic matter in calcareous sediment and sedimentary rocks by loss ignition: Comparison with other method. Journal of sedimentary petrology. Vol. 44, No. 1, p.p. 242-248.

Wofsy S.C., 1983. A simple model to predict extinction coefficient and phytoplankton biomass in eutrophic waters. Limnology and Oceanography. Vol. 28, No. 6, pp. 1144-1155.

Wu, R. S. S. 1995. Environmental Impact of Marine Fish Culture: Towards a Sustainable Future. Marine Pollution Bulletin. Vol. 31, Nos. 4-12, pp. 159-166.

Wulff, F., A. Stigebrandt and L. Rahm. 1990. Nutrient Dynamics of the Baltic Sea. AMBIO. Special Issue: Marine Eutrophication. Vol. XIX, No. 3. p 126-133.

Yanagi Tetsuo, Koh-ichi Inoue, Sigeru Montani and Machiko Yamada. 1997. Ecological modelling as a tool for coastal zone management in Dokai Bay, Japan.